Cellulose Nanocrystals Incorporated Nanocomposites for Water Treatment Applications

by

Nishil Mohammed

A thesis
presented to the University of Waterloo
in fulfillment of the
thesis requirement for the degree of
Doctor of Philosophy
in
Chemical Engineering

Waterloo, Ontario, Canada, 2017

Author's Declaration

This thesis consists of material all of which I authored or co-authored: see Statement of Contributions included in the thesis. This is a true copy of the thesis, including any required final revisions, as accepted by my examiners.

I understand that my thesis may be made electronically available to the public.

Statement of Contributions

The work presented in this thesis is the result of work performed by the author and several scientific collaborators. Contributions from each researcher and the resulting publications are described here. The literature review in Chapter 2 is currently in preparation for journal submission. Nishil and Prof. K.C Tam wrote the manuscript. Nate helped in revising the manuscript. The work in Chapter 3 has been accepted as: Nishil Mohammed, Nathan Grishkewich, Richard M. Berry and Kam Chiu Tam, Cellulose Nanocrystal–Alginate Hydrogel Beads as Novel Adsorbents for Organic Dyes in Aqueous Solutions, **Cellulose**, **2015**, 22(6), 3725-3738. Nishil performed all the experiments. Nathan helped in modeling the kinetic adsorption data. Dr. Berry proofread the manuscript. Nishil and Prof. K.C. Tam wrote the manuscript. The work in Chapter 4 has been accepted as: Nishil Mohammed, Nathan Grishkewich, Herman Ambrose Waeijen, Richard M. Berry and Kam Chiu Tam, Continuous Flow Adsorption of Methylene Blue by Cellulose Nanocrystal–Alginate Hydrogel Beads in Fixed Bed Columns, **Carbohydrate Polymers**, **2016**, 136, 1194-1202. Nishil and Nathan equally performed all the experiments and analyzed the data. Ambrose helped in performing some column adsorption experiments. Dr. Berry proofread the manuscript. Nishil, Nathan and K.C. Tam wrote the manuscript. The work in Chapter 5 is currently in preparation for journal submission. Nishil performed all the experiments. Zengqian Shi helped in functionalizing the cellulose nanocrystals. Aravind helped in performing the selective dye adsorption and antibacterial studies. Dr. Berry and Prof. Anderson proofread the manuscript. Nishil and Prof. K.C. Tam wrote the manuscript. The work in Chapter 6 has been accepted as: Nishil Mohammed, Avijit Baidya, Vasanthanarayan Murugesan, Avula Anil Kumar, Mohd Azhardin Ganayee, Jyoti Sarita Mohanty, Kam Chiu Tam and Thalappil Pradeep, Diffusion-Controlled Simultaneous Sensing and Scavenging of Heavy Metal Ions in Water Using Atomically Precise Cluster–Cellulose Nanocrystal Composites, **ACS Sustainable Chemistry and Engineering**, **2016**, 4(11), 6167-6176. Nishil performed all the experiments. Avijit, Vasanth, Anil, Azhar and Jyoti helped in the characterization of the nanocomposite. Nishil, Prof. K.C. Tam and Prof. Pradeep wrote the manuscript.

Abstract

Water is the elixir of life; however, it is being increasingly contaminated by a wide variety of contaminants from industrial, municipal and agricultural sources like dyes, heavy metal ions, food additives, pharmaceuticals, detergents, agrochemicals etc. Among the various water treatment technologies employed for the treatment of wastewater, adsorption is a technique which when implemented using well-designed system provides high quality treated water at an affordable cost. Activated carbon is the conventionally used adsorbent for water treatment. However, its production is energy intensive, expensive and also emits greenhouse gases. Hence there is an enormous interest in developing low-cost alternative adsorbents from industrial and agricultural waste and biomass. In this context, the use of sustainable nanomaterial, such as cellulose nanocrystals (CNCs) to develop sustainable platforms for wastewater treatment is a novel approach that has a negligible carbon footprint. CNCs obtained by the sulfuric acid hydrolysis of pulp fibers are rod-like nanomaterials that possess several interesting properties such as high specific surface area, high specific strength, hydrophilicity, biodegradability and surface functionalization capabilities. These properties and their large-scale availability make them attractive candidates for use in water treatment applications. However, the separation of these CNCs after use in water treatment is a challenge because of their high colloidal stability and nano-dimensions. Incorporating these CNCs into nanocomposite systems that can be easily separated after use in batch and continuous water treatment processes is an ideal strategy to address this challenge. Also, the selectivity of pristine CNCs towards a wide variety of water contaminants is limited and it is essential to surface functionalize them to impart this selectivity. Hence, this thesis explores the (i) development of CNC incorporated nanocomposites and evaluation of their adsorption characteristics using batch and fixed bed column adsorption studies, and (ii) evaluation of the selective adsorption characteristics of surface functionalized CNCs and their ability to tailor the characteristics of the nanocomposites, for use in water treatment applications.

In the first part, a new generation of recyclable adsorbent based on CNCs and alginate with superior adsorption capacity was developed. CNCs were incorporated into alginate (CNC-

ALG) hydrogel beads and their adsorption characteristics were evaluated in detail using batch adsorption studies of a model organic dye, methylene blue (MB) in aqueous solution. The influence of various parameters such as contact time, adsorbent dosage, initial dye concentration, pH, temperature, ionic strength, crosslinking time and bead size on the MB adsorption were investigated. The measured thermodynamic parameters confirmed a spontaneous exothermic adsorption process. The adsorption kinetics and mechanism of adsorption were best described using pseudo-second order kinetic and intra-particle diffusion model. Equilibrium adsorption data obeyed the Langmuir adsorption isotherm and a maximum adsorption capacity (q_{max}) of 256.41 mg/g was reported, which is comparable to activated carbon. We demonstrated that after 5 adsorption-desorption cycles, the removal efficiency of MB remained at ~97%, and the CNC-ALG hydrogel beads are effective adsorbents for the removal of organic dyes from wastewaters.

In the second part, the adsorption behavior of MB by CNC-ALG hydrogel beads in a fixed bed column was studied by varying the initial dye concentration, bed depth and flow rate. An unusual phenomenon was observed in the early phase of the adsorption, and the phenomenon was elucidated by varying other critical design parameters, such as the flow direction, diameter of column and composition of adsorbent. The swelling and shrinkage of hydrogel beads during the adsorption was responsible for the anomalous concentration versus time profile of the adsorption process. The q_{max} of the column was 255.5 mg/g, which is in agreement with the batch study determined from the Langmuir adsorption isotherm. Moreover, a comprehensive understanding of the adsorption mechanism of the CNC-ALG hydrogel beads during the early stages of adsorption was derived from this study.

In the third part, CNCs were surface functionalized and their applicability in nanocomposites for water treatment application was explored. Herein, we report for the first time the use of pristine and surface functionalized CNCs for the selective adsorption of a specific dye molecule from dye mixtures. CNCs were coated with melamine-formaldehyde (MF) and polydopamine (PD) to prepare surface functionalized CNCs such MF-CNCs and PD-CNCs respectively. The selectivity of pristine and surface functionalized CNCs were

investigated using selective dye adsorption studies and these studies showed that pristine CNCs, MF-CNCs and PD-CNCs showed an affinity towards dye having specific charge or functional group. The ability of surface functionalized CNCs to tailor the properties of nanocomposites was also explored by preparing a novel nanocomposite viz., PD-CNC-ALG hydrogel beads. PD-CNC-ALG hydrogel beads displayed very good selectivity for dyes containing Eschenmoser functional group. Batch adsorption studies performed confirmed that these hydrogel beads possessed good adsorption capacity for MB and copper with a q_{max} of 333.33 and 79.99 mg/g respectively. PD-CNC-ALG hydrogel beads can also be made antibacterial by chelating silver nanoparticles (Ag-NPs) onto PD-CNCs. The leaching of Ag-NPs from the hydrogel polymer matrix was found to be negligible as these Ag-NPs are strongly chelated to the PD-CNCs. Such systems can be used in the disinfection of bacteria contaminated water. Thus, the prepared PD-CNC-ALG hydrogel beads can be considered as a versatile adsorbent with broad capabilities for use in wastewater treatment.

In the fourth part, a novel nanocomposite system viz., bovine serum albumin protected gold nanoclusters (Au@BSA NCs) loaded cellulose nanocrystal – alginate hydrogel beads that can simultaneously sense and scavenge toxic heavy metal ions at low concentrations was developed for *in situ* monitoring and purification of contaminated water. These nanocomposites were also found to be highly selective towards mercury ions. Characterization of the system performed using scanning electron microscopy coupled with energy dispersive spectroscopy and X-ray photoelectron spectroscopy elucidated the physical and chemical characteristics of the system. Additionally, we proposed a new method to visualize the diffusion phenomenon and calculated the effective diffusion coefficient of heavy metal ions in the hydrogel beads by monitoring the fluorescence quenching dynamics of Au@BSA NCs upon binding to mercury ions. Finally, practical applications of this nanocomposite were demonstrated using batch adsorption experiments as well as using a dip pen device loaded with the hydrogel beads for *in-situ* monitoring of heavy metal ions in water.

In conclusion, this thesis provides a detailed investigation on the development and application of CNCs incorporated nanocomposites for water treatment applications.

Acknowledgements

Four years of doctoral study at the University of Waterloo has been a rewarding experience both in my personal and professional life. I would like to acknowledge several people who have supported and helped me throughout this journey.

First and foremost, I would like to express my sincere gratitude to my supervisor Prof. Michael K.C. Tam for his guidance, motivation, and patience without which this thesis would not have been possible. I would also like to thank my doctoral thesis committee members Prof. Marc Aucoin, Prof. Xianshe Feng, Prof. Sigrid Peldszus, Prof. Todd Hoare and Prof. Sheree Pagsuyoin for their insightful remarks and suggestions regarding my research and thesis.

A very special thanks to Mr. Nathan Grishkewich who collaborated with me on several projects. Dr. Zengqian Shi has been very helpful in several aspects related to functionalization of CNCs. Thank you, Nathan, and Dr. Shi for all your help.

Special thanks also go to Prof. Thalappil Pradeep, Prof. Boxin Zhao and Prof. William Anderson for allowing me to use their lab facilities. I would also like to thank all my labmates in the Laboratory of Functional Colloids and Sustainable Nanomaterials for their support and stimulating discussions. My immense gratitude also goes to all the staff members of Department of Chemical Engineering especially Judy Caron, Lis Bevan and Cathy Logan who have helped me in several administrative aspects during my graduate studies at University of Waterloo.

Most importantly, none of this could have happened without my family and friends. I am forever grateful to my parents (Mrs. V.C. Khadeeja and Mr. A.V. Kunchi Mohammed), my love (Mrs. Lamiya Ibrahim) and my in-laws (Mr. Ibrahim Ambikana, Mrs. Ayesha Ibrahim and Mr. Jassim Ibrahim) who offered their unceasing encouragement, unconditional love, support and attention. Last but not the least, my special thanks to Dr. Deepak Vishnu Dharmangadan and all other members of Canadian Tharavadu community for all their support and warmth of friendship.

Dedication

To my lovely parents V.C. Khadeeja and A.V. Kunchi Mohammed

Table of Contents

List of Figures

List of Tables

List of Acronyms

CN	Cellulose nanomaterials
CNC	Cellulose nanocrystals
CNF	Cellulose nanofibrils
MCC	Microcrystalline cellulose
NCH	Nanocomposite hydrogels
ALG	Alginate
MB	Methylene blue
PD	Polydopamine
MF	Melamine formaldehyde
TAPPI	Technical association of the pulp and paper industry
TEMPO	2,2,6,6-tetramethyl-1-piperidinyloxy
GTMAC	Glycidyltrimethylammonium chloride
SEM	Scanning electron microscopy
TEM	Transmission electron microscopy
UV	Ultraviolet
Vis	Visible
SNP	Silica nanoparticle
PAA	Poly(acrylic acid)
PB	Polyvinyl alcohol-borax
PVA	Polyvinyl alcohol
CHO-CNC	Aldehyde functionalized cellulose nanocrystal
CNC-NH_2	Amine functionalized cellulose nanocrystal
CNC-COOH	Carboxyl functionalized cellulose nanocrystal
PVAc	Poly(vinyl acetate)
NVP	N-Vinyl pyrrolidine
c-CNF	Carboxymethyl substituted cellulose nanofibril
PAM	Polyacrylamide

AM	Acrylamide
NMBA	N,N'-Methylenebisacrylamide
PEG	Polyethylene glycol
$CaCl_2$	Calcium chloride
PHEMA	Poly(2-hydroxyethylmethacrylate)
CMC-$NHNH_2$	Adipic acid dihydrazide modified carboxymethyl cellulose
Dextran-CHO	Aldehyde-modified dextran
CB[8]	Cucurbit[8]uril
APS	Ammonium persulfate
q_{max}	Maximum adsorption capacity
MA	Maleic anhydride
A-CNC	Amino functionalized cellulose nanocrystal
Q-CNF	Surface quarternized cellulose nanofibril
MnO2	Manganese dioxide
R-POSS	Polyhedral oligomeric silsesquioxane
HPAM	Partially hydrolyzed polyacrylamide
PVAm	Polyvinylamine
HIUS	High intensity ultra-sonication
TMP	TEMPO oxidization
ECNC	Electrosterically stabilized cellulose nanocrystal
DCC	Dicarboxylated chains
NaBr	Sodium bromide
NaClO	Sodium hypochlorite
PEI	Polyethylenimine
APTES	Aminopropyltriethoxysilane
CHA	Carbonated hydroxyapatite
Fe-NP	Iron nanoparticle
HNO_3	Nitric acid

HCl	Hydrochloric acid
NaOH	Sodium hydroxide
H_2SO_4	Sulfuric acid
Fe_3O_4	Iron oxide
SiO_2	Silicon dioxide
H_2S	Hydrogen sulphide
HAP	Hydroxyl-carbonated apatite
PO_4^{3-}	Phosphate
NO^{3-}	Nitrate
D-CNC	Dialdehyde functionalized cellulose nanocrystal
Hb	Haemoglobin
IgG	Immunoglobulin
TiO_2	Titanium dioxide
PAN	Poly(acrylonitrile)
PET	Poly(ethylene terephthalate)
FTIR	Fourier transform infrared spectroscopy
XPS	X-ray photoelectron spectroscopy
EDAX	Energy dispersive analysis of X-rays
FE-SEM	Field emission scanning electron microscopy
HR-TEM	High resolution transmission electron microscopy
Ag-NP	Silver nanoparticle

Chapter 1

Introduction

1.1 Overview

Water plays a vital role in sustaining life on earth. However, the quality of the water resources is deteriorating alarmingly due to the pollution caused by industrial, municipal and agricultural activities.[1] Various physical, chemical and biological water treatment methods are employed to remediate the toxic organic and inorganic contaminants in water.[2] Among all these methods, adsorption is being predominantly used worldwide due to several economic and environmental reasons such as low cost, insensitivity to toxic substances, simplicity in design and operation. High quality treated water can also be obtained at an affordable cost when a correctly designed adsorption system is used.[2–6] Activated carbons are the commonly used adsorbents in water treatment processes, but their production is energy intensive, expensive and emits greenhouse gas. Hence to reduce the carbon footprint and usage of activated carbon in water treatment processes, researchers worldwide are developing non-conventional low-cost alternative adsorbents from natural materials, biosorbents and waste materials from agricultural and industrial sources.[2,3,7–9]

Cellulose is one of the most abundant biopolymer available on this planet with many desirable properties. Hence it is a prime candidate that is considered while developing sustainable adsorbent platforms for use in water remediation.[10] Recent advances in nanotechnology have provided the scope and opportunities to the fabricate nanomaterials that are more efficient and functional than their parent materials.[11] In this context, nanomaterials derived from cellulose, namely cellulose nanocrystals (CNCs) and cellulose nanofibrils (CNFs) find promising application in various water treatment processes, such as adsorption, absorption, flocculation, membrane filtration, catalytic degradation and disinfection. Of these cellulose nanomaterials, CNCs possess higher surface area to mass ratio and reduced size which make them a superior candidate for use in adsorption of water contaminants. Studies have already

shown that CNCs can be used to adsorb various contaminants in water such as organic dyes, heavy metals, pharmaceuticals etc. The adsorption properties can also be improved by functionalizing them.[12–14] However, the high colloidal stability and nanosize dimension of CNCs makes them difficult to separate from water after adsorption of contaminants and limits their application in large-scale water treatment processes. To overcome this limitation, it is ideal to incorporate CNCs into hydrogel matrices which make their separation easier after use in batch or fixed bed column adsorption processes. The incorporation of CNCs into these hydrogel matrices also help in solving some inherent limitations of these hydrogels.[15–18]

Hydrogels are water-swollen crosslinked polymeric networks that are widely used across various fields, such as water treatment, agriculture, biomedicine etc.[19,20] However, the poor mechanical performance and limited functionalities of these hydrogels become a bottleneck for their use in the majority of these applications. Various strategies are employed to address these limitations and the idea of introducing nanoparticles into the continuous hydrogel matrix to form the nanocomposite hydrogels (NCHs) has got significant consideration among these strategies.[19,21] Various nanoparticles such as carbon nanotubes, graphene, nano/microgels, polysaccharide nanocrystals, clay, metallic, magnetic, silica, and bioactive nanoparticles have been used to reinforce NCHs.[22] Among these nanoparticles, CNCs have attracted considerable attention because of their several unique properties such as its availability, low cost, high mechanical strength, high surface area per volume and aspect-ratio.[10] CNCs can provide improved mechanical properties at very low volume fractions of the reinforced phase and also the surface functionalization possibilities of nanoparticles that can provide added functionalities to NCHs.[23] CNCs also possess many benign properties, such as non-toxicity, biocompatibility, and biodegradability, which make it an ideal candidate for developing systems that are considered green.[10] Additionally, it is also convenient to perform chemical and/or physical conjugation between CNCs and the polymer matrix because of the large number of hydroxyl groups on the surface of CNCs.[24,25]

Considering advantages of using CNCs for adsorption and its ability to solve some inherent limitations of these hydrogels, we focused on developing CNCs incorporated

nanocomposites that can be used for adsorption of contaminants in water. Batch and fixed bed column adsorption studies using these nanocomposites provided a detailed understanding of their adsorption characteristics. Studies were also carried out to evaluate the selectivity of the pristine and surface functionalized CNCs. The ability of surface functionalized CNCs to tailor the characteristics of nanocomposites that incorporates them, for use in water treatment applications was also evaluated. In summary, this thesis focused on the development and application of CNCs incorporated nanocomposites for water treatment applications.

1.2 Research Objectives

CNCs are sustainable nanomaterials that possess very good surface area and a large number of surface functional groups that makes it an ideal material for use in adsorption. Several studies have also demonstrated that pristine and surface functionalized CNCs can be used to adsorb a variety of contaminants present in water. However, the separation of these nanomaterials after adsorption requires coagulation and high-speed centrifugation, which limits their applications in large scale water treatment processes. To address this limitation, it is desirable to incorporate CNCs into hydrogel matrices which make their separation easier after use in batch as well as continuous column adsorption processes. Also, the major design parameters that should be considered while developing these CNCs incorporated nanocomposites are (a) the ability to exploit the high surface area of CNCs within the hydrogel beads for adsorption and (b) the choice of the polymer used to form the nanocomposite hydrogel network. To best of our knowledge, no studies have provided a comprehensive understanding on the development and adsorption characteristics of similar CNCs incorporated nanocomposites. Hence the first aspect of this thesis is to develop CNCs incorporated nanocomposites based on the major design parameters and study its adsorption characteristics using batch and fixed bed column adsorption studies. Surface functionalizing the CNCs with appropriate functional groups and moieties can tailor the characteristics of the nanocomposites that incorporates them, for use in water treatment applications. To this date, no studies have examined this approach in detail and hence the second aspect of this thesis encompasses this.

Therefore, based on a comprehensive literature review, the following research hypothesis and research objectives were formulated for this thesis:

Research hypothesis:

1. Incorporation of CNCs into the alginate hydrogel beads can facilitate their easy separation with negligible leaching of CNCs into the treated water during batch and continuous water treatment operations.
2. Surface functionalization of CNCs can tailor selectivity and adsorption characteristics of nanocomposites that incorporate them.

Research objectives:

1. Synthesize and characterize CNCs incorporated alginate (CNC-ALG) hydrogel beads and evaluate its adsorption characteristics for a model cationic organic dye, methylene blue (MB) using batch adsorption studies.
2. Understand the adsorption behavior of MB by CNC-ALG hydrogel beads in a fixed bed adsorption column by varying the process parameters used in the adsorption studies.
3. (a) Evaluate the selective dye adsorption characteristics of pristine CNCs and surface functionalized CNCs namely melamine-formaldehyde (MF) coated CNCs and polydopamine (PD) coated CNCs.

   (b) Study the ability of surface functionalized CNCs to tailor the characteristics of nanocomposites by using PD-CNCs incorporated CNC-ALG hydrogel beads.
4. Develop a diffusion controlled simultaneous sensor-scavenger system for heavy metal ions in water based on atomically precise cluster – CNC composite.

1.3 Thesis Outline

This thesis consists of 7 chapters. The results from all the research work carried out as part of this thesis are reported in the manuscript format in chapter 3 through chapter 6. The scope and contents of the chapters are listed as follows: Chapter 1 briefly introduces the importance of adsorption in water treatment, the role of CNCs in this adsorption and the advantages of incorporating CNCs into hydrogels. This chapter also includes the research objectives and the outline of the thesis. Chapter 2 covers a detailed literature review on the use

of cellulose nanomaterials for various water treatment applications. This chapter also provides a general introduction to cellulose nanomaterials and nanocomposite hydrogels. Chapter 3 reports on the development of CNC-ALG hydrogel beads and evaluation of their adsorption characteristics for MB using batch adsorption studies. Chapter 4 provides a detailed understanding on the adsorption behavior of MB by CNC-ALG hydrogel beads in a fixed bed adsorption column. Chapter 5 investigates the surface functionalization of CNCs and its applicability in nanocomposites for water treatment applications. Chapter 6 reports on the development of a diffusion controlled simultaneous sensor-scavenger system for heavy metal ions in water based on atomically precise cluster – CNCs composite. Chapter 7 summarizes the key conclusions of this research work and the major contributions of the author along with the recommendations for future studies.

Chapter 2*

Literature review

2.1 Introduction

This chapter reviews the literature related to various aspects of the research work performed in this thesis. Firstly, a brief introduction on cellulose nanomaterials (CNs) and its two major types cellulose nanocrystals (CNCs) and cellulose nanofibrils (CNFs) are provided. Preparation, properties and functionalization of CNCs are explained in more detail. Secondly, a detailed discussion on hydrogels and nanocomposite hydrogels (NCHs) is provided with emphasis on CNs incorporated NCHs. Effect of incorporating pristine and functionalized CNs on the properties of the NCHs are explained in more detail. Following this, a detailed literature review on CNs incorporated NCHs is also provided. Thirdly, a detailed literature review on the use of cellulose nanomaterials for various water treatment applications such as adsorption, absorption, flocculation, membrane filtration, catalytic degradation and catalysis is provided. Special effort is also made to categorize and tabulate all the reported CNs based system that can be used for water treatment application. A brief discussion on the future perspectives of CNs in water treatment applications is also included at the end of this chapter to provide a roadmap for research and development efforts in this area.

*This chapter is partially adapted from a paper "Nishil Mohammed, Nathan Grishkewich and Kam Chiu Tam, Cellulose Nanomaterials: Promising Sustainable Nanomaterials for Sorption and Other Water Treatment Processes, *Manuscript Under Preparation*."

2.2 Cellulose nanomaterials

Cellulose is the most widely available biomaterial on the planet, having many desirable properties, such as biodegradability, biocompatibility, hydrophilicity, chirality and high functionality. Its chemical structure consists of repeating β-D-glucopyranose units, classifying it as a carbohydrate polymer.[10] Cellulose fibers contain both loosely packed amorphous regions as well as tightly packed highly crystalline domains, and various processing techniques have been used to produce cellulose nanomaterials (CNs) of varying morphologies and physical properties.

Over the last 10 years, several nomenclatures have been used to describe various forms of cellulose derived nanomaterials. Some of these include; nanocrystalline cellulose, microcrystalline cellulose, cellulose nanowhiskers, polysaccharide nanocrystals, cellulose nanocrystals, nanocellulose, cellulose nanofibrils, cellulose microfibrils, cellulose nanofibers, cellulose microfibers, nanofibrillated cellulose, microfibrillated cellulose, Avicel, bacterial cellulose and any combination of the above. To consolidate the nomenclature, the Technical Association of the Pulp and Paper Industry (TAPPI), US Department of Agriculture, US Forest Service and various Canadian entities have unified the classification of CNs into two main groups, namely cellulose nanocrystals (CNCs) and cellulose nanofibrils (CNFs).[12]

Both these nanomaterials can be produced from various cellulosic sources, but they differ in the way they are manufactured. CNFs are produced by mechanical disintegration of plant cellulose fibers in an aqueous medium, such as homogenization, extrusion, or grinding. CNFs prepared in this manner can have lateral dimensions of 5-100 nm, and lengths of 0.5-5 μm, and are only 60 – 80% crystalline. Often cellulose fibers are pre-treated using various chemicals, such as 2,2,6,6-tetramethyl-1-piperidinyloxy (TEMPO), glycidyltrimethylammonium chloride (GTMAC) and periodate-chlorite in order to lower the mechanical energy required when processing raw fibers to yield CNFs.[26,27] CNFs can also be directly extracted from certain types of bacteria such as *Acetobacter xylinum* and *Gluconacetobacter xylinus*, which is often referred to as bacterial cellulose. Bacterial cellulose by definition and according to their dimensions (lateral dimensions of 10 nm and lengths of 1000 nm) are classified under CNFs.[12,28] CNCs,

on the other hand, are produced by the acid hydrolysis of the plant cellulose fibers and more details regarding this group of CNs are mentioned in the following section. Some representations of the various forms of CNs are summarized in Figure 2.1.[29] Figure 2.1 comprises of scanning electron microscope (SEM) and transmission electron microscopy (TEM) images of various forms of CNCs.

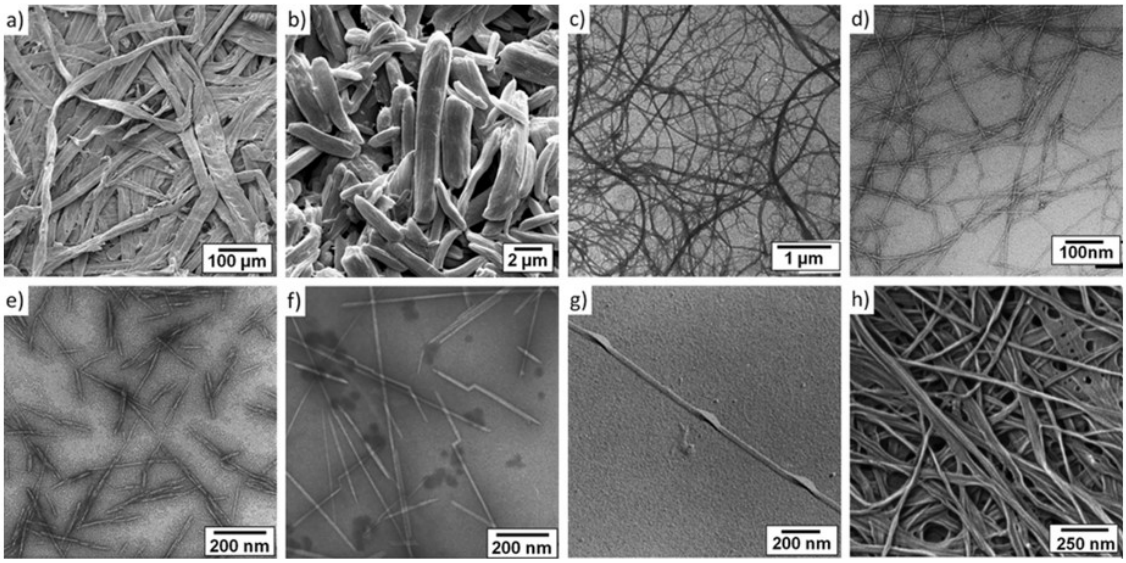

Figure 2.1. Micrographs of CNs: (a) SEM of wood fiber, (b) SEM of microcrystalline cellulose (MCC), (c) TEM of MCC (d) TEM image of TEMPO-CNFs, (e) TEM of wood CNCs, (f) TEM image of tunicate-CNCs, (g) TEM of algae CNCs (h) SEM image of bacterial cellulose.[29] (Reprinted with permission from ref. 29 © 2011 Royal Society of Chemistry)

2.2.1 Cellulose nanocrystals

CNCs are produced by acid hydrolysis of cellulose fibers that disintegrates the amorphous regions to produce well-defined crystalline domains. CNCs derived from plant sources possess lateral dimensions of 5-70 nm, with lengths ranging from 100-250 nm. When they are produced via sulfuric acid (H_2SO_4) hydrolysis, the resulting nanocrystals are decorated with negatively charged sulfate ester groups.[10,30] These sustainable nanomaterials possess very high specific surface area, good mechanical strength, biodegradability and high surface functionality. They are stiffer than aluminium and stronger than steel.[31] Depending on its source, they also possess a high aspect-ratio (length/diameter) varying between 30 to 150.[32] Sulfate ester groups are introduced to the surface of CNCs when they are produced by the

H_2SO_4 hydrolysis of cellulose and deprotonation of these sulfate groups in aqueous solutions gives CNCs their characteristic negative charge.[33] CNCs can form stable aqueous solutions due to the repulsion between these negatively charged sulfate ester groups on them,[34] and above a critical concentration these suspensions can also form chiral nematic ordered phases in solutions.[33] Figure 2.2 shows a schematic representation of cellulosic chain and its constituents.

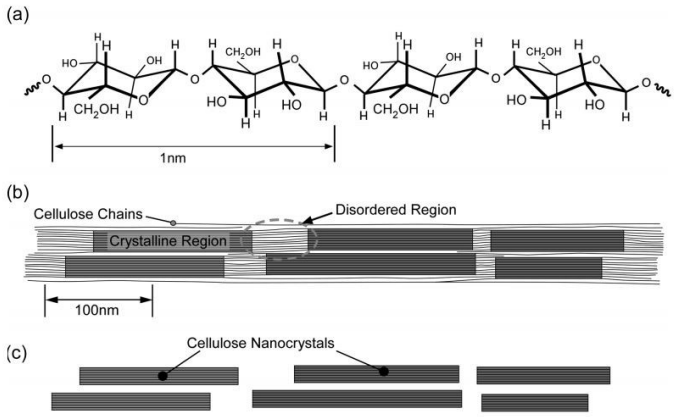

Figure 2.2. Schematics of (a) a single cellulose chain (b) a cellulose microfibril showing ordered (crystalline) and disordered (amorphous) regions (c) CNCs after acid hydrolysis dissolved the dissolved regions.[35] (Reprinted with permission from ref. 35 © 2010 American Chemical Society)

CNCs also possess a reactive surface covered with numerous active hydroxyl groups that can be employed for a wide variety of functionalization depending on the desired application. Surface functionalization of CNCs are usually done to make them possible for use as reinforcing agents in composite materials or to serve specific functions in novel nanomaterials that can find potential applications in various industrial sectors such as personal care, biomedical etc.[10,36] There are various ways in which CNCs can be functionalized and some of the most important strategies reported in literature are esterification,[37] cationization,[38] carboxylation,[39] silyation,[40] and polymer grafting.[41] Recent reports by our group also suggests that CNCs can be easily surface functionalized by coating it with polydopamine (PD),[42,43] and melamine-formaldehyde (MF).[44,45] Figure 2.3 is a schematic diagram illustrating the various types of chemical modifications on CNC surface.[10]

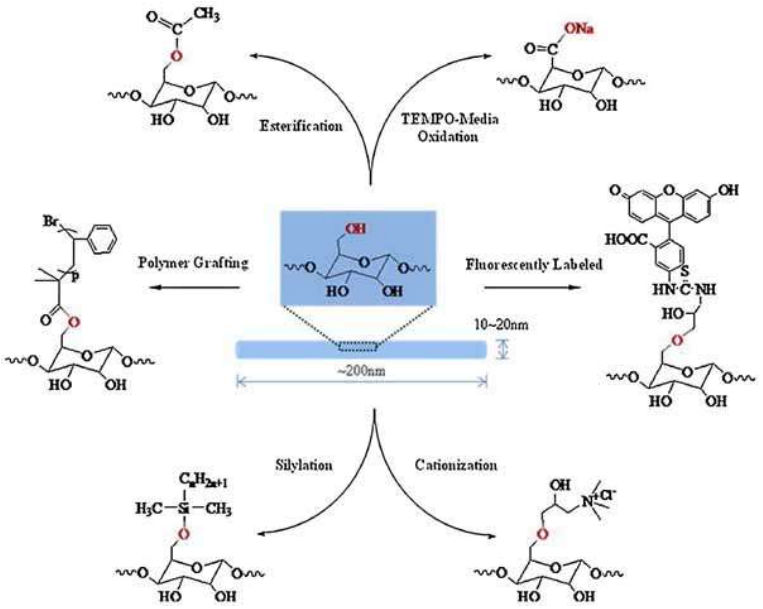

Figure 2.3. Schematic diagram illustrating the various types of chemical modifications on CNC surface.[10] (Reprinted with permission from ref. 10 © 2011 John Wiley and Sons)

PD possesses abundant functional groups such as catechol groups, amine groups and aromatic moieties that make it a promising material for various applications.[46] It can be coated as a thin layer onto virtually any material by spontaneous oxidation of dopamine in an alkaline aqueous solution,[47] and this strategy was employed by our research group to surface functionalize CNCs.[42,43] Figure 2.4 is a schematic representation of the oxidative polymerization of dopamine to form PD.[48] There are various factors that determine the coating of PD such as the concentration of dopamine, type of buffer used, the pH value of the reaction solution, use of oxidant, reaction time and temperature. The effects of all these parameters have been studied in detail previously.[46] The versatility of this PD coating also allows for further modification of substrates as in conjugation of biomolecules onto various surfaces,[49] and the creation of antibacterial surfaces by *in situ* deposition of silver nanoparticles.[50]

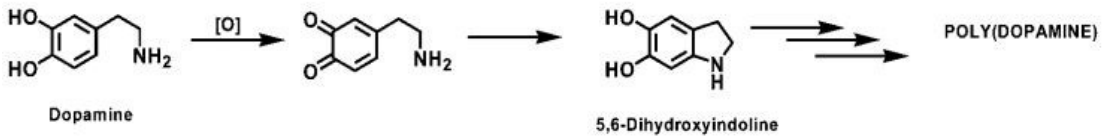

Figure 2.4. Schematic representation of the oxidative polymerization of dopamine to form Polydopamine.[48] (Reprinted with permission from ref. 48 © 2013 Royal Society of Chemistry)

MF resins are formed via the condensation reaction of formaldehyde with melamine.[51] MF can be easily coated onto CNCs via *in situ* polycondensation of the MF resin onto the surface of CNCs. This introduces a high amount of amine content on the surface of CNCs and this is a simple strategy to introduce nitrogen content on the surface of CNCs. Moreover, the coating of MF is porous in nature which can be a beneficial aspect for the adsorption characteristics of MF-CNCs. The synthesis of MF coated CNCs can be carried out using a simple procedure, which is considered to be highly efficient and industrially scalable.[44,45] Figure 2.5 is a schematic illustration of the idealized chemical reactions leadings to MF resin.

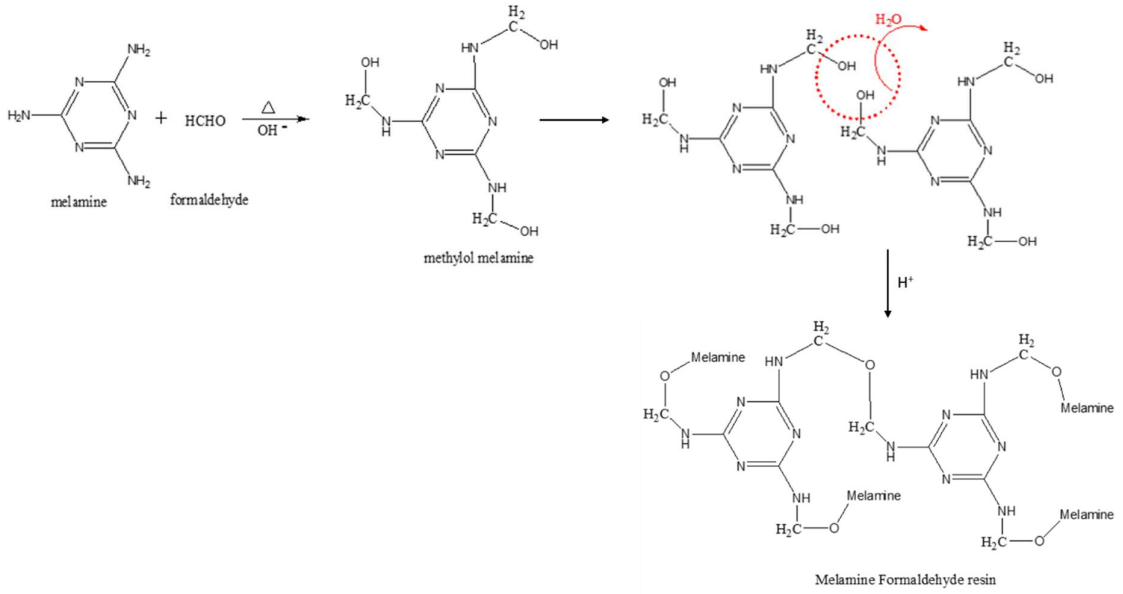

Figure 2.5. Schematic illustration of the idealized chemical reactions leadings to MF resin.

2.3 Hydrogels

Hydrogels are water-swollen, crosslinked three-dimensional polymeric network structures that find applications in water treatment (adsorption of dyes, heavy metals and other organic contaminants), agriculture (controlled release of agrochemicals), biomedical field (wound dressing, tissue engineering, artificial muscles, drug delivery, contact lens), sensors, chemical valves, separation devices, filters, optically transparent materials, metal particle preparation and catalysis.[19,20] Hydrogels have gained particular interest in the field of wastewater treatment due to their high adsorption capacities and regeneration abilities that make them reusable for continuous processes.[52] They are also widely used in biomedical

applications such as tissue engineering because of their highly hydrated 3D porous structure that mimics the biological tissue.[53] They contain a definite proportion of hydrophilic and hydrophobic parts wherein the hydrophilic chains are crosslinked by physical, ionic or covalent interactions. Because of these crosslinked hydrophilic chains, hydrogels swell when placed in an aqueous solution without either dissolving or considerably changing their shape in response to environmental stimulants, such as pH, ionic strength, solvent composition, light or electrical field.[54,55]

2.4 Classification of hydrogels

Hydrogels can be classified in several ways depending on their method of preparation, nature of crosslinking, rate of biodegradation, ionic charges, sources or nature of swelling with changes in environment.[56] Figure 2.6 shows the classification of hydrogels based on these various aspects. Based on the method of preparation, hydrogels can be classified as photopolymer hydrogels, copolymer hydrogels and interpenetrating network hydrogels. Homopolymer hydrogels are produced by crosslinking of only one type of hydrophilic monomer unit whereas copolymer hydrogels are produced by crosslinking of chains composed of co-monomer units, where at least one must be hydrophilic to render them water swellable. Interpenetrating network hydrogels are produced by polymerizing a monomer within a pre-formed crosslinked hydrogel network so that the second crosslinked structure formed by the polymerization of the monomer intermeshes with the first network.[20] Depending on the type of crosslinking, hydrogels can be categorized into chemically crosslinked and physically crosslinked hydrogels. Chemical or physical crosslinking of the polymeric chains in the hydrogels determines their network stability in their swollen state. Chemically crosslinked hydrogels also known as thermosetting or permanent hydrogels, cannot be dissolved in any solvents unless the covalent crosslink points are cleaved or be reshaped via temperature increase. On the other hand, the presence of reversible crosslinking points in the physically crosslinked hydrogels also known as thermoplastic or temporary hydrogels allows for solvent casting and/or thermal processing. Hydrogels can also be categorized based on the ionic charges on their polymeric backbone, rate of biodegradation and their physical properties.[56]

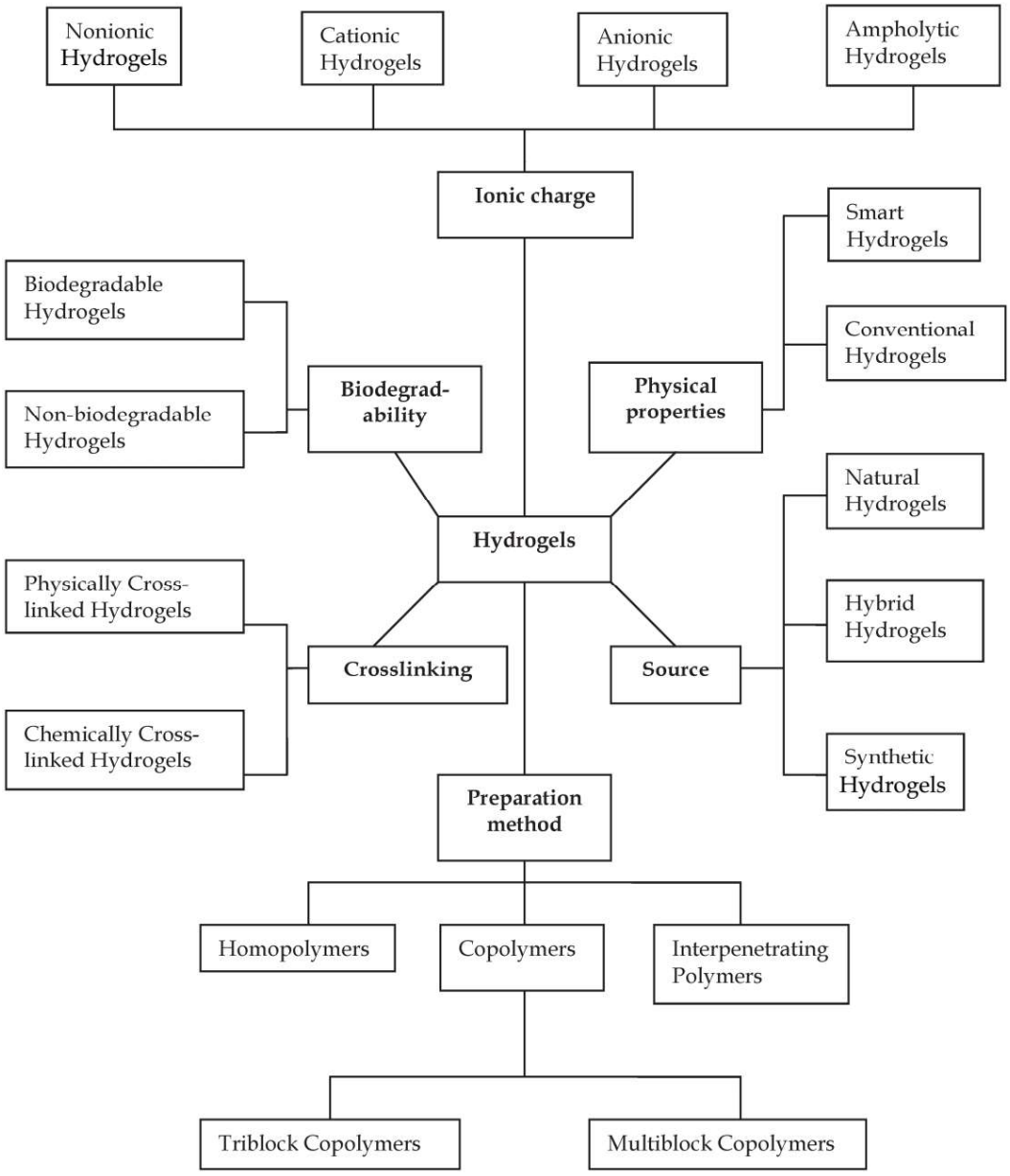

Figure 2.6. Classification of hydrogels.[56] (Reprinted with permission from ref. 56 © 2011 Intech Open)

2.4.1 Preparation of hydrogels

Hydrogels are prepared by swelling crosslinked network structures in water or biological fluids. These crosslinked network structures can be prepared by several methods, such as physical crosslinking, chemical crosslinking, photopolymerization or irradiative crosslinking.[57] Physically crosslinked hydrogels can be obtained by either heating/cooling a polymer solution, ionic interaction, complex coacervation, H-bonding, maturation (heat-

induced aggregation) or freeze-thawing.[58] Chemical crosslinking involves the direct reaction of a linear or branched polymer with the help of a di or multifunctional functional, small molecular weight crosslinking agent. Copolymerization crosslinking reaction between one or more monomers and a multifunctional monomer that is present in relatively small quantities can also be employed to prepare chemically crosslinked hydrogels. Another method to form crosslinked network structures is by combining monomer and linear polymer chains that are crosslinked using an interlinking agent in the presence of ultraviolet (UV) light. Electron beams, gamma rays or x-rays are utilized in ionizing radiation crosslinking to excite a polymer in order to produce crosslinked structure via free radical reactions.[20]

2.4.2 Limitations of hydrogels

Even though hydrogels gained a lot of interest due to their high adsorption capacities, their low mechanical stability and gel strength limits their application in wastewater treatment.[54] Burst release of the active constituents entrapped within hydrogels upon contact with the surrounding media is another major obstacle. This burst release could be attributed to highly hydrated and hydrophilic microstructure of the hydrogels.[59,60] And this could possibly restrict the application of hydrogels loaded with active water treatment agents.

Recently, several approaches are being studied for improving the gel strength and reducing the burst release. This include approaches such as increasing the crosslinking density, surface crosslinking, double network gels, interpenetrating gels, semi-interpenetrating gels and nanocomposite or hybrid gels.[19,21] Among all these strategies the introduction of reinforcing nanoparticles into the continuous hydrogel matrix to form nanocomposite hydrogels has attracted a great deal of attention recently. This is because nanoparticles that can provide enhanced functionalities like stimuli responsiveness depending on its inherent properties can also provide significant improvement in the mechanical properties at a very low volume fraction of the reinforcing phase.[23]

2.5 Nanocomposite hydrogels

Nanocomposite hydrogels (NCHs) are generally defined as crosslinked polymer network structures swollen with water in the presence of nanoparticles or nanostructures. Nanoparticles present in these NCHs either crosslink the hydrogel, adsorb or attach to polymer chains or add new properties to the hydrogel by simply being entrapped within the hydrogel network. Nanoparticles commonly used in NCHs include polysaccharide nanocrystals, clay nanoparticles, hydroxyapatite nanoparticles, metallic nanoparticles, magnetic nanoparticles, colloidal nanoparticles like micelles and nanogels, carbon nanotubes, and semiconducting nanoparticles.[22] Also, depending on the type of nanoparticles used, unique properties such as stimuli responsiveness can also be added to polymer hydrogels which makes them promising materials for applications in electronics, optics, sensors, actuators, microfluidic sectors, catalysis, separation devices, drug delivery and many other biotechnological areas.[61]

2.5.1 Preparation of nanocomposite hydrogels

NCHs can be prepared by incorporating the nanoparticles into the polymeric hydrogel matrix via three basic approaches: (1) Mechanical mixing of a polymer with nanoparticles followed by gelation, (2) *In-situ* synthesis of nanoparticles using a hydrogel matrix as template and (3) Polymerization in the presence nanoparticles. All these approached are explained in detail with the help of suitable examples in the following sections.

2.5.1.1 Mechanical mixing followed by gelation

The simplest method to prepare NCHs is to initially prepare a physical mixture of nanoparticles and polymer in a sol phase by mechanical mixing and then induce gelation, either via a change in temperature, pH or addition of crosslinking species. Depending on the type of crosslinkers used, hydrogels can be either physically or chemically crosslinked. The main advantage of this approach is that the size, morphology and surface properties of the nanoparticles used in these NCHs can be properly defined and designed. If necessary, preparation of nanoparticles can be performed in conditions such as extreme pH, organic solvents environment, high temperature and pressure that would not be compatible with the

preservation of hydrogel integrity and solubility. It is difficult to achieve homogeneous nanoparticle dispersion within the hydrogel using this approach.[62] Yan et al. have prepared single wall carbon nanotube incorporated alginate nanocomposite hydrogels by mechanically mixing the finely dispersed single-walled carbon nanotubes in a pure alginate polymer solution and then gelating it with the help of divalent calcium ions supplied by calcium carbonate in the presence of D-glucono-δ-lactone.[63] Figure 2.7a shows the schematic representation of the mechanical mixing followed by gelation approach.[62]

2.5.1.2 *In situ* synthesis of nanoparticles using hydrogel template

Another way to incorporate nanoparticles into hydrogels is to use polymer hydrogel matrix as a template for the synthesis of nanoparticles. This strategy also referred to as bio-templating approach should limit the diffusion issues encountered with preformed nanoparticles in the case of mechanical mixing. In this method, the inorganic nanoparticle precursors, ions or polyions are converted into nanoparticles within the hydrogel by a two-step reaction. During the first step, the inorganic precursor is added to the polymer sol before inducing gelation or is impregnated into the hydrogel matrix once the hydrogel is obtained. This is followed by a second step wherein the mineralization of the precursor is induced by pH changes, addition of reducing agent, carbonation or supplementation by other suitable reagents. In the case of metallic nanoparticles, metallic salts are chemically, thermally, or photo-catalytically reduced to form nanoparticles within the hydrogels. In this method, the density and size of the nanoparticle can be tuned by varying the concentration of precursor salts, pH, and reduction time. An alternative approach is to use bi-functional ions that can serve as both mineral precursors and ionic crosslinkers for the gelation.[62] Wang et al. have synthesized gold (Au) nanoparticles containing thermo-responsive nanoparticle-hydrogel composites by employing the *in-situ* method. First, they synthesized the hydrogel by crosslinking polymerization of poly(N-isopropyl acrylamide) and comonomers containing thiol functional groups that have a tendency to form complexes with Au^{3+} ions. The formation of colloidal Au nanoparticles inside the hydrogels was then modulated by an earlier prepared functional

hydrogel matrix after the addition of a reducing agent called sodium borohydride.[64] Figure 2.7b shows the *in situ* synthesis of nanoparticles using hydrogel template.[62]

2.5.1.3 Polymerization in the presence of nanoparticles

NCHs can also be prepared by polymerizing the monomers from the surface of nanoparticles. Here the nanoparticles act as both fillers and multifunctional crosslinks. Yang et al. have prepared highly flexible NCHs using silica nanoparticles (SNPs) to graft hydrophilic poly (acrylic acid) (PAA) via free radical polymerization. In this study, the primary hydroxyl groups on the SNPs surface were first chemically modified with γ-methacryloxypropyl trimethoxy silane to obtain C=C groups on the surface. This surface vinyl group functionalized SNPs were dispersed in the acrylic acid monomer solution and initiator ammonium persulfate was added. Ammonium persulfate decomposed under heat to produce free radicals that initiated the polymerization of acrylic acid to form *in-situ* SNPs reinforced NCHs via a grafting-from method.[65]

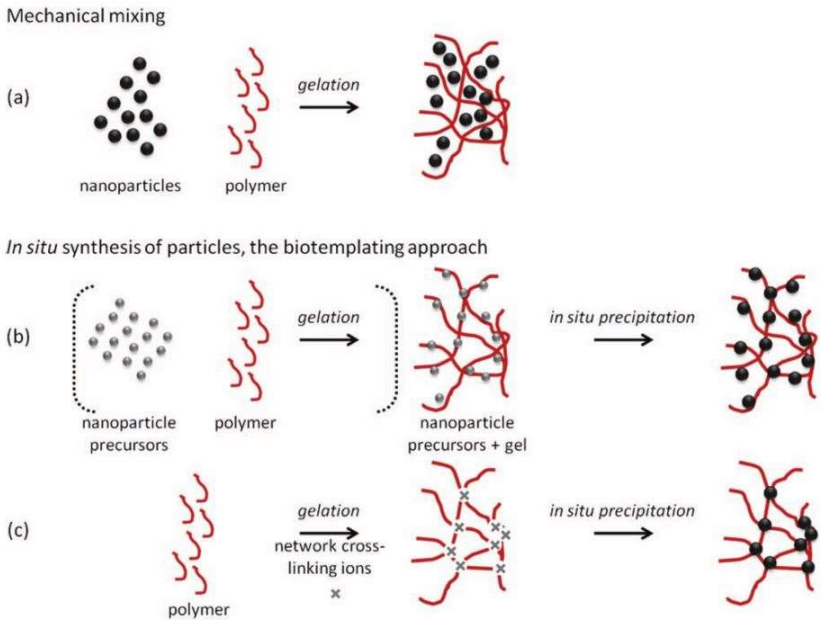

Figure 2.7. (a) Mechanical mixing followed by gelation approach. (b) *In situ* synthesis of nanoparticles using hydrogel template.[62] (Reprinted with permission from ref. 62 © 2012 John Wiley and Sons)

2.5.2 Cellulose nanomaterials incorporated nanocomposite hydrogels

Nanoparticles are normally incorporated into hydrogels to tailor the various properties of hydrogels. Among all the nanoparticles used in NCHs, cellulosic nanomaterials (CNs) have attracted significant attention, because of their distinct biocompatibility, biodegradability and other attractive properties like good processability, high water holding capacity, low density, low cost, non-toxicity and high crystallinity. CNs can itself act as a very good reinforcing agent because of their high strength to aspect ratio and high specific active surface area. Additionally, it is also convenient to perform chemical and/or physical conjugation between CNs and the polymer matrix because of the large number of hydroxyl groups on the surface of CNs.[24,25] CNs can be surface functionalized with carboxyl, amine, aldehyde and silane groups, in addition to polymer graftings to prepare NCHs with functional properties compared to pristine CNs containing NCHs. The following subsections discuss some examples of pristine and functionalized CNs incorporated NCHs and the effect of pristine and functionalized CNs on the properties of NCHs.

2.5.2.1 Pristine cellulose nanomaterials incorporated hydrogels

Zhou et al. have synthesized polyacrylamide (PAM) hydrogels reinforced with CNCs through *in situ* free radical polymerization. Here, the PAM-CNC NCHs were prepared by free radical polymerization of acrylamide (AM) monomer in aqueous suspensions of CNCs. CNCs were first dispersed homogeneously in solution and then redox initiators potassium persulfate/sodium bisulfite were added into the solution to induce hydroxyl group on the surface of CNCs to produce radicals. Subsequently AM monomer and crosslinker N,N'-methylenebisacrylamide (NMBA) were added into the previous solution mixture and stirred in a nitrogen atmosphere. Grafting points between CNCs and PAM chains arises as a result of covalent bonding and hydrogen bonding C–O formation between the free radicals formed on the surface of CNCs and the double bonds of AM monomer. Simultaneously, homo polymerization of AM to grow PAM macromolecule chains is initiated by other free radicals in solution and NMBA crosslinks these chains to form a PAM hydrogel network containing CNCs. They also studied the swelling properties of CNC reinforced PAM hydrogels and found

that the equilibrium swelling ratio gradually decreased with increasing CNC content. This decrease in swelling capacity of hydrogels with the increase in CNC content is due to the fact that only small amounts of water is absorbed by hydrophilic groups of CNCs and the increasing crosslinking density due to the formation of more junctions in the hydrogel structure by the CNCs acting as multifunctional crosslinkers. It was noted that equilibrium swelling ratio decreased up to a threshold CNC content, above which it showed a slight increase, which is attributed to the probable disturbance of large amounts of CNCs in the crosslinking polymerization reaction that inhibits some of the crosslinkers to react with the monomers. Compression stress and elastic modulus of the gel increased with CNC content until it reached a threshold CNC content. Beyond the threshold CNC content, the effective crosslinking density decreased because CNCs at a higher concentration aggregated. Hence, the decrease in stress of the gel after critical threshold CNC content can be attributed to the reduced dispersion quality of nanocrystals and the low crosslink density of hydrogels with higher CNC content. Thus, it could be explained that the swelling ability and mechanical properties of hydrogels depended on the nanofiller/matrix interactions and dispersion quality of nanofillers in the matrix.[66] Figure 2.8 shows the schematic representation of gelation mechanism of PAM-CNC NCHs.

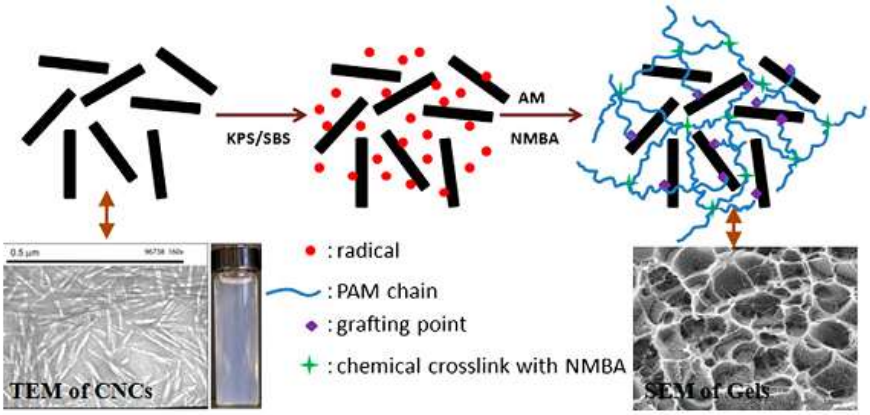

Figure 2.8. Scheme of the gelation mechanisms of PAM-CNC NCHs.[66] (Reprinted with permission from ref. 66 © 2011 Elsevier)

Han et al. have synthesized CNs reinforced polyvinyl alcohol-borax (PB) hydrogels using a facile approach in aqueous medium. CNs like CNCs and CNFs were homogeneously mixed with polyvinyl alcohol (PVA) solution and crosslinked using borax crosslinker using

optimum process conditions to prepare these NCHs. Here the CNs not only entangled with PVA through hydrogen bonds but also chemically crosslinked with borate ions to form complexes thus acting as multifunctional crosslinking agents and nanofillers to physically and chemically bridge the three-dimensional network of hydrogels. They also studied how the particle size, aspect ratio, crystal structure and crystallinity of these CNs affect the density, water content, optical transmittance and compression property of PB NCHs. Particle size and dispersion quality of the nanoparticles in the polymer system has a large influence on the visible light transmittance of NCHs. It was observed from the UV optical transmittance measurements that the transparency of the hydrogels decreases with increasing size of CNs used because particles of larger size scatter more visible light causing the reduction in the transparency of hydrogels compared to smaller ones. In addition, with increasing aspect ratio, the entanglement of polymeric chains and probability of the polymeric chains to contact with the surface of particles are promoted. These polymer chain entanglements led to the formation of numerous physical junctions in these hydrogels making it more compact, translucent and stronger. Uniaxial compression studies performed on these hydrogels revealed that the modulus and energy absorption of CNF reinforced PB is much higher than the CNC reinforced PBs which can be attributed to the larger size and aspect ratio of CNFs. This difference in mechanical reinforcement is due to the variation in the degree of crosslinking of hydrogels as a result of the difference in dimension, concentration, dispersion and polymer matrix interactions of CNs in the hydrogels. Homogeneous distribution of CNs led to the coexistence of chemical and physical cross-links in the complex network. CNs also act as multifunctional crosslinking agent and fillers to bridge the hydrogel network contributing to the enhanced reinforcement of the hydrogels.[24] Figure 2.9 shows the schematic illustration of the preparation and synthesis process of CNs reinforced PB hydrogel.

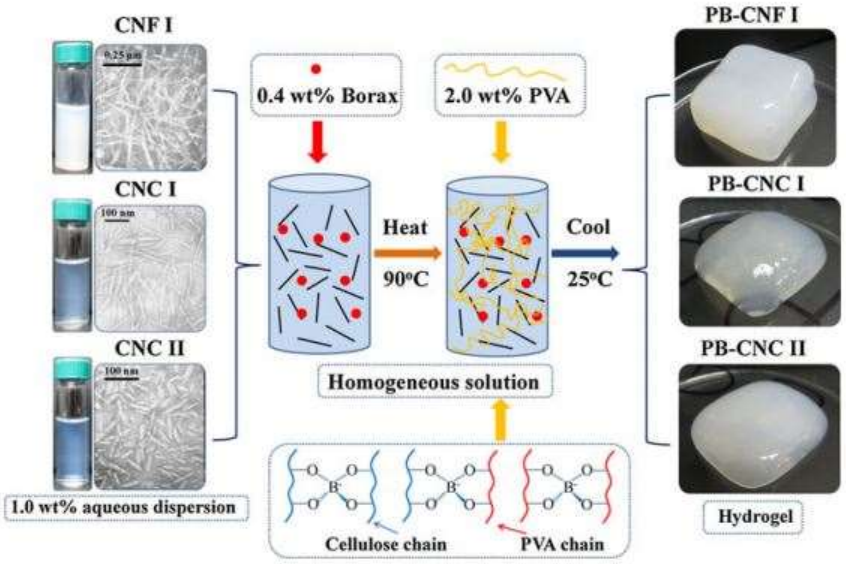

Figure 2.9. Schematic illustration of the preparation and synthesis process of CNs reinforced PB hydrogel.[24] (Reprinted with permission from ref. 24 © 2013 Springer)

Abitbol et al. have prepared CNCs reinforced PVA NCHs with improved structural stabilities and distinct microstructures by cyclic freezing and thawing. It was found that water sorption of gels increased with CNC content due to the hydrophilic nature of the cellulose that reduced the PVA crystallinity. The elastic modulus of CNC-PVA hydrogels also increased relative to pure PVA hydrogels because of the reinforcement of CNCs. They found that the equilibrium swelling ratio increased with an increase in the CNC content. It was observed that the time required to attain the equilibrium water saturation and equilibrium mass relative to the initial gel mass increased with increasing CNC content because of the hydrophilic nature imparted to the gels by CNCs, which increased the water uptake as expected for more porous and/or amorphous samples. A decrease in the crystallinity or increase in the amorphous content of the hydrogels with CNC loading was confirmed by comparing the differential scanning calorimetric thermograms of pure PVA hydrogels and CNC loaded PVA hydrogels and it can be understood that the melting point of hydrogel decreased with increase in the CNC content. The decrease in the melting point in turn indicated a reduction in the crystallinity of hydrogels.[67]

Yang et al. have synthesized CNC reinforced polyethylene glycol (PEG) NCHs by UV-initiated free radical polymerization at room temperature. Here the aqueous nanocomposite precursor solution comprising of PEG and CNCs are covalently crosslinked and this provides enhanced mechanical properties to this NCHs.[68] Lin et al. have incorporated CNCs into alginate based nanocomposite microspheres for enhancing the mechanical strength and regulating drug release behavior. These nanocomposite hydrogel microspheres were prepared by initially mixing the CNCs with sodium alginate sol by ultrasonic treatment followed by ionotropic gelation of the nanocomposite sol in a $CaCl_2$ aqueous solution.[69] Similarly Zhang et al. have also incorporated CNCs into supramolecular hydrogels based on cyclodextrins/polymer inclusion in order to enhance the mechanical strength and regulate the drug release behaviour.[25] Karaaslan et al. have synthesized CNCs reinforced poly(2-hydroxyethylmethacrylate) (PHEMA) hydrogels by *in situ* radical polymerization of the methacrylic groups from the 2-hydroxyethylmethacrylate modified hemicellulose coated cellulose nanowhiskers. It was found that the average chain length between the crosslinking points and number of effective crosslinks between the polymer chains were significantly different from pure PHEMA hydrogels that were crosslinked using the conventional crosslinking agent and the resulting NCHs had enhanced toughness, viscoelasticity and recovery behaviour.[70] Sanna et al. have reported the synthesis of thermos-responsive poly(N-vinylcaprolactam) NCHs containing CNCs by using frontal polymerization technique. It was found that CNCs decreased the swelling ratio and increased the viscosity with increasing CNC content.[71] Goetz et al. have synthesized poly(methyl vinyl ether-co-maleic acid)–polyethylene glycol NCHs crosslinked *in situ* with CNCs. Water absorption studies demonstrated that these hydrogels crosslinked by CNCs are capable of absorbing up to ~900%.[72,73] Kelly et al. have prepared photonic NCHs by photopolymerization of hydrogel precursors in the presence of CNCs. These NCHs demonstrated long-range chiral nematic structure and showed iridescence changes in response to external stimuli, such as solvent, pH or temperature due to the cation exchange within the NCHs modulated by the CNCs.[74] Spagnol et al. have synthesized two different superabsorbent NCHs based on poly(acrylamide-co-acrylate) matrix and starch-g-(sodium acrylate) matrix

filled CNCs by free radical aqueous copolymerization. These hydrogels exhibited good pH and salt responsive swelling behavior.[75,76]

2.5.2.2 Functionalized cellulose nanomaterials incorporated nanocomposite hydrogels

Yang et al. have synthesized injectable hydrogels based on carboxymethyl cellulose and dextran, reinforced with rigid rod-like pristine CNCs and aldehyde functionalized CNCs (CHO-CNCs). In this study, they demonstrated how injectable hydrogels can be reinforced physically and chemically with CNCs. A double barrel syringe was used to co-inject adipic acid dihydrazide modified carboxymethyl cellulose (CMC-$NHNH_2$) and aldehyde-modified dextran (dextran-CHO) solutions. One of the barrels of the double barrel syringe contained CMC-$NHNH_2$ and other barrel contained CNC containing dextran-CHO solution. In all cases, the solutions in both barrels were liquids with a very low viscosity that can gel quickly once mixed. The driving force for gelation is hydrazone cross-links that are rapidly formed between the amine groups of CMC and aldehyde groups of dextran once the components were mixed. In this hydrogel, the pristine CNCs were physically entrapped between the chemically crosslinked CNC and dextran whereas the CHO-CNCs have the potential to react with the CMC-$NHNH_2$ and thus be chemically crosslinked within the hydrogels. They also compared the difference in mechanical and swelling properties of these two different NCHs. Results of rheological measurements showed that for the same loadings, hydrogels with CHO-CNCs had larger storage moduli than the equivalent hydrogels with pristine CNCs consistently. This is likely attributed to the ability of CHO-CNCs to become physically entrapped within, as well as chemically bound to the hydrogel network compared to pristine CNCs. It was also observed that beyond a particular CNC loading, there is a decrease in modulus possibly because CNCs sterically block the crosslinking between adipic acid dihydrazide modified carboxymethyl cellulose and aldehyde-modified dextran. Swelling studies on these hydrogels revealed that the reduction in the swelling ratio of hydrogels upon the addition of nanocrystals is only slightly impacted in the case of CHO-CNC reinforced hydrogels when compared to pristine CNC reinforced hydrogels. This is because CHO-CNCs are more entangled or covalently crosslinked into the hydrogels.[53] Figure 2.10 is a schematic representation of the synthesis of injectable

hydrogels and the photographs of the injectable hydrogels reinforced with pristine CNCs and CHO-CNCs.

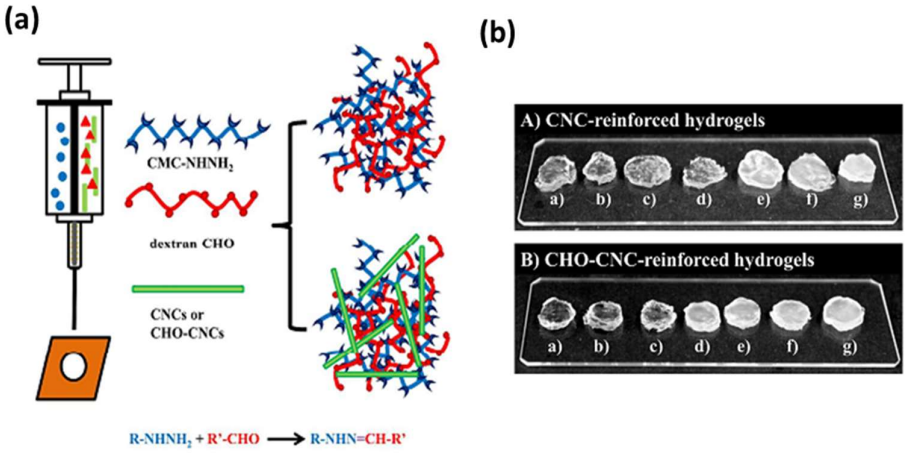

Figure 2.10. (a) Schematic representation of injectable hydrogels reinforced with CNCs prepared using a double barrel syringe. (b) Photographs of reinforced injectable hydrogels with varying loadings of (A) pristine CNCs and (B) CHO-CNCs.[53] (Reprinted with permission from ref. 53 © 2013 American Chemical Society)

Eyholzer et al. has synthesized N-Vinyl pyrrolidine (NVP) hydrogels reinforced with varying concentration and degree of carboxymethyl substituted CNFs (c-CNFs), where the concentration and degree of substitution of c-CNFs played a role on hydrogel properties. Here the precursor solution containing crosslinker, photoinitiator, monomer and c-CNFs were properly homogenized and were then injected into the molds where it is exposed to UV light for photopolymerization to produce NCHs. It was observed that for all samples, the swelling ratio decreased with increasing concentration of pristine and functionalized CNFs and for a given concentration of c-CNFs, the swelling ratio generally increased with increasing degree of substitution. A decrease in the swelling ratio with increasing pristine and functionalized CNF concentration can be attributed to an increase in the stiffness of NCHs due to more physical entanglement of NVP and c-CNFs. Whereas an increase in swelling ratio with increasing degree of substitution of c-CNFs for a given c-CNF concentration can be attributed to increased hydrophilicity of the hydrogel to absorb more water. It was also observed that for all the NCHs, the modulus of elasticity increases with increasing concentration of pristine and functionalized CNFs whereas for a particular c-CNF concentration, modulus of elasticity

decreases with increasing degree of substitution. This trend observed for modulus of elasticity can be explained by considering their respective trend in swelling ratios. Large standard deviations were observed for swelling ratio and elastic modulus values of hydrogels with pristine and functionalized CNF concentration above a critical threshold because of inhomogeneities within the hydrogels, originating from poor dispersion of the nanofibrils.[77]

Way et al. have synthesized CNCs incorporated poly(vinyl acetate) (PVAc) NCHs with pH tunable mechanical properties by incorporating two different pH-responsive CNCs, such as amine functionalized CNCs (CNC-NH_2) and carboxyl functionalized CNCs (CNC-COOH). They also studied the effects of the pH-responsive CNCs on the mechanical properties of PVAc hydrogel at different pH conditions. CNC-NH_2 gets protonated at low pH to form aqueous dispersions in water because of electrostatic repulsions of ammonium moieties that inhibit aggregation. However, at higher pH, a transition to gel is observed when CNC-NH_2 is neutral and attractive forces based on hydrogen bonding dominate. The CNC-COOH behaves opposite to CNC-NH_2, where it becomes dispersible at high pH and forms gel at acidic environment.[78]

Dash et al. have synthesized gelatin hydrogels with improved mechanical and thermal properties by crosslinking it with oxidized CNCs. Here the CNCs were oxidized in the presence of periodic acid to produce aldehyde functionalized CNCs which could act as a potential crosslinker. These aldehyde groups will react with the free amine groups of gelatin through Schiff's base formation to form the NCHs.[79] McKee et al. prepared supramolecular NCHs with superior healable, stable and stiff properties by combining polymer brush-modified 'hard' CNCs and 'soft' polymeric domains and bound together by cucurbit[8]uril (CB[8]) supramolecular crosslinks. Here the CNCs were surface functionalized with a dense set of methacrylate polymer brushes bearing naphthyl units by surface-initiated atom transfer radical polymerization. These were then non-covalently crosslinked through simple addition of poly(vinyl alcohol) polymers containing pendant viologen units as well as CB[8]s in aqueous media to form supramolecular NCHs.[80] Yang et al. synthesized two different flexible NCHs based on PAA and PAM by *in situ* free radical polymerization in the absence of chemical crosslinks. This is done by functionalizing the surface of CNCs with silane groups so as that it

can act as multifunctional crosslinks to initiate polymerization of the hydrophilic monomers such as acrylic acid and acrylamide grafted onto it.[81,82] Dai et al. have synthesized carboxylated CNCs reinforced carboxymethyl cellulose/hydroxymethyl cellulose hydrogels with the help of crosslinker divinyl sulfone.[83] Similarly Cha et al. synthesized pH and thermal sensitive poly(N-Isopropyl acrylamide) hydrogels by incorporating carboxyl functionalized CNCs.[84]

2.6 Cellulose nanomaterials for water treatment applications

The ability to fixate compounds onto cellulose fibers has been known for centuries, with the earliest examples being cotton fabric dyeing in the textile industry, as well as construction paper production in the pulp and paper industry. Such characteristics could ideally be exploited for their use in water treatment operations. To further improve the effectiveness of cellulose in water treatment processes, it is necessary to increase its external surface area by transforming pulp fibers into high surface area nanocrystals or nanofibrils.

There is a global shift in recent decades to develop low cost, bio-renewable materials for use in water treatment, with CNs being a prime candidate as evident from the number of scientific articles and patents published. This is because CNs possess many interesting properties such as high specific surface area, good mechanical strength, biocompatibility, biodegradability and high possibility of surface functionalization.[10] Also the supply of CNs for their commercial applications will not be a hindrance compared to other nanomaterials as many organizations and companies, such as Celluforce Inc., American Process Inc., Alberta Innovates, Nippon Paper Industries, Borregaard AS, Innventia AB, University of Maine, Forest Products Laboratories of US Forest Service and Department of Agriculture have the capability to produce CNs in significantly large quantities.[85] There are several studies which demonstrate the use of CNs in adsorption, absorption, flocculation, membrane filtration, catalytic degradation and disinfection based water treatment processes. Figure 2.11 is a schematic diagram showing the water treatment applications of CNs.

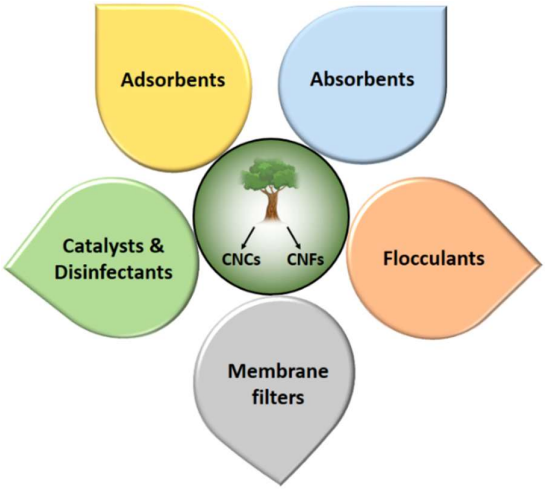

Figure 2.11. Schematic diagram showing the water treatment applications of CNs.

2.6.1 Cellulose nanomaterials as adsorbents

Adsorption is a phase transfer process wherein chemical species preferentially accumulate at the interface of two phases.[86] These phases can be liquid-liquid, liquid-solid, gas-solid or gas-solid combinations. The phase that is adsorbing is called as adsorbent and the chemical species that's being adsorbed is called as an adsorbate.[87] The driving force for adsorption depends on the adsorbate-adsorbent interaction and may differ between the phases.[86,88] Most of the adsorption processes can be grouped into one of the 3 categories namely (a) Physical adsorption (b) Chemical adsorption and (c) Electrostatic adsorption.[89] Physical adsorption is driven by weak intermolecular interactions such as van der Waals and hydrogen bonding between the adsorbate and the surface of the adsorbent whereas in chemical adsorption, the adsorption of adsorbate to an adsorbent surface takes place via the formation of a chemical bond. Electrostatic adsorption or ion exchange is driven by the coulombic attraction between the adsorbate and adsorbent surface.[88] Adsorption is a technique that is widely used for the removal of contaminants in water. Among the various methods employed for water treatment, adsorption when implemented using a well-designed system offers the best results yielding high quality treated water.[3,4] Moreover, this technique is considered superior over other techniques because of its simple design and operation, low initial investment, effectiveness and insensitivity to toxic substances.[2,5,6]

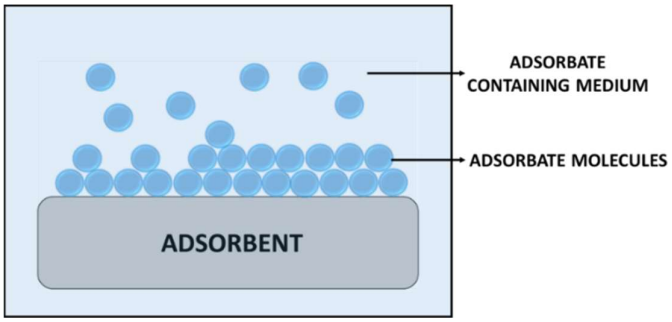

Figure 2.12. Schematic representation of adsorption process onto a solid adsorbent.

Activated carbon is the most widely used adsorbent for wastewater treatment. However, the energy required for the production and regeneration of activated carbon increases its cost. Hence there is a compelling motivation to develop alternative low-cost adsorbents from industrial and agricultural by-products.[2,3,7–9] The production and regeneration of activated carbon generate a large carbon footprint as opposed to the sustainable nanomaterials obtained from cellulose. It was calculated the annual carbon dioxide (CO_2) emissions produced during the production and regeneration of 1.0 lb granular activated carbon are around 8.5 lb and 7.0 lb respectively.[9] The production of the CNs, on the other hand, employs mechanical disintegration and sulfuric acid hydrolysis processes. Celluforce Inc. based in Canada produce around 1 ton/per day of CNCs in their pilot plant facility and they have already demonstrated that the feasibility to recycle a large quantity of sulfuric acid during the production process. Also, the raw material used for their production is the pulp waste from the paper industry. This in turn makes the overall process sustainable with a drastically lower carbon footprint as opposed to activated carbons. According to Celluforce Inc., the current cost of highly purified CNCs is around 25 $/kg. However this cost will be significantly reduced when the commercial production of CNC commences. Also, CNCs with lower purity is only required for wastewater treatment processes. Thus, it is foreseen that the pricing of CNCs will be competitive to the currently available high grade activated carbons used for wastewater treatment processes. From the point of environmental sustainability these CNCs are also superior to the majority of the ion exchange resins produced from petroleum-based polymers used in present days. Thus, the idea of developing adsorbents using CNs, such as CNCs and CNFs has gained popularity among researchers worldwide.

2.6.1.1 Adsorbents of dyes

Effluent discharge from textile, pulp and paper, dye and dye intermediates, pharmaceutical industries, food and leather tanning industries contain various types of dyes that should be removed.[2,90] Adsorbents based on CNs to decontaminate water by removing these dyes have been developed recently. He et al. used carboxylated CNCs prepared by hydrolysis of microcrystalline cellulose (MCC) using ammonium persulfate (APS) to adsorb a cationic dye, methylene blue. Negative carboxyl functional groups introduced on the surface of CNCs during the hydrolysis of MCC in APS can bind positively charged methylene blue (MB) molecules with a maximum adsorption capacity (q_{max}) of 101.2 mg/g. They also demonstrated that the adsorption capacity of CNCs approached an equilibrium within 10 min and desorption of MB from CNCs was possible using a suitable eluent, such as ethanol with more than 90% removal after 7 desorption cycles.[91] Batmaz et al. also investigated the adsorption characteristics of CNCs using methylene blue. They demonstrated that pristine CNCs possessed very good adsorption capabilities and their adsorption capacity can be improved by functionalization. Pristine CNCs produced via sufuric acid hydrolysis of wood pulp possess negative sulfate ester groups on its surface and more negative charges can be introduced by oxidizing the primary hydroxyl groups on the surface of CNCs using TEMPO reagents. The q_{max} of pristine CNCs and TEMPO-oxidized CNCs were found to be 118 mg/g and 769 mg/g respectively and these results suggested that the MB adsorption was a result of counter-ion exchange between the active anionic sites and positively charged dye molecules.[92]

Yu et al. developed a single step extraction via citric/ hydrochloric acid (HCl) hydrolysis of MCC to produce carboxylated CNCs for the adsorption of methylene blue. The maximum % dye removal by these carboxylated CNCs was compared to two other types of CNCs produced by hydrolysis of MCC using different mineral acids, such as H_2SO_4 and formic/HCl. It was found that at the same adsorbent dosage, carboxylated CNCs possessed superior dye removal when compared to two other types of CNCs. This is because of the additional carboxyl groups present on these carboxylated CNCs which act as active binding sites for dye molecules.[93] Similarly, Qiao et al. synthesized a novel carboxylate functionalized adsorbent

based on CNCs for the removal of multiple cationic dyes (Crystal Violet, Methylene Blue, Malachite Green and Basic Fuchsin). These carboxylated CNCs were produced by grafting maleic anhydride (MA) on the hydroxyl groups of pristine CNCs. The equilibrium adsorption time for pristine CNCs and MA-CNCs was determined to be about 240 min. They also compared the maximum uptake of cationic dyes on these MA-CNCs with pristine CNCs and raw cellulose, and the following order, MA-CNCs > Pristine CNCs > raw cellulose was observed. The dramatic improvement in the adsorption capacity of pristine CNCs for cationic dyes compared to pulp fibers or untreated plant wastes is due to the high surface area, increased number of surface hydroxyl groups and negative sulfate ester groups of pristine CNCs. The adsorption capacity of MA-CNCs was much higher than pristine CNCs due to the additional carboxyl groups introduced by maleic anhydride that can bind cationic dyes via electrostatic interaction. This is in agreement with the calculated q_{max} of pristine CNCs (185.2 mg/g) and MA-CNCs (243.9 mg/g). They also demonstrated that MA-CNCs exhibited a promising cycling behaviour. The desorption rate was more than 80% and the adsorption capacity of the regenerated MA-CNCs was maintained at 85.7 mg/g after the fourth consecutive adsorption-desorption cycle.[94]

Apart from the use of negatively charged CNCs, researchers have also reported the cationic modification of CNCs for the adsorption of anionic dyes. Eyley et al. demonstrated the ion exchange capability of imidazolium grafted CNCs using an anionic dye, orange II. The pristine CNCs were cationically modified by grafting imidazolium groups using a heterogeneous Cu(I) catalysed azide-alkyne cycloaddition on CNCs. The amount of dye adsorbed by these functionalized CNCs was found to be 0.28 mmol/g (98.1 mg/g) for orange II dye.[95] Figure 2.13 represents a schematic diagram showing the adsorption of an anionic dye, orange II by imidazolium grafted CNCs and UV/Vis spectrum showing their improved adsorption ability compared to pristine CNCs.

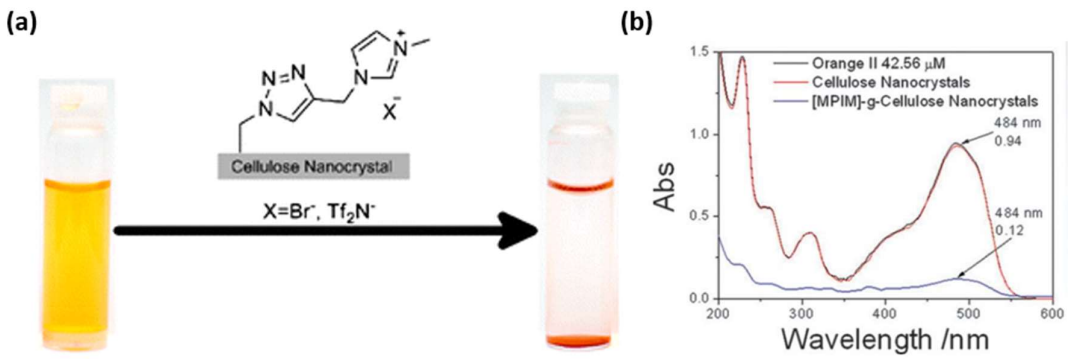

Figure 2.13. (a) Schematic diagram showing the adsorption of an anionic dye, Orange II dye by imidazolium grafted CNCs. (b) UV/Vis spectrum showing adsorption of Orange II dye by imidazolium grafted CNCs and pristine CNCs.[95] (Reprinted with permission from ref. 95 © 2011 Royal Society of Chemistry)

In another study, Jin et al. used amino functionalized CNCs (A-CNCs) as an adsorbent for anionic dyes (congo red 4BS, acid red GR and reactive yellow K-4G). The A-CNCs used in this study were prepared by grafting ethylenediamine onto sodium periodate oxidized pristine CNCs. Here the hydroxyl and primary amine groups of A-CNCs serve as active adsorption sites for the binding of anionic dyes and the q_{max} of acid red GR was found to be 555.6 mg/g.[96]

CNFs are also widely explored for their use in the adsorption of dyes. Cha et al. reported on the utilization of CNFs as a rapid adsorbent for the removal of methylene blue. CNFs were prepared from kenaf core by a delignification process using acid-chlorite bleaching method followed by defibrillation in a high-speed blender. The CNFs produced by this method have adsorption sites on the hemicellulose domains and the q_{max} of this non-acid treated CNF for MB was found to be 122.2 mg/g. They also demonstrated that this adsorbent displayed rapid adsorption performance, where the equilibrium was achieved immediately after 1 min of contact time, and it could be desorbed via a regeneration process by protonation of the CNF with 0.1M HCl. It was observed that >70% of MB could be desorbed after six adsorption-desorption cycles even though the efficiency of the adsorption process decreased to 34%. The reduction in the adsorption performance after six cycles is attributed to the pre-adsorbed MB and aggregation of CNF during desorption.[97] Surface quarternized CNFs (Q-CNFs) with high adsorption capacity for anionic dyes (congo red and acid green 25) was developed by Pei et al.

Here the Q-CNFs were prepared by mechanical disintegration of wood pulp fibers that were pre-treated by reacting with GTMAC. An optimized sodium hydroxide (NaOH) concentration was employed for this reaction in order to maximize the conversion of hydroxyl groups on the surface of CNFs to quaternary ammonium groups. They observed that the adsorption capacity of these Q-CNFs increased with increasing trimethylammonium chloride content on cellulose from 0.59 to 1.32 mmol g^{-1} with no further improvement upon increasing the charge content to 2.31 mmol g^{-1}. Q-CNFs with trimethylammonium chloride content of 1.32 mmol g^{-1} were able to adsorb 664 mg/g of congo red and 683 mg/g of acid green 25 within a few tens of seconds of contact with dye solution. This rapid equilibrium kinetics is associated to the uniform nanoscale structure, high specific surface area and surface cationic charge density of the surface Q-CNFs. They also prepared a nanopaper by freeze drying the aqueous suspension of Q-CNFs and demonstrated the dye adsorption capability of this Q-CNFs nanopaper using congo red solution. All these results demonstrated the feasibility of Q-CNFs for dye removal from aqueous waste streams.[98] Figure 2.14 illustrates the dye adsorption capability of Q-CNFs and Q-CNFs nanopaper.

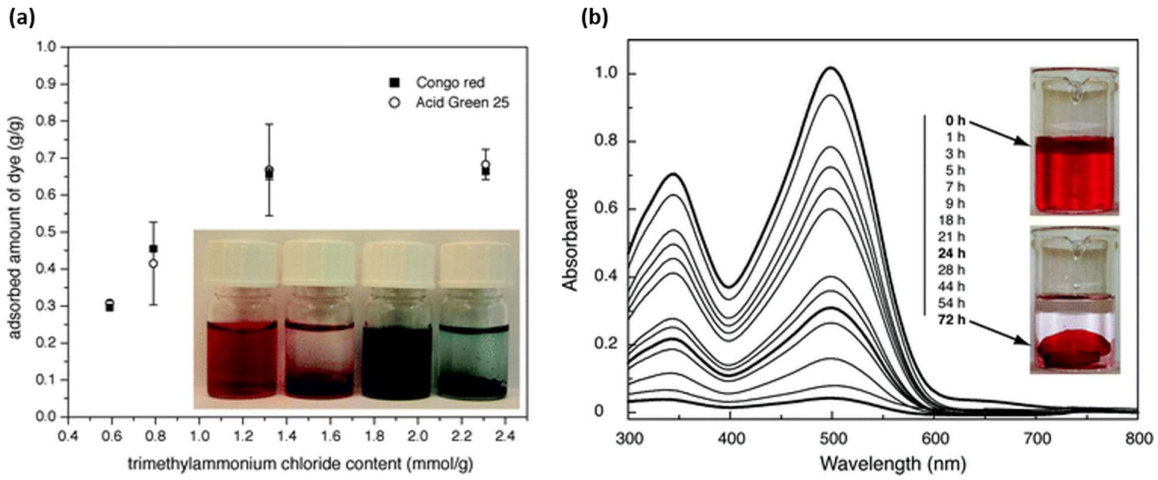

Figure 2.14. (a) Adsorbed amount of congo red and acid green 25 on Q-CNFs as a function of the trimethylammonium chloride content. (b) Time-dependent absorption spectra of the congo red solution containing Q-CNFs nanopapers with a trimethylammonium chloride content of 1.32 mmol g^{-1}.[98] (Reprinted with permission from ref. 98 © 2013 Royal Society of Chemistry)

Wang et al. developed the manganese dioxide (MnO_2) coated CNFs for the effective removal of methylene blue. Here the CNFs produced by mechanical disintegration of bamboo

pulp fibers acted as both a reducing reagent for Mn(VII) and an ultra-light support for MnO_2 nanosheets. A comparison of the % dye removal of MnO_2 coated CNFs with pristine CNFs and commercial MnO_2 indicated that the adsorption efficiency followed the order of MnO_2 coated CNFs > CNFs > commercial MnO_2. This extremely high decolourization efficiency is attributed to the excellent water dispersibility of CNFs, special lamellar morphology of MnO_2 deposited on CNFs and large surface area of layered MnO_2 nanosheets. It was also observed that complete decolourization of MB by MnO_2 coated CNFs was achieved within 5 min at an initial MB concentration of 80 mg/l and pH of 9.6.[99] Xie et al. prepared novel CNFs based nanostructured biosorbents for the adsorptive removal of reactive dyes like yellow B-4RFN and Blue B-RN. Here the CNFs based fabric were modified with reactive polyhedral oligomeric silsesquioxane (R-POSS) to introduce multi-N-methylol groups on its surface. Compared to the control CNFs based fabric, the R-POSS-CNFs hybrid fabric possessed significantly improved adsorption capacity for reactive dyes and this could be due to the organic functional groups (–C–N–) imparting cationic properties and the numerous nanosized cubic cores in the hybrid materials that act as adsorption sites for these dyes. They also found that the adsorption capacity reached equilibrium at 240 min.[100]

Several researchers have also explored the potential application of CNs incorporated nanocomposites for the adsorption of dyes. Researchers from Wu's group, fabricated porous nanocomposite hydrogels based on partially hydrolyzed polyacrylamide (HPAM) and pristine CNCs by two different methods for adsorbing MB from aqueous solutions.[101,102] In the first approach, the nanocomposite solution containing pristine CNCs and HPAM in water/ethanol mixture was electrospun and subsequently crosslinked by heat treatment to form the nanocomposite hydrogel. This porous nanocomposite hydrogel displayed a rapid swelling rate and high adsorption capacity in removing MB from low concentration dye solutions.[101] In the second method, the nanocomposite solution containing pristine CNCs and HPAM in water was formulated into a film and subsequently crosslinked by heat treatment to yield a nanocomposite hydrogel. The q_{max} for this nanocomposite gel for MB was found to be 326.08 mg/g.[102] Both of these nanocomposite hydrogels were found to approach the adsorption equilibrium after

approximately 240 min and the adsorption of MB could be attributed to the exchange or sharing of electrons between cationic groups on dye molecules and anionic groups on the adsorbent (mainly sulfate ester groups of CNCs and carboxyl from HPAM).[101,102]

Jin et al. developed a novel microgel based on CNCs and amphoteric polyvinylamine (PVAm) that can be used for adsorptive removal of anionic dyes, such as acid red GR, congo red 4BS and reactive light yellow K-4G. Here the microgel was fabricated via a two-step method wherein the first step includes the sodium periodate oxidation of CNCs to produce dialdehyde functionalized CNCs that act as crosslinkers to react with PVAm in the second step to yield pH responsive microgels bearing high density of free amine groups. Under the acidic pH environment, protonation of amine groups on the surface of microgels results in the positively charged microgel surface. This in turn aid in the electrostatic attraction between the protonated amine and negatively charged sulfate groups of anionic dyes promoting higher adsorption of anionic dyes onto the microgels. The q_{max} for acid red GR, congo red 4BS and reactive light yellow K-4G were found to be 896 mg/g, 1469 mg/g and 1250 mg/g respectvely.[103]

Nypelö et al. prepared functional microbeads that can be used for the adsorption of MB in aqueous solutions via the self-assembly of Pickering magneto-responsive CNCs. These solid microbeads with a polystyrene core was encapsulated in a hybrid shell consisting of CNCs and magnetic nanoparticles. Here the *in-situ* emulsion polymerization of styrene was stabilized by magneto-responsive CNCs. The adsorption capacity of these microbeads was estimated to be 2 mg/g for MB and the dye carrying microbeads can be easily concentrated and separated from the media using a magnet.[104] Figure 2.15 shows the SEM images of the microbeads at various magnifications and their use in the removal of MB in aqueous solution.

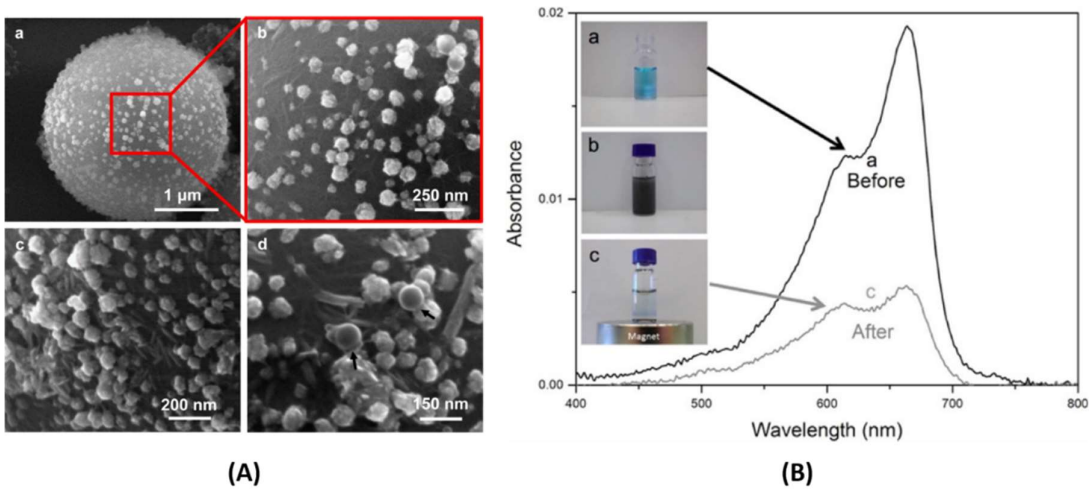

Figure 2.15. (A) SEM images of (a) an individual hybrid CNC–$CoFe_2O_4$–PS microbead and (b, c) close-ups to the surface revealing the CNC hybrid mesh formation. Arrows in (d) indicate small PS particles formed by nucleation outside emulsion droplets. (B) (a) MB removal from aqueous solution by introducing (b) CNC–Cobalt ferrite PS hybrid microbeads to the solution. MB solution after magnetic separation of the dye saturated microbeads is shown in (c) UV–Vis spectra of the MB solution before (a) and after (c) adsorption are presented on the right.[104] (Reprinted with permission from ref. 104 © 2014 American Chemical Society)

Chen et al. formulated aerogels from two differently prepared CNFs, which were used for the removal of MB and toluidine blue in aqueous solutions. CNFs were prepared from cellulose fibers by two different methods namely: (a) high intensity ultra-sonication (HIUS), (b) TEMPO oxidization (TMP) followed by ultrasonic treatment. During the freeze drying process HIUS-CNFs and TMP-CNFs self-aggregated into long fibers in the longitudinal direction and formed sheet like structures, and the diameters of the aggregated nanofibers in the sheets varied owing to the CNFs morphology and properties. The diameters of the nanofibers in HIUS-CNFs and TMP-CNFs ranged from 150-900 nm and 50-300 nm respectively. Due to this difference, the adsorption capacity of HIUS-CNFs and TMP-CNFs for MB approached 2.90 mg/g and 3.70 mg/g respectively whereas for toluidine blue approached 3.02 mg/g and 4.16 mg/g respectively.[105] Table 2.1 summarizes the various CNs based adsorbents used for the removal of dyes.

Table 2.1. Various CNs based adsorbents used for the removal of dyes.

S.No.	CNs based adsorbent	Dye	q_{max} (mg/g)	Ref.
1	Carboxylated CNCs prepared by APS hydrolysis of MCC	Methylene blue	101.2	91
2	Pristine CNCs	Methylene blue	118	92
3	Carboxylated CNCs prepared by TEMPO oxidization of pristine CNCs	Methylene blue	769	92
4	Carboxylated CNCs prepared by citric/HCl hydrolysis of MCC	Methylene blue	---	93
5	Pristine CNCs	Crystal Violet	185.2	94
6	Maleic anhydride grafted CNCs	Crystal Violet	243.9	94
7	Imidazolium grafted CNCs	Orange II	98.1	95
8	Amino functionalized CNCs	Acid red GR	555.6	96
9	Pristine CNFs	Methylene blue	112.2	97
10	GTMAC functionalized CNFs	Congo red, Acid green 25	664 (Congo red), 683 (Acid green 25)	98
11	MnO_2 coated CNFs	Methylene blue	---	99
12	R-POSS modified CNFs based fabric	Yellow B-4RFN, Blue B-RN	---	100
13	CNCs/HPAM nanocomposite hydrogels prepared using electrospinning	Methylene blue	---	101
14	CNCs/HPAM nanocomposite hydrogels prepared using casting	Methylene blue	326.08	102
15	D-CNCs/PVAm microgels	Congo red 4BS, Acid red GR, Reactive light yellow K-4G	869 (Acid red GR), 1469 (Congo red 4BS), 1250 (Reactive light yellow K-4G)	103
16	Magneto-responsive CNCs microbeads	Methylene blue	2	104
17	HIUS-CNFs aerogels	Methylene blue, Toluidine blue	2.90 (Methylene blue), 3.70 (Toluidine blue)	105
18	TMP-CNFs aerogels	Methylene blue, Toluidine blue	3.02 (Methylene blue), 4.16 (Toluidine blue)	105

2.6.1.2 Adsorbents of heavy metal ions

Apart from dyes, heavy metals are another group of contaminants that are considered to be a serious threat to both mankind and environment due to their toxic nature and other adverse effects. Many of these heavy metals are detected in industrial effluents originating from metal plating, mining activities, paint manufacture, fertilizer industries etc. They are not biodegradable and tend to accumulate in the food chain.[106] It is thus important to develop adsorbents that can remove these toxic contaminants from wastewater and in this regard, CNs based adsorbents could be applied to remove heavy metallic ions.

Researchers from Mathew's group, have explored the potential of CNs for adsorption of various heavy metal ions from aqueous solutions.[107,108] In the first study, the two major classes of CNs viz., CNCs and CNFs extracted from cellulose sludge via H_2SO_4 hydrolysis and homogenization of cellulosic fibers respectively were used for the adsorption of Ag(I) from aqueous solutions. They conducted Ag^+ adsorption experiments using both types of CNs at various pH conditions and studied the flocculation characteristics of both suspensions. After Ag^+ treatment, CNCs suspension were stable whereas CNFs suspension mostly sedimented and separated into distinct layers. This is in agreement with the surface charge characteristics of the CNs after Ag^+ ions adsorption. CNCs possess higher specific surface area or proportion of adsorption sites available to bind Ag^+ ions compared to CNFs that sedimented. Adsorption of Ag^+ ions occurs as a result of electrostatic interaction between positively charged Ag^+ ions and negatively charged functional groups of the CNs (sulfate ester groups on CNCs and carboxyl groups on CNFs) and the q_{max} was estimated to be 34.4 and 15.45 mg/g on CNCs and CNFs respectively.[107] Figure 2.16 shows the adsorption behaviour of Ag^+ ions on CNCs and CNFs at varying pH and corresponding schematic representation of the mechanism for the adsorption.

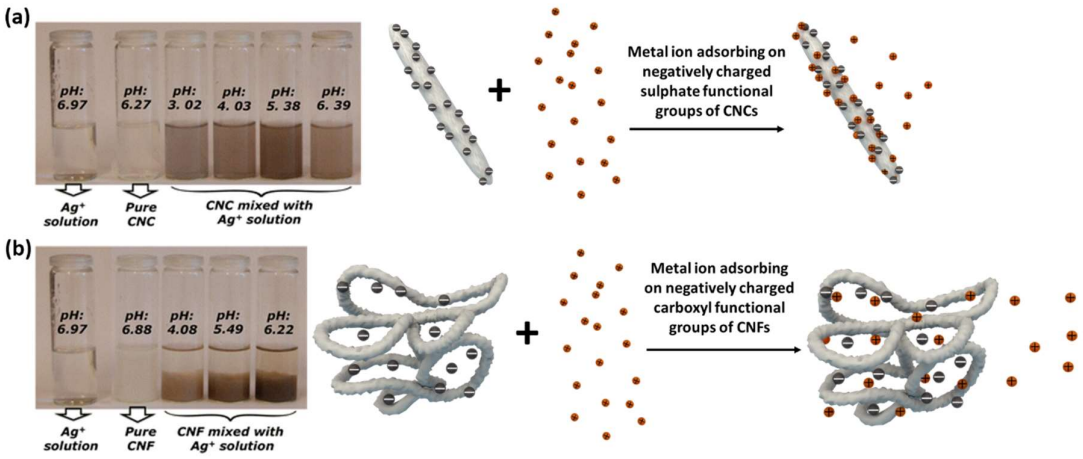

Figure 2.16. Photograph showing Ag^+ solution, pure CNs suspension and suspensions of CNs mixed with Ag^+ ions at different pH after 12 h magnetic stirring and schematic representation of their Ag^+ adsorption mechanism for (a) CNCs (b) CNFs.[107] Schematic redrawn (Reprinted with permission from ref. 107 © 2014 Springer)

In the second study, phosphorylated derivatives of CNCs and CNFs were prepared and used for the adsorption of Ag^+, Cu^{2+} and Fe^{3+} from aqueous solutions. The phosphate groups introduced on the surface of CNs via enzymatic phosphorylation contributed to improved metal sorption velocity and sorption capacity compared to pristine CNs. The q_{max} for Ag^+, Cu^{2+} and Fe^{3+} were found to be 56, 20 and 6.3 mg/g respectively for pristine CNCs, 136, 117 and 115 mg/g respectively for phosphorylated CNCs, 120, 114 and 73 mg/g respectively for phosphorylated CNFs. The high surface area of these CNs along with the nature and density of the functional groups like sulfonate group (pristine CNCs), phosphate group (phosphorylated CNCs and CNFs) act as the binding sites for the adsorption of heavy metal ions. Moreover, they also demonstrated the potential application of these phosphorylated CNs for the removal of Cu^{2+} and Fe^{3+} containing effluents from mirror making industry.[108]

Yu et al. reported on the use of surface functionalized CNCs, such as SCNCs and NaSCNCs for the adsorption of Pb(II) and Cd(II) from aqueous solution. The pristine CNCs produced by H_2SO_4 hydrolysis of cotton were chemically modified with succinic anhydride to obtain carboxyl group-bearing SCNCs and further treatment of SCNCs with saturated sodium bicarbonate ($NaHCO_3$) converted the carboxyl groups to carboxylates as in NaSCNCs. The adsorption capacities of these two types of CNCs were studied in detail using batch adsorption

studies. Results of adsorption studies revealed that the adsorption rates of Pb^{2+} and Cd^{2+} ions on SCNCs and NaSCNCs were very fast with adsorption capacity approached the equilibrium within 5 min for NaSCNCs compared to SCNCs that took 150 min. q_{max} of SCNCs and NaSCNCs for Pb(II) and Cd(II) were estimated to be 367.6, 259.7 and 465.1, 344.8 mg/g, respectively, where NaSCNCs displayed higher adsorption capacity than SCNCs. Both types of CNCs had high selectivity for Pb^{2+} in the presence of co-existing ions while in a similar environment, the adsorption of Cd^{2+} on NaSCNCs was better than SCNCs. It should be noted that NaSCNCs were easily regenerated using mild saturated NaCl. Studies on the adsorption mechanism for these types of CNCs were conducted using Fourier transform infrared spectroscopy (FTIR) and X-Ray photoelectron spectroscopy (XPS) techniques to confirm that the adsorption process of heavy metals was a result of a complexation process for SCNCs and an ion exchange mechanism for NaSCNCs. Thus, the excellent adsorption properties of NaSCNCs compared to SCNCs resulting from the ion exchange suggests the importance of converting the carboxyl groups into carboxylates for adsorbents containing carboxyl groups.[109]

Researchers from Srivastava's group, explored the potential of pristine and a wide variety of functionalized CNCs for the adsorptive removal of heavy metal ions in aqueous solutions. CNCs prepared from rice straw fibers were used for the adsorption of Cd(II), Pb(II) and Ni(II) from aqueous solutions.[110–113] Adsorption studies revealed that these CNCs possessed higher adsorption capacity compared to their parent materials like rice straw fibers and cellulose derived from rice straw. This improved adsorption efficiency may be influenced by the removal of amorphous domains in the cellulosic chains during the synthesis of CNCs, promoting the availability of more primary hydroxyl groups on its surface. Also, the acid hydrolysis of the cellulosic fibers during the synthesis of CNCs introduced negatively charged sulfate ester groups on the surface of CNCs that could act as binding sites for cationic heavy metal ions. They also showed that these CNCs can be successfully regenerated by up to three adsorption-desorption cycles using 0.5M Nitric Acid (HNO_3) as eluent with an estimated a q_{max} of 9.7, 9.42 and 8.55 mg/g for Cd(II), Pb(II) and Ni(II) respectively.[110] They also improved the adsorption performance of these CNCs toward Cd(II), Pb(II), Ni(II) and Cr(III) metal ions by

graft copolymerizing them with various monomeric units. Graft copolymerizing of CNCs with monomeric acids like acrylic acid, maleic acid and itaconic acid introduced more negatively charged carboxylate groups on the surface of CNCs.[111] Whereas graft copolymerizing with vinyl sulfonic acid introduced more negatively charged sulfonate groups on the surface of CNCs.[112] In comparison to the pristine CNCs, both these carboxylate and sulfonate groups on the graft copolymerized CNCs act as additional active sites for heavy metal ion binding leading to their enhanced adsorption capacity. It was also found that the reusability of graft copolymerized CNCs have been increased to five cycles compared to three cycles of pristine CNCs probably due to their enhanced stability.[111,112] CNCs were also functionalized via succination and amination functionalization procedures so that they could be used for the decontamination of Cr(III) and Cr(VI) respectively. It was reported that the increased surface area to volume ratio and quantum size effects of CNCs not only increased the adsorption sites but also induced the ability to tune the surface properties of CNCs through molecular modification making them ideal for surface functionalization to enrich the active sites for adsorption. Esterification of hydroxyl groups on CNCs with succinic anhydride-introduced carboxyl groups on its surface that contributed to the increase in the binding with positively charged metal ions like Cr(III). Amination of CNCs with acrylamide and ethylenediamine introduced NH_3^+ cationic ligands on its surface that contributed to binding of Cr(VI). The adsorption capacity of these functionalized CNCs approached an equilibrium in 40 min of contact time. The q_{max} of succinated CNCs/Cr(III) and aminated CNCs/Cr(VI) system was found to be 2.88 and 2.77 mg/g respectively. They also demonstrated that these CNCs could be successfully regenerated up to five regeneration cycles using 0.05M HNO_3 or 0.05M HCl eluent solutions.[113]

Electrosterically stabilized CNCs (ECNCs) were prepared by Sheiki et al. for the adsorptive removal of Cu(II). These ECNCs prepared from wood fibers through periodate/chlorite oxidation were hypothesized to possess dicarboxylated chains (DCC) protruding from the crystalline domains. These highly charged polyelectrolytes impart high charge content on the ECNCs, making them highly stable. It was found that depending on the

Cu(II) concentration, ECNCs scavenges Cu^{2+} ions by different mechanisms. ECNCs aggregate into star-like particles, which break down into individual star-like entities by shear force and Brownian motion when the Cu(II) concentration is low (≤ 200 ppm). These aggregate morphologies change from star-like to raft-like morphology when the concentration is 300 or 400 ppm, which is probably due to the ECNCs charge neutralization by copper adsorption and the collapse of protruding DCC chains. At Cu(II) concentration (≥ 500 ppm), as opposed to star-like agglomerates, these raft-like structures gradually grow and are prone to sedimentation which makes their separation easier for wastewater treatment processes. Highly charged DCC polyanions protruding from ECNCs act as active sites for Cu^{2+} binding and the q_{max} for this adsorption was found to be 185 mg/g.[114]

Sirviö et al. prepared bisphosphonate functionalized CNCs that can be used for the removal of vanadium from aqueous solution. Here the bisphosphonate functionalized CNCs were prepared by mechanical disintegration of periodate oxidized and sodium alendronate aminated wood cellulose fibers. They also found that adsorption was highly efficient at very low solution pH (2-3) wherein the adsorption of vanadium onto these CNCs could most likely be due to complexation of vanadium with bisphosphonate groups and electrostatic interaction between cationic vanadium species and anionic acid groups. The q_{max} for vanadium was found to be 1.98 mmol/g (100.9 mg/g).[115]

Ma et al. found that ultrafine CNFs can be used as efficient adsorbents for the removal of radioactive UO_2^{2+} ions in water. The ultrafine CNFs used in this study were prepared via the oxidation of wood pulp using the TEMPO/ Sodium Bromide (NaBr)/ Sodium hypochlorite (NaClO) process followed by mechanical treatment. Upon the addition of UO_2^{2+} ions to CNFs suspension, a gel formed immediately due to the coordination between the positively charged UO_2^{2+} ions and negatively charged carboxylate groups on the CNFs. The q_{max} for these ultrafine CNFs for UO_2^{2+} ions was estimated to be 167 mg/g.[116] Figure 2.17 shows the high resolution TEM images of ultrafine CNFs before and after the adsorption of UO_2^{2+} ions with the corresponding photograph of the suspension shown in the inset.

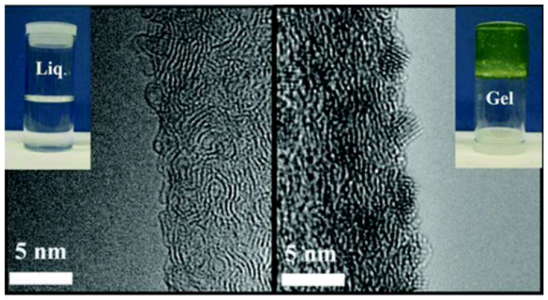

Figure 2.17. High resolution TEM images of ultrafine CNFs before and after the adsorption of $UO2^{2+}$ ions with the corresponding photograph of suspension in the inset.[116] (Reprinted with permission from ref. 116 © 2012 American Chemical Society)

Sehaqui et al. also prepared carboxylated CNFs for the adsorptive removal of Cu(II), Cr(III), Ni(II) and Zn(II) from aqueous solutions. They found that Cu(II) adsorption capacity of these carboxylated CNFs were higher compared to pristine CNFs, due to the additional carboxylate groups introduced on the surface of CNFs during TEMPO oxidation of the parent cellulosic fibers that act as anionic binding sites for the electrostatic attraction of Cu^{2+} ions. The q_{max} for Cu(II), Ni(II), Cr(III) and Zn(II) was estimated to be 135, 58, 49 and 66 mg/g respectively. They also demonstrated that this adsorbent could be also effectively regenerated using acidic HCl solution as eluent with more than 90% adsorption capacity after three adsorption-desorption cycles.[117] Zhang et al. prepared a highly functionalized adsorbent viz., TEMPO oxidized CNFs modified with polyethylenimine (PEI) for the adsorptive removal of Cu(II) from aqueous solution. Here, the CNFs were modified by first oxidizing via TEMPO reagent followed by PEI grafting using a glutaraldehyde crosslinking method. This modification introduced abundant carboxyl and amino functional groups on CNFs that could act as active sites for the binding of Cu^{2+} ions in aqueous solution, and the q_{max} was estimated to be 52.3 mg/g. Moreover, after regeneration with 1M HCl eluent, the adsorption capacity remained constant during four adsorption-desorption cycles implying the excellent regeneration ability of this adsorbent.[118]

Researchers from Sillanpää's group, developed a wide range of functionalized CNFs for adsorption of heavy metals from water.[119–123] Aminopropyltriethoxysilane (APTES) modified CNFs were prepared for the adsorption of Ni(II), Cu(II) and Cd(II) from aqueous solutions. They reported that APTES modified CNFs has a comparatively higher adsorption capacity than

unmodified CNFs. In the case of unmodified CNFs, metal ion binding is due to electrostatic interaction with just the carboxyl groups on its surface whereas in APTES modified CNFs, the amino groups contributed by the aminosilane functionalization provide additional functional groups for metal ion binding. These APTES modified CNFs can be easily regenerated using 0.1M NaOH eluent and their q_{max} for Ni(II), Cu(II) and Cd(II) ions was estimated to be 2.734 mmol/g (160.5 mg/g), 3.150 mmol/g (200.2 mg/g) and 4.195 mmol/g (471.6 mg/g) respectively.[119] Succinic anhydride modified CNFs were prepared for the removal of Zn(II), Ni(II), Cu(II), Co(II) and Cd(II) from aqueous solutions. The carboxyl groups on the surface of these modified CNFs act as adsorption sites for these heavy metal ions and the q_{max} for Zn(II), Ni (II), Cu(II), Co(II) and Cd(II) was estimated to be 1.610 mmol/g (105.3 mg/g), 0.744 mmol/g (43.7 mg/g), 1.900 mmol/g (120.7 mg/g), 1.338 mmol/g (81.8 mg/g) and 2.062 mmol/g (231.8 mg/g) respectively. It was also observed that the succinic anhydride modified CNFs could be efficiently regenerated using 1M HNO_3 eluent and assisted with ultrasonic treatment.[120] Carbonated hydroxyapatite (CHA) modified CNFs were prepared for the adsorption of Ni(II) and Cd(II) from aqueous solution. Here the adsorption of Ni(II) and Cd(II) ions possibly occurs a result of ion exchange mechanism or dissolution-precipitation mechanism. Regeneration studies using various strengths of HNO_3 showed that both the heavy metals can be effectively regenerated using weaker acid (0.01M HNO_3) with the adsorption capacity for Ni^{2+}ions decreasing after every cycle and Cd^{2+} ions remaining same even after four cycles. The q_{max} of these adsorbents for Ni(II) and Cd(II) was estimated to be 2.021 mmol/g (118.62 mg/g) and 1.224 mmol/g (137.6 mg/g) respectively.[121] Magnetic nanoparticle activated CNFs were prepared for the adsorptive removal of As(V) from aqueous solution. Here the adsorption of arsenic species occurs as a result of inner-sphere complexes with the oxidized states of Fe^{o} from iron nanoparticle (Fe-NP) present in the adsorbent. Thus, the presence of OH_2^+, OH^- and O^- functional groups on adsorbent surface have an influence on the adsorption properties. They estimated the q_{max} to be 2.460 mmol/g (184.31 mg/g) with their adsorption capacity reaching an equilibrium after approximately 75 min. They also found that this adsorbent can be effectively regenerated using 1M NaOH eluent with a regeneration efficiency

of more than 98% after three cycles.[122] Sulfonated CNFs were prepared for the recovery of ionic, nanoparticulate and metallic forms of Au(III). These anionic CNFs were synthesized by periodate oxidation of CNFs followed by sodium metabisulfite sulfonation. Introduction of additional anionic sulfonated functional groups on the surface of CNFs can enhance their adsorption capacity compared to pristine CNFs. These anionic sites can act as additional binding sites of the adsorption of cationic metal ion species. The q_{max} of these sulfonated CNFs for Au(III) was estimated to be 60 mg/g. They also found that the Au(III) adsorption was negligibly affected by the competing heavy metal ions like Cd(II), Co(II), Cr(VI), Ni(II) and As(V) present in aqueous environment and regeneration using strong complexing eluent like 0.5M thiourea in 1M HCl can effectively recover more than 83-99% of the adsorbed Au(II) ions from the adsorbent.[123] Suopajärvi et al. also used sulfonated CNFs for the adsorptive removal of Pb(II) from aqueous solutions. The q_{max} of these sulfonated CNFs was estimated to be 1.2 mmol/g (248.6 mg/g).[124]

Zhou et al. used carboxylated CNFs filled magnetic chitosan hydrogel beads as adsorbents for Pb(II). Here, the hydrogel beads were prepared by an instantaneous gelation method wherein the nanocomposite solution consisting of carboxylated CNFs, amine-functionalized magnetite nanoparticles and PVA blended chitosan was introduced into a NaOH gellant bath. A comparison of the adsorption capacity of composite hydrogel beads with and without carboxylated CNFs showed that the composite hydrogel beads with carboxylated CNFs performed better at all pH ranges. This could be attributed to the carboxyl groups on CNFs that enhances the electrostatic interaction between the adsorbent and Pb^{2+} ions. They estimated the q_{max} to be 171 mg/g with their adsorption capacity reaching an equilibrium after 200 min. They also demonstrated that these composite hydrogel beads are reusable as their adsorption effectiveness could be maintained at 90% level even after four adsorption-desorption cycles using 0.01 HNO_3 eluent.[125]

Carboxylated CNFs incorporated PVA hybrid aerogels having good metal ion adsorption capability were recently developed by Zheng et al. These hybrid aerogels were prepared by freeze drying the crosslinked carboxylated CNFs/PVA composite gel. A comparison of the

metal ion adsorption capacities of the aerogels with and without CNFs indicated that these hybrid aerogels with CNFs possessed better adsorption performance. This heightened performance could be attributed to the increased number of carboxyl groups present on the surface of CNFs resulting from the TEMPO oxidation process, which contributed more active sites for metal ion binding. The adsorption capacities of these hybrid aerogels for Hg^{2+}, Pb^{2+}, Cu^{2+}, and Ag^{+} were 157.5, 110.6, 151.3 and 114.3 mg/g respectively.[126]

Anirudhan and co-workers developed nanocomposites based on CNCs that can be used for the adsorptive removal of heavy metal ions from industrial wastewaters.[127,128] In the first work, they prepared 2-mercaptobenzamide modified itaconic acid-grafted-magnetite CNCs composite that can be used for the selective adsorption of Hg(II) from aqueous solutions. This adsorbent was prepared by graft co-polymerization of itaconic acid onto magnetite CNCs composite using ethylene glycol dimethacrylate as crosslinking agent and potassium sulfate as free radical initiator followed by modification with 2-mercaptobenzamide. Hg^{2+} ions were selectively adsorbed onto this adsorbent by virtue of the ionized carboxyl and sulfhydryl groups anchored on its surface through electrostatic attraction. They estimated the q_{max} to be 240 mg/g with their adsorption capacity reaching an equilibrium within 60 min. It was also found that spent adsorbent can be effectively regenerated using 0.1M HCl eluent and even after five adsorption-desorption cycles, the adsorption capacity was above 85%.[127] In the second work, they prepared poly(itaconic acid/methacrylic acid)-grafted-CNCs/nanobentonite composite that can be used for the effective removal of Co(II) from aqueous solutions. This adsorbent was prepared by ionic crosslinking of CNCs/nanobentonite with itaconic acid followed by radical polymerization of methacrylic acid and crosslinking with ethylene glycol dimethacrylate. They estimated the q_{max} to be 350.8 mg/g with their adsorption capacity reaching an equilibrium within 120 min. It was also found that spent adsorbent can be effectively regenerated using 0.1M HCl eluent and even after six adsorption-desorption cycles, the adsorption capacity was above 85%.[128] Table 2.2 summarizes the various CNs based adsorbents used for the removal of heavy metals.

Table 2.2. Various CNs based adsorbents used for the removal of heavy metals.

S.No.	CNs based adsorbent	Heavy metal	q_{max} (mg/g)	Ref.
1	Pristine CNCs	Ag(I)	34.4	107
2	Pristine CNFs	Ag(I)	15.45	107
3	Pristine CNCs	Ag(I), Cu(II), Fe(III)	56.0 [Ag(I)], 20.0 [Cu(II)], 6.3 [Fe(III)]	108
4	Phosphorylated CNCs	Ag(I), Cu(II), Fe(III)	136.0 [Ag(I)], 117.0 [Cu(II)], 115.0 [Fe(III)]	108
5	Phosphorylated CNFs	Ag(I), Cu(II), Fe(III)	120.0 [Ag(I)], 114.0 [Cu(II)], 73.0 [Fe(III)]	108
6	Succinic anhydride modified CNCs	Pb(II), Cd(II)	367.6 [Pb(II)], 259.7 (Cd(II))	109
7	Sodium substituted succinic anhydride modified CNCs	Pb(II), Cd(II)	465.1 [Pb(II)], 344.8 [Cd(II)]	109
8	Pristine CNCs	Cd(II), Pb(II), Ni(II)	9.7 [Cd(II)], 9.42 [Pb(II)], 8.55 [Ni(II)]	110
9	Acrylic acid/Maleic acid/Itaconic acid/Vinyl sulfonic acid graft co-polymerized CNCs	Cd(II), Pb(II), Ni(II), Cr(III)	---	111,112
10	Succinic anhydride modified CNCs	Cr(III)	2.88	113
11	Acrylamide modified CNCs	Cr(VI)	2.77	113
12	Electrosterically stabilized CNCs	Cu(II)	185	114
13	Bisphosphonate functionalized CNCs	V(V)	100.86	115
14	Carboxylated CNFs	UO_2^{2+}	167	116
15	Carboxylated CNFs	Cu(II), Cr(III), Ni(II), Zn (II)	135.0 [Cu(II)], 58.0 [Cr(III)], 49.0 [Ni(II)], 66.0 [Zn(II)]	117
16	Carboxylated CNFs modified with PEI	Cu(II)	52.32	118
17	APTES modified CNFs	Ni(II), Cu(II), Cd(II)	160.5 [Ni(II)], 200.2 [Cu(II)], 471.6 [Cd(II)]	119
18	Succinic anhydride modified CNFs	Zn(II), Ni (II), Cu(II), Co(II) Cd(II)	105.3 [Zn(II)], 43.7 [Ni (II)],	120

			120.7 [Cu(II)], 81.8 [Co(II)], 231.8 [Cd(II)]	
19	CHA modified CNFs	Ni(II), Cd(II)	118.62 [Ni(II)], 137.6 [Cd(II)]	121
20	Fe-NP modified CNFs	As(V)	184.31	122
21	Sulfonated CNFs	Au (III)	60	123
22	Sulfonated CNFs	Pb(II)	248.6	124
23	Carboxylated CNFs/Magnetic chitosan hydrogel beads	Pb(II)	171	125
24	Carboxylated CNFs/PVA hybrid aerogels	Hg(II), Pb(II), Cu(II), Ag(I)	157.5 [Hg(II)], 110.6 [Pb(II)], 151.3 [Cu(II)], 114.3 [Ag(I)]	126
25	2-mercaptobenzamide modified Itaconic acid-grafted-magnetite CNCs composite	Hg(II)	240	127
26	Poly(itaconic acid/methacrylic acid) grafted-CNCs/Nanobentonite composite	Co(II)	350.8	128

2.6.1.3 Adsorbents of other water contaminants

There are various other contaminants in wastewater, such as pharmaceuticals, pesticides and biomolecules that can be a potential threat to human health and the environment. Efforts are underway to develop techniques that can remove even trace amounts of these contaminants present in water, and some early attempts by researchers to develop CNs based materials to adsorb them have seen promising results. Chen et al. synthesized β-cyclodextrin modified CNCs@Fe_3O_4@SiO_2 superparamagnetic nanorods for the adsorption of two model pharmaceutical compounds, namely procaine hydrochloride and imipramine hydrochloride. They demonstrated that the pharmaceutical residues could be adsorbed by the hydrophobic cavity of the β-cyclodextrin grafted on the CNCs@Fe_3O_4@SiO_2 superparamagnetic nanorods and this adsorbent could be easily separated from the aqueous solution using a magnetic field. The q_{max} for procaine hydrochloride and imipramine hydrochloride was found to be 13.0 ± 0.09 and 14.8 ± 0.16 mg/g respectively. Figure 2.18 shows a schematic describing the composition

of β-cyclodextrin modified CNCs@Fe_3O_4@SiO_2 superparamagnetic nanorods and their magnetic separation and adsorption of pharmaceutical residues.[129]

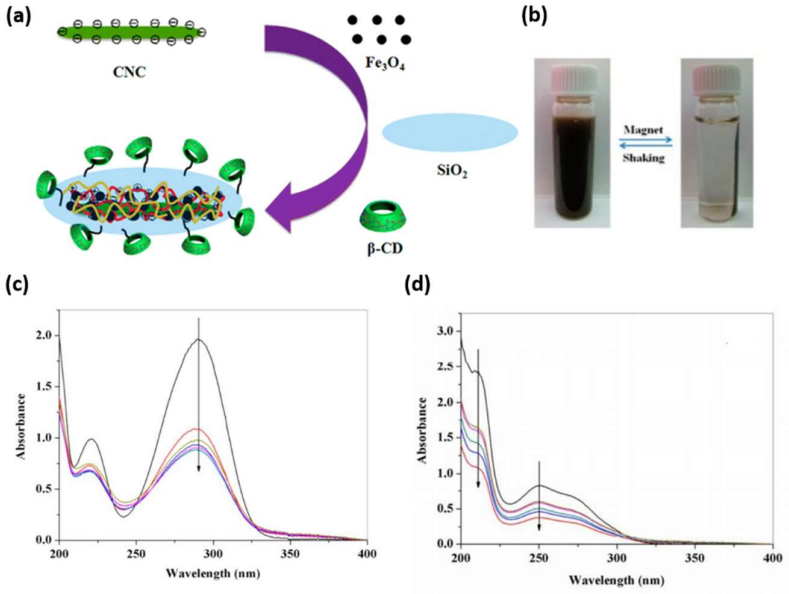

Figure 2.18. (a) Schematic diagram showing the composition of β-cyclodextrin modified CNCs@Fe_3O_4@SiO_2 superparamagnetic nanorods. (b) Magnetic separation of the superparamagnetic nanorods after adsorption. (c) UV-Vis of the upper clear procaine hydrochloride solution with different adsorption times. (d) UV-Vis of the upper clear imipramine hydrochloride solution with different adsorption times.[129] (Reprinted with permission from ref. 129 © 2014 American Chemical Society)

Researchers from Sillanpää's group,[121,130] have developed CNFs based systems that can be used for the remediation of wide variety of environmental contaminants. In one study, they modified CNFs with APTES, hydroxyl-carbonated apatite (HAP) or Epoxy to produce a novel nanostructured adsorbent for the removal of hydrogen sulphide (H_2S) from the aqueous solution and the q_{max} of these adsorbents for H_2S was found to be 103.95 mg/g, 13.38 and 12.73 mg/g for APTES-CNFs, HAP-CNFs and Epoxy CNFs respectively. The adsorption of H_2S onto APTES-CNFS could be attributed to the formation of $NH_3^+HS^-$ group as a result of weak chemical reaction between surface amine groups on APTEs-CNFs and H_2S. In case of HAP-CNFs, the adsorption could be attributed to the complex formation between positively charged calcium ions on HAP-CNFs and sulfate ions in H_2S while the adsorption for Epoxy-CNFs is due to the reaction between epoxy groups and H_2S.[130] In another study, they used CHA modified CNFs for the adsorption of phosphate (PO_4^{3-}) and nitrate (NO_3^-) from aqueous

solution. Here the adsorption of PO_4^{3-} and NO_3^- anions could be attributed to the exchange of ions with OH^- groups present on CHA modified CNFs. Regeneration studies using various concentrations of NaOH showed that PO_4^{3-} can be effectively regenerated with weaker base (0.01M NaOH) even though the adsorption capacity decreased after every cycle whereas NO_3^- is not regeneration viable. The q_{max} for PO_4^{3-} and NO_3^- was found to be 0.843 mmol/g (80.06 mg/g) and 0.209 mmol/g (12.96 mg/g) respectively.[121]

Several researchers have demonstrated the promising potential of CNs based adsorbents for the adsorption of several biomolecules and these adsorbents can be also extended for use in water treatment applications. Huang et al. prepared dialdehyde functionalized CNCs (D-CNCs) that can be used for the adsorption of creatinine. Here the dialdehyde groups were introduced on the surface of CNCs by sodium periodate oxidation of CNCs. They found that with the increase in aldehyde content, the adsorption capacity of these D-CNCs increased. They also demonstrated that the adsorption of creatinine became faster as the size of D-CNCs decreased. The q_{max} of D-CNCs with highest aldehyde content was found to be 1.50 mg/g and the adsorption of creatinine could be due to the crosslinking through Schiff-based bonds between the aldehyde groups on D-CNCs and amino groups on creatinine molecules.[131]

Anirudhan and co-workers, developed CNCs based adsorbents for the removal of biomolecules from aqueous solutions.[132–134] Carboxylate functionalized cation exchanger viz., poly(acrylic acid) modified poly(glycidylmethacrylate) grafted CNCs were used for the adsorption of trypsin from aqueous solutions. The q_{max} for trypsin was found to be 140.7 mg/g with their adsorption capacity reaching an equilibrium within 90 min. They also demonstrated that the spent adsorbent can be effectively regenerated using 0.1M potassium thiocyanate eluent without the loss in adsorption capacity even after four adsorption-desorption cycles.[132] The same group of researchers also developed a novel adsorbent viz., poly(methacrylic acid-co-vinyl sulfonic acid) grafted magnetic CNCs composite that can be used for the selective adsorption of proteins like haemoglobin (Hb) and immunoglobulin (IgG) from aqueous solutions. The magnetic properties of the adsorbent associated with Fe_3O_4 will aid in the facile separation of the adsorbent via a magnetic field. The q_{max} for Hb and IgG were found to be

248.19 and 200.21 mg/g respectively with their corresponding adsorption capacities reaching equilibrium within 2 and 3 h respectively. They have also demonstrated that this novel adsorbent can be used for the selective adsorption of Hb or IgG from their protein mixture with bovine serum albumin and can also be regenerated with 0.01M KOH eluent without much loss in adsorption capacity, even after five adsorption-desorption cycles.[133,134] In all these studies,[132–134] biomolecules were bound to the adsorbent by electrostatic interaction between the negatively charged adsorbent and positively charged protein molecule below their isoelectric point. Table 2.3 summarizes the various CNs based adsorbents used for the removal of other water contaminants.

Table 2.3. Various CNs based adsorbents used for the removal of other water contaminants.

S.No.	CNs based adsorbent	Contaminant	qmax (mg/g)	Ref.
1	β-cyclodextrin modified CNCs@Fe_3O_4@SiO_2 superparamagnetic nanorods	Procaine, Imipramine	13.0 (Procaine), 14.8 (Imipramine)	129
2	APTES modified CNFs	H_2S	103.95	130
3	HAP modified CNFs	H_2S	13.38	130
4	Epoxy modified CNFs	H_2S	12.73	130
5	CHA modified CNFs	PO_4^{3-}, NO_3^-	80.06 (PO_4^{3-}), 12.96 (NO_3^-)	121
6	Dialdehyde functionalized CNCs	Creatinine	1.50	131
7	Poly(acrylic acid) modified poly(glycidylmethacrylate) grafted CNCs	Trypsin	140.65	132
8	Poly(methacrylic acid-co-vinyl sulfonic acid) grafted magnetic CNCs	Hb, IgG	248.19 (Hb), 200.21 (IgG)	133,134

2.6.2 Cellulose nanomaterials as absorbents

In contrast to adsorption, absorption is a technique used in water treatment whereby the contaminant partitions into the bulk of the absorbent and is held within its porous structure. Oil and chemical spills from petrochemical industries have become a serious concern, and absorbents based on organic and inorganic porous materials have been developed for use in oil/water separation processes. Among these absorbents, CNs based absorbents have gained

increasing attention due to their unique properties and sustainable nature. CNFs aerogels prepared by vacuum freeze drying of aqueous CNFs suspensions possess very good absorption properties because of their highly porous nature and high surface area. Rendering them hydrophobic/oleophilic is an ideal strategy to produce these absorbents for use in oil/water separation processes.[126,135–137]

Korhonen et al. developed hydrophobic CNFs aerogels that can selectively absorb non-polar liquids and oil from water. CNFs aerogels are made hydrophobic/oleophilic by coating them with a nanoscopic layer of titanium dioxide (TiO_2). They demonstrated that depending on the density of the liquid, these aerogels possessed absorption capacities in the range 20 to 40 g/g towards a range of non-polar liquids (toluene, hexane, octane, hexadecane, petroleum benzene, dodecane, octanol, chloroform) and oils (paraffin oil, mineral oil) and the absorbed non-polar liquids can be easily removed by drying whereas oils could be extracted with solvents such as ethanol and octane. They have also shown that the hydrophobicity and absorption capacity of these aerogels do not change with repeated cycles, making them reusable.[135]

Another strategy to prepare CNF aerogels hydrophobic for use in oil/water separation is by silane coating. Zheng et al. rendered carboxylated CNFs/PVA hybrid aerogels superhydrophobic/superoleophilic by treating them with methyltrichlorosilane via a simple thermal chemical vapor deposition process. These silane treated hybrid aerogels are ideal absorbent materials for removing oil and organic solvents from water and they possess excellent absorption capacity in the range of 44 to 96 g/g for oils (diesel oil, crude oil, corn oil, pump oil) and organic solvents (gasoline, hexane, chloroform, toluene). A comparison of the silane treated PVA aerogels and carboxylated CNFs/PVA hybrid aerogels showed that the latter possessed two to three times higher adsorption capacity probably due to their unique microstructure consisting of more uniform and smaller pore sizes, higher surface area and higher degrees of interconnection within their highly porous structure.[126] In another study, Jiang et al. prepared CNFs aerogels hydrophobic/oleophilic by vapor deposition with triethoxy(octyl)silane. These aerogels demonstrated very good absorption selectivity towards

non-polar liquids and exhibited good recyclability. They also possessed excellent absorption capacities in the range of 139 to 356 g/g towards a wide range of non-polar liquids including various aliphatic (hexane, octane, decane, hexadecane), cyclic (cyclohexane) and aromatic (toluene) hydrocarbons and oils (pump, soybean).[136]

Zhang et al. recently reported a facile synthesis of hydrophobic CNF aerogels by a novel and efficient silylation process in water. This silylation process is a straightforward one step procedure whereby the CNFs water suspension was freeze-dried in the presence of methyltrimethoxysilane solution. These silylated CNFs aerogels were efficient in removing dodecane spills from water surface with excellent selectivity and recyclability. The absorption capacities of these aerogels were found to be in the range of 49 to 102 g/g for a collection of organic solvents (ethanol, dodecane, acetone, toluene, dichloromethane, chloroform) and oils (motor oil, mineral oil, silicone oil).[137]

Yang et al. have reported chemically crosslinked CNCs aerogels that can be used as superabsorbents for oil/water separations. These aerogels were prepared by freeze drying of the hydrogels formed by crosslinking the hydrazide modified CNCs and aldehyde-modified CNCs via hydrazone crosslinking chemistry. The absorption capacity of these aerogels were in 72 ± 0.5, 130 ± 10, 134 ± 8 and 160 ± 10 g/g for dodecane, ethanol, DMSO and water respectively. Even though these aerogels displayed good absorption capacities for all polar and non-polar liquids, their absorption preferences give them the ability to separate oil and water. They have demonstrated that these CNCs aerogels could preferentially absorb water from a dodecane/water mixture.[138] Figure 2.19 shows the photograph of a piece of CNCs aerogel prepared from a 0.5 wt % CNCs suspension and their use in picking up water from a dodecane/water mixture. Table 2.4 summarizes the various CNs based absorbents used for oil/water separation processes.

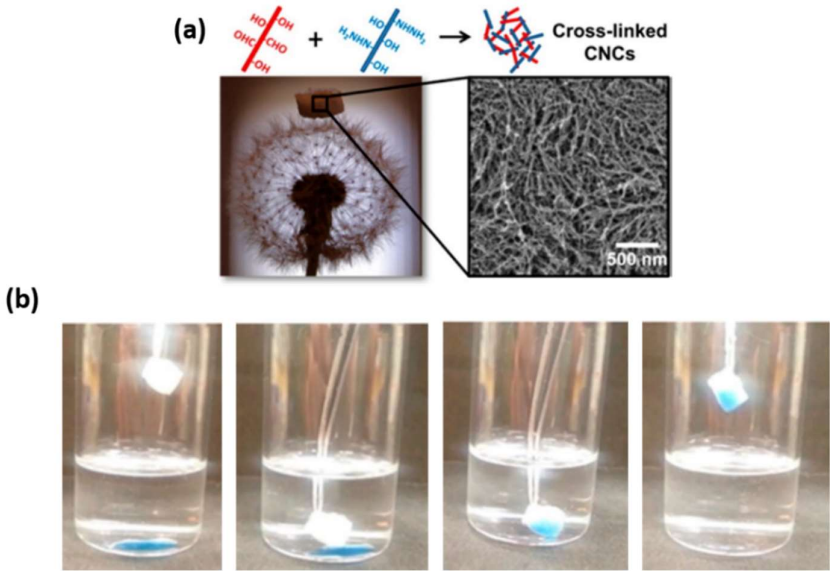

Figure 2.19. (a) A low-light photograph of a piece of CNCs aerogel (prepared from a 0.5 wt % CNCs suspension) standing on top of a dandelion flower along with the schematic showing its constituents and SEM image showing the porous nature. (b) Chronological images of an aerogel picking up water (water has been dyed with blue colour for easier visualization) from a dodecane/water mixture.[138] (Reprinted with permission from ref. 138 © 2014 American Chemical Society)

Table 2.4. Various CNs based absorbents used for oil/water separation processes.

S.No.	CNs based absorbent	Absorption capacity	Ref.
1	CNFs aerogels coated with TiO_2	20 to 40 g/g	135
2	Carboxylated CNFs/PVA hybrid aerogel treated with methyltrichlorosilane	44 to 96 g/g	126
3	CNFs aerogels treated with triethoxy(octyl)silane	139 to 356 g/g	136
4	CNFs aerogels treated with methyltrimethoxysilane	49 to 102 g/g	137
5	Chemically crosslinked CNCs aerogels	72 to 160 g/g	138

2.6.3 Cellulose nanomaterial as flocculants

Flocculation is a commonly used method to remove very fine suspended solid particles, metals, dyes and other organic matter present in municipal and industrial wastewaters. Flocculants are added to facilitate the collision of colloidal particles in solution to form larger unstable particles referred to as flocs, which eventually precipitates from solution. Often these flocculants induce the formation of flocs by electrostatically interacting with colloidal particles and bridging them to form larger flocs.[139,140] Several characteristic features of CNs make them

ideal candidates for use as flocculants. Firstly, CNs are sustainable, biocompatible and biodegradable, making them a very good alternative to widely used flocculants viz., synthetic polymers derived from oil based sources.[141] Secondly, the high aspect ratio of these CNs give rise to percolation at low concentration inducing the formation of network/floc.[141] It has been found that while forming a percolation network, the higher aspect ratio particles tend to align themselves in a more wavy or tangled pattern as opposed to straight fillers.[142] This would in turn help in containing the particle and formation of floc at low concentration. When the Thirdly, the occurrence of possible gelation as physical and chemical entanglements is reduced due to the electrostatic repulsion and rigidity of CNs which in turn makes the processing easier.[141]

Some early research using CNs as flocculants have shown promising results. Researchers from Niinimäki group developed two generation of anionic CNFs namely dicarboxylic acid CNFs and sulfonated CNFs that can be employed in the coagulation-flocculation treatment of municipal wastewaters.[143,144] These anionic CNFs were produced by nanofibrillation of their parent anionic cellulose derivatives using a homogenizer. Anionic cellulose derivatives used for this process were synthesized via periodate oxidation of cellulose followed by sodium chlorite oxidation to produce dicarboxylic acid cellulose derivate or sulfonation with sodium metabisulfite to produce sulfonated cellulose derivative. The first generation of anionic CNFs viz., dicarboxylic acid CNFs were able to flocculate wastewater efficiently and the dosages required were similar to that of the commercial flocculant. They performed as well as a commercial flocculant in COD removal while the turbidity reduction efficiency with these flocculants was 14-40% lower than commercial flocculant.[143] On the other hand, the second generation of anionic CNFs viz., sulfonated CNFs possessed comparatively higher anionic charge and thus performed better than dicarboxylic acid CNFs in removing turbidity and COD with low dosages, and their performance were comparable to the commercial flocculant.[144] It was also observed that when both CNFs were used as flocculants, there was a considerable reduction in the total chemical consumption relative to coagulation with ferric sulfite alone. The mechanism of this coagulation-flocculation with anionic CNFs relies on the charge

interaction and bridging of particles. Initially, the cationic ferric ion coagulant adsorbs onto the negatively charged particles surface to impart a non-uniform distribution of surface charges. Then anionic CNFs, in turn, produce bridges between these particles via cationic patches resulting in the formation of flocs that sediment. In the case of dicarboxylic acid CNFs, the flocculation performance is due to their high aspect ratio and negatively charged backbone constituting carboxyl groups. Under alkaline pH, these groups make the polymer chain stretch out because of electrostatic repulsion, allowing them to be extended and to produce loops and tails to promote bridging. This in turn enables them to form large flocs with an open structure. However, sulfonic groups present in sulfonated CNFs possess a larger degree of ionization compared to carboxyl groups in dicarboxylic acid CNFs and thus electrostatic affinity toward ferric ion patches of coagulant will be higher. This explains why the flocculation performance of sulfonated CNCs are better than dicarboxylic acid CNFs. They also demonstrated that the wastewater flocs produced with sulfonated CNFs were smaller, rounder and more stable under shear compared to flocs produced with commercial flocculant. Niinimäki and co-workers suggested that anionic CNFs are good alternatives for use as flocculants in the coagulation-flocculation treatment of wastewater.[143,144] Figure 2.20 is a schematic representation of anionic CNFs synthesis and their use in flocculation of fine particles during the coagulation-flocculation treatment of municipal wastewater.

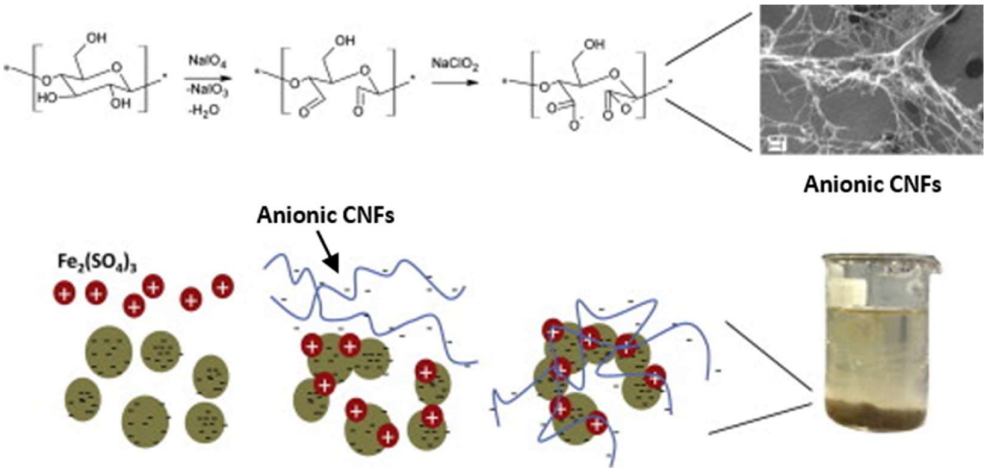

Figure 2.20. Schematic illustration showing the synthesis of anionic CNFs and mechanism of fine particles flocculation by anionic CNFs during coagulation-flocculation treatment of municipal wastewater.[143] (Reprinted with permission from ref. 143 © 2013 Elsevier)

Yu et al. demonstrated that the CNCs produced by the one step citric/HCl hydrolysis of MCC possessed comparatively higher flocculation performance of suspended kaolin clay particles compared to two other types of CNCs derived from H_2SO_4 and formic/ HCl hydrolysis in the coagulation-flocculation. The enhanced performance of the carboxylated CNCs is dependent on the surface chemical groups as these carboxylated CNCs possess more anionic functional groups compared to other types of CNCs with the same specific surface area. These functional groups can act as active binding sites to flocculate suspended particles through charge neutralization mechanism via the electrostatic adsorption with the anion groups of carboxylated CNCs, anionic kaolin and cationic coagulant $CaCl_2$ particles.[93] Quinlan et al. studied the flocculation of an anionic azo dye reactive orange 16 from aqueous solution using cationic CNFs produced by the quaternization of CNFs with GTMAC reagent. They also compared the removal efficiency of CNFs with varying degree of quaternization and they demonstrated that the removal efficiency depended on the charge density on the CNFs. Flocs were formed instantaneously when CNFs with the highest charged density were added to the anionic dye due to the immediate electrostatic interaction between the cationic functional groups on CNFs and anionic groups on dye resulting in charge neutralization and precipitation from solution and the maximum removal efficiency for this system was estimated to be 295.1 mg/g.[140] Similarly Jannah et al. demonstrated the flocculation of another anionic dye ethyl orange using chitosan grafted CNCs.[145] Sun et al. reported on the flocculation of negatively charged bacteria using rod-shaped CNCs. The flocculation of bacteria to form bioflocs is one of the important colloidal activity in water treatment that needs to be controlled. Here the CNCs act as a non-adsorbing system that aid in microbial aggregation by depletion mechanism.[146]

Several other interesting studies have been reported, and they demonstrated the promising potential of CNs based flocculants in other functional areas. They can also be extended for use in water treatment applications, such as TEMPO-oxidized CNFs for flocculation of kaolin clay,[147] ECNCs for flocculation of precipitated calcium carbonate,[148] cationic CNCs grafted with pyridinium groups for flocculation of *Chlorella vulgaris*,[141] CO_2 responsive CNCs grafted with imidazolium groups for flocculation of *Chlorella vulgaris*,[149,150]

and amine functionalized CNCs for the flocculation of negatively charged surfactants.[151] Table 2.5 summarizes the various CNs based flocculants for the flocculation of water contaminants.

Table 2.5. Various CNs based flocculants used for the flocculation of water contaminants.

S.No.	CNs based flocculant	Contaminant	Ref.
1	Dicarboxylic acid CNFs	Municipal wastewater solid particles	143
2	Sulfonated CNFs	Municipal wastewater solid particles	144
3	Carboxylated CNCs	Kaolin clay	93
4	Quaternized CNFs	Reactive orange 16	140
5	Chitosan grafted CNCs	Ethyl orange	145
6	Pristine CNCs	Bacteria (Pseudomonas aeruginosa)	146
7	Carboxylated CNFs	Kaolin clay	147
8	Electrosterically stabilized CNCs	Calcium carbonate	148
9	CNCs grafted with pyridinium groups	Microalgae (Chlorella vulgaris)	141
10	CNCs grafted with imidazolium groups	Microalgae (Chlorella vulgaris)	149,150
11	Amine functionalized CNCs	Negatively charged surfactants	151

2.6.4 Cellulose nanomaterials based water filtration membranes

Water filtration membranes remove contaminants in water by size exclusion and charge mediated adsorption. CNs find applications in these water filtration membranes owing to their nano dimensions, high surface area and good mechanical strength. CN based membranes have been fabricated as pristine CN mats and as CN incorporated polymer composites. CN based membranes have been employed within a wide range of membrane separation processes, such as ultrafiltration, microfiltration, nanofiltration and membrane distillation. The inclusion of CNs within the polymer matrices markedly changes the membrane properties, such as tensile strength, surface hydrophilicity, pore size, porosity, permeability, selectivity and biofouling resistance.[12]

Various CNs incorporated water filtration membranes have been developed. CNCs reinforced polyvinylideneflouride-co-hexafluoropropylene membranes developed by Laila et al. were used in membrane distillation.[152] Metreveli et al. developed *Cladophora* CNCs based

filter paper capable of removing virus (Swine influenza virus) solely based on size exclusion principle.[153] These *Cladophora* CNC based filter paper was further crosslinked using citric acid to make them ideal for removing tracer particles, such as Au nanoparticles as small as 20 nm.[154] *Cladophora* CNC based filter paper prepared by Metreveli et al. were used for the removal of xenotropic murine leukemia virus particles.[155] Karim and co-workers, developed a wide range of CN-based membranes that can be used for wastewater treatment application.[156–158] Nanoporous membranes with CNCs as the functional entities in chitosan matrix were developed to remove cationic dyes, such as victoria blue, methyl violet and rhodamine 6G.[156] In an another study, CN-based functional membranes consisting of CNFs nanopaper dip coated with CNCs having sulfate or carboxyl surface groups were prepared for the removal of heavy metal ions (Ag^{+} and $Cu^{2+}/Fe^{3+}/Fe^{2+}$) from industrial effluents.[157] They have also developed high flux affinity membranes based on layered cellulose nanocomposite membrane consisting of cellulose microfiber sludge as a supporting layer and CNCs in a gelatin matrix as a functional layer for the removal of heavy metal ions (Ag^{+} and $Cu^{2+}/Fe^{3+}/Fe^{2+}$) from industrial effluents.[158] Figure 2.21 shows a schematic representation of the fabrication process of layered cellulose nanocomposite membranes and their use in heavy metal ion capture.

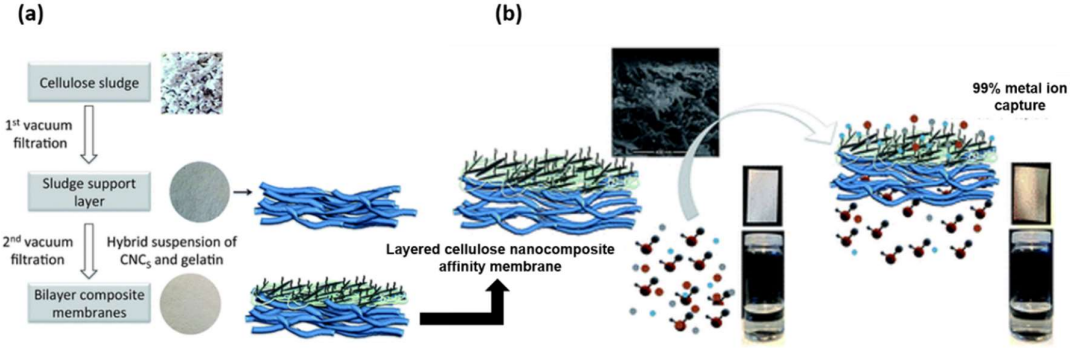

Figure 2.21. (a) The fabrication process of layered cellulose nanocomposite membranes using vacuum filtration process. (b) Heavy metal capture using the layered cellulose nanocomposite membranes.[158] (Reprinted with permission from ref. 158 © 2016 Royal Society of Chemistry)

Researchers from Bismarck's group developed a wide variety of CNFs based nanopapers that can be used as membranes.[159–161] These CNFs based nanopapers can be used for nanofiltration of organic solvents (tetrahydrofuran, n-hexane) and water.[159] They have also enhanced the use of these nanopapers as tight ultrafiltration membranes.[160] Nanopaper ion

exchangers prepared from phosphorylated CNFs can also be used for the continuous removal of Cu(II) from aqueous solution.[161] Polyethersulfone composite membranes blended with CNFs prepared by Qu et al.[162] and cellulose triacetate composite membranes blended with TEMPO oxidized CNFs prepared by Kong et al.[163] were used for ultrafiltration.

Chu and co-workers, prepared a wide range of nanofibrous microfiltration, nanofiltration and ultrafiltration membranes by infusing CNFs into or by creating CNFs based barrier top layer on electrospun poly(acrylonitrile) (PAN) nanofibrous scaffold supported by poly(ethylene terephthalate) (PET) non-woven substrate.[164–171] CNF infused PAN/PET membranes were used to remove bacteria (*Escherichia coli*, *Brevundimonas diminuta*), virus (MS2 Bacteriophage) and dye (Crystal violet) contaminants.[165] Amino modified CNFs infused PAN/PET membranes were used to remove bacteria (*Escherichia coli*), virus (MS2 Bacteriophage) and/or toxic heavy metal ions (Cr^{6+}, Pb^{2+}). Here the amino modified CNFs were prepared by grafting carboxylated CNFs with polyvinylamine.[166] CNF based barrier top layer containing PAN/PET membranes were used to remove virus like MS2 Bacteriophage and for the ultrafiltration of oil/water emulsions.[167,168] They have also prepared PAN/PET membranes containing CNFs based nanocomposite barrier top layer made of either crosslinking poly(ethylene glycol) and CNFs or polymerizing polyamide around CNFs that can be used for filtration purposes.[169,170] Apart from these membranes, thiol modified cellulose nanofibrous composite membranes for the adsorption of Cr(VI) and Pb(II) have been developed as well. Thiol modified CNFs were anchored by thermal crosslinking in an electrospun PAN nanofibrous scaffold to prepare this nanofibrous composite membrane. Here the thiol modification of CNFs was performed by grafting oxidized CNFs with cysteine so as to provide additional active sites for metal ion adsorption, apart from the active sites provided by the high surface area and the carboxyl groups of these CNFs. The q_{max} for Cr(VI) and Pb(II) was estimated to be 87.5 and 137.7 mg/g respectively.[171]

2.6.5 Cellulose nanomaterial for advanced water treatment

Advanced water treatment techniques using catalysts and disinfectants are typically employed for the chemical degradation of contaminants and disinfection of biological hazards,

such as microorganisms. Because of their high surface area, crystallinity, water dispersibility and surface functionalization capabilities, CNs can be used as an ideal support for these catalysts and disinfectants so as to produce systems with increased activity for use in water treatment applications.[172–174]

Various CNs based catalytic systems have been developed to degrade contaminants in water. Wu et al.[175] prepared CNC coated with palladium nanoparticles for the catalytic reduction of methylene blue. Synder et al.[176] have produced CNFs/TiO_2 composite films that were further functionalized with Ag or Au nanoclusters for the photodegradation of methylene blue. Figure 2.22 represents a schematic of the application of CNFs for use as a framework for catalytic films.

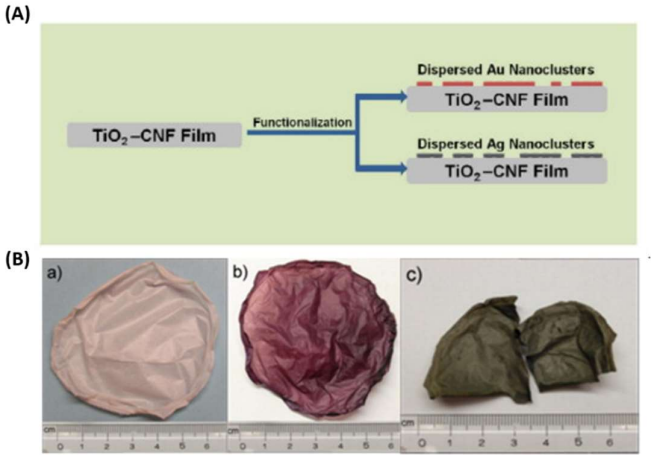

Figure 2.22. (A) Schematic diagram showing the framework of a potential catalytic degradation film based CNFs/TiO_2 composite doped with Au and Ag nanoclusters. (B) Digital images of the (a) dried CNFs/TiO_2 film, (b) Au–TiO_2–CNF film, and (c) Ag–TiO_2–CNF film.[176] (Reprinted with permission from ref. 176 © 2013 Elsevier)

Liu et al.[177] developed CNCs coated with TiO_2 nanoparticles for the photocatalytic degradation of methyl orange dye. Apart from these systems, Kaushik et al.[172] have described various other CN based catalytic systems in their review paper, and these systems have not been explored for use in functional water treatment processes.

There are also many other promising materials based on CNs that can have potential application as disinfectants in water treatment, for instance, researchers have developed various systems, where CNs were modified to possess antibacterial properties by (1) depositing Ag

nanoparticles or nanoclusters on its surface,[42,178–183] (2) depositing ZnO-Ag heterostructure nanoparticles on its surface,[184] (3) conjugating CNs with allicin or lysozyme,[185] as well as (4) coating with antibacterial polyrhodanine.[186] However, these systems have not been tested in functional water treatment processes.

2.6.6 Future perspectives of CNs in water treatment applications

Even though CNs have been widely studied for use in water treatment applications; there are still scope for improvements when compared to conventional materials currently being used. Some of the challenges of CNs are:

1. Currently, they are less cost effective compared to activated carbon and petroleum based polymers,
2. The surface area of CNs is lower when compared to the highest grades of activated carbon are currently available in the market,
3. Due to their high colloidal stability and nanosized dimensions, CNs may be harder to separate in some water treatment processes. Therefore it may be necessary to embed them within matrices. However, their dispersibility within other hydrophobic matrices limits their application in membranes and this necessitates the surface functionalization of CNs before their use.

On the other hand, CNs possess many desirable properties over conventional materials, such as activated carbon and petroleum-based polymers used in water treatment applications. These are:

1. Their production does not require high-temperature processes resulting in the lower emission of carbon dioxide compared to the production of activated carbon. Thus, CNs have less carbon footprint comparatively compared to activated carbon produced by thermal processes,
2. They are more sustainable and environmentally friendly compared to petroleum-based polymer counterparts,
3. Moreover, the increased surface area to volume ratio and quantum size effects of CNs produced from cellulosic sources not only increases the amount of adsorption sites but

also offers the possibility of tuning the surface properties of CNs through molecular modification. This makes CNs ideal for surface functionalization compared to native cellulose, thereby creating active sites for adsorption,

4. They possess good mechanical strength and dispersibility in water, making them ideal for use in filtration membranes and as flocculants respectively.

All these characteristics open the door for their use in various water treatment applications. And in view of the enormous potential of CNs, research and development should focus on reducing the cost of production as well as tailoring their surface functionalities for deployment in wastewater treatment systems. CN supported catalysts and disinfectants are emerging functional nanomaterials that may find new applications in wastewater treatments. We need to exploit new and novel CN based nanohybrids that are intelligent by functionalizing them with responsive moieties that can be tailored to specific applications, such as selective adsorption, simultaneous sensing and scavenging etc. Also, the adoption of these functional nanomaterials in scalable chemical engineering processes needs to be developed as most of the researchers currently only focus on the design and synthesis of functional nanomaterials. This points to the need for collaborative research between material scientists, chemists and chemical engineers, where scalable water treatment processes can be developed and implemented. Considering the pace of work being carried out in all these areas, we believe that the wastewater treatment processes employing these sustainable nanomaterials will become a reality in the near future.

2.7 Summary

In this chapter, a brief introduction on CNs especially CNCs, hydrogels and nanocomposite hydrogels are presented. CN incorporated hydrogels and the effect of incorporation of CNs were reviewed. This chapter also provides a comprehensive review of CN-based systems used for the removal of a plethora of contaminants in wastewater. Adsorbents based on CNs are ideal for removing dyes, heavy metal ions and pharmaceutical compounds in wastewater. Absorbents based on CNs have been proven to be effective for the removal of oil-based contaminants from water. CNs have also been used as reinforcement agents and fillers in the membrane for the filtration of a wide variety of pollutants. Flocculants

based on CNs can flocculate dyes, heavy metal ions, clay particles and bacterial biomass. They can also be used as supports for catalysts and disinfectants for treating organic and pathogenic contaminants in water. Thus, CNs offer many possibilities in water remediation in industries such as textile, pulp and paper, leather tanning, metal plating, mining, paint, fertilizer, food and pharmaceuticals. Based on the current literature review, it can be concluded that the use of CNs for water treatment application is a promising area of research. In this context, addressing the limitation associated with separation and functionality of CNCs for use in large scale water treatment processes will have implications in the near future. Thus, our goal is to develop novel CNCs incorporated nanocomposites with improved properties for use in water treatment applications.

Chapter 3*

Cellulose Nanocrystal–Alginate Hydrogel Beads as Novel Adsorbents for Organic Dyes in Aqueous Solutions

A new generation of recyclable adsorbents comprising of cellulose nanocrystals and alginate (CNC-ALG) with superior adsorption capacity was developed. Sustainable nanomaterials like cellulose nanocrystals (CNCs) derived from pulp fibers and cellulosic biomass are ideal systems for removing contaminants in our water systems as their use will also contribute to the lesser dependence on adsorbents like activated carbon that generate greenhouse gases during its production. Adsorption characteristics of CNC-ALG hydrogel beads were evaluated using batch adsorption studies of a model organic dye called methylene blue (MB) in aqueous solution. The influence of various parameters such as contact time, adsorbent dosage, initial dye concentration, pH, temperature, ionic strength, crosslinking time and bead size on the MB adsorption were also investigated. The measured thermodynamic parameters confirmed a spontaneous exothermic adsorption process. The adsorption kinetics and mechanism of adsorption were best described using pseudo second order kinetic model and intra-particle diffusion model. Equilibrium adsorption data are fitted well using Langmuir adsorption isotherm and a maximum adsorption capacity of 256.41 mg/g was reported, which is comparable to that of activated carbon. We demonstrated that after five adsorption-desorption cycles, the removal efficiency of MB remained at ~97%, and the CNC-ALG hydrogel beads are effective adsorbents for the removal of organic dyes from wastewaters.

*This chapter is adapted from a paper "Nishil Mohammed, Nathan Grishkewich, Richard M. Berry and Kam Chiu Tam, Cellulose Nanocrystal–Alginate Hydrogel Beads as Novel Adsorbents for Organic Dyes in Aqueous Solutions, *Cellulose*, 2015, 22(6), 3725-3738."

3.1 Introduction

Water is one of the commodities essential for the continual prosperity of developed and developing nations. The demand for clean water is increasing due to rapid population growth and industrial activity. Both ground and surface water reservoirs are being polluted by contaminated wastewater from industrial, municipal, and agricultural sources.[1] Among the contaminants that pollute these water bodies, dye-containing effluents from wet processing textile industries are becoming a major issue, especially in countries such as India and China.[187,188] The volume of dye-containing effluent discharged into water bodies in these countries is alarming, both from a toxicological and esthetic perspective,[189] and hence the treatment of these effluents before their discharge is crucial. Methylene blue (MB) is the most common dye used for dyeing cotton, wood and silk. Exposure to MB molecules can cause eye burns, breathing complications, nausea, vomiting, profuse sweating, mental confusion and methemoglobinemia.[90]

Various physical, chemical and biological treatment methods can be employed for dye removal.[2] Among these treatment methods is adsorption, which when implemented using a well-designed system is considered to offer the best solution for producing high quality treated water.[3,4] This technique offers many advantages such as simple design and operation, low initial investment, effectiveness and insensitivity to toxic substances.[2,5,6] Activated carbon is considered the most widely used adsorbent for water treatment. However, the high cost and energy involved in producing and regenerating the absorbent have inspired the development of alternative low-cost adsorbents based on sustainable materials.[3,90]

The use of sustainable nanomaterials such as cellulose nanocrystals (CNCs) for the adsorption of dyes from water was reported recently.[91,92] Previous research from our research group have reported that CNCs possess a very good adsorption capacity for a model cationic dye, MB with a maximum adsorption capacity (q_{max}) of 118 mg/g. It was also found that this q_{max} further increased to 769 mg/g upon the introduction of additional carboxyl groups on the surface of CNC by TEMPO oxidation. These nanomaterials were also found to outperform several conventional adsorbents widely used in developing countries.[92] CNCs are rod-like

nanoparticles obtained from cellulose, having diameters ranging from 5-20 nm and lengths of up to a few hundred nanometers. They can be produced at the industrial scale by acid hydrolysis of pulp fibers. Because of their high specific surface area, good mechanical strength, biodegradability and high functionality,[10] adsorbents based on these nanomaterials have the capacity to remove wide varieties of pollutants from wastewater. However, the separation of these nanomaterials after adsorption requires coagulation and high-speed centrifugation, which limits their applications in large scale water treatment process.[92]

Hydrogels are crosslinked polymer network structures capable of swelling and absorbing large quantities of water without dissolution. They contain various proportions of hydrophilic and hydrophobic components. Due to their high adsorption, recyclability and reusability for continuous processes, these hydrogels have gained a particular interest in wastewater treatment.[54] Alginate is a widely used natural polysaccharide for the preparation of hydrogels. They are obtained from the cell walls of brown seaweed and the sodium salt of this polysaccharide is produced in large scales as sodium alginate. It is an anionic polysaccharide composed of (1-4) linked β-D-mannuronate (M) and α-L-guluronate (G) units linked by β-1, 4 and α-1, 4 glycosidic bonds. In the presence of divalent cations, such as Ca^{2+}, they form hydrogels via ionic crosslinking of calcium bridges between the M and G units of adjacent chains. Alginate is also biocompatible, biodegradable; readily available, inexpensive and non-toxic.[190] Due to the presence of carboxylate groups along the polymeric chains, they are widely used as biosorbents for dyes, metal ions, etc.[191,192]

There is an increasing interest in using sustainable nanomaterials, such as CNCs to remove contaminants from wastewater. However, the practical challenge of separating these high surface area nanoparticles from wastewater needs to be addressed before they can be adopted for use in large-scale wastewater treatment plant. The present research describes a solution to this challenge by impregnating CNCs into alginate hydrogel beads that can be easily separated using sieves after use in batch adsorption system or can be packed in fixed column for continuous water treatment processes. The choice of the alginate biopolymer used for preparing the CNC incorporated hydrogel beads was decided based on several factors. Firstly,

the simplicity in the synthesis procedure as the alginate hydrogel beads can be easily prepared using ionic crosslinking method. Secondly, the materials used for the synthesis of the alginate hydrogel beads, such as sodium alginate and calcium chloride are eco-friendly and sustainable in nature. Thirdly, the inherent ionic charge and porous structure of alginate hydrogel beads can also promote their adsorption capabilities thereby yielding adsorbents with high adsorption capacity and recyclability. The incorporated CNCs can also provide added functionality to this hydrogel system by providing improved surface area, enhanced mechanical property, selectivity through surface modification of CNCs and crosslinking if CNCs are functionalized with crosslinkable groups. Also, the use of porous hydrogel matrix for the treatment of textile effluents can provide an added advantage compared to the hard substrate like activated carbon. The compressible nature of these porous hydrogel beads, as opposed to the hard substrates, provides the ability to squeeze out the adsorbed organic dyes after use in the adsorption process. Thus, these hydrogel beads act as a dye concentrators that help in recycling process for textile dyeing industries. The spent hydrogel matrix material after dye extraction can be burned to generate energy making the entire process, a zero-waste generating process.

Although CNCs have been incorporated into alginate microsphere with the motivation of enhancing the mechanical strength and regulating the drug release behavior,[69] no studies have been reported till date on the use of similar CNC embedded hydrogel beads for removal of organic dyes in aqueous solutions. We demonstrate their utility for the same by examining its performance in the adsorption of MB, a well-known textile dye. The proposed strategy can also mitigate the dependence on commonly used adsorbents, such as activated carbon, which has high activation cost, which also contributes to the release of greenhouse gases during its activation step for wastewater treatment. The potential of using environmentally friendly nanomaterials to remove contaminants from wastewater will have an enormous impact on third world countries where water pollution is becoming a major environmental issue. Figure 3.1 is a schematic illustration showing the synthesis of CNC-ALG hydrogel beads and their use in batch adsorption studies.

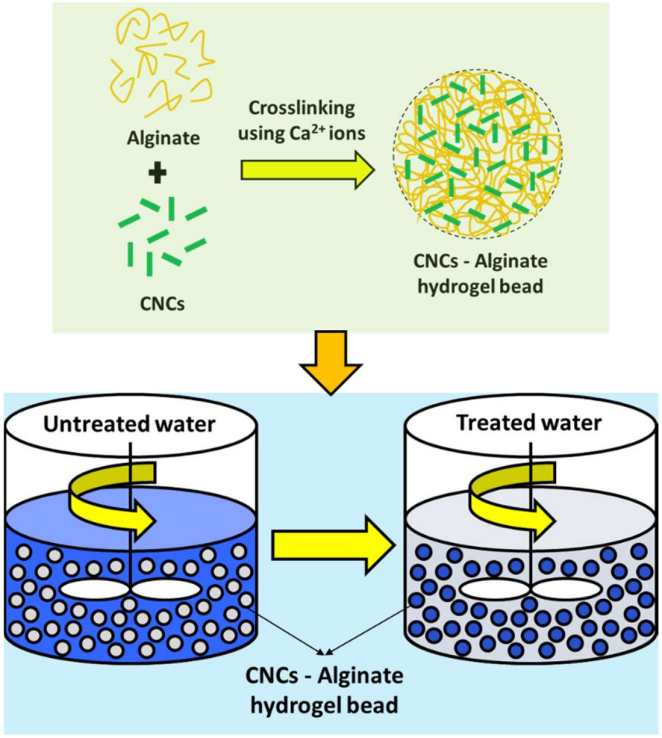

Figure 3.1. Schematic illustration showing the synthesis of CNC-ALG hydrogel beads and their use in batch adsorption studies.

3.2 Experimental section

3.2.1 Materials used

Spray dried CNCs (average dimensions of 100 nm length and 5nm diameter, surface area of ~500 m^2/g) were supplied by CelluForce Inc. Sodium alginate (ALG) was purchased from FMC Biopolymer. Methylene Blue (MB) and Sodium chloride (NaCl) were purchased from Sigma-Aldrich. Calcium chloride ($CaCl_2$) was purchased from Fisher Scientific. All chemicals were used without further purification, and purified water from a Milli-Q Millipore system (>18 MΩcm) was used to prepare the samples.

3.2.2 Preparation of hydrogel beads

CNC-ALG hydrogel beads were prepared by an ionotropic gelation method using Ca^{2+} ions. Depending on the beads, 0.2 to 2 wt% CNCs were thoroughly mixed with 1 to 4 wt% of sodium alginate solution in a homogenizer. The homogenized solution was loaded into syringes and extruded through 22-gauge size needles using a syringe pump at a flow rate of 5 mL/min into 50 mL of 2 wt% $CaCl_2$ solution that was gently stirred to prevent the beads from adhering

to each other. The beads were allowed to crosslink in $CaCl_2$ solution for 15 min, after which they were washed with water to remove residual $CaCl_2$ and the beads were used for batch adsorption studies.

3.2.3 Characterization of hydrogel beads

Digital photographs of pure ALG and CNC-ALG hydrogel beads were recorded for measuring the size. The mean diameter of the hydrogel beads was determined from the optical micrographs using an image analysis software (Analyzing Digital Images). The morphology and porous nature of freeze-dried beads were examined using a field emission scanning electron microcopy (FE-SEM, Zeiss LEO 1550) at 10 kV accelerating voltage.

Gravimetric method is employed to calculate the water content, void fraction and swelling ratio of hydrogel beads. Beads were dried to a constant weight at 40°C and the water content (WC) was calculated using Equation 3.1.

$$WC = \frac{W_w - W_d}{W_w} \tag{3.1}$$

where W_w (g) and W_d (g) are the weights of wet and dried beads respectively. The void fraction (ε) of the CNC-ALG hydrogel beads was calculated from Equation 3.2 based on the density of the bead matrix (alginate and CNC) and the weight change before and after drying.[193]

$$\varepsilon = \left[\frac{(W_w - W_d)/\rho_w}{W_d/\rho_m + (W_w - W_d)/\rho_w} \right] \tag{3.2}$$

where W_w (g) and W_d (g) are given above, and ρ_m and ρ_w are the densities of the bead matrix (ρ_m = 1.60 g/cm^3) and water (ρ_w = 1 g/cm^3) respectively. A fixed amount of freeze-dried hydrogel beads were swollen in Millipore water for 5 h and the acquired water content is calculated as percentage to express the swelling ratio of hydrogel beads.

To study the influence of CNCs on the mechanical properties of hydrogel beads, 0.5 wt% ALG hydrogel beads with and without CNCs were compressed using CETR UNMT testing machine. A constant load of 10 g was applied to compress the hydrogel beads to a constant height and measure the force which it can withstand.

Dynamic light scattering measurements were performed using a Brookhaven light scattering system to further prove that almost all CNCs are incorporated into the gel network formed by alginate. Intensity weighted particle size distribution of $CaCl_2$ crosslinking solution before and after hydrogel bead formation were taken and compared to that CNCs dispersed in water.

3.2.4 Batch adsorption studies

Each batch adsorption experiment was performed by stirring CNC-ALG hydrogel beads at 500 rpm for 1 h in 50 mL of dye solution. All experiments were conducted at neutral pH and 25 °C. The initial and final concentration of the bulk dye was measured using a Cary 100 UV-Vis spectrophotometer. The calibration curve of MB at 664 nm was used to convert the absorption values of MB to its corresponding concentration. Dye removal % and amount of MB adsorbed (q_e) on CNC-ALG hydrogel beads were calculated using the Equation 3.3 and 3.4 respectively.[194,195]

$$\text{Dye Removal } \% = \frac{(C_0 - C_e)}{C_0} \times 100 \tag{3.3}$$

$$q_e = \frac{(C_0 - C_e)V}{m} \tag{3.4}$$

where q_e is the amount of dye adsorbed for 1 g of adsorbent (mg/g), C_e is the equilibrium concentration of free dye molecules in the solution (mg/L), C_0 is the initial dye concentration (mg/L), V is the volume of solution (L) and m is the mass of adsorbent (g).

3.2.5 Effect of various parameters on dye adsorption

The adsorption of dye onto the CNC-ALG hydrogel beads can be influenced by various parameters and hence the effect of contact time, adsorbent dosage, initial dye concentration, pH, ionic strength, crosslinking time, bead size and temperature on their ability to adsorb dye was studied.

3.2.5.1 Effect of contact time

The effect of adsorption time on dye removal was studied by measuring the dye concentration at regular time intervals from 0 to 180 min. Adsorption experiments were carried

out by stirring 445 mg (dry weight basis) of CNC-ALG beads in 50 mL of 200 mg/L dye solution at 500 rpm.

3.2.5.2 Effect of adsorbent dosage

The effect of adsorbent dosage on dye removal was studied by stirring varying amounts (35 to 600 mg (dry weight basis)) of CNC-ALG beads in 50 mL of 200 mg/L dye solution at 500 rpm for 1 h.

3.2.5.3 Effect of initial dye concentration

The effect of initial dye concentration on dye removal was studied by varying the dye concentration from 100 to 1200 mg/L. Adsorption experiments were carried out by stirring 445 mg (dry weight basis) of CNC-ALG beads in 50 mL of dye solution at 500 rpm for 1 h.

3.2.5.4 Effect of pH

The effect of pH on dye removal was studied by performing the dye adsorption studies and changing the pH of the dye solution to 2.5, 6.5 and 10 at 25 °C. Adsorption experiments were carried out by stirring 445 mg (dry weight basis) of CNC-ALG beads in 50 mL of 200 mg/L dye solution at 500 rpm for 1 h.

3.2.5.5 Effect of ionic strength

The effect of ionic strength on dye removal was studied by performing dye adsorption studies in the presence of 0, 0.25, 0.5 and 1 M NaCl. Adsorption experiments were carried out by stirring 445 mg (dry weight basis) of CNC-ALG beads in 50 mL of 200 mg/L dye solution at 500 rpm for 1 h.

3.2.5.6 Effect of cross-linking time

The effect of cross-linking time on dye removal was studied by performing dye adsorption studies using CNC-ALG beads crosslinked in $CaCl_2$ for various time intervals 15, 30 and 60 min. Adsorption experiments were carried out by stirring 445 mg (dry weight basis) of CNC-ALG beads in 50 mL of 200 mg/L dye solution at 500 rpm for 1 h.

3.2.5.7 Effect of bead size

The effect of crosslinking time on dye removal was studied by performing dye adsorption studies using CNC-ALG beads prepared with needles of varying gauge sizes 18G, 22G and 25G inches. These needles produced beads having diameters of 3.4, 2.8 and 1.9 mm respectively. Adsorption experiments were carried out by stirring 445 mg (dry weight basis) of CNC-ALG beads in 50 mL of 200 mg/L dye solution at 500 rpm for 1 h.

3.2.5.8 Effect of temperature

The effect of temperature on dye removal was studied by performing dye adsorption studies at three different temperatures of 25, 35, 45 and 55°C at a pH 7. Adsorption experiments were carried out by stirring 445 mg (dry weight basis) of CNC-ALG hydrogel beads in 50 mL of 200 mg/L dye solution at 500 rpm for 1 h.

3.2.6 Kinetic studies

The kinetics of dye adsorption was studied by measuring dye concentrations of 5 different batches of CNC-ALG hydrogel beads stirred in dye solutions for 3 h. Each batch consisted of 445 mg (dry weight basis) of beads stirred in a dye solution of varying initial concentration (100 mg/L, 200 mg/L, 400 mg/L, 600 mg/L and 800 mg/L) respectively. The dye uptake (q_t) was then plotted against time (t) and analyzed using various models to obtain the kinetic parameters of adsorption.

3.2.7 Adsorption isotherm

The adsorption isotherm of this hydrogel bead system was determined by stirring 445 mg (dry weight basis) of CNC-ALG hydrogel beads with various initial dye concentrations (600 mg/L, 1000 mg/L, 1400 mg/L, 1800 mg/L and 2000 mg/L). Beads were stirred at 500 rpm for 1 h at pH 7 and 25°C. The equilibrium dye uptake (q_e) was then plotted against equilibrium concentration of dye (C_e) and modeled using various mathematical models to determine the adsorption isotherms.

3.2.8 Desorption study

The reusability of CNC-ALG hydrogel beads after dye adsorption was studied via 5 consecutive adsorption – desorption cycles. A mixture of 1 M HCl and 98% ethanol with a volume ratio of 1:1 was chosen as the eluent to restore the adsorption sites of the CNC-ALG hydrogel beads. 75 mg (dry weight basis) of MB preloaded CNC-ALG hydrogel beads were separated from the batch adsorption runs and mixed with 20 mL of eluent, where MB was desorbed from the beads. For each cycle, 15 mL of 50 mg/L dye solution was employed for adsorption and 20 mL of eluent was employed for desorption. The adsorption and desorption cycle was 60 and 30 min respectively.

3.3 Results and discussion

3.3.1 Preparation of hydrogel beads

Hydrogel beads were formulated in varying ratios of CNCs and alginate to study their individual contributions to the adsorption of MB. Figure 3.2a shows the dye removal % of freeze-dried hydrogel beads having a constant 2 wt% ALG and various wt% (0, 0.1, 0.5 and 1 wt%) of CNCs. With increasing CNCs wt%, the percentage dye removal increased. Dye removal % of 2 wt% ALG bead with 1 wt% CNCs is almost three times higher than hydrogel beads with no CNCs. This increase in dye removal % is due to the increased number of adsorption sites contributed by the high surface area CNCs. A non-linear increase in the dye removal % with increase in CNC content was observed and this is possibly due to more aggregation of CNCs within the hydrogel beads at higher CNC content. CNCs tend to undergo gelation in the presence of Ca^{2+} ions which can be also one reason for the aggregation of CNCs. Hence, the adsorption capability of the CNCs is compromised to some extent. However, the effective increase in number of CNC active sites present inside the hydrogel beads still contributed to the non-linear increase in the adsorption. It was also found that, compared to freeze-dried hydrogel beads, wet hydrogel beads displayed better adsorption capacity even with half the adsorbent dosage. This lower adsorption capacity may be attributed to a decrease in porosity as a result of the drying, creating a structural barrier that limits the diffusion of dye molecules to the adsorption sites.[192] Lagoa et al. reported that dry alginate beads possessed a

lower porosity and hence they adsorbed metal ions at a slower rate compared to wet beads.[196] Figure 3.2b shows the dye removal % of wet hydrogel beads having a constant 1 wt% of CNCs and various wt% (2, 1 and 0.5 wt %) of ALG. It shows that the dye removal % increased with decreasing alginate content, due to the better accessibility of dye molecules to the adsorption sites on the CNCs arising from the loose network structure formed on reducing the alginate content. Figure 3.2c and 3.2d shows the improvement in dye adsorption characteristics of 0.5 wt% ALG + 1 wt% CNC hydrogel beads compared to pure 0.5 wt% ALG hydrogel beads. Considering all these results, wet 0.5 wt% ALG + 1 wt% CNC hydrogel beads were chosen for further characterization and adsorption studies.

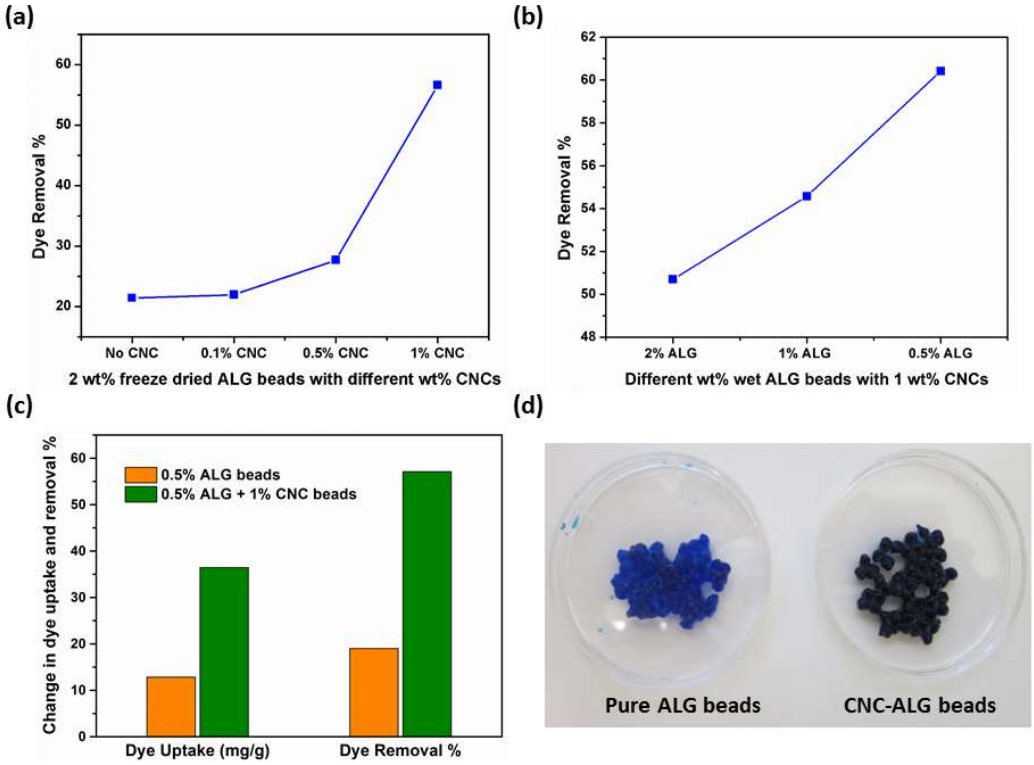

Figure 3.2. (a) Dye Removal % of 2 wt% ALG hydrogel beads with different wt% of CNCs (Concentration of dye solution = 200mg/L, Volume of dye solution = 50 mL, Dosage of freeze-dried hydrogel beads = 200 mg). (b) Dye Removal % of 1 wt% CNC containing hydrogel beads of different wt% ALG (Concentration of dye solution = 200 mg/L, Volume of dye solution = 50 mL, Dosage of wet hydrogel beads = 150 mg). (c) Comparison in dye adsorption properties of pure ALG and CNC-ALG hydrogel beads (Concentration of dye solution = 200mg/L, Volume of dye solution = 50 mL, Dosage of wet hydrogel beads = 150 mg). (d) Illustration of dye adsorption capability of pure ALG and CNC-ALG hydrogel beads.

3.3.2 Characterization of hydrogel beads

Digital photographs of pure ALG (Figure 3.3a) and CNC-ALG (Figure 3.3b) hydrogel beads revealed that the incorporation of CNCs into the ALG hydrogel beads imparted a characteristic white colour. The optical micrograph of wet CNC-ALG hydrogel beads (Figure 3.3c) showed that they possess a smooth and uniform surface with an average diameter of around 2.9 mm (Table 3.1).

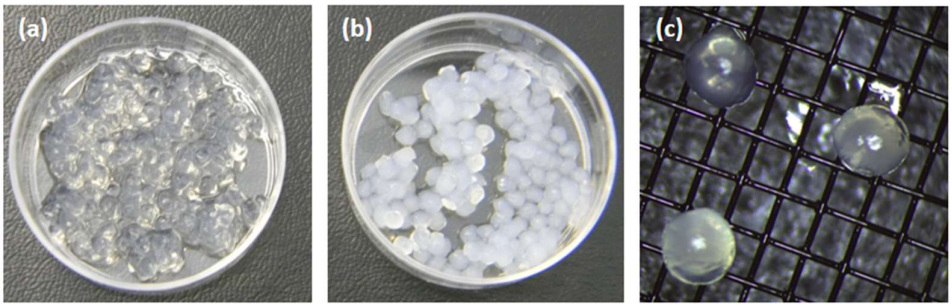

Figure 3.3. (a) Digital photograph of pure ALG hydrogel beads. (b) Digital photograph of CNC-ALG hydrogel beads. (c) Optical micrograph of CNC-ALG hydrogel beads.

Table 3.1. Mean diameter of CNC-ALG hydrogel beads using Analyzing Digital images.

Bead No.	Diameter (mm)
1	2.90
2	2.84
3	2.89
4	2.92
5	2.95
6	2.93
Average	2.905

The surface morphology and porous nature of beads were studied by characterizing the freeze-dried hydrogel beads using SEM. Figure 3.4a and 3.4b shows the surface morphology of both pure ALG and CNC-ALG hydrogel beads. The surface of pure ALG hydrogel beads was smoother and less dense in comparison to the CNC-ALG hydrogel beads. Incorporating CNCs into the hydrogel structure generated more undulations and folds on the bead surface, effectively increasing the surface area available for dye adsorption. These observations are in agreement with those reported previously.[197,198] Figures 3.4c and 3.4d show the crosslinked and porous nature of the CNC-ALG hydrogel beads respectively. Figure 3.4d provides a visual

representation of the porous nature of the hydrogel beads and it does not facilitate the determination of the exact porosity. Moreover, the freeze-dried hydrogel beads used for the SEM experiments does not provide the exact visualization of the porous nature that the hydrogel beads in their native wet swollen state possess.

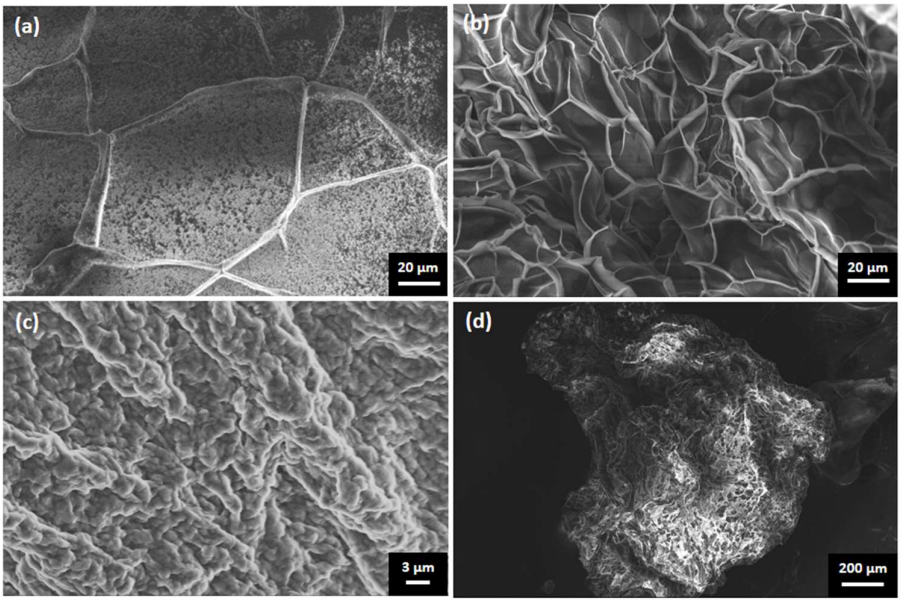

Figure 3.4. (a) Surface morphology of pure ALG hydrogel beads. (b) Surface morphology of CNC-ALG hydrogel beads. (c) Crosslinked nature of CNC-ALG hydrogel beads. (d) Porous nature of CNC-ALG hydrogel beads.

Figure 3.5 summarize the water content and void fraction of the pure ALG and CNC-ALG hydrogel beads. These results indicate the CNCs have a negligible effect on the water content and void fraction of the hydrogel when they are incorporated into its structure. Thus, the addition of CNCs in the ALG hydrogel beads increased the amount of binding sites available for adsorption without compromising their inherent porous nature. This contributed to the improved dye adsorption characteristics of CNC-ALG compared to ALG hydrogel beads.

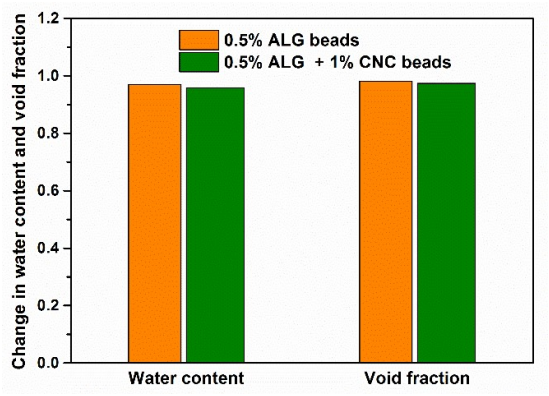

Figure 3.5. (a) Comparison of water content and void fraction of pure ALG and CNC-ALG hydrogel beads.

The swelling ratio (Figure 3.6) of hydrogel beads with and without CNCs were also evaluated and it was found that the CNC-ALG beads have be comparatively lower swelling ratio than that of the ALG hydrogel beads which can be attributed to the high crystallinity of CNCs. This high crystallinity reduces the overall amorphous nature of the hydrogel matrix which is more favorable for swelling. Also, the CNCs that gets entangled within the alginate network chains, contributes to the mechanical reinforcement effect that also, in turn, lowers the swelling ratio.

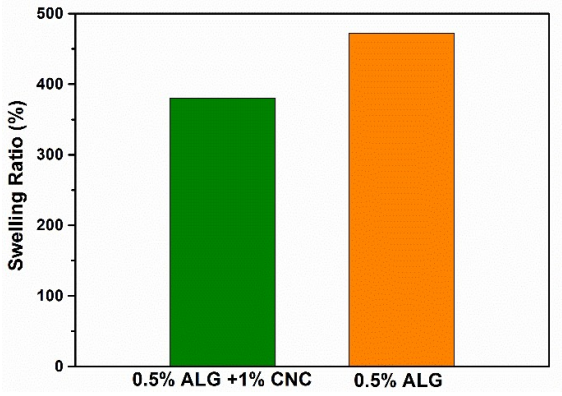

Figure 3.6. (a) The swelling ratio of hydrogel beads.

Apart from this addition of CNCs could also reinforce the hydrogels and various studies have shown that CNCs improved the mechanical properties of hydrogels.[53,66,67] Preliminary compression testing performed on 0.5 wt% hydrogel beads containing varying CNC content (1 – 2 wt% CNC) showed improvement in their compressive strength upon increasing CNCs content. 0.5 wt% ALG hydrogel beads without CNCs were fragile and proper compression

testing could not be done on them. 2 wt% CNC containing hydrogel beads withstood higher force compared to 1wt % CNC containing beads as shown in Figure 3.7.

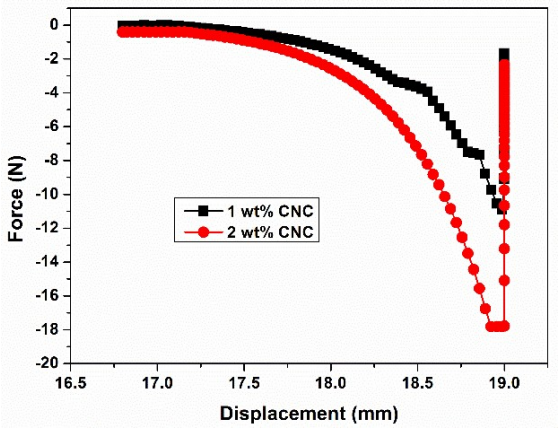

Figure 3.7. (a) Compression testing of 0.5 wt% ALG hydrogels with 1wt % and 2 wt% CNCs.

Dynamic light scattering measurements proved that CNCs were completely entrapped into the hydrogel beads. Intensity weighted particle size distribution (Figure 3.8) of crosslinking solution after bead formation was near to 0 kcps as compared to the CNCs dispersed in water having around 80 kcps. This denotes that CNCs are not present in the crosslinking solution and denotes are CNCs are completely entrapped within gel network formed by alginate.

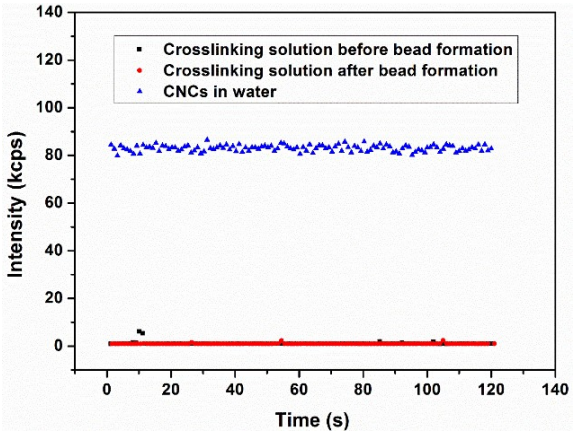

Figure 3.8. Dynamic light scattering measurements to prove the CNCs incorporation into hydrogel beads (Please note that the red dots is overlapping the black dots).

3.3.3 Effect of various parameters on dye adsorption

Effect of various parameters such as contact time, contact time, adsorbent dosage, initial dye concentration, pH, ionic strength, crosslinking time, bead size and temperature on the dye adsorption characteristics of CNC-ALG hydrogel beads are discussed in the following sections.

3.3.4 Effect of contact time

Figure 3.9 shows the effect of contact time on dye removal %. The rapid uptake of dye was observed within the first 30 min, which was followed by a slower uptake process until it approached equilibrium. During the initial stage, there was a large number of vacant sites available for adsorption, and with increasing time the occupied sites induced repulsive interactions between solute molecules on the surface and the bulk solution.[199] From the binding isotherm, the equilibrium time for adsorption was determined to be approximately 1 h, hence all future adsorption studies were performed for a duration of 1 h.

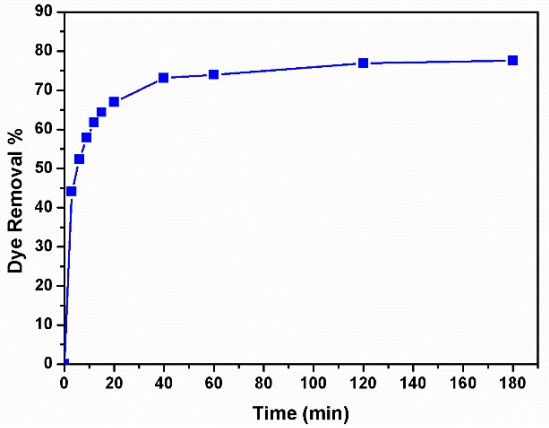

Figure 3.9. Dye removal % of CNC-ALG hydrogel beads with varying contact time.

3.3.4.1 Effect of adsorbent dosage

The effect of adsorbent dosage was investigated by varying the dosage of CNC-ALG beads (adsorbent) from 35 to 600 mg (dry weight basis) in 50 mL of 200 mg/L dye solution. Figure 3.10 shows that with increasing the amount of adsorbent, the dye removal % increased from 57 to 82% and equilibrated at around 445 mg of adsorbent. As the adsorbent dosage was increased, more active sites would be available for dye adsorption and would ultimately enhance dye uptake. This observation is consistent with the results of Deng et al.[200] However, the amount of dye adsorbed per unit mass (q_e) decreased from 150 to 14 mg/g with increasing

adsorbent dosage, which is attributed to the unsaturation of active sites on adsorbent due to the increase in the ratio of adsorption sites to dye molecules.[201]

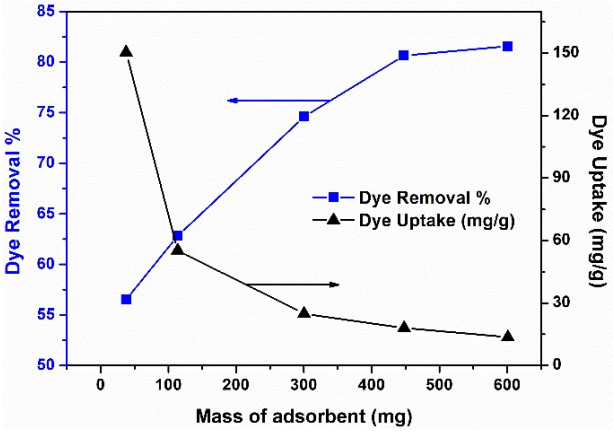

Figure 3.10. Dye removal % of CNC-ALG hydrogel beads with varying adsorbent dosage.

3.3.4.2 Effect of initial dye concentration

Adsorption of MB onto CNC-ALG beads was measured for five different initial dye concentrations for a fixed amount of adsorbent. Figure 3.11 shows that with increasing initial dye concentration, dye removal % initially increased and then decreased gradually. This initial increase in dye removal % at low dye concentration is attributed to the low ratio of initial number of dye molecules to adsorption sites. However, at higher dye concentration, the ratio of increase in dye concentration to the increase in the amounts of dye adsorbed becomes lower due to the availability of less adsorption sites, which agrees with the result of Saha et al.[202] Even though the removal percentage decreased with increasing dye concentration, the amount of dye adsorbed increased from 8 to 89 mg/g for an increase in initial dye concentration from 100 to 1200 mg/L. A higher initial dye concentration provides the driving force for Fickian diffusion between the aqueous and solid phases and the number of dye molecules available for adsorption was greater for the same number of adsorption sites.[194,203]

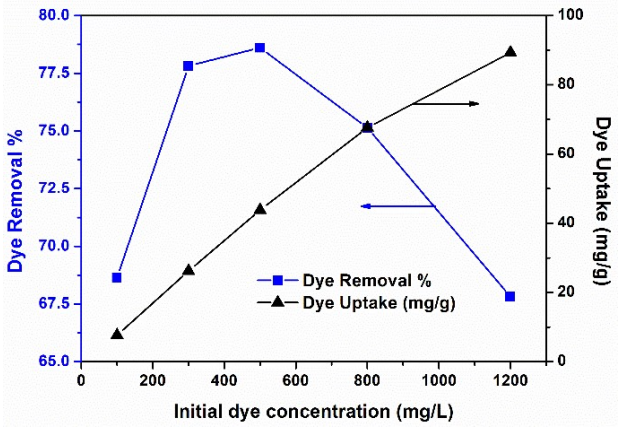

Figure 3.11. Dye removal % of CNC-ALG hydrogel beads with varying initial dye concentration.

3.3.4.3 Effect of pH

The pH of the medium plays a major role in tailoring the surface charge of adsorbent via protonation or deprotonation of the functional groups. Hence understanding the influence of pH on the adsorption capacity of the adsorbent is important. Figure 3.12 shows that when the pH was increased from 2.5 to 10, the dye removal % did not change drastically. However, a slight increase in dye removal % from 82.0 to 84.5% was observed (as shown in the Figure 3.12 inset). This result shows that the CNC-ALG beads can maintain a high adsorption capacity over a wide pH range. For the adsorbents possessing carboxyl ($–COO^-$) and sulfate ($–OSO_3^-$) functional groups, the negative surface charge decreased as pH approached the pKa of the functional groups. The pKa of $–OSO_3^-$ groups on the CNCs is ~1.9,[30] and $–COO^-$ groups on the alginate ranges from 3 to 5.[204] The slight increase in the dye removal % observed for CNC-ALG hydrogel beads in the pH range (2.5 – 10) can be attributed to the change in the ionic characteristics of the alginate chains. There may be an excess of H^+ ions competing with the cationic dye for adsorption sites at low pH. Operating at a higher pH is useful for absorbing more cationic dyes like MB as the surface of the adsorbent would become more anionic with increasing pH as reported previously.[192,198,199,205]

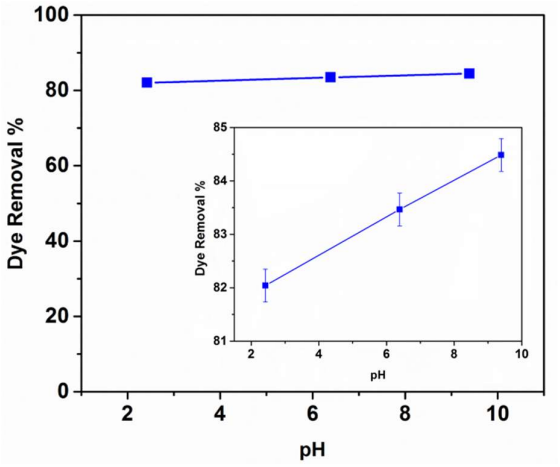

Figure 3.12. Dye removal % of CNC-ALG hydrogel beads with varying pH.

3.3.4.4 Effect of ionic strength

Effluents from the dye industry contain many components, such as acids or alkalis, salts, suspended or dissolved compounds, metal ions and other toxic compounds. The presence of these impurities increases the ionic strength of the medium, which may alter the adsorption performance.[206] The effect of ionic strength on the adsorption of MB was investigated by adding varying amounts of NaCl to the dye solution. Figure 3.13 shows that when the ionic strength was increased from 0 to 1 M, the dye removal % decreased significantly from 75 to 7%. This can be attributed to the screening of electrostatic interactions between the adsorbent and dye molecules due the presence of Na^+ and Cl^- ions in the solution.[207,208]

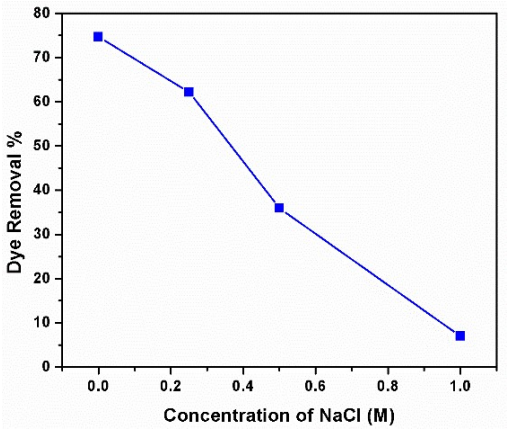

Figure 3.13. Dye removal % of CNC-ALG hydrogel beads with varying ionic strength.

3.3.4.5 Effect of crosslinking time

Figure 3.14 shows that the dye removal % did not decrease drastically with the increase in the crosslinking time for the time range used in this study. However, a slight decrease in the dye removal % from 69.08 to 68.35 % was observed with increasing cross-linking time (as shown in the Figure 3.14 inset). This can be attributed to the fact that with increasing crosslinking time, more Ca^{2+} ions can diffuse into the beads and increase the crosslinking density within the beads. This in turn reduces the free volume, i.e., the number of binding sites per unit volume of gel and the amount of dye adsorption decreases accordingly.[209]

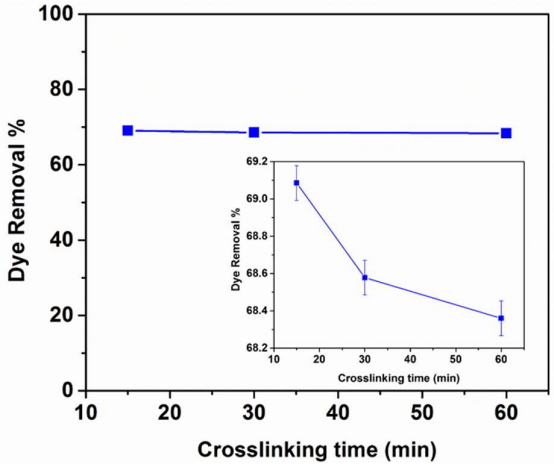

Figure 3.14. Dye removal % of CNC-ALG hydrogel beads with varying crosslinking time.

3.3.4.6 Effect of bead size

The size of the beads depends on many factors, such as needle diameter, charge applied to the bead surface, viscosity and concentration of the alginate solution. An easy way to control the bead size is to use needles with the desired diameter as identified by its gauge number. To study the effect of bead size on dye adsorption, beads were produced using needles of various gauge sizes. As shown in Figure 3.15, the dye removal % did not increase drastically with decreasing the size of the beads. However, a slight increase in the dye removal % from 83.49 to 85.80 % was observed with decreasing size of beads (as shown in the Figure 3.15 inset). This can be attributed to the higher external surface area of smaller beads and the availability of functional groups that are responsible for dye adsorption on the bead surface.[210]

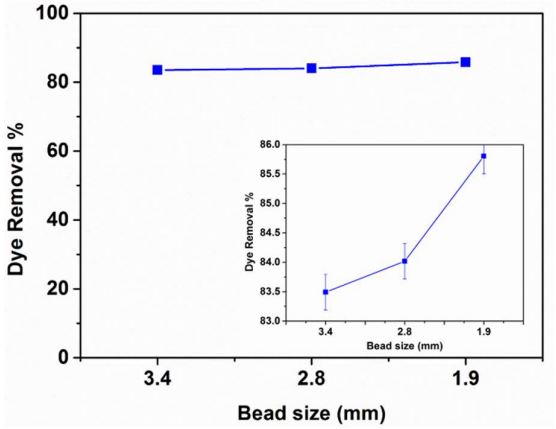

Figure 3.15. Dye removal % of CNC-ALG hydrogel beads with varying bead size.

3.3.5 Thermodynamic study

The effect of temperature is an important parameter to be studied to understand the thermodynamics of adsorption. It was found that the dye removal % decreased from 77 to 69% when the temperature was increased from 25 to 55°C as shown in Figure 3.16a, which suggests that dye adsorption becomes less favorable at higher temperatures. To further understand the effect of temperature on the adsorption process, thermodynamic parameters, such as standard free energy (ΔG°), enthalpy (ΔH°) and entropy (ΔS°), were determined using the following equations:

$$K_d = \frac{C_a}{C_e} \tag{3.5}$$

$$\Delta G = \Delta H° - T\Delta S° \tag{3.6}$$

$$\ln K_d = \left(\frac{\Delta S°}{R}\right) - \left(\frac{\Delta H°}{RT}\right) \tag{3.7}$$

where K_d is the distribution coefficient for the adsorption, C_a is the amount of dye (mg) adsorbed on the adsorbent per liter of the solution at equilibrium and C_e is the equilibrium concentration (mg/L) of the dye in the solution, T is the solution temperature (K) and R is the gas constant. ΔH° and ΔS° were calculated from the slope and intercept of Van't Hoff plots of ln K_d versus 1/T (Figure 3.16b). The results are summarized in Table 3.2.

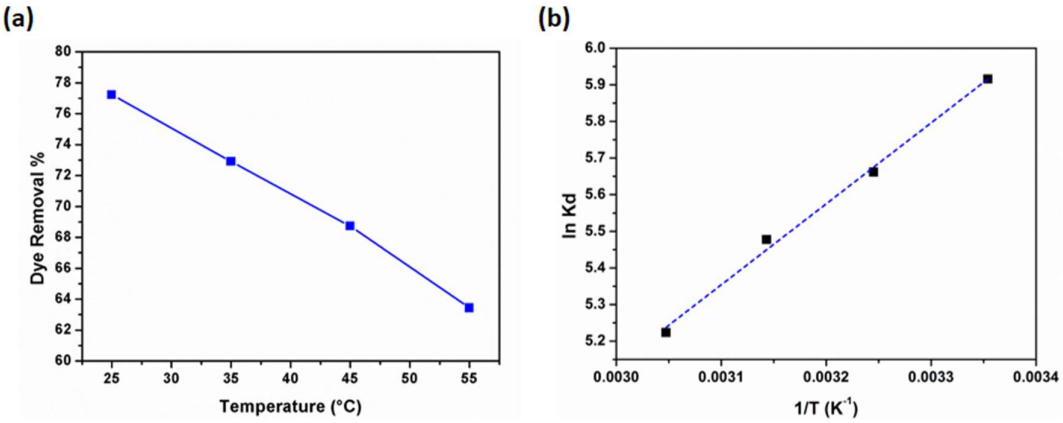

Figure 3.16. (a) Dye removal % of CNC-ALG hydrogel beads with varying temperature. (b) Plot of ln K_d versus 1/T.

Table 3.2. Thermodynamic parameters for adsorption of MB on CNC-ALG hydrogel beads.

Temperature (°C)	K_d (L/g)	$\Delta G°$ (KJ mol^{-1})	
25	370.85	-14.66	**$\Delta H°$ = -18.39 kJ mol^{-1}**
35	287.59	-14.54	**$\Delta S°$ = -12.50 J mol^{-1} K^{-1}**
45	239.21	-14.41	
55	185.50	-14.29	

The distribution coefficient (K_d) is a useful parameter describing the capability of the alginate hydrogel beads to retain a solute and also the extent of its diffusion in a solution.[211] It can be also used to compare the adsorption capacities of different adsorbents, when measured under similar conditions.[212] The values of K_d were further used to determine $\Delta H°$, $\Delta S°$ and $\Delta G°$, $\Delta H°$ and $\Delta S°$ were found to be −18.39 kJ $mol^{-1}$and −12.50 J $mol^{-1}K^{-1}$ respectively. Negative $\Delta H°$ values reflect the exothermic nature of the process, whereas a small negative value $\Delta S°$ suggests that no noticeable change in the structure of the CNC-ALG hydrogel beads occurs during the adsorption process. Our results agree with previous studies.[213,214] Generally, the absolute magnitude of free energy change for physisorption is between −20 and 0 kJ mol^{-1}, and chemisorption has a range of −80 to −400 kJ mol^{-1} [215]. $\Delta G°$ values calculated for the dye adsorption onto CNC-ALG hydrogel beads at temperatures 25, 35, 45 and 55°C were −14.66, −14.54, −14.41 and -14.29 kJ mol^{-1} respectively, with an initial concentration of 200 mg/L. Hence, this process can be considered as physisorption, and the negative values of $\Delta G°$ indicate that the adsorption process is spontaneous. It can be also noted that $\Delta G°$ increases with increasing temperature, suggesting a decrease in adsorption with temperature. The decrease in

adsorption capacity with increasing temperature may be influenced by the weakening hydrogen bonding and van der Waals interaction between the adsorbent and adsorbate.[216,217]

3.3.6 Kinetic studies

The adsorption kinetics were studied to elucidate the rate of dye adsorption, adsorption mechanism and possible rate-controlling steps.[102,218] The influence of adsorption time on the dye adsorption capacity of CNC-ALG hydrogel beads for various initial dye concentrations is shown in Figure 3.17a. In the present investigation, the adsorption data was analyzed and simulated using three kinetic models, namely the pseudo-first-order, pseudo-second-order kinetic and intraparticle diffusion models. These models can be expressed in the following forms:

Pseudo-first-order model.[219]

$$\frac{dq_t}{dt} = k_1(q_e - q_t) \tag{3.8}$$

Pseudo-second-order model.[220]

$$\frac{dq_t}{dt} = k_2(q_e - q_t)^2 \tag{3.9}$$

Intra-particle diffusion model.[221]

$$q_t = k_{id}\sqrt{t} \tag{3.10}$$

where q_e (mg/g) is the amount of dye adsorbed at equilibrium, q_t (mg/g) is the amount of dye adsorbed at time t (min), and k_1 (min^{-1}) is the rate constant of the pseudo-first-order model, k_2 (g mg^{-1} min^{-1}) is the rate constant of the pseudo-second-order model and k_{id} (mg g^{-1} $min^{-1/2}$) is the intra-particle diffusion rate constant. The initial absorption rate constant k_{2i} (mg g^{-1} min^{-1}) for the pseudo-second-order absorption kinetic model can be calculated using the Equation 3.11.[222]

$$k_{2i} = k_2 q_e^2 \tag{3.11}$$

The experimental kinetic data for various initial dye concentrations was fitted using the linearized form of the pseudo-first-order (Equation 3.12**)** and pseudo-second-order model equation (Equation 3.13) respectively to determine the kinetic parameters of adsorption.

$$\log(q_e - q_t) = \log q_e - \frac{k_1}{2.303}t \tag{3.12}$$

$$\frac{t}{q_t} = \frac{1}{k_2 q_e^2} + \frac{1}{q_e} t \qquad (3.13)$$

For the pseudo-first-order model, the rate constant (k_1) and q_e were determined from the slopes and intercepts of log ($q_e - q_t$) versus t. For the pseudo-second-order model, the rate constant (k_2) and q_e were determined from the slope and intercepts of t/q_t versus time t plots. The value of q_e determined experimentally q_e(expt), calculated q_e(calc), and the correlation coefficient (R^2) together with the kinetic adsorption rate constants k_1, k_2 and k_{2i} are summarized in Table 3.3. It was observed that the R^2 values for the pseudo-first-order kinetic model were lower than those for the pseudo-second-order kinetic model. The pseudo-second-order kinetic model gave a linear plot with an average regression coefficient of $R^2 = 0.99$. Also, q_e(calc) using pseudo-second-order kinetic model agreed well with q_e(expt), confirming that the kinetics of dye adsorption by CNC-ALG hydrogel beads are better described by the pseudo-second-order kinetic model rather than the pseudo-first-order model. The kinetic adsorption data and the prediction using the pseudo-second-order model are depicted using Figures 3.17a and 3.17b respectively.

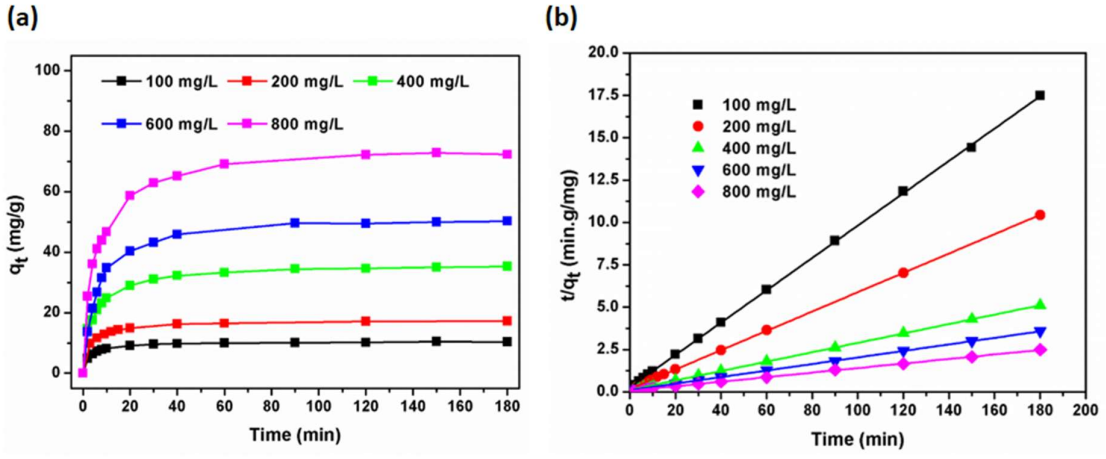

Figure 3.17. (a) Plot of qt versus time for various initial dye concentrations. (b) Pseudo-second-order kinetic model fitting for batch adsorption of MB of various initial dye concentrations on CNC-ALG hydrogel beads.

Table 3.3. Adsorption kinetic parameters for MB on CNC-ALG hydrogel beads estimated using (a) Pseudo-First-Order and (b) Pseudo-Second-Order Model.

(a) Pseudo-First-Order Model					
Concentration (mg/L)	**q_e(expt) (mg/g)**	**q_e(calc) (mg/g)**	**K_1 (min^{-1})**	**R^2**	**Standard error**
100	10.41	3.03	0.025	0.83	16.55
200	17.24	5.43	0.031	0.95	8.59
400	35.28	14.58	0.030	0.93	10.46
600	50.29	24.75	0.034	0.93	10.80
800	72.84	35.77	0.032	0.94	9.68

(b) Pseudo-Second-Order Model						
Concentration (mg/L)	**q_e(expt) (mg/g)**	**q_e (calc) (mg/g)**	**K_2 (g mg^{-1} min^{-1})**	**K_{2i} (mg g^{-1} min^{-1})**	**R^2**	**Standard error**
100	10.41	10.48	0.03	3.66	0.99	0.72
200	17.24	17.51	0.02	5.45	1.00	0.44
400	35.28	35.97	0.01	8.23	0.99	0.58
600	50.29	51.81	0.00	9.45	0.99	0.58
800	72.84	74.63	0.00	14.41	0.99	1.04

Kinetic modelling using pseudo-second-order model also showed that as the initial dye concentration increased, the initial adsorption rate constant (k_{2i}) increased while the rate constant of adsorption (k_2) decreased. This explains that the rate of adsorption depends on the concentration of dye molecules. With the increase in the dye concentration, the higher amount of dye molecules contributed to the increased concentration gradient promoting increased adsorption rate at the initial phase (k_{2i}). However, the overall adsorption rate (k_2) decreases considering the longer time it takes to reach the equilibrium.

Since the adsorption process involves the transport of dye molecules from the bulk solution to the pores of the adsorbent beads, this transport process could be considered as the rate determining step. Since both the rate models cannot identify the diffusion mechanism during the adsorption process, our experimental data was also tested using intra-particle diffusion model. The experimental kinetic data for various initial dye concentrations was fitted using the linearized form of the intraparticle diffusion model (Equation 3.14) wherein the k_{id} and C provide can be obtained from the slope and intercept of q_t vs $t^{0.5}$ plots.

$$q_t = k_{id} t^{0.5} + C \tag{3.14}$$

Figure 3.18a and 3.19a to 3.19d are the plots of q_t versus $t^{0.5}$ for 100, 200, 400, 600 and 800 mg/L dye concentration. It was observed that all these plots were not linear over the whole-time range, suggesting that more than one process affected the adsorption. The three stages in the plot describe the mass transfer of dye into the CNC-ALG hydrogel beads wherein the first stage could be explained using boundary layer diffusion and second two stages using intraparticle diffusion. According to intraparticle diffusion model, the if the plot passed through the origin, intraparticle diffusion was the sole rate-limiting step and if not boundary layer diffusion controlled the adsorption to some degree.[223,224] As seen in the figures, the lines did not pass through the origin and all the plots have an intercept which implies that intraparticle diffusion was not only the rate limiting step. The intercept value, C of the plots denotes the boundary layer thickness and intercept observed for all these plots suggest that a boundary layer resistance between the adsorbate and adsorbent is the rate-limiting factor for the adsorption process.

The intraparticle diffusion constants $k_{id.1}$, $k_{id.2}$ and $k_{id.3}$ which describe the diffusion rates of different stages of the adsorption process could be determined from the three slopes, each corresponding to one diffusion behavior. The numerical values of these intra-particle diffusion constants are summarized in Table 3.4.

Table 3.4. Intra-particle rate parameters for various initial dye concentrations.

Concentration (mg/L)	**$k_{id.1}$ (mg g^{-1} $min^{-0.5}$)**	**$k_{id.2}$ (mg g^{-1} $min^{-0.5}$)**	**$k_{id.3}$ (mg g^{-1} $min^{-0.5}$)**
100	2.05	0.51	0.07
200	2.41	0.85	0.14
400	6.15	2.35	0.33
600	12.58	3.47	0.52
800	13.15	5.84	0.71

The adsorption rate displays the trend, $k_{id.1} > k_{id.2} > k_{id.3}$, which suggests that a rapid first stage controls diffusion of dye molecules into the bead, and a slower second and a much slower third stage until it reached an equilibrium. The first stage corresponds to the rapid diffusion ($k_{id.1}$) of large amounts of dye molecules (about 50%) from the bulk dye solution to the surface of the adsorbent. When the adsorption sites on the exterior surface become saturated, dye

molecules enter the pores described by the $k_{id.2}$ in the second stage. With dye molecules entering the pores, the diffusion resistance increases, leading to a reduction in the diffusion rate ($k_{id.2}$). In the third stage, dye molecules diffuse into the interior of the adsorbent described by $k_{id.3}$, and the rate of diffusion slowly decreases until the system reaches equilibrium.

The obtained rate parameters $k_{id.1}$, $k_{id.2}$ and $k_{id.3}$ were also plotted and correlated with the initial dye concentrations. The intra-particle diffusion parameter could also be correlated to the initial dye concentration by an equation of the form:

$$k_{id.i} = A_i \text{ (Initial dye concentration)}^{B_i} \quad (3.15)$$

$$\log k_{id.i} = \log A_i + B_i \log \text{(Initial dye concentration)} \quad (3.16)$$

where the subscript i possesses values 1, 2 or 3 referring to the diffusion parameters in the three regions respectively.[225] A plot of log k_{id} versus log (Initial dye concentration) in the three regions is shown in Figure 3.18b, and it was observed that when the initial dye concentration was increased, intra-particle diffusion rate would increase correspondingly.

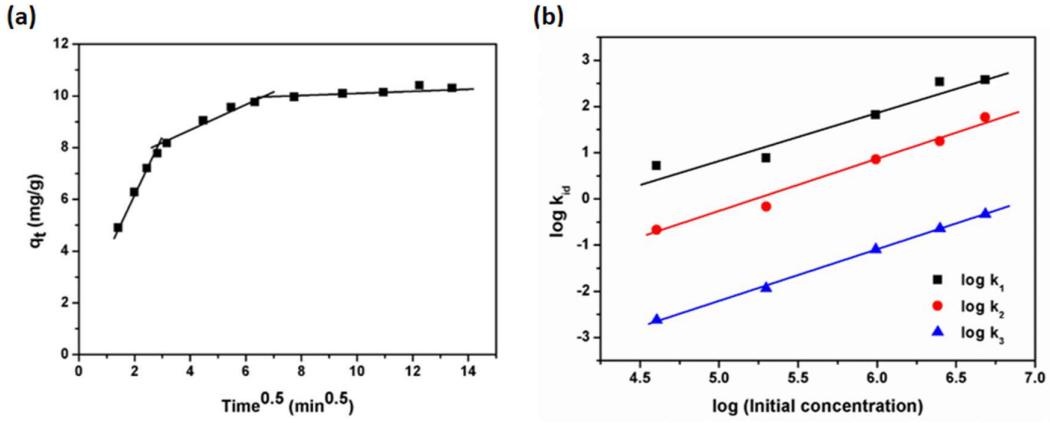

Figure 3.18. (a) Intraparticle diffusion kinetic model fitting for batch adsorption of 100 mg/L MB solution on CNC-ALG hydrogel beads. (b) The plot of log k_{id} versus log (initial dye concentration).

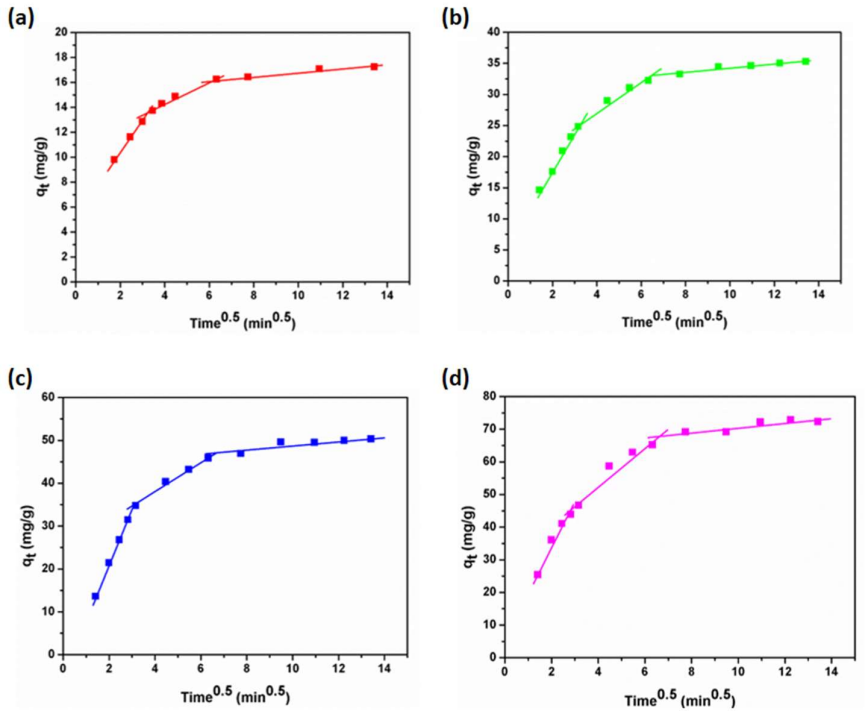

Figure 3.19. Plot of q_t versus $t^{0.5}$ for (a) 200mg/L (b) 400 mg/L (c) 600 mg/L (d) 800 mg/L initial dye concentration.

3.3.7 Adsorption isotherm

An equilibrium between adsorption and desorption will be established, when an adsorbent is exposed to an adsorbate for longer period of time and for the development of an adsorption process, it is necessary to have a sound understanding on the properties of the system at equilibrium. Adsorption isotherms are normally used to model the equilibrium adsorption process and they describe the equilibrium of an adsorption system at a constant temperature by relating the concentration of adsorbate in the bulk to the specific adsorption of the adsorbent. There are several adsorption isotherm models used to describe the equilibrium distribution. Two commonly used adsorption isotherm models, the Langmuir and Freundlich adsorption isotherms, were used to fit our experimental data.

The Langmuir isotherm model assumes monolayer adsorption over a homogeneous adsorbent surface with adsorption sites that are identical and energetically equivalent. The Langmuir isotherm can be mathematically expressed by Equation 3.17.[226]

$$q_e = \frac{q_m K_L C_e}{1 + K_L C_e} \qquad (3.17)$$

where q_e is the amount of dye adsorbed per g of adsorbent (mg/g) at equilibrium, q_m is the maximum amount of dye that can be adsorbed per g of adsorbent (mg/g) in equilibrium, C_e is the equilibrium concentration of free dye molecules in the bulk solution (mg/L), and K_L is a constant related to the energy of adsorption (L/mg) which shows the affinity between the dye and adsorbent. The values of K_L and q_m can be extracted by using the linearized form of the Langmuir isotherm (Equation 3.18). The linearized form of the Langmuir isotherm can be represented by a plot of $1/q_e$ versus $1/C_e$, where q_m and K_L can be found from the intercept and slope, respectively.

$$\frac{1}{q_e} = \frac{1}{K_L q_m C_e} + \frac{1}{q_m} \tag{3.18}$$

Furthermore, a dimensionless constant obtained from the Langmuir model, R_L (Separation factor) can be used to determine the favorability and feasibility of the adsorption process. R_L can be calculated from Equation 3.19.[227]

$$R_L = \frac{1}{1 + K_L C_0} \tag{3.19}$$

where C_0 is the initial dye concentration in solution (mg/L) and K_L is the Langmuir constant (L/mg). The isotherm is unfavorable if $R_L > 1$, linear if $R_L = 1$, favorable if $0 < R_L < 1$ and irreversible if $R_L = 0$.

The Freundlich model assumes multilayer adsorption with non-uniform distribution of adsorption heat and affinities over a heterogeneous adsorbent surface. The Freundlich isotherm can be mathematically expressed using Equation 3.20.[228]

$$q_e = K_F C_e^{1/n} \tag{3.20}$$

where q_e is the amount of dye adsorbed per g of adsorbent (mg/g) at equilibrium, K_F is related to the adsorption capacity, 1/n is heterogeneity factor which ranges from 0 to 1 and C_e is the equilibrium concentration of free dye molecules in the solution (mg/L). The values of K_F and 1/n can be extracted by using the linearized form of the Freundlich isotherm (Equation 3.21). The linearized form of the Freundlich isotherm can be represented by a plot of log q_e versus log C_e, where K_F and 1/n can be determined from the intercept and slope respectively.

$$\log q_e = \log K_F + \frac{1}{n} \log C_e \tag{3.21}$$

Values of 1/n also indicate whether the adsorption process is irreversible (1/n=0), favorable (0<1/n<1) and unfavorable (1/n >1).[198] The calculated parameters q_m, K_L, K_F, n and the correlation coefficients (R^2) are summarized in Table 3.5. The R^2 values of the linear form of Langmuir model were much closer to unity in comparison of those from the Freundlich model, indicating that the Langmuir isotherm better describes the adsorption process.[227] The maximum adsorption capacity (q_m) of the CNC-ALG hydrogel beads was found to be 256.4 mg/g for MB, which is a significant improvement over the dye adsorption capacity of CNC alone (118 mg/g) reported previously.[92] Considering the monolayer adsorption characteristics of Langmuir adsorption isotherm, it can be inferred that the adsorption of the dye occurs in a monolayer pattern along the entire porous hydrogel bead matrix comprising of CNCs and alginate polymer. The linearized Langmuir and Freundlich adsorption isotherm plots are shown Figures 3.20a and 3.20b respectively.

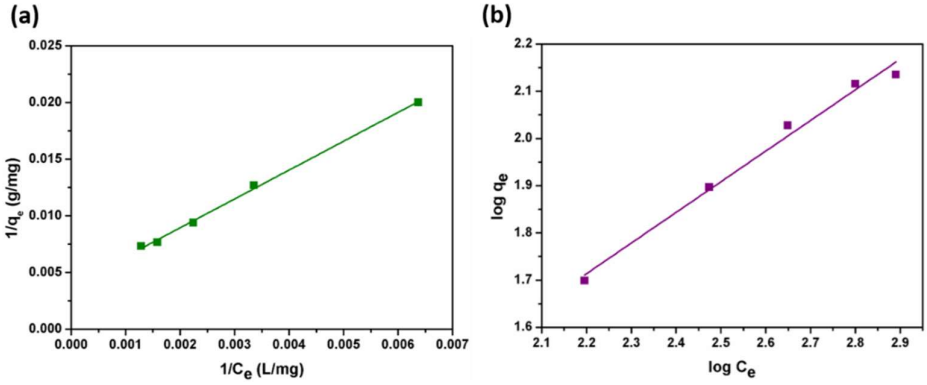

Figure 3.20. Linearized (a) Langmuir (b) Freundlich plots for adsorption of MB onto CNC-ALG hydrogel beads.

Table 3.5. Langmuir and Freundlich constants and regression coefficients of linearized plots for adsorption of MB on CNC-ALG hydrogel beads.

Model	**Parameters**			
Langmuir	**q_m**	**K_L**	**R^2**	**Standard error**
	256.410	0.002	0.998	0.0001
Freundlich	**n**	**K_F**	**R^2**	**Standard error**
	1.541	1.931	0.988	0.0346

The R_L values for various initial dye concentrations were also found to be between 0 and 1, indicating that the adsorption is favorable (Figure 3.21). Also, the values of 1/n calculated

using Freundlich model equation, were smaller than 1, again indicating the favorable adsorption conditions.

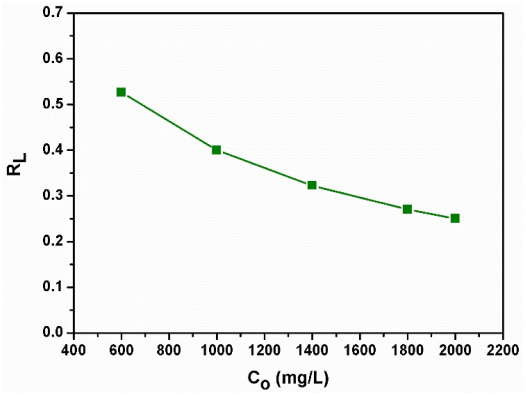

Figure 3.21. The plot of separation factor at various initial dye concentrations.

3.3.8 Desorption study

Adsorbent reusability can be important if the material has to be employed in practical wastewater treatment systems. The reusability of CNC-ALG hydrogel beads was examined through repeated adsorption–desorption cycles. After regenerating the beads using a 1:1 HCl – ethanol eluent mixture, the removal efficiency of MB after five adsorption-desorption cycles remained at ~97% and their adsorption capacity was almost fully recovered as shown by their adsorption capacity over 5 adsorption cycles (Figure 3.22). From this result, it can be concluded that the adsorbent can be readily regenerated and has considerable potential in wastewater treatment applications.[198]

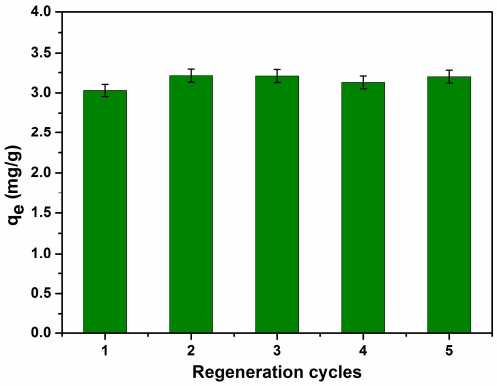

Figure 3.22. The adsorption capacity of CNC-ALG hydrogel beads for MB during regeneration cycles.

3.4 Conclusions

CNC-ALG hydrogel beads were prepared and their dye adsorption behavior was investigated in batch adsorption studies. These hydrogel beads displayed improved adsorption capabilities in comparison to pure ALG hydrogel beads. Adsorption isotherm studies revealed that the Langmuir isotherm described the adsorption process better than the Freundlich isotherm, and the maximum adsorption capacity of these hybrid hydrogel beads was found to be 256.4 mg/g for MB. CNC-ALG hydrogel beads were also found to be reusable, as these hydrogel beads showed more than 97% dye removal efficiency even after 5 successive adsorption-desorption cycles. All these results indicate that CNC-ALG hydrogel beads can be used as an effective adsorbent for the removal of dyes and has the potential to be used in industrial and environmental applications.

Chapter 4*

Continuous Flow Adsorption of Methylene Blue by Cellulose Nanocrystal–Alginate Hydrogel Beads in Fixed Bed Columns

The adsorption behavior of methylene blue by cellulose nanocrystal-alginate (CNC-ALG) hydrogel beads in a fixed bed column was studied by varying the initial dye concentration, bed depth and flow rate. An unusual phenomenon was observed in the early phase of the adsorption, and the phenomenon was elucidated by varying other critical design parameters, such as the flow direction, diameter of column and composition of adsorbent. The swelling and shrinkage of hydrogel beads during the adsorption was responsible for the anomalous concentration versus time profile of the adsorption process. The maximum adsorption capacity of the column was 255.5 mg/g, which is in agreement with the batch study determined from the Langmuir adsorption isotherm. Moreover, a comprehensive understanding of the adsorption mechanism of the CNC-ALG hydrogel beads during the early stages of adsorption was derived from this study.

*This chapter is adapted from a paper "Nishil Mohammed, Nathan Grishkewich, Herman Ambrose Waeijen, Richard M. Berry and Kam Chiu Tam, Continuous Flow Adsorption of Methylene Blue by Cellulose Nanocrystal–Alginate Hydrogel Beads in Fixed Bed Columns, *Carbohydrate Polymers*, 2016, 136, 1194-1202."

4.1 Introduction

Dyes used across textile industries, pulp and paper industries, dye and dye intermediate industries, pharmaceutical industries, tannery and kraft bleaching industries etc. are considered one of the important organic contaminants introduced to the natural water resources or wastewater streams.[229] This is alarming both from toxicological and esthetical perspectives and hence the treatment of this dye effluent before discharging into water bodies is crucial [189]. Several researchers have considered methylene blue (MB) as a model cationic organic dye for adsorption studies.[92,218,230] This is because of the high solubility of MB in aqueous solution and harmful side effects of MB which necessitates its removal from waste water.[90,231,232] MB is used extensively for dying cotton, wood and silk and exposure to MB molecules can cause eye burns, breathing complications, nausea, vomiting, profuse sweating, mental confusion and methemoglobinemia.[90]

Among the various treatment methods employed for dye removal, adsorption is considered superior because of its simple design and operation, low initial investment, effectiveness and insensitivity to toxic substances.[2,5,6] Moreover, this technique when performed using a well-designed system offers the best results that produce high quality treated water.[3,4] Activated carbon produced from various sources is the most widely used adsorbent for wastewater treatment.[195,233,234] However, the high cost and energy involved in its production and regeneration has resulted in an increasing interest to develop alternative low-cost adsorbents, such as rice husk, fly ash, hazelnut shell, banana peel, orange peel, kaolin etc.[2]

Recently, our group has demonstrated that adsorbents based on the sustainable nanomaterial called cellulose nanocrystals (CNCs) can outperform the adsorption capacity of these non-conventional low-cost adsorbents.[92] CNCs are rod-like nanoparticles having a diameter of 10-20 nm and lengths of several hundred nanometers obtained by the H_2SO_4 hydrolysis of pulp fibers.[235] These CNCs possess high specific surface area, good mechanical strength, biodegradability and high functionality.[10] Moreover, the use of CNCs provides a more sustainable alternative compared to other conventional nanostructures produced from petrochemical and activated carbon sources because of the negligible carbon footprint,

biodegradability and non-toxicity. Reports suggest that the CNCs can be produced on a large scale (1 ton/day) by a Canadian industry named Celluforce and the synthesis process employed by them is eco-friendly and sustainability as it gives thrust to the regeneration of sulphuric acid used for the sulphuric acid hydrolysis.[236–238] Hence, adsorbents based on these nanomaterials should have an enormous capability for adsorbing a wide variety of pollutants from wastewater. However, the practical application of these nanomaterials in large scale water treatment processes is limited due to the difficulty of separating them from aqueous solutions.[92] To address this problem, it is desirable to embed these nanomaterials into three-dimensional networks that can facilitate their easy separation using sieves after batch adsorption or use in a continuous fixed bed system.

Hydrogels are crosslinked three-dimensional polymer network structures that have gained a particular interest in wastewater treatment due to their high adsorption capacities, regeneration capacities and reusability for continuous processes.[54] Alginate obtained from cell walls of brown seaweed is the most widely used biopolymer to prepare hydrogel beads for wastewater treatment due to their biocompatibility, biodegradability, large-scale availability, lower cost and non-toxicity.[190,239] Our group has recently developed CNCs incorporated alginate (CNC-ALG) hydrogel beads having excellent adsorption capability that can be easily used in fixed bed columns for large scale water treatment processes. CNC-ALG hydrogel beads possess an overall anionic charge and batch adsorption studies have shown that they have very good adsorption capacity for a model cationic dye called methylene blue.[15]

Application of adsorption techniques for large-scale wastewater treatment usually employs continuous operations, such as fixed bed units, as this allows for large volumes of contaminated water to be treated within a shorter time period. These units may be easily scaled up from the laboratory to pilot unit, and the process is easy to monitor and operate.[218,230] Continuous adsorption processes using fixed bed columns are an effective process for cyclic sorption/desorption as it makes the best use of the concentration gradient as a driving force for adsorption. This in turn allows for efficient utilization of the sorbent capacity and results in better quality of the effluent.[239]

Several studies have reported on the use of hydrogel beads made from biopolymers such as alginate and chitosan in fixed bed columns for the adsorption of contaminants from water.[239–243] However, none of the studies have concentrated on the adsorption behavior of these hydrogel beads when used in fixed bed column studies. Moreover, until now there is no reported study where CNCs based hydrogel beads have been used for fixed bed column studies. Hence this work reports on the study of the adsorption behavior of CNC-ALG hydrogel beads in a fixed bed column for adsorption of MB. Figure 4.1 is a schematic diagram of a fixed bed adsorption column process employing CNC-ALG hydrogel beads as dye adsorbents.

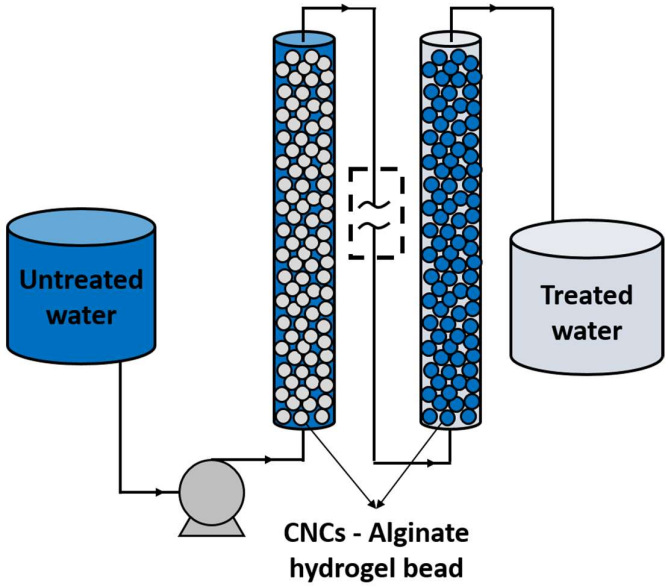

Figure 4.1. Schematic diagram of a fixed bed adsorption column process employing CNC-ALG hydrogel beads as dye adsorbents.

4.2 Experimental section

4.2.1 Materials used

The Acrylic tubing of 1/2" (1.27 cm) outer diameter and 3/8" (0.95 cm) inner diameter, as well as 1" (2.54 cm) outer diameter and 7/8" (2.22 cm) inner diameter were purchased from P&A Plastics Inc. located in Hamilton, Ontario. Plastic and brass couplings were purchased from Lowes/Home Depot. CNCs (spray dried) used in this study was supplied by CelluForce Inc. Sodium alginate (ALG) was purchased from FMC Biopolymer. Methylene blue (MB) was purchased from Sigma-Aldrich. Calcium chloride ($CaCl_2$) was purchased from Fisher

Scientific. All the chemicals were used without further purification and purified water from a Milli-Q Millipore system (>18 MΩcm) was used in preparing the sample solutions.

4.2.2 Preparation and characterization of hydrogel beads

CNC-ALG hydrogel beads were prepared by mixing the CNCs with alginate solution and then dispensing small droplets into a gelation bath containing $CaCl_2$ using a syringe and hypodermic needle. Here the CNC-ALG composite solution was prepared by mixing equal volumes of 1 wt % ALG solution and 2 wt % CNC solution so that the final composition that can be used to formulate the hydrogel beads is 0.5 wt% ALG and 1 wt% CNC. After thoroughly mixing the solution using a homogenizer, the solution was loaded into syringes and extruded through 22-gauge size needles using a syringe pump at a flow rate of 5 mL/min into 50 mL of 2 wt% $CaCl_2$ solution that was gently stirred to prevent the beads from adhering to each other. Hydrogel beads were formed instantaneously in the gelation bath and were crosslinked for another 15 min. The preparation of hydrogel beads was carried out at neutral pH and 25°C. These hydrogel beads were characterized using several techniques and the effect of incorporating CNCs into the ALG hydrogel beads was studied by comparing the characteristics of 0.5 wt% ALG hydrogel beads with and without CNCs.[15]

4.2.3 Fixed bed column adsorption experiments

A 30 cm long acrylic tube of 0.95 cm diameter having a volume of 21.26 cm^3 was used as the column for the majority of the fixed bed experiments. Steel mesh was placed at both ends of the column to prevent the hydrogel beads from exiting the column. Silicone tubing was connected to either end of the plastic couplings to draw the solution in and out of the column. CNC-ALG hydrogel beads were then suspended in the column filled with water so that they would not adhere to the sides of the column or to each other. Prior to each experiment, water was passed through the column to evacuate air bubbles and impurities. Then, the dye solution was pumped through the fixed bed from the bottom using a peristaltic pump at a desired flow rate. Effluent samples were collected from the top of the column at different intervals and the concentration of MB was analyzed by measuring the absorbance at 664 nm with a UV/Visible spectrophotometer. Breakthrough curves were obtained by plotting C_t/C_o (mg/L) against t

(min) where C_t is the effluent dye concentration; C_o is the influent dye concentration and t is the service time. All tests were carried out at room temperature, 25°C (±2).

4.2.4 Effect of various operating parameters

The shape of the breakthrough curve and time for breakthrough appearance are very important characteristics for determining the operation and the dynamic response of a fixed bed adsorption column. The influence of various parameters such as initial MB concentrations, bed depth and flow rates on the initial 90 min of the breakthrough curves was studied.[244]

4.2.4.1 Effect of initial dye concentration

The effect of initial dye concentration on the breakthrough curves was investigated using feed solutions of initial MB concentrations of 50, 150 and 250 mg/L. The investigation was done using fixed beds with a bed depth of 22 cm and flow rate of 4.40 mL/min.

4.2.4.2 Effect of bed depth

The effect of bed depth on the breakthrough curves was investigated using fixed beds of varying volumes, having bed depths of 22, 44 and 66 cm. The feed solution had an initial MB concentration of 50 mg/L in all cases and was allowed to flow through the hydrogel beads with a flow rate of 4.40 mL/min.

4.2.4.3 Effect of flow rate

The effect of flow rate on the breakthrough curves was investigated using flow rates of 1.17, 2.34 and 4.40 mL/min. In all cases, a feed solution having an initial MB concentration of 50 mg/L was passed through a fixed bed of depth 22 cm.

4.2.5 Assessment of trend in the breakthrough curves

Fixed bed column adsorption experiments were performed by changing the composition of the adsorbent and altering the vessel design parameters such as reversing the direction of flow and increasing the adsorption vessel diameter to examine their effect on the breakthrough profile. These experiments would confirm if the adsorbent itself caused the unique breakthrough curve observed during the initial 90 min or if it was a consequence of the current adsorption vessel design and setup.

4.2.5.1 ALG hydrogel beads with and without CNCs

To investigate whether CNCs inside the hydrogels have any contribution to the observed phenomenon, column adsorption experiments using alginate hydrogel beads with and without CNCs were carried out. In this study, a feed solution of initial MB concentration of 50 mg/L was passed upwards through a 30 cm long column of 0.95 cm diameter containing 22 cm bed depth of pure ALG or CNC-ALG hydrogel beads. Effluent samples were collected from the top of the column at different intervals and the concentration of MB was analyzed by measuring the absorbance at 664 nm with a UV/Visible spectrophotometer.

4.2.5.2 Reverse flow

To understand whether the direction of flow had an influence on the breakthrough curve, the flow of the feed solution was reversed. For this, a feed solution of initial MB concentration 50 mg/L was passed downwards through a 30 cm long column at a flow rate of 4.4 mL/min. Effluent samples were collected from the bottom of the column at different intervals and were analyzed similar to above.

4.2.5.3 Larger column diameter

To understand whether the diameter of the column had an influence on the breakthrough curve, the feed solution was passed through a column having a larger diameter than the one used for the operating parameter experiments. A 50 cm long column with a diameter of 2.22 cm was used. The investigation was done by passing a feed solution of initial MB concentration 50 mg/L upwards through a fixed bed with bed depth of 46 cm at a flow rate of 24 mL/min. Effluent samples were collected from the top of the column at different intervals and were analyzed similar to above.

4.2.5.4 Larger diameter column with reverse flow and very low flow rate

A column adsorption experiment featuring a combination of the above-mentioned two parameters was operated at a very low flow rate to test further whether the phenomenon still existed. A 15 cm column having a diameter of 2.22 cm was used. The investigation was performed by passing a feed solution of initial MB concentration of 50 mg/L downwards through a fixed bed with bed depth of 10 cm at a flow rate of 1 mL/min. Effluent samples were

collected from the bottom of the column at different intervals and were analyzed similar to above.

4.2.6 Dynamic bed depth study

The effect of initial dye concentration on the bed depth was studied using a set of fixed bed column experiments. Feed solutions of different initial MB concentrations 100, 250, 400 and 550 mg/L were passed through 30 cm long columns having a bed depth of 22 cm at a flow rate of 4.40 mL/min. Then the decrease in bed depth over time was measured for 4 h using a measuring scale.

4.2.7 Hydrogel beads swelling study

To further understand the mechanism behind the shrinkage of the adsorbent bed during the column studies, the adsorbent was subject to a constant exterior dye concentration with their size changes documented over time. Three hydrogel beads of uniform size were placed within a Petri dish containing 250 mg/L of dye. The hydrogel beads were placed on a wire mesh in the Petri dish to immobilize them within the solution. The hydrogel beads were then photographed with the help of a microscope over a period of 4 h. These images were analyzed using the Analyzing Digital Images software to calculate the percentage change in the volume of hydrogel beads. The percentage change in bead volume was plotted by taking the average volume of 3 hydrogel beads.

4.2.8 Analysis of fixed bed adsorption data

To calculate the maximum adsorption capacity of the hydrogel beads and other useful parameters pertaining to adsorption column process, the adsorbent bed was completely exhausted with MB. This was accomplished by passing a feed solution of initial MB concentration 250 mg/L at 4.40 mL/min through a 10 cm long column having a bed depth of 7.4 cm. High removal of MB was noticed when the dye solution initially came in contact with the fresh porous adsorbent, which gradually changed with time until breakthrough profile was established. Various parameters were calculated as in previous reported studies [218,244].

The treated effluent volume V_t (mL) was determined using Equation 4.1.

$$V_t = Qt_e \tag{4.1}$$

where Q is the volumetric flow rate (mL/min) and t_e is the time at exhaustion (min).

For a given concentration of feed and flow rate, the maximum column capacity q_{total} (mg) can be obtained from the area above the breakthrough curve. Subsequently the area under the curve of the concentration adsorbed versus time will give the maximum column capacity, which was calculated by integrating the C_{ad} (mg/L) versus t (min) plot using the Equation 4.2.

$$q_{total} = \frac{Q}{1000} \int_{t=0}^{t= t_{total}} C_{ad}\, dt \tag{4.2}$$

C_{ad} used in the above equation can be found from the difference between influent and effluent dye concentrations as shown in Equation 4.3.

$$C_{ad} = C_o - C_t \tag{4.3}$$

where C_{ad}, C_o, C_t, t_{total} and Q are the adsorbed dye concentration (mg/L), influent dye concentration (mg/L), effluent dye concentration (mg/L), total flow time (min) and volumetric flow rate (L/min) respectively.

The maximum adsorption capacity of the hydrogel beads q_m (mg/g) used in the column is defined by Equation 4.4 as the total amount of dye adsorbed (q_{total}) per gram of sorbent at the end of total flow time.

$$q_m = \frac{q_{total}}{m} \tag{4.4}$$

where m is the total amount of adsorbent (g) in the column.

The total amount of dye sent to the column W_{total} (mg) was calculated using Equation 4.5.

$$W_{total} = \frac{C_o Q t_{total}}{1000} \tag{4.5}$$

The total amount of dye removed R using the current column can be calculated in percentage using Equation 4.6.

$$R = \frac{q_{total}}{W_{total}} \times 100 \tag{4.6}$$

4.3 Results and discussion

4.3.1 Preparation and characterization of hydrogel beads

Alginate is an anionic polysaccharide composed of (1-4) linked β-D-mannuronate (M) and α-L-guluronate (G) units. They can form hydrogels via intermolecular crosslinking of the G residues with divalent cations like Ca^{2+}.[190] When the aqueous alginate solution containing CNCs is dropped into the $CaCl_2$ ionic crosslinking solution, the structure of the G residues in the alginate chain allows for a high degree of coordination of the Ca^{2+} ions. This is because the sugar ring of the guluronic acid is in the $^1C_4$ conformation, and the polymer chain adopts a characteristic zigzag shape which creates pocket-like cavities in which Ca^{2+} cations can be easily accommodated. This leads to the egg-box model of crosslinking wherein the G blocks of one polymer form junctions with the G blocks of adjacent polymer chains [245–247]. A comprehensive characterization of hydrogel beads was performed in our previous study.[15]

From our previous work, using equilibrium batch adsorption studies it was shown that the adsorption of methylene blue onto CNC-ALG hydrogel beads followed the Langmuir adsorption isotherm, implying homogeneous mono-layer coverage. In addition, it was found from monitoring the kinetics of these batch experiments that the adsorption followed the pseudo-second-order model and intra-particle diffusion model. The results of the batch experiments conducted at various temperatures and ionic strength suggest that the adsorption is physisorption contributed by both hydrogen bonding and electrostatic interactions.[15]

4.3.2 Fixed bed column adsorption experiments

When assessing the usability of an adsorbent for a fixed bed adsorption unit, it is important to study the changes in the breakthrough profile as the initial adsorbate concentration, volumetric flow rate, and bed depth are altered. These breakthrough profiles will yield two important times, breakthrough time (when $C_t=0.05C_0$) and exhaustion time (when $C_t=0.95C_0$), and the variations in these times with changes to the flow rate and initial adsorbate concentration give insight to changes to the size of the mass transfer zone.[248] The focus of this study is to depict how the mass transfer zone was affected by these parameter changes; however, a unique phenomenon was witnessed at the early stages of each breakthrough

experiment. Until now no literatures have reported on this type of breakthrough profile for fixed bed adsorption of hydrogel based adsorbents. Hence, we studied this breakthrough profile in detail to elucidate the effect of various parameters on the breakthrough curve, and the physical reason for this behavior.

4.3.3 Effect of various operating parameters

The influences of various operating parameters, such as initial MB concentration, bed depth and volumetric flow rate on the fixed bed adsorption of MB by CNC-ALG hydrogel beads were studied and the breakthrough curves for the initial 90 min of the adsorption are shown in Figures 1 to 4. Breakthrough curves demonstrated a dramatic increase (Region 1) followed by a gradual decrease (Region 2) with increasing concentration until the point of saturation (the last region being characteristic of a breakthrough curve). This was very different from the S-shaped breakthrough curves reported previously,[218,241,242] where the height of bed containing rigid adsorbent (e.g. activated carbon) does not change with dye adsorption. This peculiar phenomenon observed in the breakthrough curve depicted in Region 1 and 2 may be due to the characteristic swelling and shrinkage of the hydrogel beads respectively during the adsorption of the MB. During the swelling of adsorbent hydrogel beads, the rearrangement of the adsorbent within the bed occurs and this causes alteration in the void spaces between the beads. This results in lesser contact of the bulk fluid with the adsorbent, leading to an increase in effluent dye concentration. During the shrinkage of hydrogel beads, the fixed bed achieves a more efficient packing, decreasing channeling along the walls of the column. This results in better contact with the bulk solution, promoting the mass transfer of dye molecules and helping to achieve a lower effluent dye concentration. The prominence of this phenomenon increases with increase in the flux of dye molecules into the hydrogel beads.

4.3.3.1 Effect of initial dye concentration

Breakthrough curves for MB adsorption at influent concentrations of 50 mg/L, 150 mg/L, and 250 mg/L, a flow rate of 4.40 mL/min and a bed depth of 22 cm are shown in Figure 4.2a. At a lower influent dye concentration, longer time was required for the available active sites of the hydrogel beads to be fully saturated as a result of lower adsorbate dosage and slower

transport of dye molecules.[218] The driving force for adsorption is between the adsorbate ion concentration on the adsorbent and in the bulk fluid.[244,249] A lower influent concentration resulted in a smaller concentration gradient which contributed to a slower transport of dye molecules into hydrogel beads, compared to a higher influent dye concentration. Hence at a lower dye concentration, more time was required to saturate the active sites of hydrogel beads resulting in a higher efficiency of adsorption that leads to a decrease in effluent dye concentration. Apart from this, the characteristic phenomenon observed in the breakthrough curves became more prominent with higher influent dye concentration. This was due to the higher flux of dye molecules moving into the hydrogel beads as a result of the higher concentration gradient, as shown in Figure 4.2b.

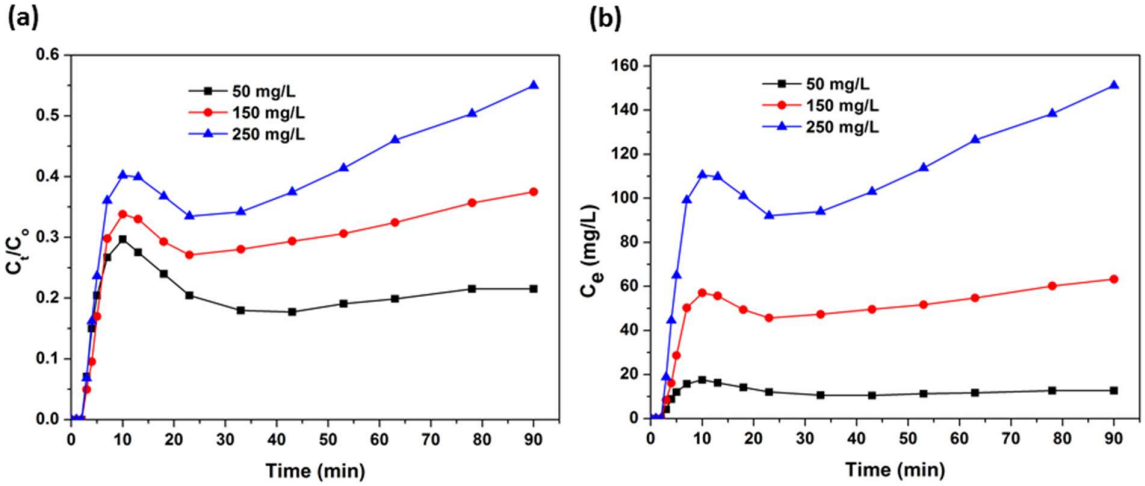

Figure 4.2. (a) Breakthrough curves for MB adsorption at different initial dye concentrations. (b) Effluent dye concentration for MB adsorption at different initial dye concentrations.

4.3.3.2 Effect of bed depth

Breakthrough curves for MB adsorption obtained at bed depths of 22, 44, and 66 cm, and a flow rate of 4.40 mL/min and initial dye concentration of 50 mg/L are shown in Figure 4.3. It was observed that the amount of MB removed from the influent was greater at increased bed depths. This was due to a larger service area available for adsorption, or an increase in the active adsorbent sites.[218,250] Apart from this, the characteristic phenomenon observed in breakthrough curves became less prominent with the increase in bed depth as the flux of dye per bead decreased. The fact that the effluent concentration is not zero after the first plug of dye passed through the column in these experiments indicates that the mass transfer zone is, in

fact, larger than each of these bed depths. Ideally, this situation would be avoided in practice by increasing the bed depth.

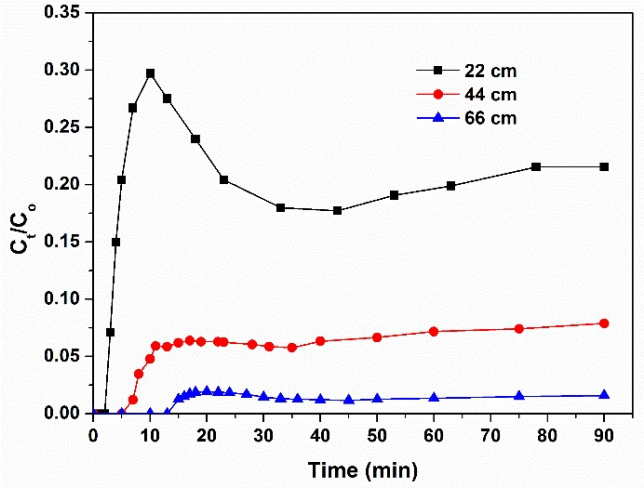

Figure 4.3. Breakthrough curves for MB adsorption at different bed depths.

4.3.3.3 Effect of flow rate

The flow rate is an important parameter as it determines the contact time between the solute and adsorbent surface. Breakthrough curves for MB adsorption at flow rates of 1.17, 2.34, and 4.40 mL/min, the initial dye concentration of 50 mg/L, and bed depth of 22 cm are shown in Figure 4.4. It was observed that the amounts of MB adsorbed onto CNC-ALG hydrogel beads decreased with increasing flow rates since the residence time of the solute in the fixed bed is directly proportional to the flow rate, and a large residence time will allow a greater amount of dye to be adsorbed.[251] Thus, the contact time of MB with CNC-ALG hydrogel beads is very short at higher flow rate resulting in lower efficiency of adsorption that leads to an increase in the effluent dye concentration.[244] Apart from this, the characteristic phenomenon observed in breakthrough curves becomes more prominent and occurs at an earlier time with the increase in flow rate as the flux of dye into the hydrogel bead increases.

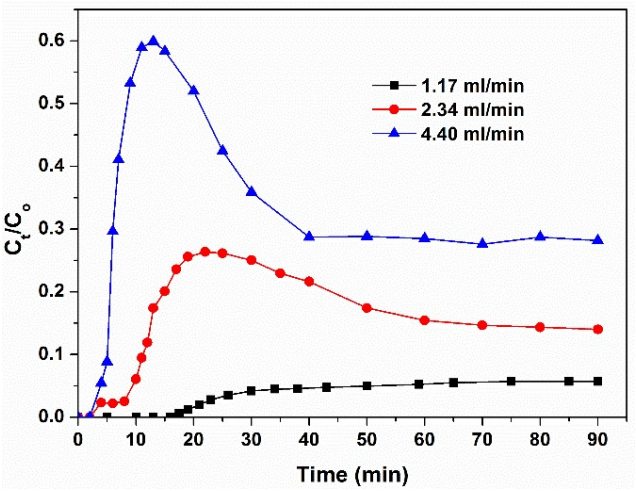

Figure 4.4. Breakthrough curves for MB adsorption at different flow rates.

4.3.4 Assessment of trend in the breakthrough curves

To ensure that the above characteristic phenomenon observed in breakthrough curves was influenced by the adsorbent and not the experimental setup, we evaluate the breakthrough curves by varying adsorbent composition and vessel design parameters.

4.3.4.1 ALG hydrogel beads with and without CNCs

To evaluate whether this phenomenon was related to the presence of the cellulose nanocrystals in the alginate matrix, adsorption experiments were carried out using pure ALG and CNC-ALG hydrogel beads separately. Both the adsorption experiments showed this characteristic phenomenon in breakthrough curves (Figure 4.5) which necessitates the importance to study the swelling response of the hydrogel beads in detail. It was also observed that even though the swelling associated overshoot peak for both the hydrogel beads was similar, the normalized effluent concentration (C/C_0) has a lower plateau value for CNC-ALG hydrogel beads at longer times. This could be attributed to the higher adsorption capacity of the CNC-ALG hydrogel beads compared to the pure ALG hydrogel beads observed earlier.

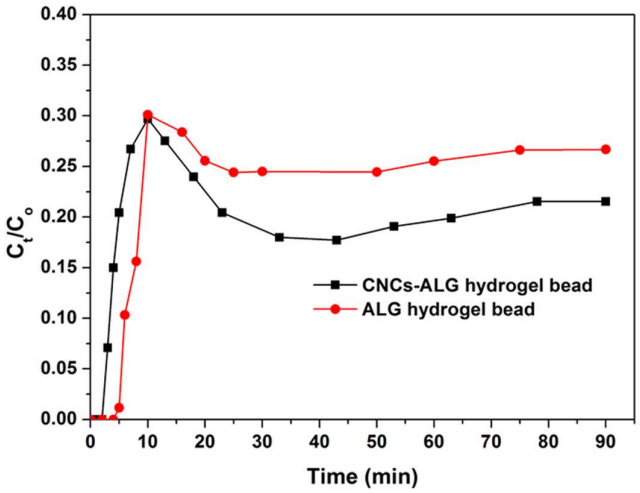

Figure 4.5. Breakthrough curve for MB adsorption when the bead composition was changed.

4.3.4.2 Reverse flow

The direction of flow was reversed and the influent dye was pumped through the column from above as opposed to all other experiments wherein the dye was pumped from the bottom. It was observed that the characteristic phenomenon observed in the breakthrough curve still persists (Figure 4.6) and hence we concluded that the direction of flow was not responsible for the observed phenomenon.

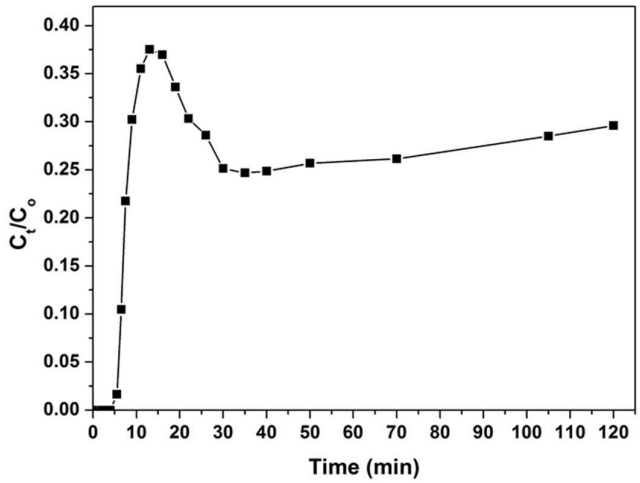

Figure 4.6. Breakthrough curve for MB adsorption when the flow direction was reversed.

4.3.4.3 Larger diameter column

When a larger diameter adsorption vessel was used for the adsorption experiments, this characteristic phenomenon was still evident in the breakthrough curve (Figure 4.7). From this, we inferred that the overshoot in the breakthrough curve is most likely related to the swelling

and shrinkage of the hydrogel beads instead of channeling associated with flow through smaller diameter columns.

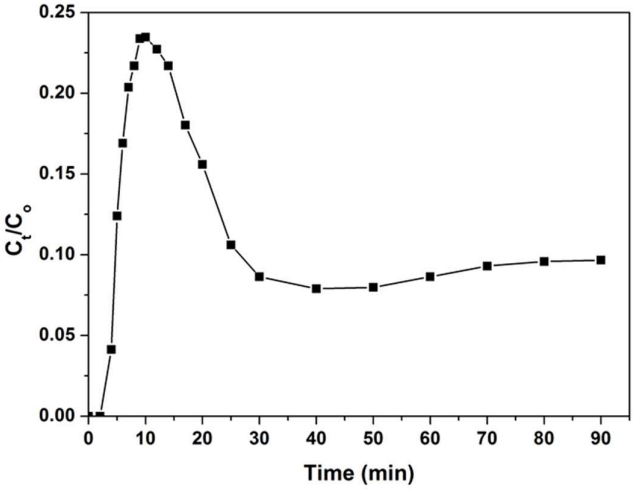

Figure 4.7. Breakthrough curve for MB adsorption when a larger diameter column was used.

4.3.4.4 Larger diameter column with reverse flow and very low flow rate

An adsorption experiment using a combination of the previous two parameters was carried out at a very low flow rate to further evaluate the influence of fixed bed operation parameters on the occurrence of this characteristic phenomenon in the breakthrough curves. It was observed that the phenomenon still persists (Figure 4.8) reaffirming the need to study the swelling response of hydrogel beads during the adsorption.

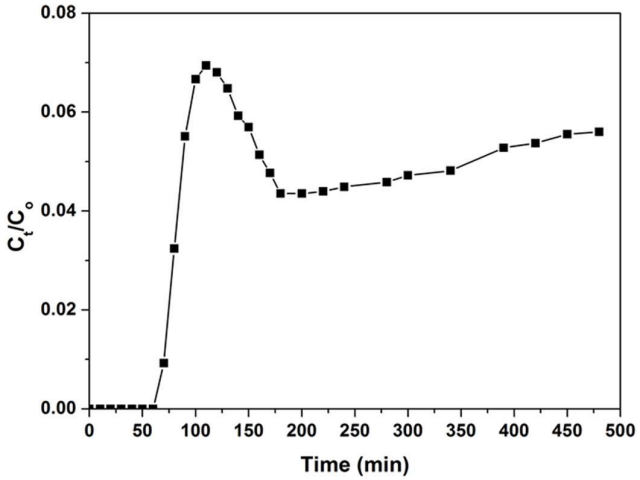

Figure 4.8. Breakthrough curve for MB adsorption when a larger diameter column was used with reverse flow and very low flow rate.

4.3.4.5 Breakthrough dependency on column diameter

It was reported that due to increased bed voidage along the wall, the longitudinal flow velocity will be maximum, resulting in an earlier breakthrough. Breakthrough for the flow near the wall occurs earlier when the bed voidage is within three pellet diameters or larger. This effect is small for a bed/pellet diameter ratio greater than 20.[248] When the bed/pellet diameter is larger than 21, a plug flow profile can be assumed where the entrance and wall effects were minimized.[252,253] In the present study, the average diameter of the hydrogel beads (d) was 2.9 mm, with the small column having a diameter (D) of 9.5 mm and the larger column having a diameter of 22.2 mm. Therefore, the D/d ratio for the small and larger diameter columns were 3.28 and 7.66 respectively. Therefore, we would expect that for a larger diameter column, the adsorption efficiency should increase as a result of larger number of hydrogel beads along the cross-sectional area of the column that facilitates more contact with the hydrogel beads and decrease channeling along the column wall.

4.3.4.6 Long term behavior of breakthrough curves

The main focus of this study was to investigate the characteristic phenomenon occurring at the early stage of the breakthrough curve, however, not much was said on the long-term breakthrough behavior. Based on the later portion of the breakthrough curves and comparing it to additional sources, [254] this plateau in effluent concentration followed by a slight increase at later times indicates that our choice of operating region has resulted in a system where film diffusion is the controlling factor for dye adsorption within the hydrogel beads. This can be characterized by the low flow rate used in the system, which increases the size of the stagnant fluid barrier (film) surrounding each bead, decreasing the mass transfer to the surface of the hydrogel beads and ultimately the rate of adsorption.

4.3.5 Dynamic bed depth study

Figure 4.9a shows the photographs of changes in the bed depth over four h when a feed solution of initial MB concentration 250 mg/L was passed through the fixed bed. Photographs clearly show that depth of the bed decreases with time and the hydrogel beads used in the column have decreased in size (Figure 4.9b). Bed depth was also measured over time and the

normalized bed depth was plotted against time as shown in Figure 4.9c. It was also observed that the percentage bed shrinkage at the end of 4 h increased with increasing influent dye concentration and reached an equilibrium bed depth beyond which there was no longer a decrease in bed depth. Figure 4.9d shows the percentage decrease in bed height with influent dye concentration. The decrease in bed depth was a consequence of the hydrogel bead shrinkage because of water being expelled from the interior of the hydrogel beads during adsorption of MB. Even though the hydrogel beads swell initially, no visible increase in the bed depth was observed along that time. This is due to the swelling of the hydrogel beads within their void spaces and rearrangement of the hydrogels beads within the bed.

Given the small column diameter to bead ratio, any decrease in bead size would result in an increased packing factor due to more hydrogel beads fitting within the cross-sectional area of the column, as well the ability of the hydrogel beads to fill more void space than their larger counterparts. Two processes are occurring in the bed shrinkage: (a) the decrease in bead size and (b) the decrease in the void volume of the bed. Hence, the swelling response of the hydrogel beads is an important contributory factor controlling the breakthrough curves for these kinds of hydrogel based adsorbents. Also, such a decrease in bed depth for porous hydrogel based sorbents was reported for the first time and this understanding can be very important for the process engineers trying to use adsorbent systems in the future.

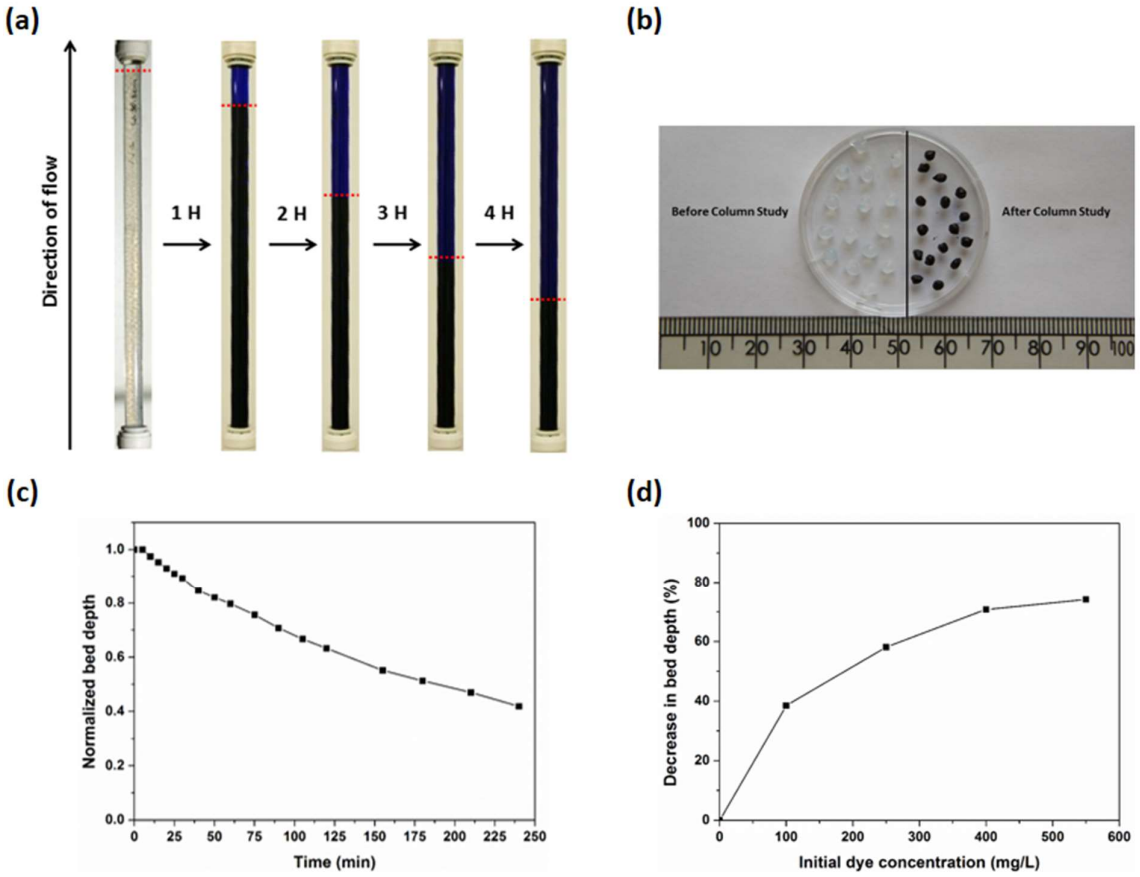

Figure 4.9. Photographs of (a) bed depth changes during the adsorption of 250 mg/L dye solution in a fixed bed column study over a period of 4 h (b) hydrogel beads before and after fixed bed column study. (c) Bed depth changes during the adsorption of 250 mg/L dye solution in a fixed bed column study over a period of 4 h. (d) The percentage decrease in bed depth at the end of 4 h of fixed bed column dye adsorption study for various initial dye concentrations.

4.3.6 Hydrogel beads swelling study

Figure 4.10 shows the percentage change in volume of the hydrogel beads over time when placed in a Petri dish containing 250 mg/L initial MB concentration for four h. The figure shows three distinct phases of the hydrogel beads viz., (I) Native phase (II) Swelling phase and (III) Shrinkage phase as represented by the schematic at the bottom of the figure. The hydrogel beads showed an initial increase followed by a decrease in their volume. This swelling behavior had a significant influence on the phenomenon observed in the breakthrough curves. The initial increase in the volume of hydrogel beads was caused by osmotic swelling. When fresh beads were placed in the dye solution, the concentration of dye molecules outside of the hydrogel beads was much higher than the interior of the hydrogel beads. The larger concentration

gradient caused the diffusion of the dye molecules into the hydrogel beads resulting in a higher osmotic pressure inside the hydrogel beads that triggered the hydrogel beads to swell. Following this phase, the volume of hydrogel beads decreased with time due to charge shielding and hydrophobic interactions of the dye molecules. As more dye molecules were getting adsorbed into the hydrogel beads, the charge shielding effect on the ionized groups within the hydrogel was enhanced resulting in charge repulsion between the ionized carboxyl groups of the alginate polymer within the crosslinked network of the hydrogel beads. Diffusion of MB into the hydrogel beads produced a less polar environment within the hydrogel due to the hydrophobicity of the MB which produced a more compact structure.[255,256]

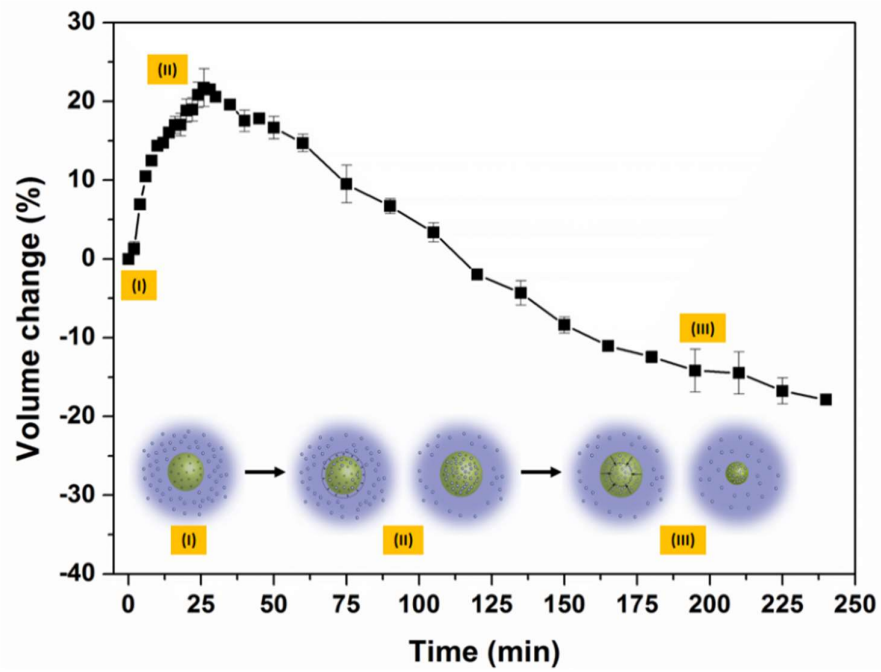

Figure 4.10. Percentage change in volume of the hydrogel beads when subjected to a constant exterior dye concentration over time. (Inset: Schematic diagram of the swelling behavior of CNC-ALG hydrogel beads during fixed bed column adsorption of methylene blue.)

4.3.7 Analysis of fixed bed adsorption data

The maximum adsorption capacity of the hydrogel beads and the influence of various parameters on the column adsorption experiment were calculated by performing an experiment where the adsorbent was completely saturated with the dye (Figure 4.11). The maximum adsorption capacity (q_m) of the CNC-ALG hydrogel beads used in the fixed bed was found to be 255.5 mg/g which was approximately equal to the reported q_m value determined from batch

adsorption experiment reported in our other paper.[15] Table 4.1 summarizes the various column operating parameters used in the experiment.

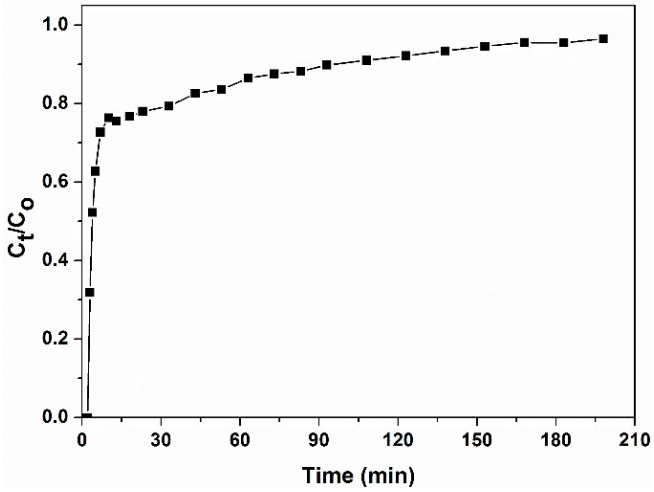

Figure 4.11. Breakthrough curve for MB adsorption for fixed bed column dye adsorption experiment carried out at 250 mg/L initial dye concentration, bed depth 7.4 cm, flow rate 4.17 mL/min.

Table 4.1. Column operating parameters determined using a fixed bed column dye adsorption experiment.

S. No.	Column Parameters	Values
1	Volumetric flow rate, Q (mL/min)	4.17
2	Time at exhaustion, t_e (min)	291.08
3	Treated effluent volume, V_t (mL)	1214.71
4	Maximum column capacity, q_{total} (mg)	19.37
5	Adsorbed dye concentration, C_{ad} (mg/L),	15.95
6	Total flow time, t_{total} (min)	234.00
7	Total amount of dye sent to the column, W_{total} (mg)	254.60
8	Total amount of dye removed, R (%)	7.61

Apart from this in our previously reported paper, the reusability of the hydrogel beads have been evaluated by desorbing MB using a 1:1 HCl – Ethanol eluent mixture and it showed that the hydrogel beads retain their full adsorption capacity even after five adsorption/desorption cycles.[15] Therefore, a lifetime of the generated hydrogel beads used in the fixed bed is at least for five adsorption/desorption cycles which support the reusability of this fixed bed column for a minimum of 5 times.

4.4 Conclusions

Fixed bed column studies using CNC-ALG hydrogel beads to remove methylene blue were conducted. The effect of various column operating parameters, such as initial dye concentration, bed depth and flow rate on the breakthrough curves was studied. A unique phenomenon in the breakthrough curves was observed in the early time period of dye adsorption. Breakthrough curves demonstrated a dramatic increase followed by a gradual decrease to a plateau at saturation. The hydrogel beads in the column exhibited an osmotic swelling followed by a charge shielding assisted shrinkage during the dye adsorption which affected the packing of the fixed bed resulting in the particular phenomenon observed in the breakthrough curve. It was found that this phenomenon improved the performance of the adsorbent, as lower void fraction meant more contact between the bulk fluid and adsorbent hydrogel beads. The maximum adsorption capacity of the hydrogel beads was found to be 255.5 mg/g and various other parameters pertaining to column adsorption experiment were calculated from the breakthrough curve.

Chapter 5*

Surface Functionalized Cellulose Nanocrystals for Selective Adsorption in Water Treatment Applications

Incorporating surface functionalized CNCs into hydrogel beads open a whole new world of possibilities for the application of CNCs in the removal of contaminants in waste water. Herein, we report for the first time the use of pristine and surface functionalized CNCs for the selective adsorption of a specific dye from a mixture of dye molecules. CNCs were coated with melamine-formaldehyde (MF) and polydopamine (PD) to prepare surface functionalized CNCs such as MF-CNCs and PD-CNCs respectively. The selectivity of pristine and surface functionalized CNCs was investigated using selective dye adsorption studies. PD-CNC-ALG hydrogel beads have very good selectivity for dye containing Eschenmoser functional groups. Batch adsorption studies confirmed that these hydrogel beads possessed very good adsorption for methylene blue and copper. Silver nanoparticles (Ag-NPs) were also chelated to PD-CNC-ALG hydrogel beads and these hydrogel beads showed excellent antibacterial activity with minimal leaching of Ag-NPs. Such system may find application in organic dyes removal, heavy metal ions removal and the disinfection of bacteria contaminated water. Thus, PD-CNC-ALG hydrogel beads could be versatile adsorbents that possess multi-functional capabilities in wastewater treatment systems.

*This chapter is partially adapted from "Nishil Mohammed, Zengqian Shi, Nathan Grishkewich, Richard M. Berry and Kam Chiu Tam, Pristine and Surface Functionalized Cellulose Nanocrystals for Selective Adsorption of Cationic Dyes, *Manuscript Under Preparation*" and "Nishil Mohammed, Aravind Ramaraju, Zengqian Shi, Nathan Grishkewich, Richard M. Berry, William A. Anderson and Kam Chiu Tam, Polydopamine Functionalized Cellulose Nanocrystal–Alginate Nanocomposites as Versatile Adsorbent for Efficient Removal of Organic Dyes and Heavy Metal Ions in Water, *Manuscript Under Preparation*"

5.1 Introduction

Water is the elixir of life; however, it is contaminated by a wide variety of contaminants from industrial, municipal and agricultural activities. Effluent discharges from these activities contains a plethora of compounds such as organic dyes, heavy metal ions, pharmaceuticals, detergents, food additive, agrochemical, microbial contaminant etc.[1,257] Hence, to ensure water is safe for human consumption and is suitable for a wide variety of recreational activities, several water treatment methods including membrane filtration,[165,166] adsorption,[15,258] ion exchange,[95,134] coagulation-flocculation,[139,143] photocatalysis,[11,176] etc. were adopted. Among all these methods, adsorption is one technique that offers promising results at an affordable cost if they are employed using well-designed system. Activated carbon is the conventional and most common adsorbent used, however, its production is energy intensive, expensive and a contributor to greenhouse gas emission. Hence, there is a growing interest to develop low-cost alternatives from forest products and agricultural biomass.[2,3,7–9] In this context, the use of sustainable nanomaterials such as cellulose nanocrystals (CNCs) to prepare sustainable platforms for wastewater treatment is a novel approach that has a negligible carbon footprint.[12–14]

CNCs are rod-like nanoparticles extracted from cellulosic sources using H_2SO_4 hydrolysis. CNCs produced by this method bear negative sulfate ester groups on its surface and they are rod-shaped with a length of 100 to 250 nm and lateral dimensions of 5 to 70 nm. They also possess several attractive characteristics such as high specific surface area, high specific strength, hydrophilicity, biodegradability and surface functionalization capabilities.[10] In addition, their large-scale availability make them attractive candidates for use in wastewater treatment applications.[12] However, the separation of these nanomaterials after use in water treatment is a challenge because of their high colloidal stability and nanosize. Therefore, it is ideal to incorporate CNCs within a polymer matrix forming macrobeads that can be readily separated, besides offering the possibility of adding new functionalities. Previous studies in our laboratory revealed that these CNCs could be easily incorporated into alginate hydrogel beads via simple ionotropic gelation process using divalent cations such as Ca^{2+} ions.[15–18]

Several studies have shown that the functionalization of nanoparticles affords them the capability of selective binding to compounds bearing a specific charge or functional groups. The strategy of functionalizing CNCs for the selective adsorption has not yet been explored. Thus, we report for the first time how pristine and surface functionalized CNCs can be used for the selective adsorption of a specific dye from a mixture dye molecules. CNCs were coated with melamine-formaldehyde (MF) and polydopamine (PD) to prepare surface functionalized CNCs such as MF-CNCs and PD-CNCs respectively. MF functionalization introduces the porous character to pristine CNCs in addition to the introduction of positive charges and enriches its surface with a large number of amine groups.[42,44] This would make them ideal for the adsorption of anionic compounds. PD functionalization introduces catechol groups, amines and aromatic moieties on the surface of pristine CNCs, making them selective to compounds with Eschenmoser functional groups. Studies have already shown that polydopamine selectively bind to organic dyes such as methylene blue (MB) that bear Eschenmoser functional groups. This selective adsorption process is driven by Eschenmoser salt assisted 1,4-Michael addition reaction between the ortho position of catechol phenolic hydroxyl group of polydopamine and Eschenmoser group in MB.[258]

Thus, surface functionalization of CNCs opens a whole new world of possibilities for the application of CNCs incorporated nanocomposites in various water treatment applications. In this work, we developed a novel nanocomposite viz., PD-CNC-ALG hydrogel beads containing PD-CNCs that possess specific interactions and surface area as an adsorbent for use in water treatment application. These hydrogel beads were found to be highly selective to MB bearing Eschenmoser functional group. They also displayed very good adsorption for heavy metal ions like Pb^{2+}, Hg^{2+}, Cr^{3+} and Cu^{2+}. Silver nanoparticles (Ag-NPs) were also deposited on the surface of PD-CNCs prior to being incorporated into the hydrogel beads. The prepared Ag-NP@PD-CNC-ALG hydrogel beads showed good antibacterial activity against gram positive and gram negative bacteria thus making them applicable as an ideal disinfectant for water treatment processes. The anchoring of Ag-NPs onto the PD-CNCs before incorporating into hydrogel beads also significantly reduce the leaching of ions associated with porous

hydrogel matrix materials. Figure 5.1 is a schematic diagram showing the synthesis and versatile application of PD-CNC-ALG hydrogel beads for water treatment application.

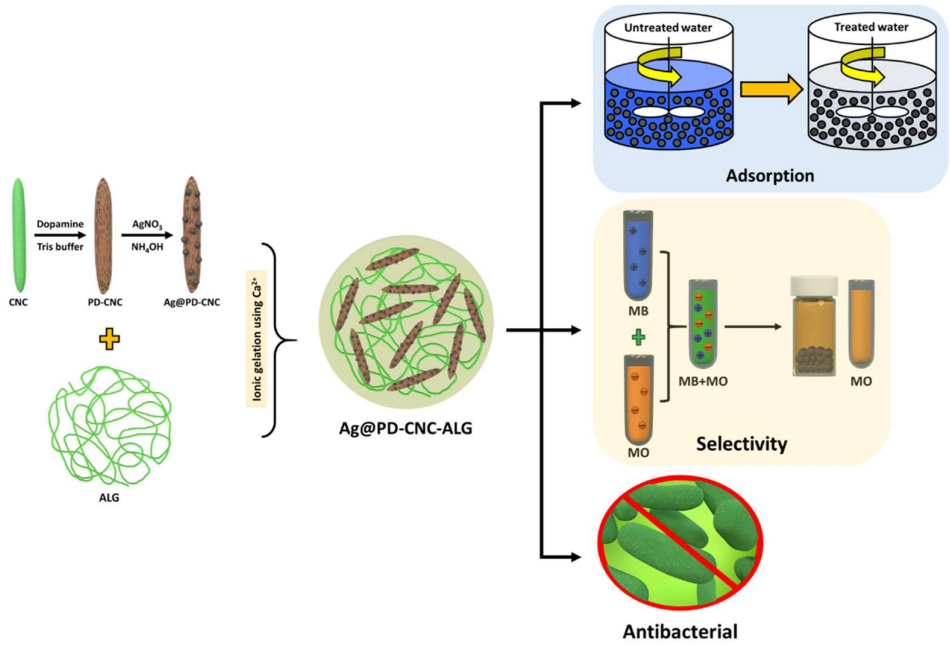

Figure 5.1. Schematic diagram showing the synthesis and versatile application of PD-CNC-ALG hydrogel beads for water treatment application.

5.2 Experimental section

5.2.1 Materials used

CNCs used in this study were supplied by CelluForce Inc. Dopamine hydrochloride, tris(hydroxymethyl)aminomethane, silver nitrate, ammonium hydroxide (NH_4OH), melamine, formaldehyde, NaOH, methylene blue hydrate (MB), methyl orange (MO), rhodamine B (RB), crystal violet (CV) and copper (II) sulfate pentahydrate were purchased from Sigma-Aldrich. Divalent acetates of mercury, copper, zinc, nickel, lead, cadmium, manganese and cobalt were purchased from Merck. Chromium (III) nitrate nonahydrate ($Cr(NO_3)_3.9H_2O$) was purchased from Lobachemie and sodium arsenite ($NaAsO_2$) was purchased from SD Fine Chemicals Limited. Calcium chloride and nutrient broth powder (OptiGrow™ Preweighed LB Broth, Lennox) were purchased from Fisher-Scientific. Sodium alginate (Protanal® GP 3550) was purchased from FMC BioPolymer and plate count agar (DifcoTM Ref. 247940) was purchased from Becton Dickinson and Company. All these chemicals were used as received without further purification. *Escherichia coli* and *Bacillus subtilis* bacteria were purchased from

Cedarlane Laboratories, in Burlington, Ontario. Purified water from a Milli-Q Millipore system (>18 MΩcm) was used in preparing the sample solutions.

5.2.2 Surface functionalization of CNCs

Preparation of MF-CNCs, PD-CNCs and Ag-NP@PD-CNCs were carried out using the previously reported protocols with slight modifications,[42–45] and the typical procedures used to synthesize them are described below:

5.2.2.1 Preparation of MF-CNCs

In a typical synthesis procedure, MF precursor solution was initially prepared and mixed with CNC suspension. In this step, 2.2 g of melamine and 4.0 mL of formaldehyde (37% in water) was added to 10 mL Millipore water in a 50-mL flask. The pH of the solution was adjusted to 8 and 9 with 1 M NaOH and the temperature was raised to 80 °C while the solution was magnetically stirred. Within 5 min, the precursor solution turned from cloudy to transparent and after 30 min, this solution was added to the CNC suspension. In the second step, MF precursor solution was added to 100 mL of CNC suspension (1%), followed by adjusting the pH between 4 and 5 using 1 M HCl and stirred at 80 °C for 2 h. The solution was then allowed to cool to room temperature and purified via repeated filtration and washing with Millipore water until the filtrate became clear.

5.2.2.2 Preparation of PD-CNCs

In a typical synthesis procedure, 1.0 g of CNCs was dispersed in 200 mL Millipore water using an IKA T25 homogenizer. This is followed by the addition of 0.3 g of tris(hydroxymethyl)aminomethane to maintain the pH at 8.0. Then, 1.0 g of dopamine hydrochloride was added to this solution and stirred using a magnetic stirrer for 3 h at 60 °C. The final product solution was then purified using an ultrafiltration cell equipped with a 0.1µm filtration membrane and several times of washing with 200 mL Millipore water until the filtrate became clear.

5.2.2.3 Preparation of Ag-NPs@PD-CNCs

PD-CNCs were also deposited with silver nanoparticles for use in antibacterial studies. In a typical synthesis procedure, 3.0 wt% NH_4OH solution was slowly added to a 20 mL of silver nitrate solution (0.25 wt%) under mild stirring until the solution became transparent indicating the formation of diamine silver (I). Then 0.5 mL of PD-CNC solution (3.0 wt%) was added to this solution and stirred at room temperature for 1 h. This is followed by the addition of 1 mL dopamine hydrochloride solution (0.4 wt%) to facilitate the reduction of silver ion. After 30 min, the resulting solution was purified via centrifugation at 8000 rpm for 10 min and washed with Millipore water three times to remove unbound silver nanoparticles. As a control, free silver nanoparticles (Ag-NPs) without PD-CNCs were also prepared under similar conditions.

5.2.2.4 Preparation of hydrogel beads

PD-CNC-ALG hydrogel beads were prepared using a similar protocol reported previously.[15–17] Simple ionotropic gelation of PD-CNCs containing sodium alginate solution using divalent cations like Ca^{2+} could instantaneously form hydrogel beads. In a typical synthesis procedure, 2 wt% of the PD-CNCs solution was thoroughly mixed with equal volume of 1 wt% sodium alginate solution using a homogenizer and transferred to a syringe equipped with 22 G gauge needle. Using an injection pump, the solution was extruded at a rate of 5mL/min into a gellant bath containing 50 mL of 2 wt% $CaCl_2$ solution. Slight stirring was also applied to the gellant bath while dispensing the polymer solution to prevent the hydrogel beads from sticking to each other. The beads were then allowed to crosslink in $CaCl_2$ solution for 15 min after which they were washed with 10 mL water to remove residual $CaCl_2$. As a control, CNC-ALG beads were also prepared in a similar manner. To demonstrate the versatile application of these hydrogel beads as water disinfectant, antibacterial Ag-NP@PD-CNC-ALG hydrogel beads were also prepared using the same protocol.

5.2.3 Characterization

Transmission electron microscopy (TEM) characterization of pristine CNCs, PD-CNCs, Ag-NPs, Ag-NPs@PD-CNCs and MF-CNCs were performed using a Philips CM10 electron

microscope. TEM samples were prepared by spraying the aqueous solution (0.005 wt% solid) sample onto a carbon-coated copper grid and air drying overnight at room temperature. Zeta potential of pristine CNCs, MF-CNCs and PD-CNCs were measured with a Zetasizer (Malvern, Nano ZS90). Visual difference in the appearance of hydrogel beads after the incorporation of PD-CNCs was observed by studying images of the CNC-ALG and PD-CNC-ALG hydrogel beads. Porous nature and elemental analysis of the Ag-NP@PD-CNC-ALG hydrogel beads were examined using a field emission scanning electron microscopy (FE-SEM) (Zeiss LEO 1530) at 10 kV of accelerating voltage equipped with energy dispersive analysis of X-rays (EDAX) (Pegasus 1200).

5.2.4 Selectivity studies

The affinity of pristine and surface functionalized CNCs towards dye molecules bearing a specific charge or functional group was studied by performing selective dye adsorption experiments. In this experiment, three different stock solutions of mixed dyes viz., MB/MO (Dark green colour), MB/RB (Purple colour) and MB/CV (Dark blue colour) having 1:1 molar ratio were prepared by mixing equal volumes of respective individual dye such as MB (Blue colour), MO (Orange colour), RB (Pink colour) and CV (Crystal violet) stock solutions. The concentration of each individual dye present in the stock solutions of dye mixtures was 10 ppm. Stock solutions of pristine CNCs, PD-CNCs and MF-CNCs in Millipore water (20 mg/mL) were used as the adsorbents. Additional selective dye adsorption experiments were also performed using CNC-ALG and PD-CNC-ALG hydrogel beads as adsorbents in order to study whether surface functionalized CNCs have the potential of manipulating the selectivity of the hydrogel beads. The widely used equations to calculate the removal % and uptake of a contaminant are described by Equation 5.1 and 5.2 respectively.[194]

$$\text{Removal } \% = \frac{(C_0 - C_e)}{C_0} \times 100 \tag{5.1}$$

$$q_e = \frac{(C_0 - C_e)\, V}{m} \tag{5.2}$$

where q_e is the amount of contaminant adsorbed for 1 g of adsorbent (mg/g), C_0 is the initial contaminant concentration (mg/L), C_e is the equilibrium concentration of free contaminant

molecules in the solution (mg/L), V is the volume of solution (L) and m is the mass of adsorbent (g). All the selective dye adsorption studies were performed at a neutral pH and 25 °C using procedures described below:

5.2.4.1 Selectivity study for pristine CNCs and surface functionalized CNCs

In this experiment, 5 mL of adsorbent stock solution and 5 mL of MB/MO mixture were placed in a 20-mL vial and the solution was stirred at 500 rpm for 1 h. The effective dosage of adsorbent and concentration of individual dye used in this study was 10mg/mL mg and 5 ppm respectively. After 1 h, the mixture was centrifuged in a Heraeus Megafuge at 8000 rpm for 15 min to separate the adsorbent from the dye solution. For adsorbents CNCs and PD-CNCs, the mixture was transferred to a centrifuge tube containing 96.5 µL of $CaCl_2$ solution (2.16 M) prior to centrifugation. This induces the agglomeration of adsorbent – dye complex thereby improving their separation from dye solution during centrifugation. The concentration of the dye in the dye mixture before and after adsorption was quantified using a Cary 100 UV-Vis spectrophotometer. Control adsorption experiments using individual dye solutions were also conducted. Selective dye adsorption studies using various dosages of pristine CNCs (5, 10, 15, 20 and 25 mg/mL) were performed to examine the influence of adsorbent dosage on selectivity. To elucidate the improved selectivity of PD-CNCs for Eschenmoser group containing dyes, additional selective dye adsorption studies were performed for PD-CNCs using MB/RB and MB/CV dye mixtures. The removal% of individual dye molecules in all these experiments were calculated using Equation 5.1.

5.2.4.2 Selectivity study for CNC-ALG and PD-CNC-ALG hydrogel beads

In this experiment, 75 mg (dry weight basis) of PD-CNC-ALG hydrogel beads were mixed at 500 rpm for 1 h in a 20-mL vial containing 10 mL of MB/MO, MB/RB and MB/CV (5 ppm) dye mixtures h. After stirring, the concentration of individual dye molecules in the dye mixtures before and after adsorption was determined. A comparative selective dye adsorption study using the same dosage of CNC-ALG and PD-CNC-ALG hydrogel beads was also performed to evaluate the improved selectivity of PD-CNC-ALG hydrogel beads for

Eschenmoser group containing dyes over CNC-ALG hydrogel beads. The removal% of individual dye molecules in all these experiments was calculated using Equation 5.1.

5.2.5 Dye adsorption studies

Batch adsorption studies using a model Eschenmoser group containing organic dye, MB were carried out to evaluate the adsorption characteristics of pristine CNCs, PD-CNCs, CNC-ALG and PD-CNC-ALG hydrogel beads. All the batch adsorption studies were conducted at a neutral pH and 25 $^{\circ}$C using procedures described below:

5.2.5.1 Dye adsorption study for pristine CNCs and PD-CNCs

In this experiment, stock solutions of dye (25 ppm) and adsorbents, i.e. pristine CNCs and PD-CNCs (10 mg/mL) were first prepared. Then 5 mL of adsorbent stock solution and 5 mL of dye stock solution were mixed in a 20-mL vial and the solution was stirred at 500 rpm for 1 h. After stirring, the mixture was transferred to a centrifuge tube containing 96.5 µL $CaCl_2$ (2.16 M) and centrifuged in a Heraeus Megafuge at 8000 rpm for 15 min on order to separate the adsorbent from dye solution. The concentration of MB in the supernatant was then measured using UV-Vis spectrophotometer. The removal% and uptake of dye were calculated using Equation 5.1 and 5.2 respectively.

5.2.5.2 Dye adsorption study for CNC-ALG and PD-CNC-ALG hydrogel beads

In this experiment, two adsorption cycles employing a fresh batch of respective hydrogel beads in each cycle were carried out and the concentration of dye solution after each cycle was determined. 135 mg (dry weight basis) of hydrogel beads were stirred in a 20-mL vial containing 15 mL of 100 ppm MB solution at 500 rpm for 1 h. After stirring, the beads were separated from the solution and a new batch of beads (135 mg) was added to this solution and stirred for another 1 h. The decrease in the initial dye concentration using the first set and second set of beads was measured using UV-Vis spectrophotometer. The removal% and uptake of dye were calculated using Equation 5.1 and 5.2 respectively.

5.2.6 Heavy metal ion adsorption studies

Batch adsorption experiments were carried out using various heavy metal ions such as As^{3+}, As^{5+}, Cd^{2+}, Co^{2+}, Cr^{3+}, Cu^{2+}, Fe^{3+}, Mn^{2+}, Ni^{2+}, Pb^{2+}, Zn^{2+} and Hg^{2+} to evaluate the heavy metal adsorption ability of PD-CNC-ALG hydrogel beads. In a typical batch adsorption experiment, 7.5 mg of water-swollen hydrogel beads were stirred overnight in a 20-mL vial containing 5 mL of 50 ppm concentration heavy metal ion solution at 500 rpm for 1 h. All the adsorption experiments were carried out at a neutral pH and room temperature (25 ºC). The initial and final concentrations of the heavy metal ion solutions were measured using ICP-MS after acidification (5% HNO_3 for all heavy metal ions except Hg^{2+} and 5% HCl for Hg^{2+}). The removal% of heavy metal ions can be calculated using Equation 5.1.

5.2.7 Kinetic studies

Kinetics of adsorption was studied by measuring the MB concentration of 5 different batches of PD-CNC-ALG hydrogel beads stirred in dye solutions at 500 rpm for 3 h. Each batch consisted of 75 mg (dry weight basis) of PD-CNC-ALG hydrogel beads in 250 mL flasks containing 50 mL solutions of MB with various initial concentrations (100, 200, 300, 400 and 500 ppm) respectively. Then the concentration of MB was measured at regular time intervals and these concentrations were used to calculate the uptake of MB over time t (q_t) using Equation 5.2. The uptake of MB (q_t) was then plotted against time (t) and the obtained data was further analyzed using various models to obtain the kinetic parameters of adsorption.

5.2.8 Adsorption Isotherm

Adsorption isotherms can be used to determine the maximum adsorption capacity (q_{max}) of PD-CNC-ALG hydrogel beads for commonly found water contaminants such as organic dyes and heavy metal ions. The model compounds chosen to evaluate the adsorption capacity of organic dyes and heavy metal ions are MB and copper respectively as these hydrogel beads were found to have very good adsorption for MB and Copper. In this experiment, adsorbate solutions of MB and copper were prepared by dissolving varying amounts of methylene blue hydrate and copper (II) sulfate pentahydrate in Millipore water. Then 75 mg (dry weight basis) of PD-CNC-ALG hydrogel beads were dispersed in 250 mL flasks containing 50 mL solutions

of the respective adsorbate solution (MB or Copper) of various initial concentrations (100, 200, 300, 400 and 500 ppm) respectively. The hydrogel beads were mixed at 500 rpm for 24 h at a neutral pH and 25 ºC. After 24 h stirring, the concentrate of adsorbate before and after adsorption was measured using the UV-Vis spectroscopy. For the concentration of MB, the absorbance values at 664 nm were determined using UV-Vis spectrophotometer. For the concentration of copper, ethylenediamine was first added to the solution containing Cu^{2+} ions and the complex formed by ethylenediamine with Cu^{2+} ions yielded absorbance value at 556 nm that were determined using UV-Vis spectrophotometer.[259] The equilibrium uptake of adsorbate q_e was then calculated using Equation 5.2 and the q_e was plotted against equilibrium concentration of adsorbate C_e. This equilibrium data was fitted to a linearized form of Langmuir adsorption isotherm equation as shown in Equation 5.3.

$$\frac{1}{q_e} = \frac{1}{K_L q_m C_e} + \frac{1}{q_m} \tag{5.3}$$

where q_m is the maximum amount of adsorbate adsorbed per gram of adsorbent (mg/g) in equilibrium and K_L is a constant related to the energy of adsorption (L/mg) that depicts the affinity between the heavy metal ion and adsorbent. Parameters q_m and K_L were determined from the intercept and slope of the plot of $1/q_e$ versus $1/C_e$, respectively.

5.2.9 Antibacterial studies

The antibacterial characteristics of PD-CNC-ALG hydrogel beads were achieved by depositing Ag-NPs onto PD-CNCs in these hydrogel beads. To evaluate its antibacterial activity, varying dosages of Ag-NP@PD-CNC-ALG hydrogel beads (10, 20 and 30 mg) were added to three scintillation vials containing 10 mL of medium containing the bacteria. This bacterium containing medium was prepared by inoculating 100 µL of bacterial inoculum into 10 mL of LB Broth. The scintillation vials containing the different doses of hydrogel beads and a control glass vial without beads were incubated at 37 °C and shaken at 250 rpm for 24 h. After 24 h, the turbidity of the solution was noted and the solutions from each of these vials were serially diluted and plated onto agar plates to count the colony forming units (CFU). This experiment was performed using both Gram-negative bacteria (*Escherichia coli*) and Gram-

positive bacteria (*Bacillus subtilis*) to evaluate the performance of the system against both bacterial types.

5.2.10 Leaching studies

Experiments were performed to evaluate if there is any leaching of the components from the PD-CNC-ALG hydrogel beads into the bulk solution. This is to demonstrate the practical applicability of these hydrogel beads for use in water treatment applications. The test involved immersing 40 mg of freeze-dried hydrogel beads in 20 mL of Millipore water for 24 h at 25 ºC. After 24 h, the hydrogel beads were separated from the solution to ascertain if there is any visible leaching of PD-CNCs from the hydrogel beads into the solution. The release of Ag-NPs from the Ag-NP@PD-CNC-ALG hydrogel beads was also determined using the UV-Vis spectrophotometer at 430 nm.[260]

5.3 Results and discussion

5.3.1 Preparation and characterization

Pristine CNCs, when dispersed well in aqueous solutions, possess high surface area that is fully accessible for functionalization with PD and MF resin. MF-CNCs are formed by the *in situ* polycondensation of MF resin on the surface of CNCs when the pristine CNCs are mixed with MF precursor.[44,45] Upon the polycondensation of MF-resin onto pristine CNCs, the colour of the pristine CNC solution turns to milky white as shown in Figure 5.2. Polydopamine can be coated as a thin layer onto virtually any material by spontaneous oxidation of dopamine in an alkaline solution and this strategy is employed to coat polydopamine onto CNCs.[42,43,47] Coating of polydopamine onto pristine CNCs transform the pristine CNC solution into a black dispersion as shown in Figure 5.2.

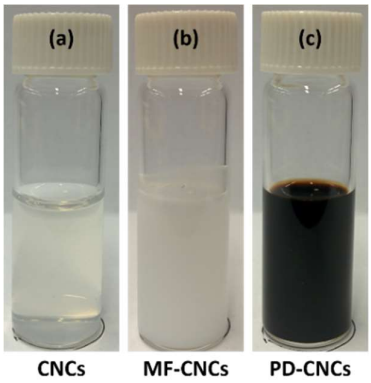

Figure 5.2. Photographs of the glass vials containing 1 wt% of the pristine CNCs, MF-CNCs and PD-CNCs.

TEM images of pristine CNCs, MF-CNCs and PD-CNCs are shown in Figure 5.3. Comparing the TEM images of MF-CNCs and PD-CNCs with that of pristine CNCs, we noted MF and PD were successfully coated onto CNCs. TEM images of pristine CNCs lacks the contrast, while with the coating of CNCs with MF and PD resulted in a better contrast.

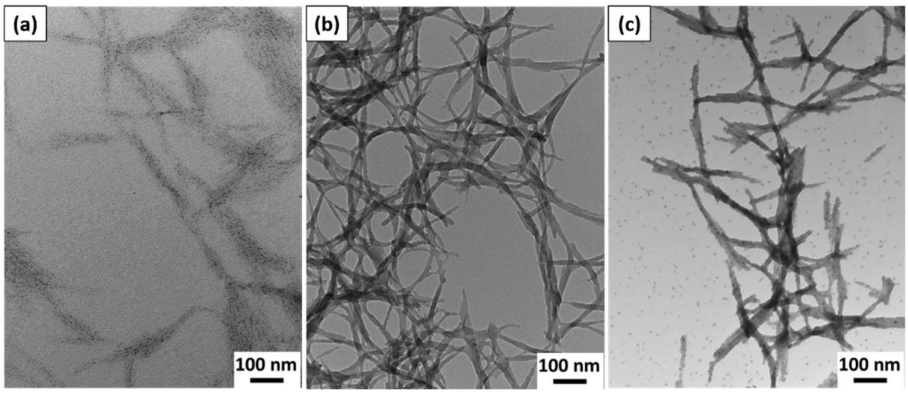

Figure 5.3. TEM images of (a) Pristine CNCs (b) MF-CNCs (C) PD-CNCs.

Ag-NPs can also be deposited onto PD-CNCs by *in situ* reduction of silver nitrate with PD-CNCs.[42,43] The morphology of the Ag-NPs@PD-CNCs (Figure 5.4b) revealed that Ag-NPs were deposited on the surface of PD-CNC with lower aggregation compared to pure Ag-NPs (Figure 5.4a) which formed large clusters when dried on the copper grid. It is well-known that pure Ag-NPs tends to agglomerate.[261] Depositing Ag-NPs onto PD-CNCs is an effective strategy to minimize the agglomeration and preserve the large surface area thereby having a greater impact on their antibacterial activity.[42] With Ag-NPs chelated onto PD-CNCs, the

leaching of Ag-NPs from the hydrogel beads is negligible, it is thus effective when used for water treatment applications.

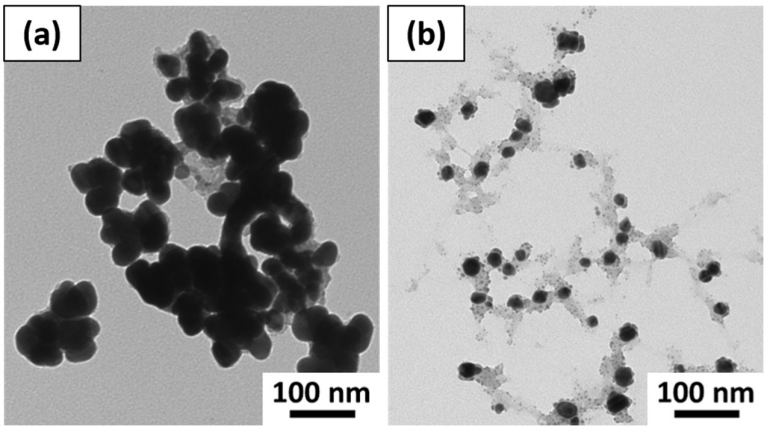

Figure 5.4. TEM images of (a) Ag-NPs (b) Ag-NPs@PD-CNCs.

Zeta potential measurements were performed to elucidate the surface charge characteristics of pristine and surface functionalized CNCs. Figure 5.5 shows the zeta potential measurements of pristine CNCs, MF-CNCs and PD-CNCs in different pHs. The surface of pristine CNCs and PD-CNCs were negative at all the pH values, while MF-CNCs displayed a strong dependence on pH; with positive values in acidic, neutral and near basic pH conditions and negative value in strong base.

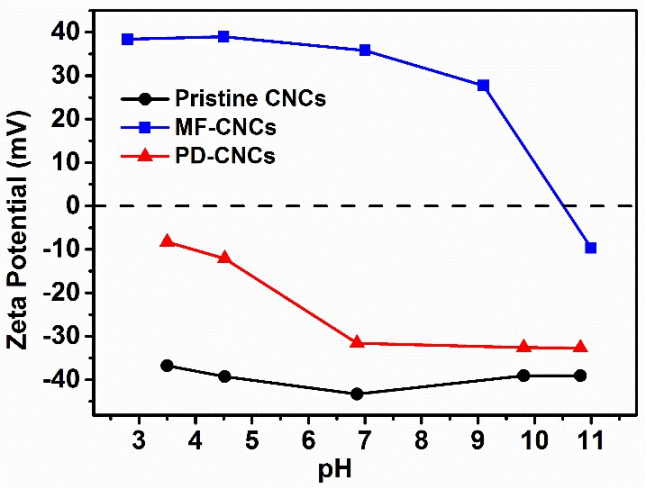

Figure 5.5. Zeta potential of pristine CNCs, MF-CNCs and PD-CNCs as a function of pH.

Ag-NP@PD-CNC-ALG hydrogel beads can be easily prepared by ionotropic gelation of alginate polymer chains present in the nanocomposite solution comprising of Ag-NPs@PD-CNCs using divalent cations like Ca^{2+} ions.[15–18] Photographs of the CNC-ALG and Ag-

NP@PD-CNC-ALG hydrogel beads are shown in Figure 5.6 respectively. CNC-ALG hydrogel beads are white whereas PD-CNC-ALG beads are black in colour since polydopamine functionalization of CNCs gives this characteristic black colour to the PD-CNC-ALG beads.

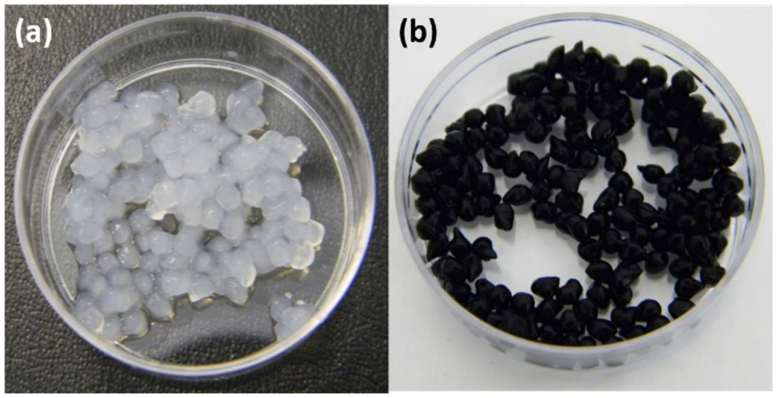

Figure 5.6. Digital photograph of (a) CNC-ALG hydrogel beads (b) PD-CNC-ALG hydrogel beads.

Cross-sectional SEM image (Figure 5.7) of the Ag-NP@PD-CNC-ALG hydrogel beads revealed the porous nature of the hydrogel beads. This porous nature of the hydrogel beads can contribute to the increased surface area for the adsorption of contaminants, such as organic dyes and heavy metal ions. Figure 5.7 provides a visual representation of the porous nature of the hydrogel beads and it does not facilitate the determination of the exact porosity. Moreover, the freeze-dried hydrogel beads used for the SEM experiments does not provide the exact visualization of the porous nature that the hydrogel beads in their native wet swollen state possess. SEM elemental analysis performed on a smaller section of the hydrogel matrix (shown at the top right corner of the figure) confirmed the existence of all the expected elements present in the Ag-NP@PD-CNC-ALG hydrogel beads, and the percentage content of the elements are also shown.

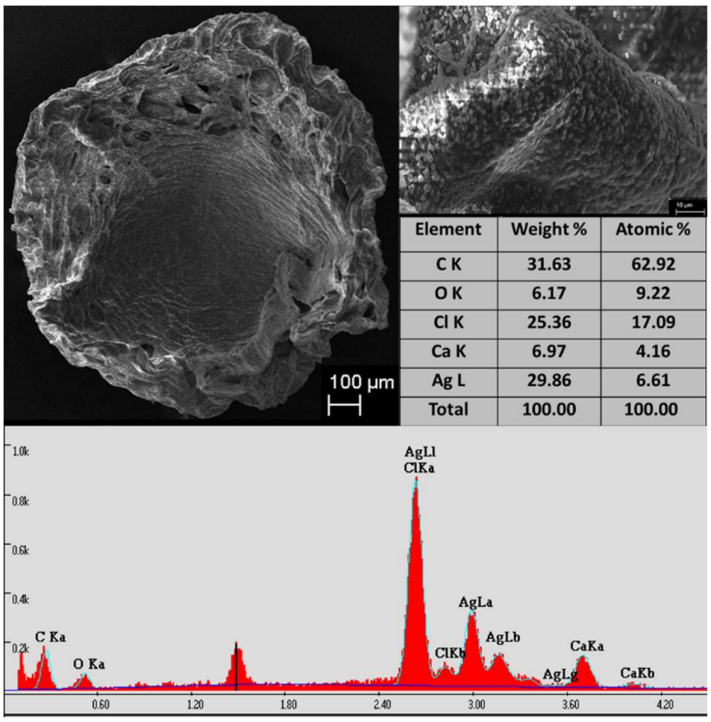

Figure 5.7. SEM-EDAX characterization of the Ag-NP@PD-CNC-ALG hydrogel beads.

5.3.2 Selectivity studies

Sulfate ester groups introduced on the surface of pristine CNCs during their production from pulp fibers via H_2SO_4 hydrolysis impart an overall negative charge to the pristine CNCs.[10] The anionic charges on this pristine CNCs interact strongly with the cationic compounds as demonstrated previously.[92] Surface functionalization is an ideal strategy to improve its affinity towards compounds bearing a specific charge or functional group. MF coating on CNCs can transform the charges on pristine CNCs from negative to positive. This will facilitate the binding to negative compounds. Also, PD possesses higher affinity towards Eschenmoser functional groups,[258] and hence coating of pristine CNCs with PD can also improve the affinity of CNCs towards compounds bearing Eschenmoser functional group. Thus, the surface functionalization of CNCs can be performed to tailor their selectivity to a wide range of compounds. This is further demonstrated by performing various selective dye adsorption experiments using pristine and surface functionalized CNCs. Figure 5.8 shows the chemical structures of the entities used for the functionalization of CNCs (Dopamine and Melamine-

Formaldehyde) and organic dyes (MB, MO, RB and CV) used in the selective dye adsorption studies.

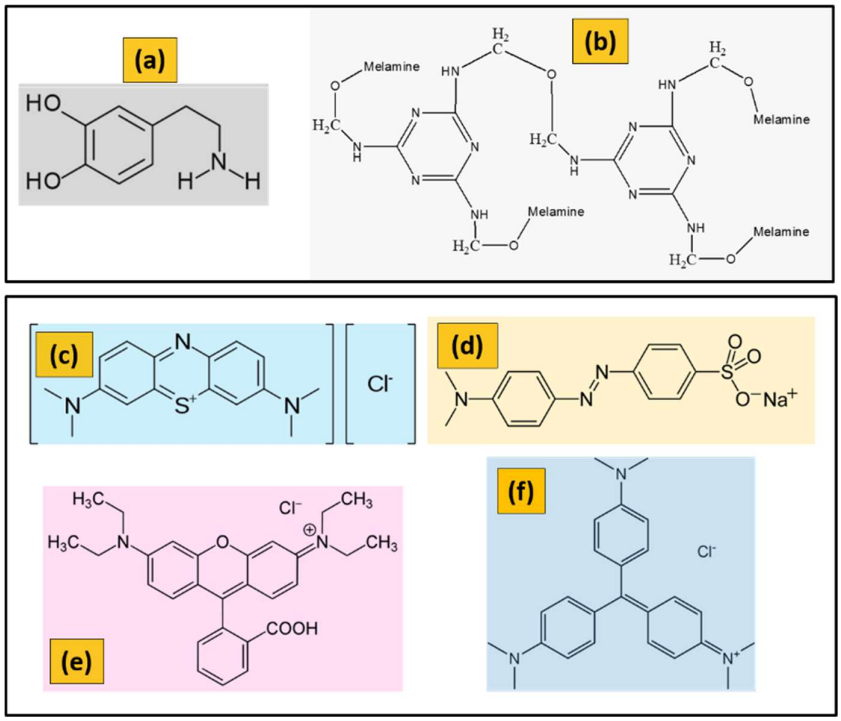

Figure 5.8. Chemical structure of (a) Dopamine (b) Melamine-Formaldehyde (c) MB (d) MO (e) RB and (f) CV.

Figure 5.9 shows the selective dye adsorption capability of pristine CNCs, MF-CNCs and PD-CNCs. When adsorption experiments were performed on MB/MO dye mixture using the same dosage of pristine CNCs, MF-CNCs and PD-CNCs, dark green colour of the MB/MO dye mixture changed to light green, blue and orange colour respectively. The light green colour is due to the presence of MB in the solution even though the majority of MB was removed from MB/MO. Negatively charged pristine CNCs bind to positively charged MB resulting in the removal of MB. The blue colour of the MB/MO dye mixture in the presence of MF-CNCs is due to the complete removal of MO leaving behind MB. Positively charged MF-CNCs bind to negatively charged MO resulting in the completely remove MO. The orange colour for PD-CNCs is due to complete removal of MB from MB/MO mixture, leaving behind MO. PD has a higher affinity towards Eschenmoser group containing MB resulting in the complete removal of MB.[258] UV-Vis spectrophotometer measurements performed on these solutions for individual dyes at their absorbance maximum validated these results. Thus, the affinity of

pristine CNCs to MB can be effectively improved by the complete removal of MB from MB/MO by PD coating. The selective adsorption of MB is driven by the 1,4-Michael addition reaction between the Eschenmoser structure of MB and the ortho position of the catechol phenolic hydroxyl group of PD.[258]

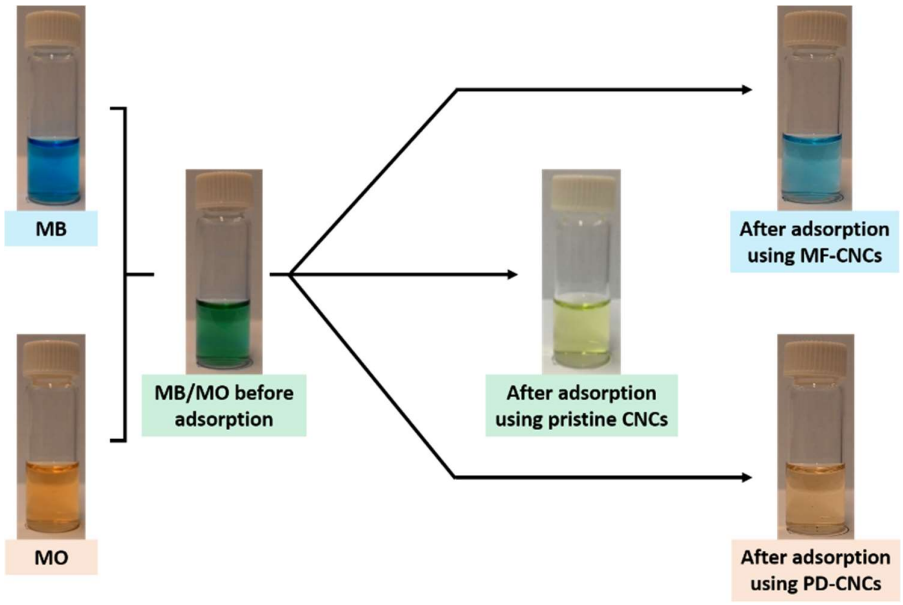

Figure 5.9. Selective dye adsorption study of MB/MO using pristine and surface functionalized CNCs.

Selective dye adsorption studies performed using varying dosages of pristine CNCs is shown in Figure 5.10. Results show that relatively higher amount of MB could be removed from MB/MO by increasing the concentration of pristine CNCs. However, increasing the dosage above 40 mg/mL did not have any significant improvement on the affinity towards the MB rather it binds to more MO because of the higher number of adsorption sites.

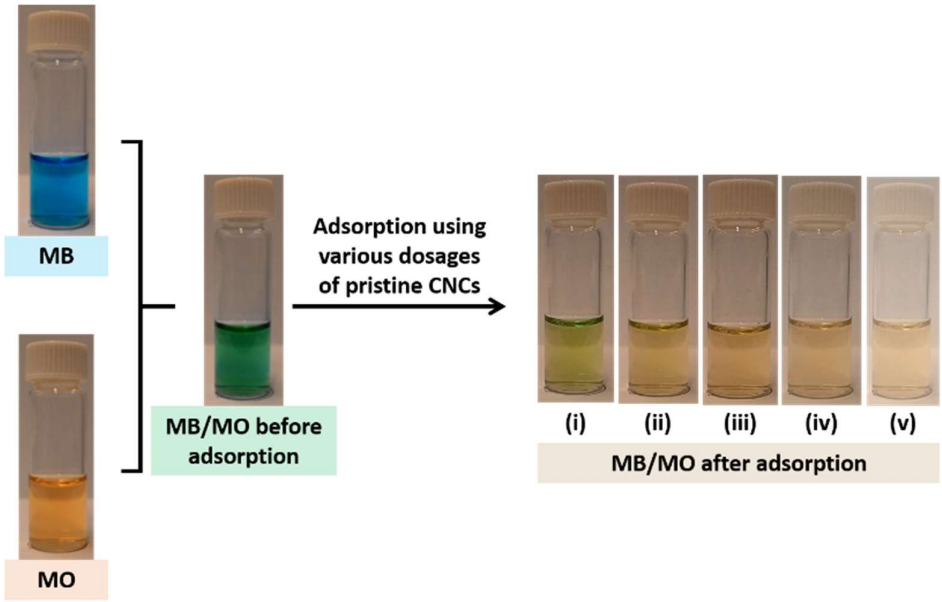

Figure 5.10. Selective dye adsorption study of MB/MO using varying dosages (i) 5 (ii) 10 (iii) 15 (iv) 20 and (v) 25 mg/mL of pristine CNCs.

Selective adsorption studies on MB/RB and MB/CV using PD-CNCs was performed to further confirm the improved affinity of PD towards Eschenmoser functional groups. RB and CV were chosen in accordance to their chemical similarity to MB with respect to Eschenmoser functional group. Figure 5.11 indicates that the purple colour of MB/RB and dark blue colour of MB/CV dye mixtures change to pink colour and colourless when selective dye adsorption studies were performed using PD-CNCs as adsorbents. This is because RB remained in the case of MB/RB dye mixture as opposed to no dye left behind in the case of MB/CV dye mixture. This is because of CV bears Eschenmoser functional group like MB as opposed to RB and this clearly validates the improved affinity of PD towards Eschenmoser functional groups. Also, it should be noted that the as the selectivity for PD-CNCs was imparted by 1,4-Michael addition reaction their reversibility may be limited to only single use as opposed to another type of CNCs whose selectivity was based on electrostatic interaction.

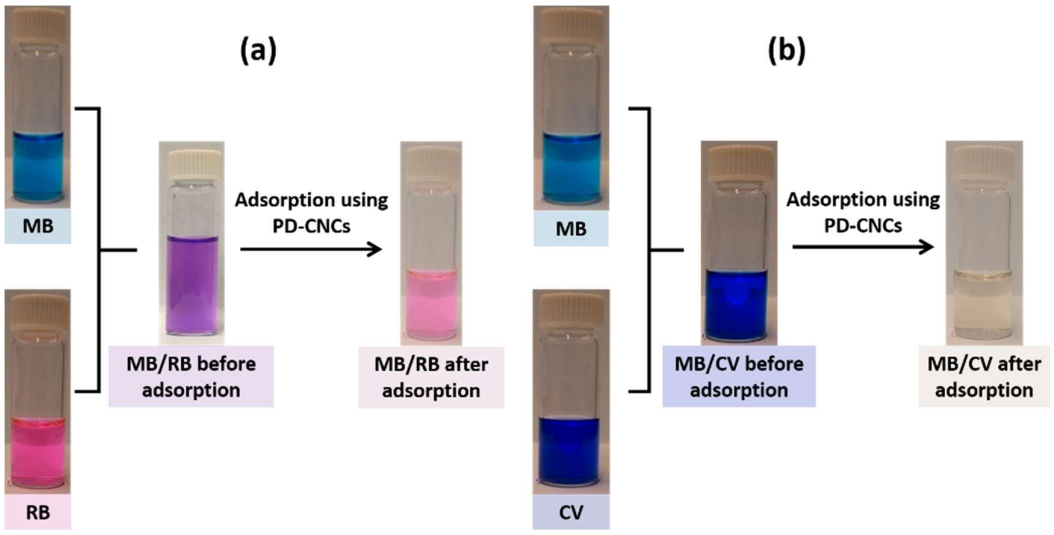

Figure 5.11. Selective dye adsorption of (a) MB/RB and (b) MB/CV using PD-CNCs.

Surface functionalized CNCs can also impart this selectivity property to the hydrogel beads and this is demonstrated by performing selective dye adsorption experiments using PD-CNC-ALG hydrogel beads wherein the PD-CNCs have an affinity for Eschenmoser functional groups bearing compounds. Figure 5.12 shows that the colours of the dye mixtures of MB/MO and MB/RB changed from dark green and purple to yellow and pink colour when PD-CNC-ALG hydrogel beads were used. UV-Vis spectrophotometer measurements on both the residual solutions after adsorption indicated the 100% removal of MB by PD-CNC-ALG hydrogel beads from MB/MO and MB/RB dye mixtures leaving behind MO and RB respectively. In case of MB/CV dye mixture, the solution turned completely colourless after adsorption denoting the complete removal of both MB and CV from the MB/CV dye mixture. This is because both MB and CV possess Eschenmoser functional groups with strong affinity to PD-CNCs.

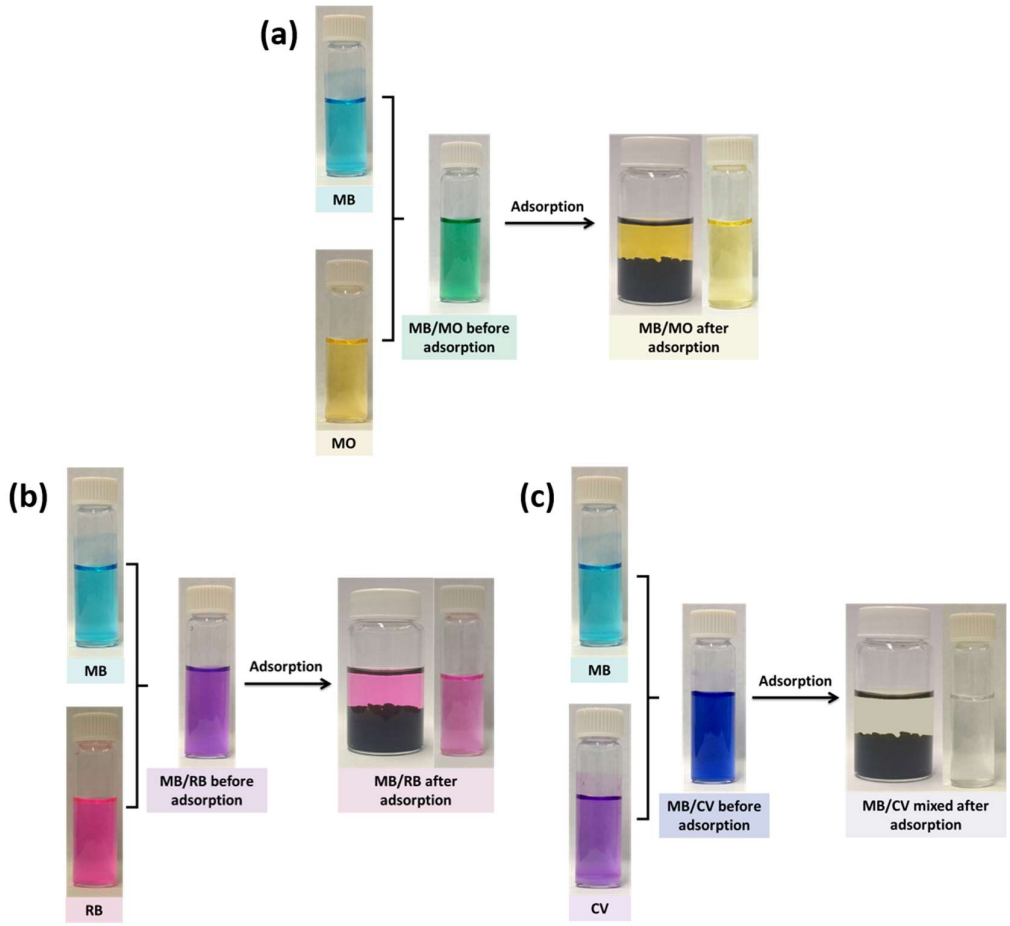

Figure 5.12. Photographs of selective adsorption of MB from (a) MB/MO (b) MB/RB (c) MB/CV mixed solutions by using PD-CNC-ALG hydrogel beads.

Figure 5.13 shows the colour of the MB/MO dye mixture before and after adsorption using CNC-ALG and PD-CNC-ALG beads. The colour of MB/MO dye mixture after adsorption using CNC-ALG hydrogel beads, retained a slight green colour indicating the presence of MB in the solution whereas the colour of MB/MO dye mixture after adsorption using PD-CNC-ALG beads changed from green to yellow indicating the complete removal of MB. The CNC-ALG beads were capable of removing only 72% MB from the MB/MO dye mixture as opposed to 100% removal reported for the PD-CNC-ALG hydrogel beads. This selective dye adsorption study performed with MB/MO dye mixture using CNC-ALG and PD-CNC-ALG hydrogel beads revealed the increased affinity of PD-CNC-ALG hydrogel beads towards MB compared to CNC-ALG hydrogel beads.

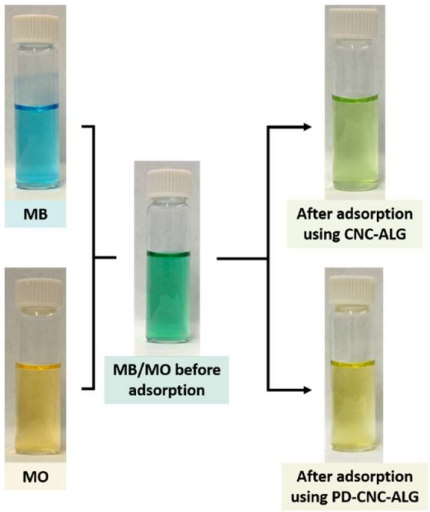

Figure 5.13. Photographs of selective adsorption of MB from MB/MO mixed the solution by using CNC-ALG and PD-CNC-ALG hydrogel beads.

5.3.3 Dye adsorption studies

Figure 5.14a shows the colour of MB solution after each batch adsorption cycle for CNC-ALG and PD-CNC-ALG hydrogel beads. The colour of MB solution clearly indicated that PD-CNC-ALG hydrogel beads adsorb comparatively more dye than CNC-ALG hydrogel beads during the batch adsorption cycles and at the end of the second cycle, where the MB solution became colourless in PD-CNC-ALG hydrogel beads denoting the complete removal of MB. Figure 5.14b shows the concentration of MB during each batch adsorption cycle for CNC-ALG and PD-CNC-ALG hydrogel beads. At the end of first and second cycles, the concentration of MB was 21.89 mg/L and 7.56 mg/L respectively for CNC-ALG hydrogel beads whereas for PD-CNC-ALG hydrogel beads it had lower values of 14.35 mg/L and 0 mg/L respectively. This proves that at the same dosage of PD-CNC-ALG hydrogel beads, it is possible to adsorb more MB compared to CNC-ALG hydrogel beads. The effectiveness of the PD-CNCs was further confirmed by comparing its MB adsorption ability with that of pristine CNCs. Figure 5.15 shows 90.05% of the dye was removed with PD-CNCs and only 71.35% was removed with pristine CNCs. This is because polydopamine functionalization of CNCs provides an improved affinity for CNCs towards Eschenmoser group containing dyes. It was already reported that there is an Eschenmoser salt assisted 1,4-Michael addition reaction between the

ortho position of catechol phenolic hydroxyl group of polydopamine and Eschenmoser group in MB that drives the adsorption process.[258]

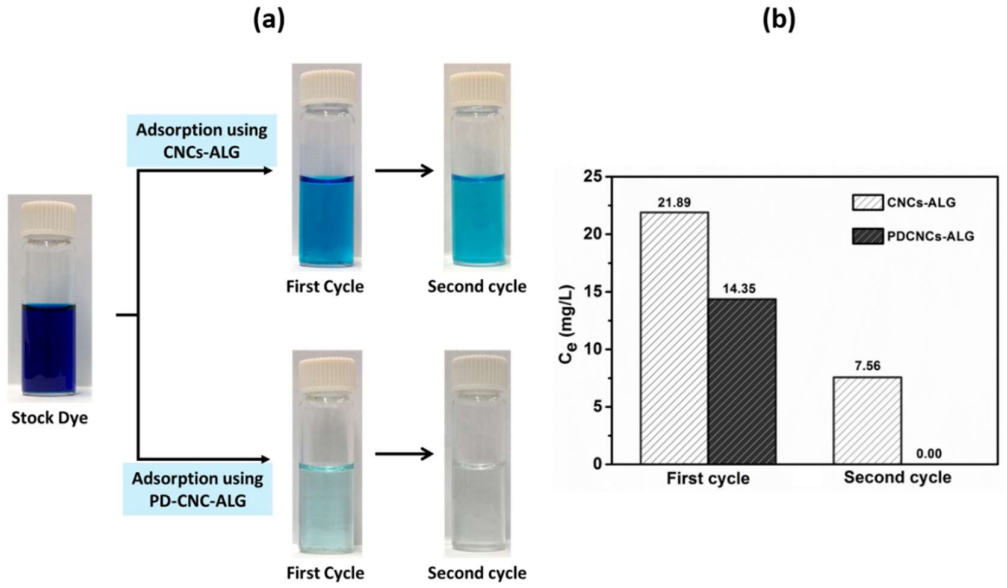

Figure 5.14. (a) Photographs of MB adsorption by CNC-ALG and PD-CNC-ALG beads during two successive equilibrium batch adsorption cycles. (b) The concentration of MB during the two successive equilibrium batch adsorption cycles for CNC-ALG and PD-CNC-ALG beads respectively.

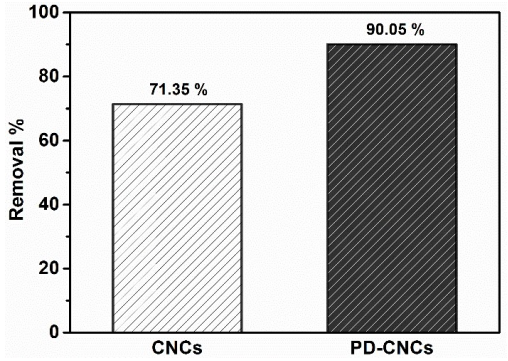

Figure 5.15. Dye Removal % of pristine CNCs and PD-CNCs.

5.3.4 Heavy metal ions adsorption studies

Figure 5.16 shows the removal % of various heavy metal ions by PD-CNC-ALG hydrogel beads. The result suggests that PD-CNC-ALG hydrogel beads are very effective in removing Pb^{2+}, Hg^{2+}, Cr^{3+} and Cu^{2+} as more than 80% of all heavy metal ions were removed. The hydroxyl and amine groups present on the polydopamine coating of CNCs can serve as binding sites to chelate the heavy metal ions.[258]

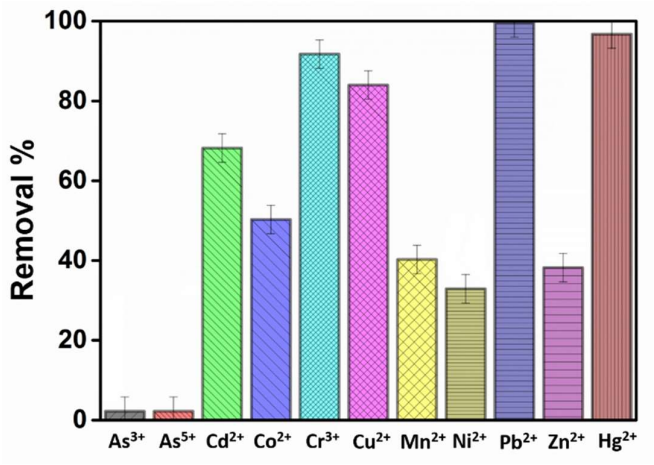

Figure 5.16. Removal % of various heavy metal ions by PD-CNC-ALG hydrogel beads.

5.3.5 Kinetic studies

Adsorption kinetic study of an adsorbent is essential to understand the rate of adsorption, mechanism of adsorption and possible rate controlling steps. The kinetics of CNC-ALG hydrogel beads was reported previously.[15] Similar to CNC-ALG hydrogel beads; pseudo-second order kinetic model fitted well to model the adsorption kinetics of MB on PD-CNC-ALG hydrogel beads. This model can be expressed using Equation 5.4.[220]

$$\frac{dq_t}{dt} = k_2(q_e - q_t)^2 \tag{5.4}$$

where q_e (mg/g) is the amount of dye adsorbed at equilibrium, q_t (mg/g) is the amount of dye adsorbed at time t (min), and k_1 (min^{-1}) is the rate constant of pseudo first order model, k_2 (g mg^{-1} min^{-1}) is the rate constant of pseudo second order model. The experimental kinetic data for various initial dye concentrations were fitted using the linearized form of pseudo-second-order model equation (Equation 5.5) to determine the kinetic parameters of the adsorption process.

$$\frac{t}{q_t} = \frac{1}{k_2 q_e^2} + \frac{1}{q_e}t \tag{5.5}$$

The pseudo second order rate constant (k_2) and q_e were determined from the slope and intercepts of the plots of t/q_t versus time t. The value of experimentally determined q_e (q_e(expt)), calculated q_e (q_e(calc)), correlation coefficient (R^2) are shown in Table 5.1. The pseudo-second-order kinetic model gave an excellent fit with an average regression coefficient of R^2 = 0.99.

Also, q_e(calc) determined from the pseudo-second-order kinetic model agreed well with q_e (expt), confirming that the kinetics of dye adsorption by CNC–ALG hydrogel beads are better described by the pseudo- second-order kinetic model rather than the pseudo- first-order model. The kinetic adsorption data and their fitting using pseudo-second order equation is shown in Figure 5.17.

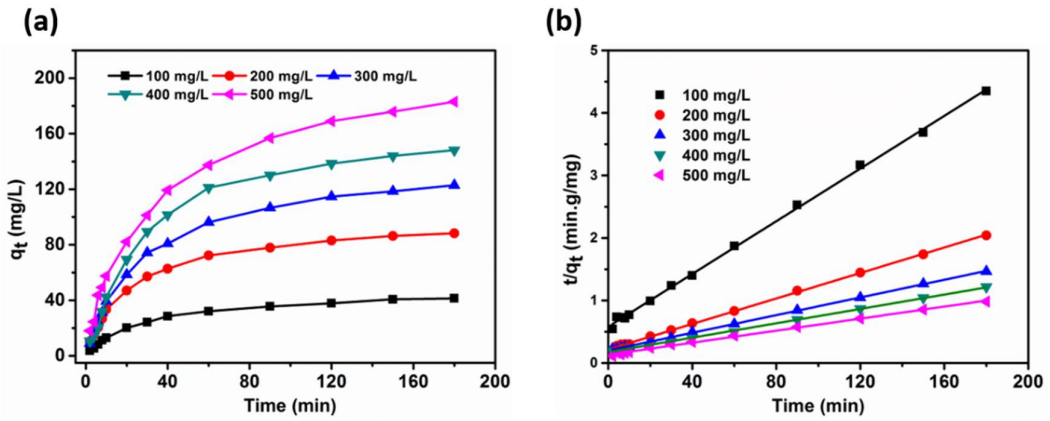

Figure 5.17. (a) Plot of qt versus time for various initial dye concentrations. (b) Pseudo-second-order kinetic model fitting for batch adsorption of various initial dye concentrations onto PD-CNC-ALG hydrogel beads.

Table 5.1. Estimated absorption kinetic parameters for MB on PD-CNC-ALG beads determined using Pseudo-second-order kinetic model.

Concentration (mg/L)	q_e (expt) (mg/g)	q_e (calc) (mg/g)	$k_2 \times 10^{-4}$ (min^{-1})	R^2
100	48.20	47.39	7.65	0.99
200	98.15	98.03	4.80	0.99
300	138.21	140.84	2.51	1.00
400	169.19	172.41	1.92	0.99
500	208.66	208.33	1.75	0.99

5.3.6 Adsorption isotherm

The abundant functional groups present in polydopamine such as catechol groups, amine groups, and aromatic moieties are expected to offer a large number of active sites to bind heavy metal ions and organic pollutants like dyes via electrostatic interaction, coordination or chelation, hydrogen bonding, or π–π stacking interaction.[46] The ability of PD-CNC-ALG beads to adsorb MB and Cu^{2+} ions was evaluated by plotting the adsorption isotherm. The equilibrium adsorption data needed to construct the Langmuir adsorption isotherm was obtained from the

concentration values of MB and Cu^{2+} ions. UV-Vis spectroscopy was used to measure the concentration values of MB and Cu^{2+} ions. MB possesses an absorbance peak at 664 nm whereas for Cu^{2+} ions it is essential to form a coloured complex with ethylenediamine prior to measurement so that an absorbance maxima can be obtained at 556 nm.[259] Figure 5.18 shows the formation of Cu^{2+} – Ethylenediamine complex and the corresponding calibration curve used for the determination of Cu^{2+} concentration.

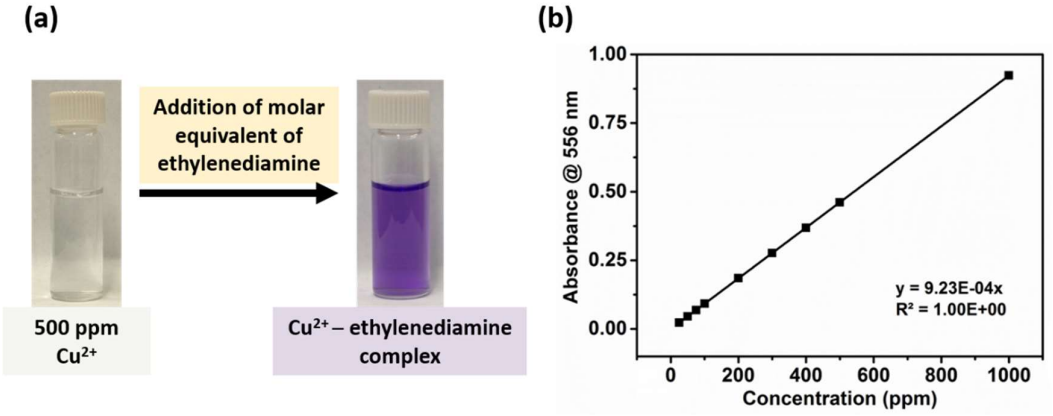

Figure 5.18. (a) Formation of Cu^{2+} – Ethylenediamine coloured complex (c) Calibration curve used for the calculation of Cu^{2+} concentration.

Adsorption isotherms were used to show the relationship between the mass of adsorbate adsorbed per unit mass of the sorbent (q_e) and the liquid phase adsorbate concentration (C_e) at equilibrium. The equilibrium adsorption data was modeled using the Langmuir adsorption isotherm and the maximum adsorption capacity of PD-CNC-ALG beads for MB and Cu^{2+} ions was determined. The Langmuir isotherm is described by using Equation 5.6.[226]

$$q_e = \frac{q_m K_L C_e}{1 + K_L C_e} \tag{5.6}$$

where q_e is the amount of dye adsorbed per g of adsorbent (mg/g) in equilibrium, q_m is the maximum amount of dye which can be adsorbed per g of adsorbent (mg/g) in equilibrium, C_e is the equilibrium concentration of free dye molecules in the solution (mg/L) and K_L is a constant related to the energy of adsorption (L/mg) which shows the affinity between the dye and adsorbent. The values of K_L and q_m can be extracted using the linearized form of the Langmuir isotherm (Equation 5.7).

$$\frac{1}{q_e} = \frac{1}{K_L q_m C_e} + \frac{1}{q_m} \tag{5.7}$$

The linearized form of the Langmuir isotherm is described by a plot of $1/q_e$ versus $1/C_e$ (Figure 5.19a for MB and Figure 5.19b for Copper), and q_m is determined from the slope. The q_m of MB and Cu^{2+} ions onto the PD-CNC-ALG beads were calculated to be 333.33 mg/g and 72.99 mg/g respectively. It was also observed that polydopamine functionalization of CNCs has resulted in a 30% increase in the q_m of hydrogel beads for MB compared to pristine CNCs incorporated hydrogel beads which has a reported q_m value of 256.41 mg/g.[15]

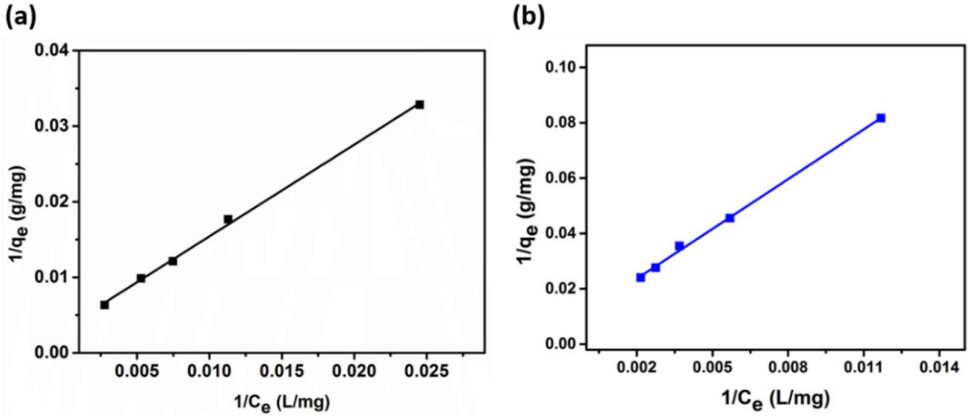

Figure 5.19. Linearized Langmuir plot for adsorption of (a) MB and (b) Cu2+ onto PD-CNC-ALG hydrogel beads.

5.3.7 Antibacterial studies

In this study, PD-CNC-ALG hydrogel beads were made antibacterial so that they can be used for the disinfection of bacteria in the water. This was done by depositing Ag-NPs onto PD-CNCs before incorporating within into the alginate hydrogel bead. Ag-NP@PD-CNC-ALG beads were then evaluated for their antibacterial activity on Gram-positive bacteria *Bacillus subtilis* and Gram-negative bacteria *Escherichia coli*. Figure 5.20 shows the CFU on the agar plates for *Escherichia coli* and *Bacillus subtilis* with varying dosage of Ag-NP@PD-CNC-ALG hydrogel beads respectively. Figure 5.21 shows the vials containing various dosages of the Ag-NP@PD-CNC-ALG hydrogel beads in the bacteria containing media for both *Escherichia coli* and *Bacillus subtilis* respectively. The CFU and turbidity of various dosage samples were compared to the control sample with no hydrogel beads. 1 mg/mL dosage sample appeared slightly turbid whereas both 2 mg/mL and 3 mg/mL dosage samples were

clear suggesting the presence of bacteria in 1 mg/mL dosage sample and no bacteria in the rest. This was confirmed from the CFU counts done on the gar plates. CFU counts for *Escherichia coli* were 4.32×10^9, 4.16×10^9 and 0 for control, 1mg/mL and rest of the samples (2 mg/mL and 3 mg/mL) respectively. CFU counts for *Bacillus subtilis* were 4.2×10^9, 6.3×10^7 and 0 for control, 1mg/mL and rest of the samples (2 mg/mL and 3 mg/mL) respectively. For both the bacteria, as the number of Ag-NP@PD-CNC-ALG hydrogel beads increased, the density of bacterial colonies decreased because of the increased silver content present that contributes to the increased antibacterial activity.

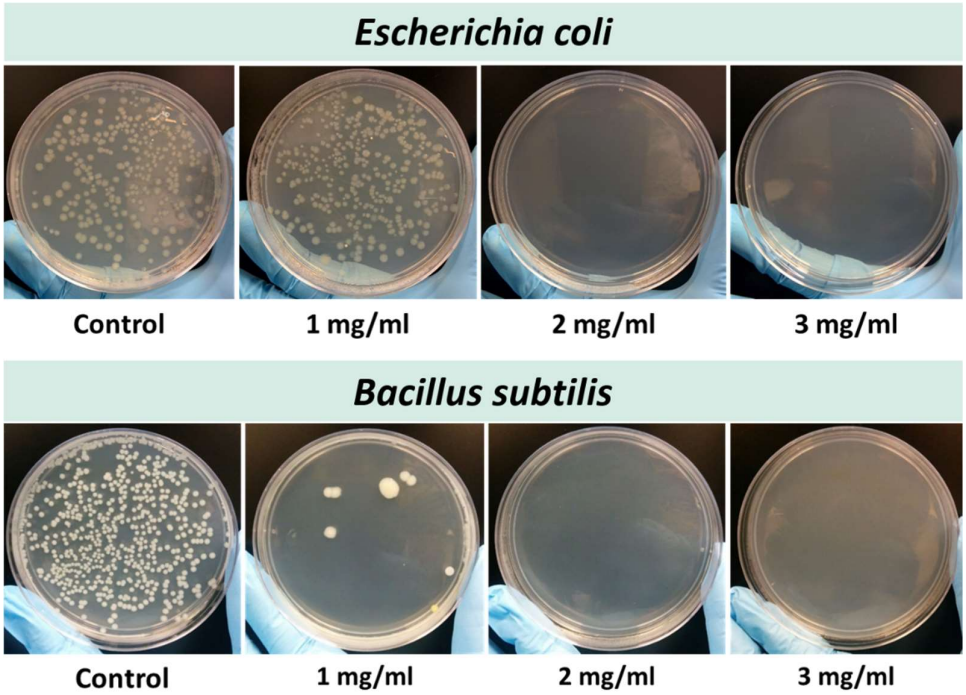

Figure 5.20. CFU on the agar plates for *Escherichia coli* and *Bacillus subtilis* with varying dosage of Ag-NP@PD-CNC-ALG hydrogel beads respectively.

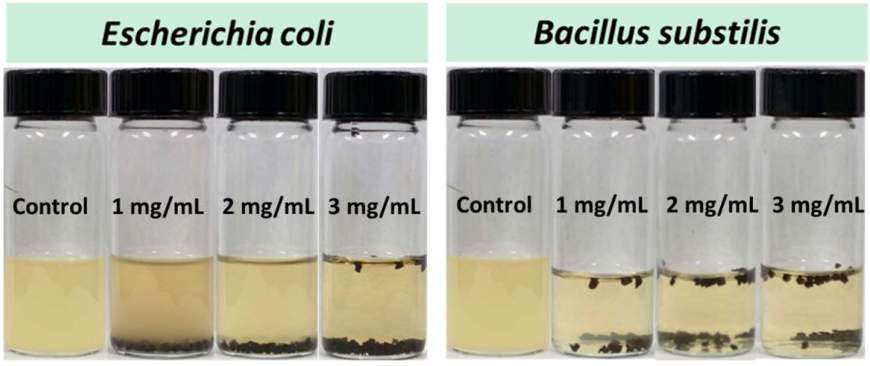

Figure 5.21. Vials containing various dosages of the Ag-NP@PD-CNC-ALG hydrogel beads in the bacteria containing media for both *Escherichia coli* and *Bacillus subtilis*.

5.3.8 Leaching studies

Ag-NPs possessed excellent antimicrobial properties against a wide variety of microorganisms.[262] However the massive deployment of Ag-NPs for water treatment applications has been hindered due to non-availability of suitable anchoring substrates that prevent Ag-NPs release into water and dislodgement of the Ag-NPs from the polymeric matrix.[263,264] In this work, this problem was addressed by chelating Ag-NPs on PD-CNCs before they were incorporated in alginate hydrogel matrix which can prevent the leaching of Ag-NPs. Ag-NPs possesses a characteristic peak at around 430 nm due to the surface plasmon resonance,[260] and hence the release of Ag-NPs can be determined by UV-Vis spectrophotometer with a detection limit of 0.1µg/L. Figure 5.22 shows the UV-Vis spectra various standard concentrations and release a sample of Ag-NPs. The release samples did not show the typical peak of Ag-NPs indicating that the concentration of Ag-NPs in the sample was below 0.1µg/L which is far below the WHO's recommended limit for total Ag concentration in drinking water of 100 µg/L.[264] This may due to strong chelation of Ag-NPs on the PD-CNCs within the crosslinked alginate hydrogel matrix. Also, no visible leaching of PD-CNCs from the Ag-NP@PD-CNC-ALG hydrogel beads was observed when the hydrogel beads were stored in water for a prolonged period of time.

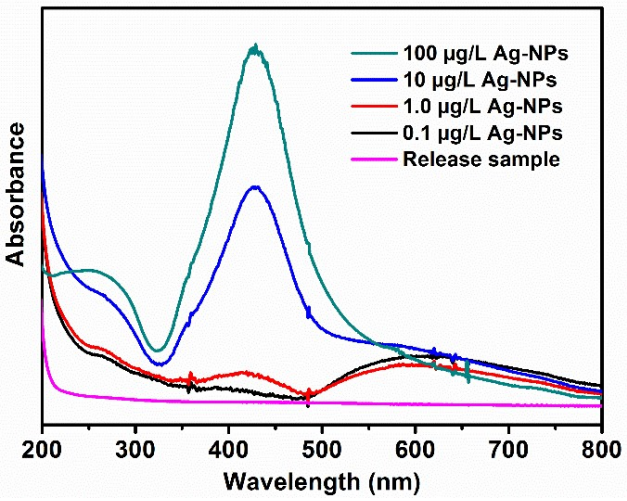

Figure 5.22. UV-Vis spectra of Ag-NPs of various standard concentrations and release sample.

5.4 Conclusions

Pristine CNCs were coated with melamine-formaldehyde (MF) and polydopamine (PD) to prepare MF-CNCs and PD-CNCs respectively. Selective dye adsorption studies performed using pristine CNCs and surface functionalized demonstrated that the selectivity of the CNCs can be tailored by surface functionalization. When methylene blue (MB)/methyl orange (MO) dye mixtures were subjected to adsorption using pristine and surface functionalized CNCs, negatively charged pristine CNCs showed an affinity for positively charged dye MB. Whereas, positively charged MF-CNCs were found to have a high affinity for negatively charged dye MO. The selectivity of pristine CNCs for MB was further improved upon coating with PD as it has high affinity towards Eschenmoser functional groups present in MB. This is validated by performing additional adsorption experiments using dye mixtures of MB with rhodamine B and crystal violet respectively. The ability of the surface functionalized CNCs to tailor the properties of nanocomposites that incorporate them was further explored by preparing a novel nanocomposite viz., PD-CNC-ALG hydrogel beads. The applicability of these hydrogel beads for water treatment application was demonstrated using selectivity studies, batch adsorption studies and antibacterial studies. Selective dye adsorption studies have demonstrated that PD-CNC-ALG hydrogel beads have selectivity towards Eschenmoser group containing dyes like MB and have improved adsorption ability for these dyes compared to CNC-ALG hydrogel beads. They also showed the good binding ability for heavy metal ions like Pb^{2+}, Hg^{2+}, Cr^{3+} and Cu^{2+}. Kinetics of MB adsorption onto PD-CNC-ALG beads was modelled using the pseudo-second-order kinetic model and the rate constants of adsorption were determined. The maximum adsorption capacity of PD-CNC-ALG hydrogel beads for MB and Cu^{2+} ions were found to be 333.33 mg/g and 72.99 mg/g respectively. Ag-NPs can also be chelated with PD-CNC-ALG hydrogel beads thereby reducing the leaching of Ag-NPs from their polymeric matrix. Thus, the prepared PD-CNC-ALG hydrogel beads can be considered as a versatile adsorbent with a wide range of capabilities for use in water treatment.

Chapter 6*

Diffusion-Controlled Simultaneous Sensing and Scavenging of Heavy Metal Ions in Water Using Atomically Precise Cluster–Cellulose Nanocrystal Composites

Development of a system that can simultaneously sense and scavenge toxic heavy metal ions at low concentrations is an ideal solution for *in-situ* monitoring and purification of contaminated water. In this paper, we report on the synthesis and application of a novel system, luminescent atomically precise cluster – cellulose nanocrystal composite namely bovine serum albumin protected gold nanoclusters (Au@BSA NCs) loaded cellulose nanocrystal – alginate hydrogel beads, that can simultaneously sense and scavenge heavy metal ions, specifically mercury ions in water. Characterization of the system performed using scanning electron microscopy coupled with energy dispersive spectroscopy and X-ray photoelectron spectroscopy elucidated the physical and chemical characteristics of the system. Additionally, we proposed a new method to visualize the diffusion phenomenon and calculate the effective diffusion coefficient of heavy metal ions in hydrogel beads by monitoring the fluorescence quenching dynamics of Au@BSA NCs upon binding with mercury ions. Finally, practical applications of this nanocomposite were demonstrated using batch adsorption experiments as well as using a dip pen device loaded with the hydrogel beads for *in-situ* monitoring of heavy metal ions in water.

*This chapter is adapted from a paper "Nishil Mohammed, Avijit Baidya, Vasanthanarayan Murugesan, Avula Anil Kumar, Mohd Azhardin Ganayee, Jyoti Sarita Mohanty, Kam Chiu Tam and Thalappil Pradeep, Diffusion-Controlled Simultaneous Sensing and Scavenging of Heavy Metal Ions in Water Using Atomically Precise Cluster–Cellulose Nanocrystal Composites, *ACS Sustainable Chemistry and Engineering*, 2016, 4 (11), 6167-6176."

6.1 Introduction

Water is being increasingly contaminated by a wide variety of pollutants from industrial, municipal and agricultural sources like heavy metal ions, dyes, food additives, pharmaceuticals, detergents, agrochemicals, etc. Thus, access to clean water is becoming more challenging and efficient technologies that can purify this contaminated water have become essential.[1,257] Among all these pollutants, toxic heavy metal ions, which accumulate in the food chain, continue to be a major concern. Various physical, chemical and biological treatment methods can be employed to remove heavy metal ions from water. Of all these treatment methods, adsorption implemented using a well-designed system offers the best solution for producing high quality treated water at affordable cost. This technique offers many advantages, such as simplicity in design and operation, low initial investment, effectiveness and insensitivity to other substances present in the water stream. Researchers round the globe are seeking for a various low-cost non-conventional adsorbent materials.[2,3,7,8,265]

In this context, the use of sustainable nanomaterials such as cellulose nanocrystals (CNCs) for the adsorption of heavy metal ions from water is gaining momentum and several researchers have examined its feasibility.[107,109,113,114,171,266] CNCs are rod-like nanoparticles obtained from cellulosic biomass, having diameters in the range of 5-20 nm and lengths of a few hundred nanometers. They can be produced at the industrial scale by acid hydrolysis of pulp fibers. Because of their high specific surface area, good mechanical strength, biodegradability and high functionality,[10] adsorbents based on these nanomaterials have the capacity to remove a wide variety of pollutants from wastewater.[12,13] Even though these nanomaterials were found to outperform several conventional adsorbents used in developing countries, their practical application for large-scale water treatment systems is limited as they are difficult to separate from the water bodies after adsorption. This can be solved by incorporating them into matrices, like hydrogel beads that can be easily used in batch as well as column adsorption processes.[15–17]

Mercury, in both organic and inorganic forms, is one of the most hazardous environmental contaminants among all heavy metal ions.[267] Different approaches have been

used for the determination of trace levels of mercury. Fluorescence-based techniques are important in the determination of ionic mercury. However, for trace levels of heavy metals, ultrasensitive methods that are readily implementable in the field have to be developed, working at the limit of single ions.[268]

Aspicules,[269] atomically precise quantum clusters of noble metals, have been gaining attention in the field of sensor owing to their enhanced photostability, high quantum yield and ease of functionalization. Their discrete energy states resulting from a size range corresponding to Fermi wavelength of electrons, endow them with luminescent properties in the visible range. Though a wide range of ligands have been utilized for synthesizing aspicules, biomolecules like proteins and peptides are emerging owing to their simplicity in synthesis, biocompatibility and wide range of applications. Noble metal clusters protected with BSA, lysozyme, and lactoferrin are some notable examples.[270–275] Xie et al.,[276] first reported the use of BSA protected gold nanoclusters (Au@BSA NCs) for sensing Hg^{2+} ions. Several other groups have used the protein protected quantum cluster systems for sensing heavy metal ions like Hg^{2+}, Cu^{2+} and Pb^{2+}. Though highly sensitive, the colloidal stability of these clusters limit their application in the field and thus a suitable substrate to anchor them is required. We have previously demonstrated the ability of Au@BSA to bind with nanofibers and have used it for detecting Hg^{2+} ions. Such confinement on a substrate also leads to an increase in the luminescence intensity.[277]

Until now there have been no reports on CNCs based nanocomposites that can be used for the simultaneous sensing and scavenging of heavy metal ions in water. In this paper, we report on the synthesis and application of novel nanocomposite hydrogel beads, viz., Au@BSA NCs loaded cellulose nanocrystal-alginate hydrogel beads that can simultaneously sense and scavenge heavy metals ions, specifically Hg^{2+} ions in water. Several researchers have attempted to probe diffusion and calculate the effective diffusion coefficient using various techniques that are rather complex. Herein, we reported a novel approach based on the fluorescence quenching dynamics of Au@BSA NCs upon Hg^{2+} ion binding, which can be used as a tool to probe diffusion and determine the diffusion coefficient of Hg^{2+} ions in the hydrogel

beads. Here the sensing occurs as a result of the adsorption of Hg^{2+} ions on Au@BSA NCs which is controlled by several parameters like analyte concentration, porous and anionic nature of the hydrogel bead, etc. We performed batch adsorption experiments to elucidate the adsorption characteristics that are pertinent to the sensing application. At this stage of development, the practical application of this system for the removal of Hg^{2+} ions in contaminated water is limited to small scale operations. Finally, the practical application of these hydrogel beads is demonstrated using a dip pen device containing these hydrogel beads for *in-situ* monitoring of heavy metal ions in water. Figure 6.1 is schematic representation showing the preparation of atomically precise cluster-cellulose nanocrystal composites and their simultaneous sensing and scavenging of Hg^{2+} ions in water.

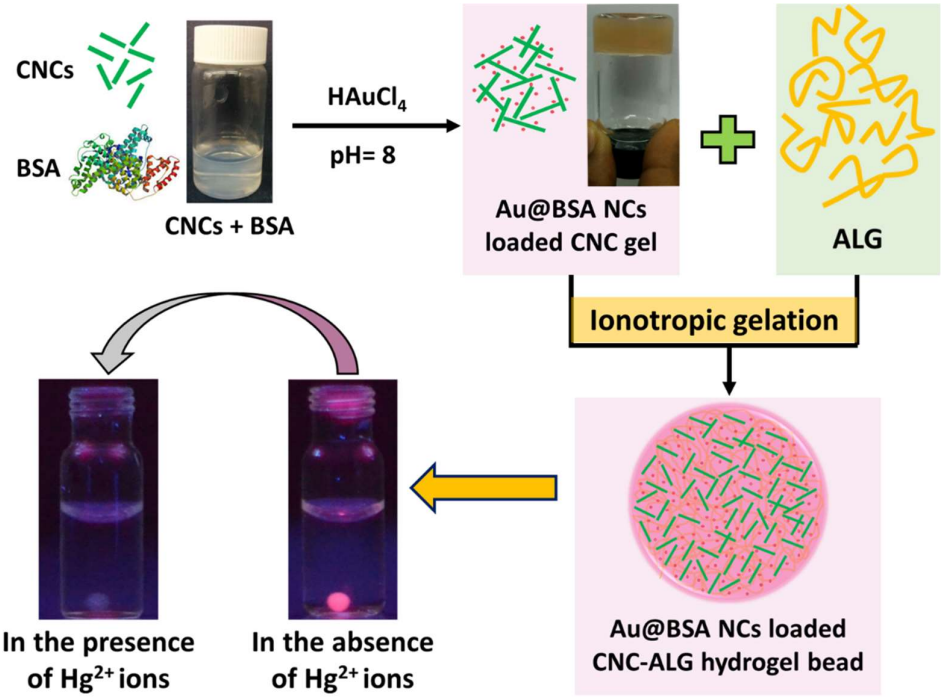

Figure 6.1. Schematic representation showing the preparation of atomically precise cluster-cellulose nanocrystal composites and their simultaneous sensing and scavenging of Hg^{2+} ions in water.

Experimental section

6.1.1 Materials used

CNCs supplied by University of Maine Process Development Centre were used in this study (Please note: Both Celluforce and UMaine CNCs are sulfated CNCs, however for this work included in Chapter 6, we used UMaine CNCs because of proprietary reasons). Sodium alginate (ALG) was purchased from FMC Biopolymer. Sodium chloride (NaCl), calcium chloride ($CaCl_2$) and tetrachloroauric acid trihydrate ($HAuCl_4.3H_2O$) were purchased from Sigma-Aldrich. Bovine serum albumin (BSA) was purchased from Sisco Research Laboratories Pvt. Ltd. Divalent acetates of mercury, copper, zinc, nickel, lead, cadmium, manganese, cobalt, iron, and magnesium were purchased from Merck. Chromium (III) nitrate nonahydrate ($Cr(NO_3)_3.9H_2O$) was purchased from Lobachemie and sodium arsenite ($NaAsO_2$) was purchased from SD Fine Chemicals Limited. Purified water from a Milli-Q Millipore system (>18 MΩcm) was used for all the experiments. All chemicals were used directly without additional purification.

6.1.2 Preparation of nanocomposite

Preparation of nanocomposite was performed in two steps. In the first step, synthesis of Au@BSA NCs loaded CNC gel was carried out. During this step, 1 mL of 6 mM $HAuCl_4.3H_2O$ aqueous solution was added dropwise to a 4-mL reaction mixture containing 25 mg BSA and 150 mg CNCs, stirred overnight. After 30 min, the pH of this solution was adjusted to ~12 by adding 200 µL of 1 M NaOH and then the whole reaction mixture was stirred overnight. The reaction mixture turned into a gel-like structure and the formation of Au@BSA NCs was indicated by the characteristic colour change from pale yellow to deep brown, with intense red fluorescence under UV light. In the second step, the final nanocomposite, viz. Au@BSA NCs loaded CNC-ALG hydrogel beads was prepared by further crosslinking the earlier synthesized Au@BSA NCs loaded CNC gel using ALG by ionotropic gelation method in the presence of Ca^{2+} ions. During this step, the desired ratio of Au@BSA NCs loaded CNC gel and ALG solution were thoroughly homogenized and loaded into syringes. This homogenized solution was then extruded through syringes mounted with 24-gauge size needle using a syringe pump

at a flow rate of 0.8 μL/min into 20 mL of 2 wt% $CaCl_2$ solution that was gently stirred to prevent the beads from adhering to each other. The hydrogel beads that were formed were then allowed to crosslink in $CaCl_2$ solution for 15 min, after which they were washed with water several times to remove residual $CaCl_2$ and BSA, and used for further experimentations.

6.1.3 Batch adsorption studies

In a typical batch adsorption experiment, 500 mg of water-swollen hydrogel beads were stirred overnight in a vial containing 5 mL of heavy metal ion solution of either Hg^{2+} or Cu^{2+} at neutral pH and 25 °C. The initial and final concentrations of the heavy metal ion solutions were measured using ICP-MS after acidification (5% HCl for Hg^{2+} and 5% HNO_3 for Cu^{2+}). Removal % and uptake of heavy metal ions (q_e) by hydrogel beads were calculated using Equation 6.1 and 6.2 respectively.[194,195]

$$\text{Removal \%} = \frac{(C_0 - C_e)}{C_0} \times 100 \tag{6.1}$$

$$\text{Uptake } (q_e) = \frac{(C_0 - C_e)V}{m} \tag{6.2}$$

where q_e is the amount of heavy metal ions adsorbed per g of adsorbent (mg/g) in equilibrium, C_e is the equilibrium concentration of free heavy metal ions in the bulk solution (mg/L), C_0 is the initial heavy metal ion solution concentration (mg/L), V is the volume of solution (L) and m is the mass of adsorbent (g).

The adsorption capacity of this nanocomposite for Hg^{2+} and Cu^{2+} uptake was also evaluated using Langmuir adsorption isotherm. This was performed by plotting the equilibrium heavy metal ion uptake (q_e) against the equilibrium concentration of heavy metal ion (C_e) for batch adsorption experiments performed with different initial heavy metal ion concentrations, ranging from 20 to 100 ppm. This equilibrium data was fitted using the linearized form of Langmuir adsorption isotherm model mentioned in Equation 6.3.

$$\frac{1}{q_e} = \frac{1}{K_L q_m C_e} + \frac{1}{q_m} \tag{6.3}$$

where q_m is the maximum amount of heavy metal ions which can be adsorbed per gram of adsorbent (mg/g) in equilibrium and K_L is a constant related to the energy of adsorption (L/mg)

which depicts the affinity between the heavy metal ion and adsorbent. Parameters q_m and K_L were determined from the intercept and slope of the plot of $1/q_e$ versus $1/C_e$, respectively.

6.1.4 Development of an ideal sensor-scavenger system

Three hydrogel bead systems containing the CNC:ALG ratios of 1:2, 1:1 and 2:1, were prepared by mixing different ratios of Au@BSA NCs loaded CNC gel and ALG solutions. Leaching of Au@BSA NCs from the hydrogel beads placed in water for 2 days were analysed by inspecting the supernatant, both visually under UV light and measuring the absorbance at 280 nm using UV-Vis spectrophotometer. Also, the mercury removal % of the three systems were compared using batch adsorption studies.

6.1.5 Sensing experiments

Further, the sensitivity of this nanocomposite to various heavy metal ions was also analyzed. For the single hydrogel bead sensing experiment, one bead was placed in each HPLC vial containing 1 mL of 1 ppm concentration of various heavy metal ion solutions like Hg^{2+}, Cu^{2+}, Zn^{2+}, Ni^{2+}, Pb^{2+}, Cd^{2+}, Cr^{3+}, As^{3+}, Mn^{2+}, Co^{2+} and Fe^{2+}. The fluorescence of Au@BSA NCs inside the hydrogel beads, when immersed in these heavy metal ion solutions, was monitored to evaluate the sensitivity and selectivity of the system. Hydrogel bead was also placed in the solution of Mg^{2+} and Ca^{2+} ions, which are the common ions contributing to the hardness of water, in order to study the effect of counter ions.

6.1.6 Characterization of nanocomposite

Photographs of the hydrogel beads were recorded and the mean diameter of hydrogel beads was measured using a vernier caliper. Morphology, elemental analysis and elemental mapping studies of the hydrogel beads were performed using a scanning electron microscopy (SEM) equipped with energy dispersive analysis of X-rays (EDAX) (FEI Quanta 200). For the SEM and EDAX measurements, freeze-dried hydrogel bead samples were spotted on an aluminium sample stub. X-ray photoelectron spectroscopy (XPS) measurements were conducted using an Omicron ESCA Probe spectrometer with unmonochromatized AlKα X-rays (energy = 1486.6 eV). High-resolution transmission electron microscopy (HR-TEM) of Au@BSA NCs was performed with JEOL 3010, a 300-kV instrument. The samples for HR-

TEM was prepared by dropping the dispersion on a carbon-coated copper grid. UV-Visible absorption spectra and photoluminescence spectra of Au@BSA NCs was acquired using Perkin Elmer Lambda 25 UV-Vis spectrophotometer and Jobin Yvon NanoLog spectrofluorometer, respectively.

6.1.7 Quenching dynamics to study diffusion

Dark field fluorescence microscopy was employed to monitor the quenching dynamics of Au@BSA NCs upon the diffusion of Hg^{2+} ions into the hydrogel beads. Fluorescence imaging and spectra of hydrogel beads were performed using the Cytoviva HSI system containing an Olympus BX-41 microscope equipped with a Dage high-resolution camera. Dark field fluorescence microscopy was used in an excitation window corresponding to DAPI/FITC/TEXAS RED (DAPI, 452−472 nm; FITC, 515−545 nm; TEXAS RED, 600−652 nm), and emission was collected using a triple pass emission filter DAPI/FITC/TEXAS RED (DAPI, 452−472 nm; FITC, 515−545 nm; TEXAS RED, 600−652 nm). We have chosen similar excitation and emission filters for simultaneous visualization of the fluorescent area along with the quenched area. The distinct red fluorescence of the cluster allows us to easily distinguish between the quenched and fluorescent part of the hydrogel bead.

Hydrogel beads of a size greater than 1 mm were imaged under a dark field fluorescence microscope. The intense red colour of the bead indicates the uniform distribution of the clusters. Hydrogel beads were initially kept in Millipore water and the fluorescence intensity was observed for some time to confirm that it did not change in the control condition. Then a single bead was immersed in 100 ppm Hg^{2+} ion solution and time-dependent quenching of red emission from Au@BSA NCs was observed. Images were captured at regular time intervals. By monitoring the fluorescence area from these images, the diffusion kinetics of the Hg^{2+} ions was studied. The rate of diffusion of ions corresponds to the rate of fluorescence quenching. As the time scale of reaction between the metal ion and the cluster which quenches the luminescence is much faster than ionic diffusion, the error due to the former event is insignificant. The diffusion of Hg^{2+} ions into the hydrogel bead was monitored by studying the reduction in the fluorescence diameter of the bead.

Diffusion coefficient (D) is an essential parameter for modelling diffusion and can be obtained by solving Fick's second law.

$$\frac{\partial^2 C}{\partial x^2} = -\frac{1}{D}\frac{\partial C}{\partial t} \tag{6.4}$$

where C is the concentration, x is the position and t is the time. Solving this equation requires knowledge of flux and concentration varying over time. The rate of change of mercury concentration (dC_o) can be equated to the rate of change in fluorescence intensity (dF_I) using the following equation:

$$dC_0 = dF_I \tag{6.5}$$

By substituting the above equation in Fick's law, we obtain the coefficient for fluorescence quenching which is similar to D for Hg^{2+} ions and was calculated by analyzing the variation of red intensity along the bead diameter at various time points. The variation in red intensity along the diameter of the bead was extracted using an image analysis code run using the open software called R. The R-code written using the JPEG library is mentioned in the appendix.

For ease of calculation, the equation representing the concentration was assumed to be a multiple of two independent functions, distance and time. The variation in red intensity for various time points was fitted to a sine curve representing the variation along the diameter. Then, the maximum intensity (taken from the center of the sine curve) was plotted against time, to obtain the function for a change of intensity with time. This was fitted to an exponential curve. The solution for Fick's equation under homogenization seems to fit the equation of fluorescence as a function of distance and time as given by:

$$F = 0.66 \sin\left(\frac{x\pi}{1260}\right) e^{\left(-t/1594\right)} - 0.11 \tag{6.6}$$

Also, the minimum measurable distance, i.e. length of one pixel, and the error from fitting the exponential decay for time constant were used to calculate the error. The detailed error calculation is mentioned below.

$$D = \frac{l^2}{\pi^2 \tau} \tag{6.7}$$

To calculate error,

$$\Delta D = \frac{l(2\tau\Delta l + \Delta\tau l)}{\pi^2\tau^2} \quad (6.8)$$

Here, τ = 1594 s, l = 0.126 cm, $\Delta l = 0.75 \times 10^{-4}$ cm (size of one pixel) and $\Delta\tau$ = 478.7 sec (error from fitting the decay equation). Substituting this in the equation, we get $\Delta D = 0.3 \times 10^{-6}$ cm^2/sec.

6.1.8 Dip pen experiments

A concept dip pen device was fabricated to demonstrate the application of these hydrogel beads for *in-situ* monitoring of heavy metal ions in water. A capillary column of inner diameter 2 mm and length 5 cm was filled with hydrogel beads of diameter 1.9 mm along the length of the column. This capillary column was dipped into a glass vial containing 5 mL of 50 ppm mercury ion solution. Photographs of the dip pen device placed in the mercury ion solution were taken at regular intervals to monitor fluorescence quenching of Au@BSA NCs, as a result of the capillary rise of mercury ion solution through the hydrogel beads.

6.2 Results and discussion

6.2.1 Preparation of nanocomposite

Highly fluorescent Au@BSA NCs with a characteristic red emission are formed as a result of *in-situ* reduction of Au ions encapsulated in BSA protein upon adjusting the reaction pH to ~12 by the addition of NaOH.[276] When the synthesis of these nanoclusters takes place in the reaction mixture containing CNCs, it leads to the formation of a gel-like structure due to the ion-mediated gelation of CNCs by the cationic Au ions. Chau et al.[278] and Shafiei-Sabet et al.[279] have reported that CNCs at a particular concentration tend to form gel-like structure upon the addition of cations due to stronger propensity of CNCs for side-by-side association. Gelation of CNCs can be induced by the increasing ionic strength of CNC suspension with the addition of salts. Salt addition reduces the Debye length of CNCs and as a result the electrostatic repulsion between them is suppressed and dominant attractive forces like van der Waals forces and hydrogen bonding come into play.[278,279]

When the nanocomposite solution containing Au@BSA NCs, CNCs and ALG was introduced to $CaCl_2$ solution, hydrogel beads were instantaneously formed, as a result of

ionotropic gelation of ALG by Ca^{2+} ions. ALG is an anionic polysaccharide composed of (1-4) linked β-D-mannuronate (M) and α-L-guluronate (G) units which in the presence of divalent cations, such as Ca^{2+} form hydrogels via ionic crosslinking of calcium bridges between the M and G units of the adjacent chains.[190] Figure 6.2 shows the Au@BSA NCs loaded CNC gel and Au@BSA loaded CNC-ALG hydrogel beads under white light and UV light.

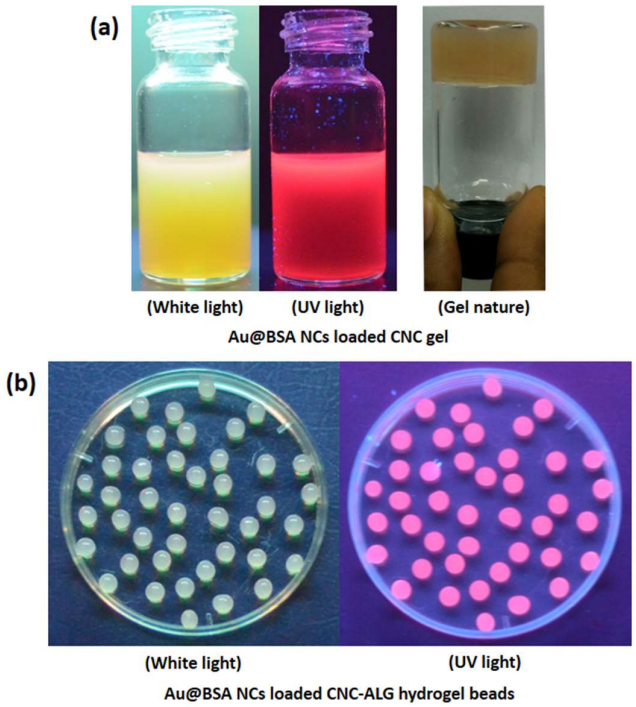

Figure 6.2. Photographs of (a) Au@BSA NCs loaded CNC gel, (b) Au@BSA NCs loaded CNC-ALG hydrogel beads under white light and UV light. The luminescence intensity in the sample bottle ((a), middle) is non-uniform as the excitation is from the top and it becomes attenuated at the bottom.

Au@BSA clusters were studied independently in the group and previous studies including ours[280,281] have established that the clusters showing emission at 660 nm are composed of 30 atoms of Au. They also exhibit well-defined mass spectra, measured using matrix-assisted laser desorption ionization (MALDI). However, as the focus here is on sensing and scavenging, we are not discussing these aspects in greater detail.

6.2.2 Development of an ideal sensor-scavenger system

Among the three nanocomposite hydrogel bead systems, 1:2 CNC:ALG system was found to be an ideal sensor-scavenger system. This system showed lesser leaching of Au@BSA

NCs as compared to 1:1 and 2:1 systems when placed in water for 2 days. Figure 6.3a shows the photographs of the vials containing the 3 systems, taken at the start and end of the leaching experiment. More intense red luminescence was observed for the supernatant for the 1:1 and 2:1 system compared to 1:2 system, due to the higher leaching of Au@BSA NCs from these systems. This is further confirmed by the higher UV absorbance of the supernatants from the 1:1 and 2:1 systems compared to the 1:2 system measured at 280 nm, as shown in Figure 6.3b. Mechanical integrity tests performed by stirring the beads vigorously overnight showed that the 1:2 was more robust compared to other systems as shown in Figure 6.3c Figure 6.3d shows that the 1:2 system also displayed higher Hg^{2+} removal compared to the 1:1 and 2:1 systems.

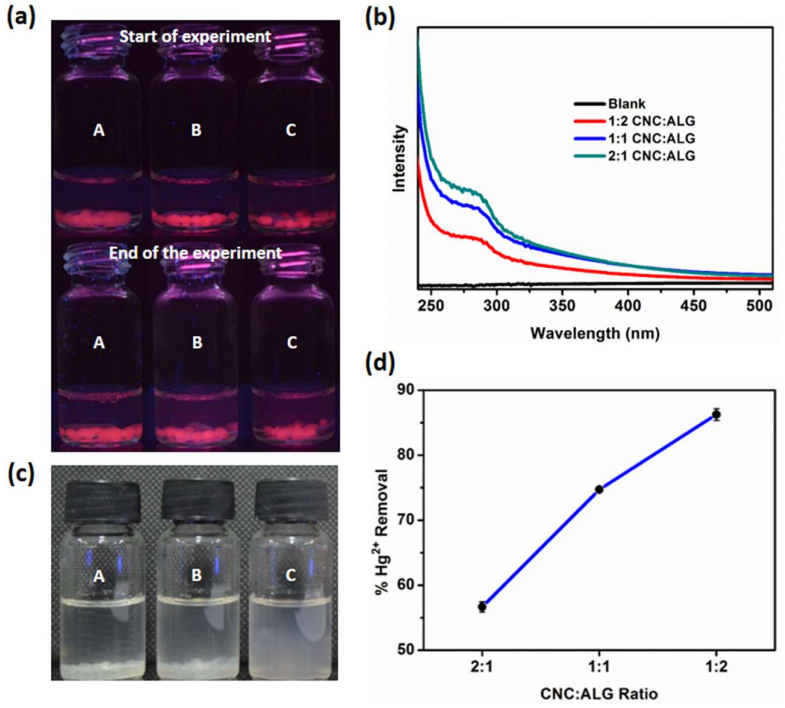

Figure 6.3. (a) Photographs of the vials containing (A) 1:2 (B) 1:1 and (C) 2:1 CNC:ALG nanocomposite hydrogel systems taken at the start and end of the leaching experiment. (b) UV absorbance spectra of the supernatant from the three systems taken at the end of the leaching experiment. (c) Photographs of the vials containing (A) 1:2 (B) 1:1 and (C) 2:1 CNC:ALG nanocomposite hydrogel systems taken at the end of mechanical integrity experiment. (d) Plot of Hg^{2+} removal % with varying CNC:ALG ratio.

Because of the high surface area and negative charge of CNCs, they are also capable of absorbing heavy metal ions. A control batch adsorption experiment performed by stirring 10

mg/mL CNCs and 50 ppm Hg^{2+} at pH 7 and 25 °C overnight showed that CNCs themselves were capable of removing 50% Hg^{2+} (Figure 6.4).

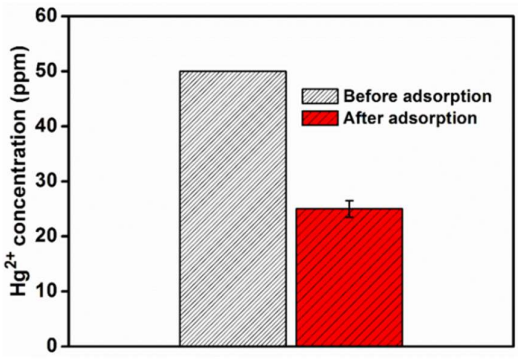

Figure 6.4. Concentration of Hg^{2+} before and after adsorption with CNCs (Adsorbent dosage = 10 mg/mL, Adsorbate concentration = 50 ppm, pH = 7, Temperature = 25 °C).

The carboxylate groups present along the polymeric chains of ALG coupled with the porous nature of the hydrogel beads also contribute to the adsorption of heavy metal ions.[191,192] Thus, the synergistic adsorption by the CNCs and ALG in the nanocomposite contributed to an increased adsorption performance of 1:2 system compared to the other two systems.

6.2.3 Sensing experiments

Au@BSA NCs fluoresce with a deep red emission which when entrapped inside these hydrogel beads also impart the characteristic red fluorescence to the beads under UV light. Single hydrogel bead sensitivity experiment, performed using 1 ppm concentration of all the major heavy metal ions such as Hg^{2+}, Cu^{2+}, Zn^{2+}, Ni^{2+}, Pb^{2+}, Cd^{2+}, Cr^{3+}, As^{3+}, Mn^{2+}, Co^{2+} and Fe^{2+} employing 1:2 CNC:ALG system showed that the nanocomposite is highly selective to Hg^{2+} ions. The nanocomposite itself was prepared using $CaCl_2$ that dissociates into Ca^{2+} and Cl^- ions, where Ca^{2+} ions will aid in the crosslinking of alginate chains and Cl- ions remain free in the solution or diffuse into hydrogel beads. No fluorescence quenching of Au@BSA NCs was observed when the nanocomposites were stored in this solution for several hours and hence it is clear that Au@BSA NCs are not sensitive to Cl- ions. No sensitivity to Ag+ was seen for this cluster system.[275] In addition, Xie et al.[275] and Hu et al.[272] have reported on the selectivity of Au@BSA NCs using various chemical species and have demonstrated that they are highly selective to Hg^{2+} ions. Figure 6.5 shows that the fluorescence of hydrogel beads were

completely quenched in the presence of Hg^{2+} ions and slight fluorescence quenching also occurred in the presence of Cu^{2+} ions.

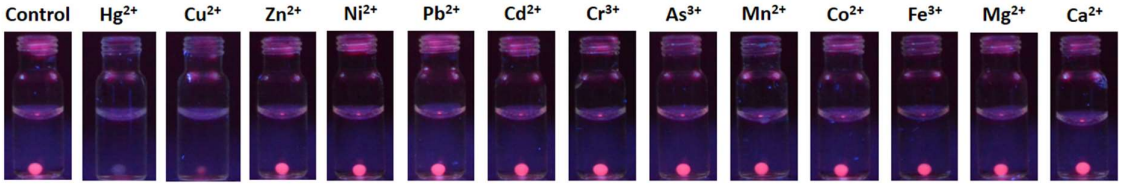

Figure 6.5. Photographs of vials containing hydrogel bead placed in 1 ppm concentration of various heavy metal ions.

There are several proposed mechanisms for the fluorescence quenching of Au@BSA NCs by Hg^{2+} ions,[273] such as (a) high affinity metallophilic bonding between the d^{10} centers of Hg^{2+} and Au^{+} that disrupts the fluorescence from Au-BSA interactions[275] and (b) photo-induced electron transfer process wherein the Hg-S bonds are formed with BSA which causes the reduction of Hg^{2+} to Hg^{+} and the latter species creates interference during excitation, thereby quenching the fluorescence.[272] Apart from this at a similar heavy metal ion concentration, the binding affinities of Hg^{2+} with Au^{+} is much stronger compared to other toxic metal ions, which also makes Au@BSA NCs more sensitive to Hg^{2+} ions.[275] The selectivity of the nanocomposite to heavy metal ions is based on the type of gold nanoclusters incorporated in them. For example, Pb and As selectivity can be imparted to the nanocomposite by incorporating gold nanoclusters reported earlier by Zhu et al.[282] and Subhasish et al.,[283] respectively. Earlier reports have also shown that Cu^{2+} ions can also quench the fluorescence of Au@BSA NCs via ion-induced aggregation as they possess a strong affinity towards BSA and histidine.[284,285] And hence the slight fluorescent quenching of hydrogel beads observed in the case of Cu^{2+} ions can be attributed to this fact. Copper interference for this sensor is due to the nature of the Au@BSA NCs that was selected in the design of this nanocomposite. Choosing another cluster system that is highly selective and specific to Hg^{2+} would be the ideal solution to tackle this limitation.

The fluorescence of the hydrogel beads after exposure to varying concentration of Hg^{2+} was examined. The experiment showed that hydrogel beads are sensitive to as low as 1 ppm. Even though the sensitivity of this nanocomposite has been studied using a much lower concentration of Hg^{2+} ions, the minimum sensitivity reported in this study is 1 ppm. The

quenching of Au@BSA NCs fluorescence upon binding to Hg^{2+} ions is limited by the diffusion of Hg^{2+} ions into the hydrogel beads, which in turn is controlled by several other factors, such as size, charge, concentration gradient of diffusing ions,[286] crosslinking density of hydrogels,[286] interfacial properties of hydrogel matrix materials with the solute,[287] etc. At a lower concentration of Hg^{2+} ions, the rate of diffusion will be drastically reduced and visual detection of the fluorescence quenching of Au@BSA NCs upon Hg^{2+} ions diffusion may require a sufficiently longer time for the current nanocomposite. For the dynamic quenching experiments, we have conducted studies using 100, 10 and 1 ppm Hg^{2+}, and noticed that the Au@BSA NCs was completely quenched in 45 min, 3 h and 24 h, respectively. Further studies are underway to develop systems that can detect a lower concentration of Hg^{2+} within a shorter time span. As a preliminary experiment, we have investigated the ability of the nanocomposite in detecting the smaller concentration of Hg^{2+} ions relevant to drinking water. For this, we have studied the sensitivity of Au@BSA NCs CNC-ALG nanocomposite to 1 ppb, 2 ppb and 10 ppb Hg^{2+} in both de-ionized water and tap water using photoluminescence spectroscopy. Emission spectra after subjecting the nanocomposite to various concentrations of Hg^{2+} ions are shown in the figure below. From the Figure 6.6, it is evident that the material is sensitive down to 1 ppb in both de-ionized water and tap water. The nanocomposite being a gel shows multiple features due to scattering.

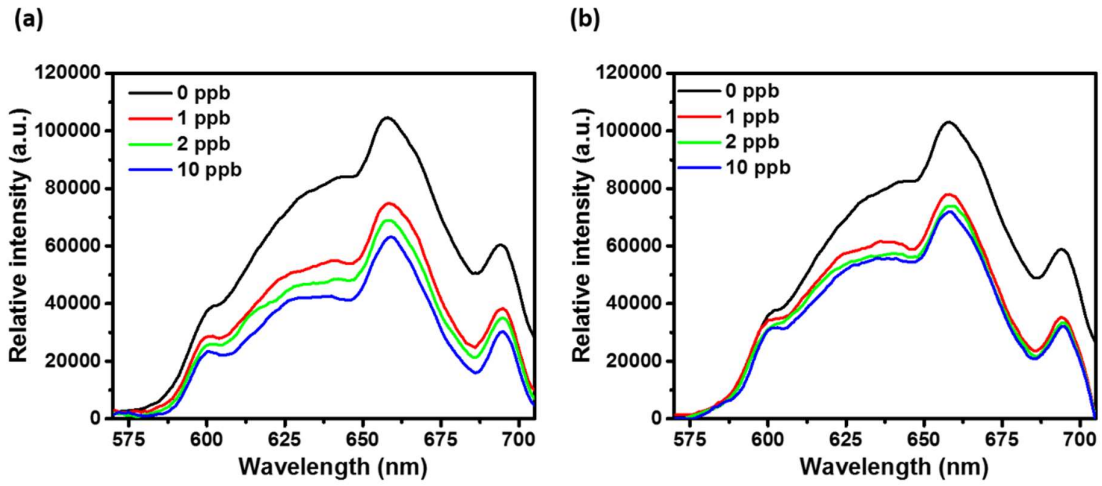

Figure 6.6. (a) Emission spectra of Au@BSA NCs CNC-ALG composite with different concentrations of Hg^{2+} ions in de-ionized water. (b) Emission spectra of Au@BSA NCs CNC-ALG nanocomposite with different concentrations of Hg^{2+} ions in tap water.

6.2.4 Adsorption of heavy metal ions

Among all the heavy metal ions tested for the sensing experiments, the adsorption capability of the nanocomposite for the most sensitive ion, namely Hg^{2+} was estimated using the Langmuir isotherm. Figure 6.7a shows the fitting of equilibrium data using the linearized form of Langmuir adsorption isotherm and the maximum adsorption capacity (q_m) was calculated to be 26 mg/g. Figure 6.7b displays the photographs of the crushed and freeze-dried nanocomposite material before and after adsorption, under white light and UV light. After binding to Hg^{2+}, the colour of the nanocomposite changed from yellowish brown to deep brown. Also, the fluorescence of the nanocomposite was completely quenched confirming the higher binding of Hg^{2+} to the nanocomposite. Adsorption studies were also carried out using Cu^{2+}, which also showed some fluorescent quenching during the single hydrogel bead sensing experiment (Figure 6.8).

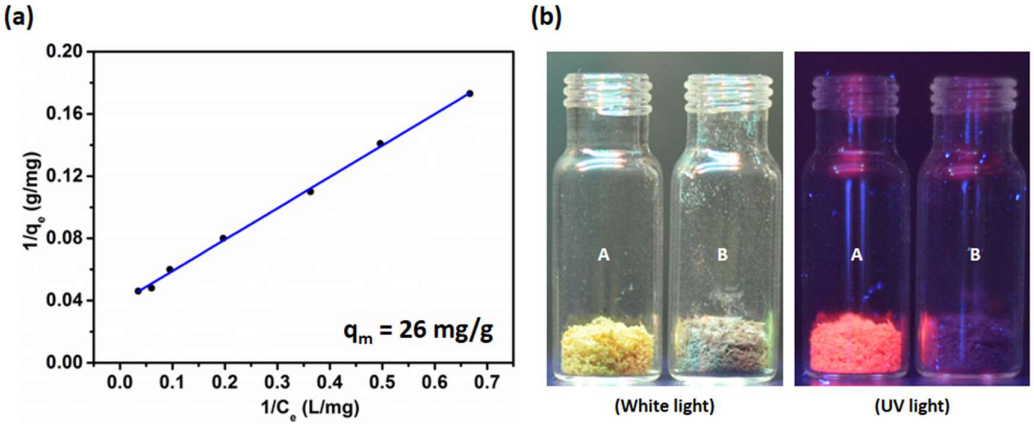

Figure 6.7. (a) Equilibrium Hg^{2+} batch adsorption data, fitted using linearized form of Langmuir adsorption isotherm. (b) Photographs of the vials containing nanocomposite (A) before and (B) after adsorption of Hg^{2+} ions under white light and UV light, respectively.

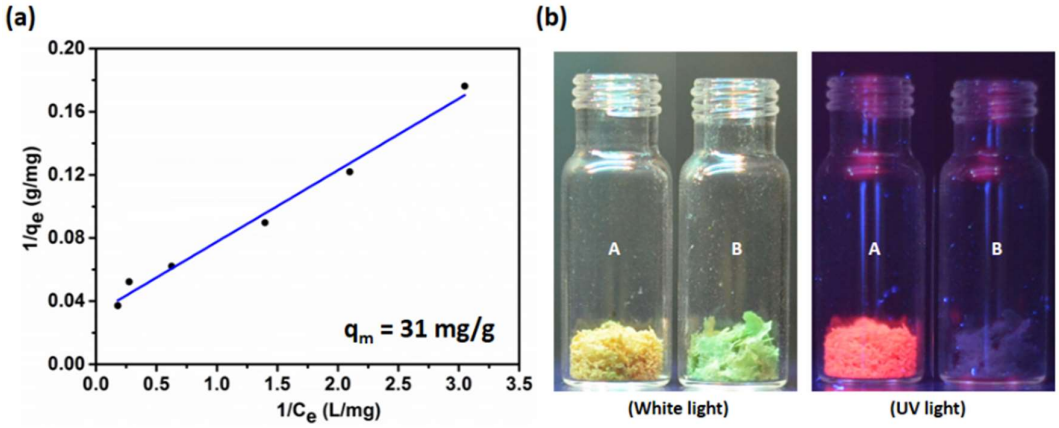

Figure 6.8. (a) Equilibrium Cu^{2+} batch adsorption data, fitted using linearized form of Langmuir adsorption isotherm. (b) Photographs of the vials containing nanocomposite (A) before and (B) after adsorption of Cu^{2+} ions under white light and UV light, respectively.

6.2.5 Characterization of nanocomposite

The average diameter of the hydrogel beads measured using a vernier caliper was 2.70 mm, which was illustrated in Figure 6.9. Ten hydrogel bead samples were used for this measurement.

(a)

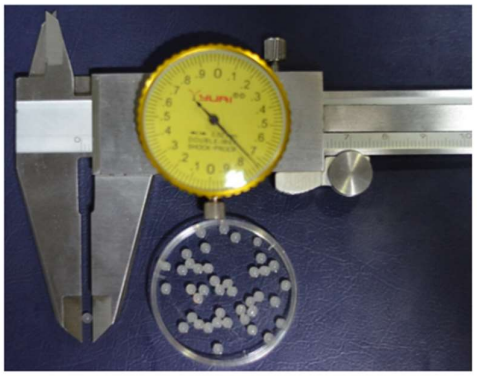

(b)

Bead number	Diameter (mm)
1	2.75
2	2.80
3	2.60
4	2.70
5	2.60
6	2.70
7	2.80
8	2.70
9	2.70
10	2.70
Average	**2.705**

Figure 6.9. (a) Photograph of the vernier caliper used for the measurement of hydrogel bead diameter. (b) The average diameter of the hydrogel beads used to measure the bead diameter.

SEM image of the freeze-dried hydrogel bead (Figure 6.10a) shows undulations and folds on the bead surface. The inset of the Figure 6.10a also shows these investigations at a higher magnification. Cross-sectional image of the hydrogel bead (Figure 6.10b) shows the porous nature of the nanocomposite which can also contribute to increased surface area of binding as well as diffusion of heavy metal ions. Figure 6.10b provides a visual representation of the porous nature of the hydrogel beads and it does not facilitate the determination of the exact porosity. Moreover, the freeze-dried hydrogel beads used for the SEM experiments does not provide the exact visualization of the porous nature that the hydrogel beads in their native wet swollen state possess.

(a) (b)

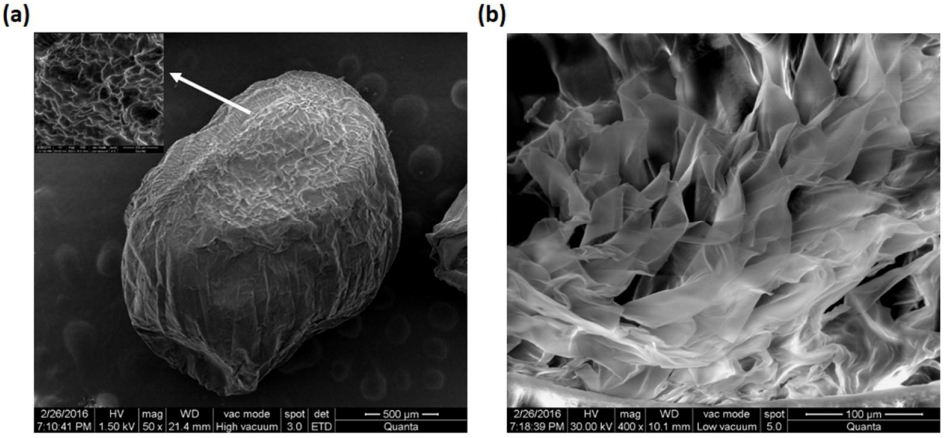

Figure 6.10. SEM image showing (a) surface morphology and (b) porous nature of the hydrogel bead, after drying.

SEM-EDAX elemental analysis and elemental mapping of the control, Hg^{2+} saturated and Cu^{2+} saturated nanocomposite are presented in Figures 6.11, 6.12 and 6.13, respectively. A comparison of the results from Figures 6.11 and 6.12, confirms the homogeneous adsorption of Hg^{2+} throughout the nanocomposite. Similarly, comparison of Figures 6.11 and 6.13 revealed the homogeneous adsorption of Cu^{2+} throughout the nanocomposite.

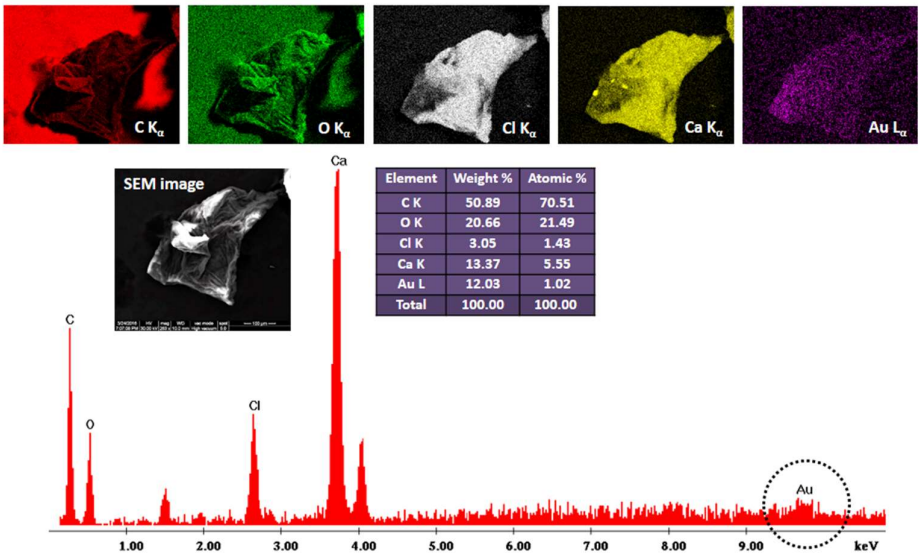

Figure 6.11. SEM-EDAX elemental analysis and elemental mapping of control nanocomposite.

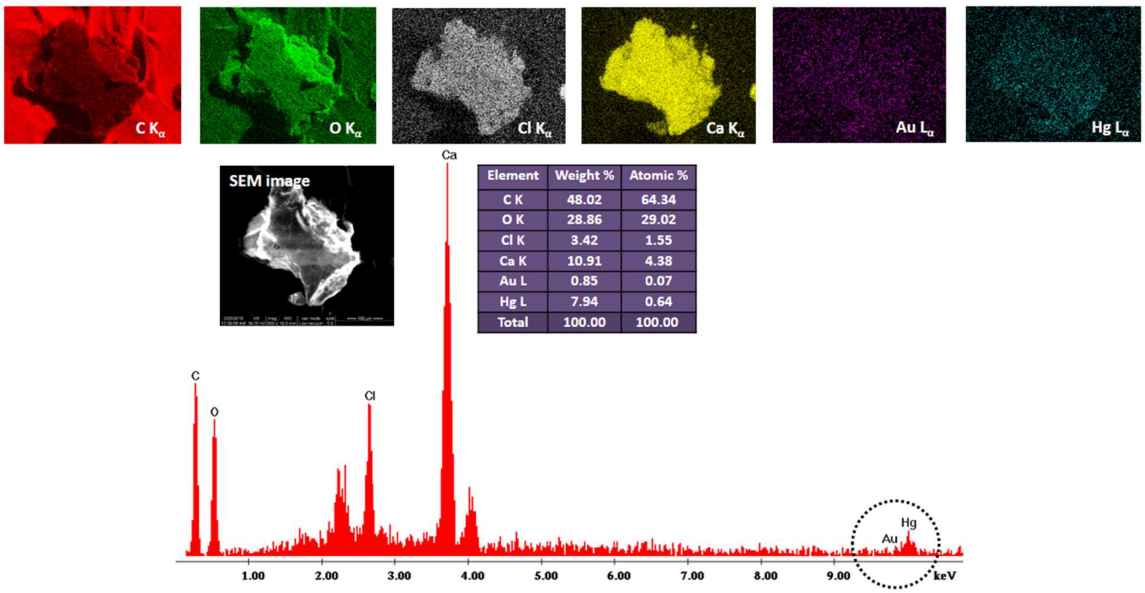

Figure 6.12. SEM-EDAX elemental analysis and elemental mapping of Hg^{2+} saturated nanocomposite.

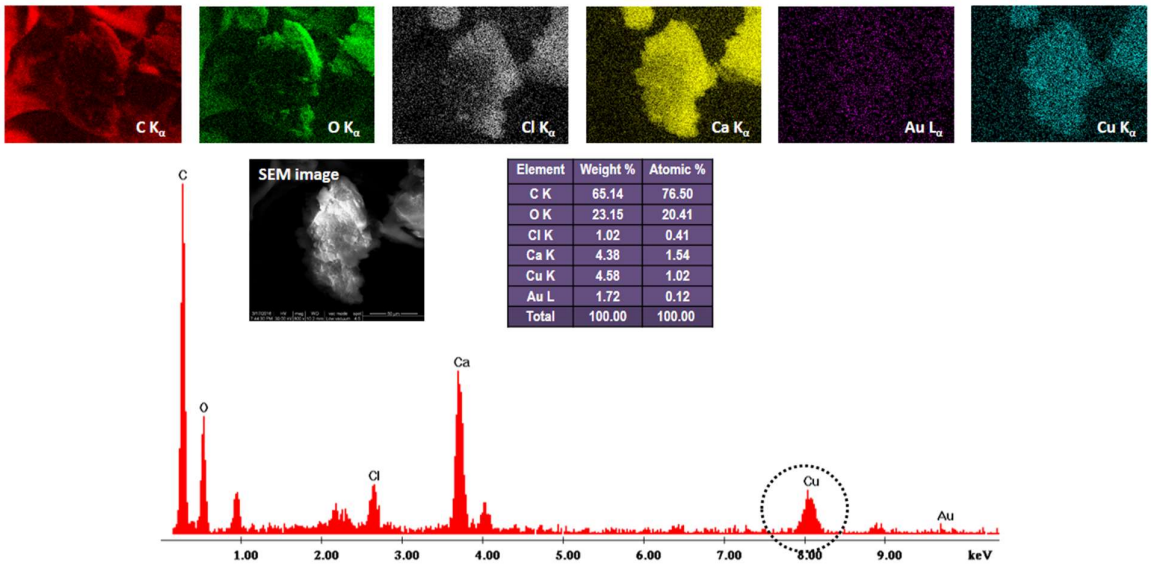

Figure 6.13. SEM-EDAX elemental analysis and elemental mapping of Cu^{2+} saturated nanocomposite.

Au@BSA NCs which gives the characteristic red fluorescence as well the sensing property to the nanocomposite has also been characterized. TEM image (Figure 6.14a) shows that these nanoclusters are around 2 nm in size. UV-Vis spectrum (Figure 6.14b) shows a peak at ~280 nm and photoluminescence spectrum shows an emission maximum at 660 nm when excited at 365 nm. These are the characteristic features for BSA protected Au nanoclusters.[277,280]

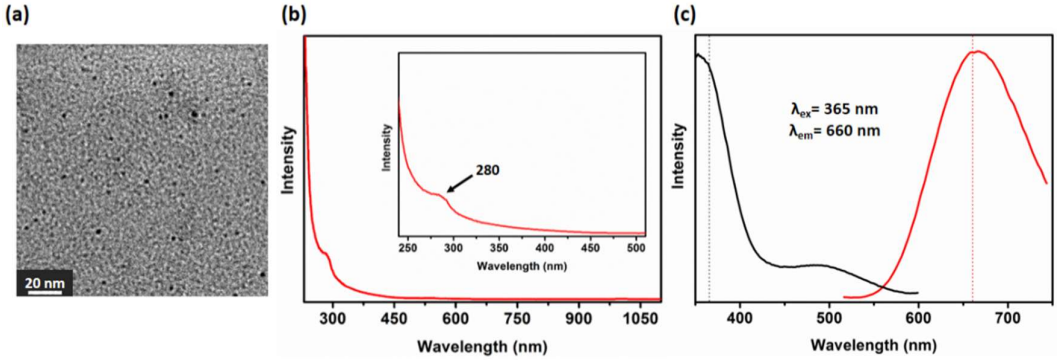

Figure 6.14. (a) TEM image (b) UV-Vis absorbance spectrum and (c) Photoluminescence spectra showing the excitation (black line) and emission (red line) peaks of Au@BSA NCs.

Although we have studied such clusters through mass spectrometry in earlier studies,[27] this was not possible in view of the nanocomposite nature of the present material which prevents ionization and desorption of the cluster. XPS analysis of the nanocomposite was performed to elucidate the fluorescence quenching as well as to confirm the adsorption of Hg^{2+}

by the nanocomposite. XPS spectra in the Au 4f region of nanocomposite before and after adsorption of Hg^{2+} are shown Figure 6.15a. Comparing the XPS spectra, it is observed that the adsorption of Hg^{2+} on the nanocomposite has led to an increase in the binding energy of Au from 84.5 eV to 84.9 eV. This is reportedly due to oxidation of Au core by the Hg^{2+}, which causes quenching of red fluorescence.[277] Also the peak of Hg $4f_{7/2}$ seen at 101.8 (Figure 6.15b) implies that there is a reduction of Hg^{2+} to Hg^{0}, which occurs when $Hg^{2+}$are adsorbed on the nanocomposite.[277]

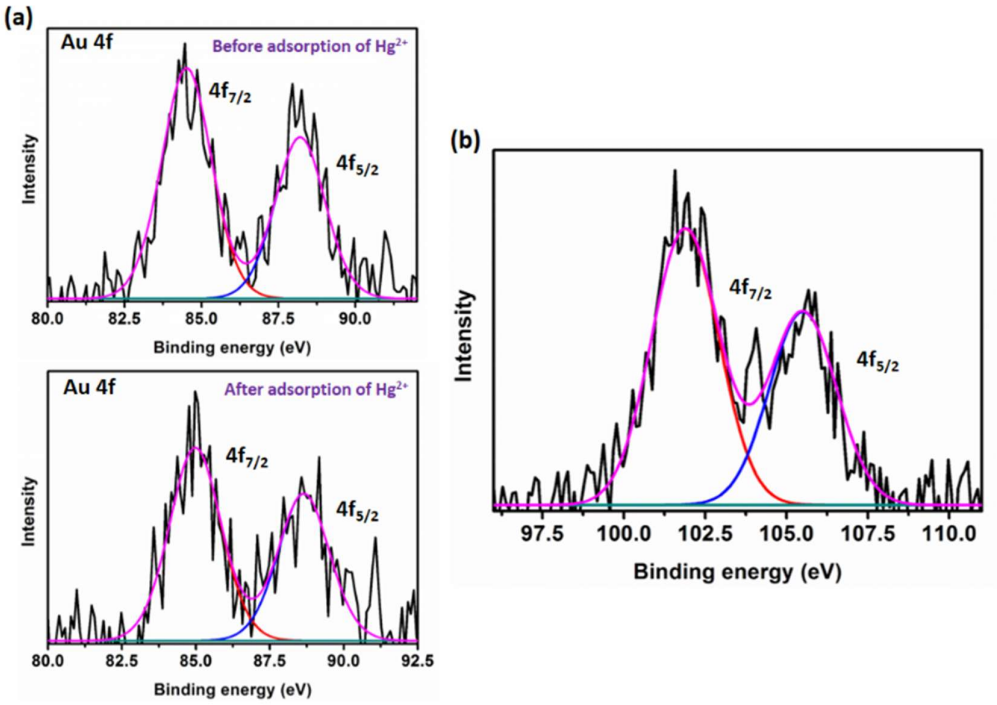

Figure 6.15. (a) XPS spectra of Au 4f region for the nanocomposite before (up) and after (down) Hg^{2+} adsorption. (b) XPS spectra of Hg 4f region of the nanocomposite after Hg^{2+} adsorption (Hg 4f data are given only after Hg^{2+} adsorption as the control nanocomposite does not have Hg^{2+}).

6.2.6 Quenching dynamics to study diffusion

Practical knowledge of the mass transfer characteristics of the sorption process, especially diffusion occurring through porous media during this sorption process is essential for various applications, especially from an industrial standpoint. It is necessary to determine the optimal flow rate and the residence time in columns and reactors. Numerous methods and experiments have been devised to estimate the value of D, which is an essential parameter for

modelling diffusion. However, all the methods are elaborate, involving diffusion cell set up, couette flow set-up, radio tracers, rotation disc measurement, and scanning electrochemical micrograph. The coefficient can also be estimated by monitoring the bulk solution concentration, but it often contains many uncertainties.[288] In this study, a novel and relatively simpler method were used, wherein the quenching dynamics of the Au@BSA NCs was observed under dark field fluorescence microscopy upon diffusion of Hg^{2+} into the hydrogel bead.

Figure 6.16 shows the quenching of nanocomposite fluorescence with respect to the diffusion of Hg^{2+} ions at various time intervals. It is seen that the intensity of red emission was slowly quenched from the surface of the bead and progressed inwards. The blue and green intensities, also seen in the images were found to be constant over time.

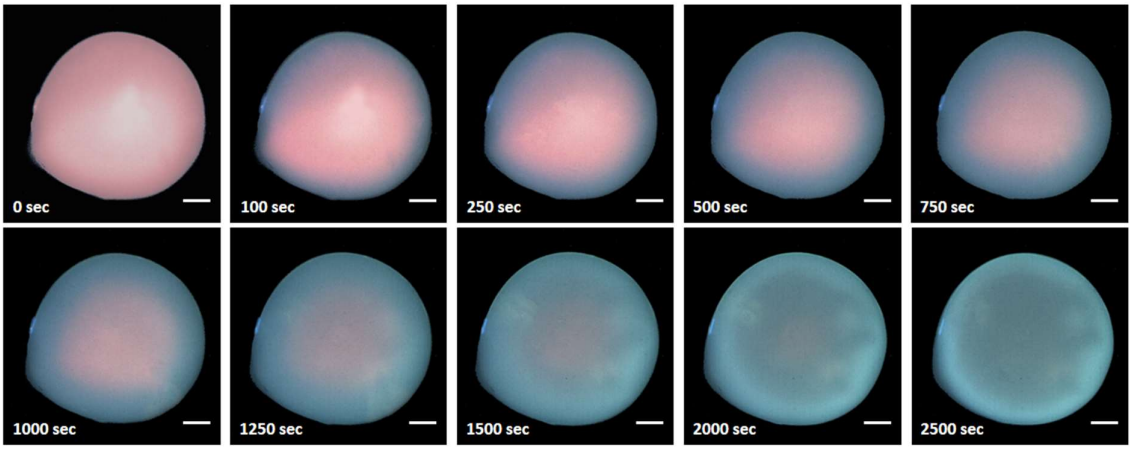

Figure 6.16. Quenching of nanocomposite fluorescence with respect to the diffusion of Hg^{2+} ions at various time points (Scale bar shown in the pictures is 200 μm). The initial concentration of Hg^{2+} in the solution 100 ppm.

The plot showing the variation in red intensity along the bead diameter at time t = 100 s for 100 ppm concentration of Hg^{2+} is given in Figure 6.17a. It was observed that the fluorescence of hydrogel bead was completely quenched after time t = 2500 s. The red intensity from a completely quenched bead (t = 2500 s) was subtracted from the other images, thus ensuring that intensity used for calculation was only from the fluorescent cluster. Our previous reports indicate that the reaction of Au@BSA NCs with Hg^{2+} ion is generally fast and uniform[277] and hence we also assume that the reaction rate far exceeds the diffusion rate. Figure

6.17b shows the sine curve fitting of the variation in red intensity for various time intervals. The maximum intensity (taken from the center of sine curve) plotted against time as shown in Figure 6.17c follows a typical exponential decay.

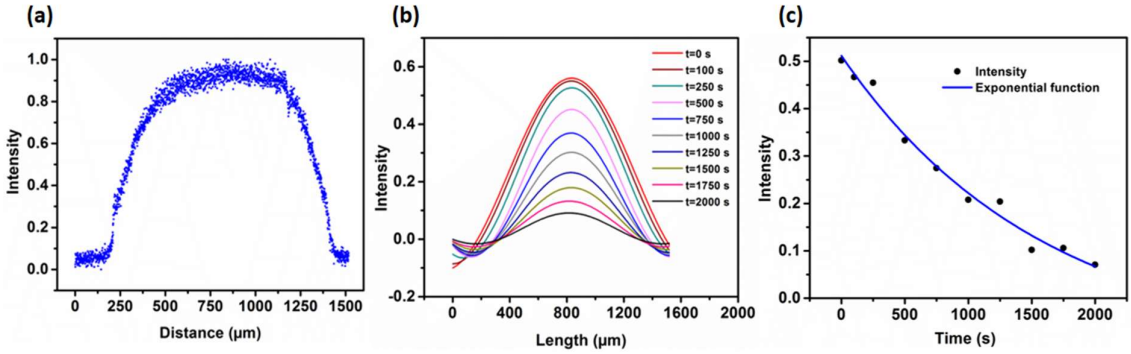

Figure 6.17. (a) Plot showing the variation in red intensity along the bead diameter at t = 100 s for 100 ppm concentration of Hg^{2+}. (b) Plot showing the fitting of the variation in red intensity for various time points to a sine curve. (c) The plot of the maximum intensity (taken from the center of sine curve) plotted against time.

The variation of the concentration as a function of distance and time (Equation 6.6) was obtained by multiplying the individual equations of distance and time, respectively. We solved for D by inserting this function in Fick's equation (Equation 6.4). The diffusion coefficient of the bead calculated using this technique was found to be 1.01 (±0.3) x 10^{-6} cm^2/s. There were no data in the literature on the diffusion of mercury through these beads and hence were unable to make any comparison. However, the diffusion coefficient for Cu^{2+} in water was measured by Marcinkowsky and Phillips[289] using radioactive tracers and by Quickenden and Jiang[290] using a rotating disk electrode. Both these investigators measured diffusion coefficient in the range of 6.2 × 10^{-6} to 7.5 × 10^{-6} cm^2/s. Jang et al. measured the diffusion coefficient of Cu^{2+} for 3.2% calcium alginate beads to be in the range of 1.0 × 10^{-5} to 1.4 × 10^{-5} cm^2/s.[291] However, for small analytes, the diffusion rate through a bead is similar to that of the diffusion in water.[291] Hg^{2+} ions being heavier than the Cu^{2+} ions, seemingly diffuse slower through the hydrogel bead. The lower diffusion rate could also be due to the binding of Hg^{2+} ions with the clusters and high affinity of this reaction.

To ensure that the diffusion coefficient can be equated to the fluorescent intensity of the bead, we have placed a single hydrogel bead in control solution (Millipore water) for nearly 24

h and monitored any reduction in nanocomposite fluorescence as a result of leaching of Au@BSA NCs. No visible change in colour of the control solution was observed indicating no leaching of the Au@BSA NCs. However, in the sample the complete quenching of the Au@BSA fluorescence was observed within 2500 s when we used 100 ppm Hg^{2+}. In general, we have placed the hydrogel bead in water for at least 15 min before the start of the experiment to ensure that there is no visible leaching of Au@BSA NCs. Within the time span of 1 h of the experiment, we do not believe that there would be any leaching of clusters to impact our calculation of diffusion coefficient.

The analysis and calculations reported here can be improved through better mathematical models. The use of confocal fluorescence microscopy can yield detailed real-time three-dimensional visualization of the diffusion process. Here, we have presented a simpler procedure that allows for the direct visualization of the diffusion in porous beads. The scope can be extended to study the diffusion of other molecules, especially proteins and DNA, which can be tagged to a fluorescent moiety.

6.2.7 Dip pen experiments

The hydrogel beads that were placed along the length of a dip pen device quenched its red fluorescence gradually when it was dipped in the mercury solution. The capillary rise of the mercury solution through the capillary column promoted the diffusion of Hg^{2+} ions through the hydrogel beads that contained Au@BSA NCs. Figure 6.18 shows the photographs of the dip pen device and gradual change in the fluorescence of the hydrogel beads upon exposure to the mercury solution.

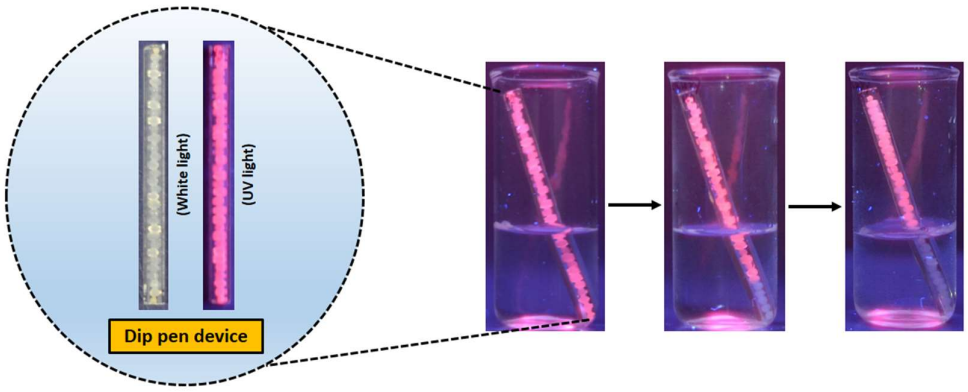

Figure 6.18. Photograph of the dip pen device and the gradual change in the fluorescence of the hydrogel beads within them when the device was dipped in the mercury solution.

Even though the use of Au@BSA NCs in our nanocomposite raises questions regarding its appropriateness for commercial applications, there are several reasons that make this nanocomposite promising for use in water treatment applications, namely, the following:

(a) The Au@BSA NCs provides excellent fluorescence signals even at a reduced concentration, hence only less than 19.7 µg of Au is needed to produce one hydrogel bead, thus in most cases, cost may not be an issue. This quantity could be reduced further, depending on the fluorescence intensity required for detection.

(b) Au@BSA NCs have very good selectivity and sensitivity towards Hg^{2+} ions as demonstrated in several earlier reports,[272,275,277] and their incorporation into the current nanocomposite makes it also selective towards Hg^{2+} ions.

(c) Au@BSA NCs, when incorporated into this nanocomposite, were found to be stable at high temperature without much loss in their characteristic red fluorescence. This was evident when we oven dried the nanocomposite at a temperature of 100 ºC. The freeze-dried nanocomposite containing Au@BSA NCs was stable and they fluoresce with bright red emission even after six months when stored at room temperature. This improved stability is due to the protective environment provided by the alginate polymer chains wrapping around the fluorescent Au@BSA NCs. Figure 6.19 also shows the photograph of the freeze-dried nanocomposite hydrogel beads which have been stored for more than six months, under UV light. Thus the practical applicability

of the nanocomposites containing Au@BSA NCs with respect to storage and usability in high-temperature conditions, such as in mining effluents is possible.

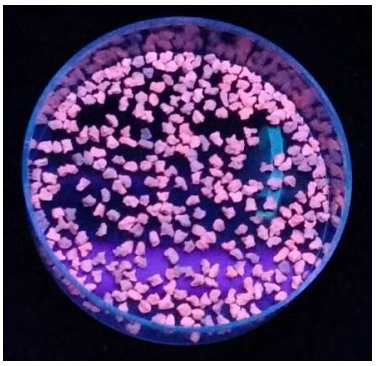

Figure 6.19. Photograph of the freeze-dried nanocomposite hydrogel beads which have been stored for more than 6 months, under UV light.

(d) The sensing and adsorption of Hg^{2+} are controlled by diffusion, hence this nanocomposite can be used as a probe to visualize the diffusion phenomena, allowing us to determine the diffusion coefficient. This is the first time such a method was proposed and this was possible because of several properties of the nanocomposite hydrogel bead, such as three-dimensional spherical structure, high porosity, hydrophilic and anionic matrix that drives the diffusion of cationic Hg^{2+} ions via electrostatic interaction and homogeneous nanocluster distribution giving uniform florescence intensity throughout the nanocomposite.

(e) The protein templated nanocluster such as Au@BSA NCs can be synthesized *in-situ* via a one pot synthesis procedure. In contrast, most metallic clusters are synthesized separately and then incorporated in the substrate. Here leaching of nanoclusters can become a challenging problem when used in a continuous process. On the other hand, here the synthesis of Au@BSA NCs takes place in a reaction mixture containing CNCs. Due to the ion-mediated gelation of CNCs by the cationic Au ions, a gel-like structure is formed and hence the leaching of nanoclusters is drastically reduced. Apart from gold, only biomolecule (BSA), biodegradable polymers (CNCs, Alginate) and eco-friendly chemicals (NaOH, $CaCl_2$) were used in the synthesis when compared to systems prepared from electrospun nanofibers based on petroleum based polymers, etc.[277]

(f) Also, the binding affinity of mercury did not vary after incorporating the cluster into the matrix. This was studied by comparing the sensitivity of the clusters alone and cluster-incorporated nanocomposites to different concentrations of Hg^{2+} ions using photoluminescence spectroscopy. Figure 6.20 shows the variation of normalized fluorescence intensities of Au@BSA NCs and Au@BSA NCs CNC-ALG nanocomposite after binding with Hg^{2+} ions at regular time intervals. The similar trend observed for Au@BSA NCs and Au@BSA NCs CNC-ALG nanocomposite reveals that the affinity of mercury did not vary after incorporating the cluster into the matrix.

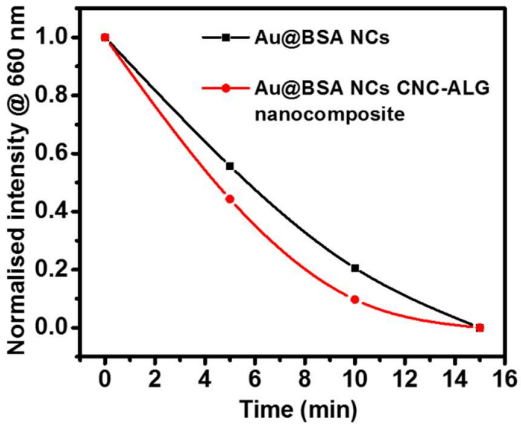

Figure 6.20. Normalized fluorescence intensities of Au@BSA NCs and Au@BSA NCs CNC-ALG nanocomposite after binding with Hg^{2+} ions at regular time intervals.

(g) In terms of response and sensitivity, there are greater possibilities of improvement of this system compared to other reported systems. Because this nanocomposite can be manipulated into smaller size hydrogel beads and also into various shapes such as film, stick or candle, depending on the end use, diffusion of Hg^{2+} ions can be enhanced using forced diffusion processes such as vacuum suction. In terms of selectivity, there is also an ability to incorporate different types of gold nanoclusters into the nanocomposite to make them selective to other heavy metal ions species of interest. Selectivity can be brought in also though molecular functionalization of the clusters.

In summary, a novel nanocomposite that can simultaneously sense and scavenge the toxic heavy metal ions like Hg^{2+} in contaminated water was developed and demonstrated. Nanostructures of the components, namely cellulose nanocrystals and protein protected

clusters allowed the creation of this fast responsive system. The sensing and scavenging property of this system is controlled by the diffusion of ions. At this stage of development, the system was not reusable due to the poor recovery of fluorescence of Au@BSA NCs upon Hg^{2+} binding. Better analysis and calculations may be performed to improve the modelling of quenching dynamics to study the diffusion of Hg^{2+} ions in hydrogels.

6.3 Conclusions

In conclusion, we have developed a novel nanocomposite that can simultaneously sense and scavenge toxic heavy metal ions in contaminated water. Au@BSA NCs leaching experiments and batch adsorption experiments using Hg^{2+} ions suggested that a nanocomposite with 1:2 CNC:ALG ratio is an ideal sensor-scavenger system. The sensitivity of this nanocomposite was found to be highly selective to Hg^{2+} ions among all other heavy metal ions tested. The fluorescence of the nanocomposite was found to be completely quenched in the presence of Hg^{2+} due to high affinity metallophilic Hg^{2+}/Au^{2+} interaction on the Au@BSA NCs surface. Adsorption of Hg^{2+} by the nanocomposite showed a visible change in their colour and the maximum adsorption capacity measured using Langmuir adsorption isotherm was 26 mg/g. We also reported a novel method to probe diffusion and calculated the diffusion coefficient by visualizing the dynamic fluorescence quenching of Au@BSA NCs as the Hg^{2+} ions diffuse into the hydrogel beads. The diffusion coefficient calculated using this novel method was 1.01 ($\pm$0.3) x 10^{-6} cm^2/s which is considered to be in the same range as reported for other ions in polymeric matrices using various other techniques. Further, the practical application of this nanocomposite was demonstrated using a dip pen experiment wherein the fluorescence of the capillary column containing these hydrogel beads quenched as the Hg^{2+} ions got adsorbed and diffused through them. Similar types of novel nanocomposites selective to other heavy metal ions can be designed. Systems incorporating these nanocomposites can be used as a simultaneous sensor-scavenger system and also as a tool to probe diffusion. The possibility to create various sustainable formulations with simultaneous sensing and scavenging offers new possibilities of applications for such materials.

Chapter 7

Original Contributions and Recommendations

7.1 Original contributions to research

Developing sustainable platforms for wastewater treatment using eco-friendly and biodegradable nanomaterials and biopolymers can drastically reduce the carbon footprint and secondary environmental pollution. Various studies have reported that cellulose nanocrystals (CNCs) are promising candidates that can be used for the adsorption of contaminants in wastewater. However, the difficulty in separation of CNCs after use in adsorption limits their application in large-scale water treatment processes. In this context, incorporation of CNCs into matrices with enhanced adsorption capabilities is extremely desirable. Also, the selectivity of pristine CNCs towards a wide variety of water contaminants is limited, and it is essential to surface functionalize them to impart this selectivity. Considering all these important factors, the following four main objectives of this thesis have been formulated: (a) Development of CNCs incorporated alginate (CNC-ALG) hydrogel beads and evaluation of their adsorption characteristics for methylene blue (MB) using batch adsorption studies. (b) Understanding of the adsorption behavior of MB by CNC-ALG hydrogel in a fixed bed column adsorption (c) Evaluation of the selective dye adsorption characteristics of pristine and surface functionalized CNCs and their ability to tailor the characteristics of the nanocomposites that incorporates them, for use in water treatment applications (d) Development of diffusion controlled simultaneous sensor-scavenger system for heavy metal ions in water based on atomically precise cluster – CNC composite. The following sections summarize the main findings of the research work carried out as part of this thesis.

7.1.1 Development of CNC-ALG hydrogel beads and evaluation of their adsorption characteristics using batch adsorption studies

CNC-ALG hydrogel beads were prepared using simple ionotropic gelation method. Nanocomposite solution comprising of CNCs and alginate were dispensed into $CaCl_2$ gelation batch to form crosslinked hydrogel beads instantaneously. Their adsorption properties for a

model cationic dye, MB was evaluated using batch adsorption studies. CNC-ALG hydrogel beads were found to have better adsorption capabilities compared to pure ALG hydrogel beads. The influence of various parameters such as contact time, adsorbent dosage, initial dye concentration, pH, temperature, ionic strength, crosslinking time and size of the beads on the dye adsorption characteristics of CNC-ALG hydrogel beads was determined. Adsorption kinetic data fitted well to pseudo-second-order kinetic model and intra-particle diffusion model was used to explain the mechanism of adsorption. Adsorption isotherm studies indicated that the Langmuir isotherm was adequate in describing the adsorption process, and the maximum adsorption capacity of these beads was found to be 256.4 mg/g for MB. CNC-ALG hydrogel beads were also found to be reusable as these beads demonstrated more than 95% regeneration efficiency even after five adsorption - desorption cycles.

7.1.2 Understanding the adsorption behavior of MB by CNC-ALG hydrogel beads in fixed bed column adsorption

A series of fixed bed column adsorption studies were carried out to investigate the adsorption behavior of MB by CNC-ALG hydrogel beads. The effect of various column operational parameters, such as initial dye concentration, bed depth and flow rate on the breakthrough curves was studied. A unique phenomenon in the breakthrough curves was observed in the initial phase of dye adsorption. Breakthrough curves demonstrated a dramatic increase followed by a gradual decrease before they steadily increased in concentration until the point of saturation. It was found that the column operational parameters had an impact on this phenomenon. To confirm that this was not an artifact due to the column design parameters, the existence of this phenomenon was verified by changing the flow direction, the diameter of the column and composition of adsorbent. It was determined that this, in fact, was not an artifact, but a property of the hydrogel beads themselves. The shrinkage of the bed over time was observed during the experiment. Hence the hydrodynamics of the beads were studied to elucidate the phenomenon observed in the breakthrough curve. It was found that hydrogels undergo osmotic swelling followed by a charge shielding assisted shrinkage during the dye adsorption which affected the packing of the fixed bed resulting in the particular phenomenon

observed in the breakthrough curve. It was found that this particular phenomenon assisted in improving the performance of the adsorbent, as lower void fraction meant more contact between the bulk fluid and adsorbent beads. The maximum adsorption capacity (q_m) of the beads was found to be 255.5 mg/g which corroborated with the q_m calculated from the batch adsorption studies. Various parameters pertaining to column adsorption experiments were also calculated from the breakthrough curve.

7.1.3 Surface functionalized CNCs for selective adsorption in water treatment applications

Surface functionalized CNCs were prepared by coating them with MF and PD. Selective dye adsorption studies performed using pristine and surface functionalized CNCs demonstrated that the selectivity of the CNCs can be tailored by surface functionalization. Negatively charged pristine CNCs showed an affinity for positively charged dye, whereas, positively charged MF-CNCs showed an affinity for negatively charged dye. The selectivity of pristine CNCs for dye containing Eschenmoser functional group was improved by coating them with PD. The ability of the surface functionalized CNCs to tailor the properties of nanocomposites was further explored by preparing a novel nanocomposite viz., PD-CNC-ALG hydrogel beads. Selective dye adsorption studies demonstrated that PD-CNC-ALG hydrogel beads have selectivity towards Eschenmoser group containing dyes like MB showing the improved adsorption capability for these dyes compared to CNC-ALG hydrogel beads. They also showed good binding to heavy metal ions like Pb^{2+}, Hg^{2+}, Cr^{3+} and Cu^{2+}. Kinetics of MB adsorption onto PD-CNC-ALG beads was modelled using pseudo-second-order kinetic model and the rate constants of adsorption were found out. The maximum adsorption capacity of PD-CNC-ALG hydrogel beads for MB and Cu^{2+} ions were found to be 333.33 mg/g and 72.99 mg/g respectively. When Ag-NPs were chelated onto PD-CNC-ALG hydrogel beads, they displayed good antibacterial activity with negligible leaching of Ag-NPs from their polymeric matrix and these systems hold promise for disinfecting bacteria in contaminated drinking water.

7.1.4 Development of diffusion controlled simultaneous sensor-scavenger system for heavy metal ions in water based on atomically precise cluster – CNC composite

A novel nanocomposite viz., bovine serum albumin protected gold nanoclusters (Au@BSA NCs) loaded CNC-ALG hydrogel beads that can simultaneously sense and scavenge toxic heavy metal ions in contaminated water was developed. This nanocomposite was found to be highly selective to Hg^{2+} ions among all other heavy metal ions tested and can also sense low concentrations of Hg^{2+} ions in water. The fluorescence of the nanocomposite was found to be completely quenched in the presence of Hg^{2+} due to high-affinity metallophilic Hg^{2+}/Au^{2+} interaction on the Au@BSA NCs surface. Adsorption of Hg^{2+} by the nanocomposite showed a visible change in their colour and the maximum adsorption capacity measured using Langmuir adsorption isotherm was 26 mg/g. A novel method to probe the diffusion and calculate the diffusion coefficient was also proposed based on the dynamic fluorescence quenching of Au@BSA NCs as the Hg^{2+} ions diffuse into the hydrogel beads. The diffusion coefficient calculated using this novel method was 1.01 (±0.3) x 10^{-6} cm^2/s which is in the same range as reported for other ions in polymeric matrices using various other techniques. Further, the practical application of this nanocomposite was demonstrated using a dip pen experiment wherein the fluorescence of the capillary column containing these hydrogel beads quenched as the Hg^{2+} ions diffused and bind to the Au@BSA NCs surface.

7.2 Recommendations for future studies

In summary, this thesis focused on the development and application of CNCs incorporated nanocomposites for water treatment applications. The following recommendations are suggested for future studies based on the results of the research work conducted. Considering the ionically crosslinked nature of these nanocomposites, their practical use in an aqueous environment containing a high concentration of competing binding ions may be limiting as it can lead to the extraction of calcium ions from the matrix due to the competitive binding of ions. However, no visible change in the nanocomposite integrity was observed after all the studies performed using a different concentration of organic dyes and

heavy metal ions. Hence, further studies may be performed to design better nanocomposite for improved performance in an aqueous environment containing a higher concentration of competing binding ions.

In Chapter 3, a novel recyclable adsorbent based on CNCs and alginate was developed and their adsorption characteristics for MB was evaluated using batch adsorption studies. Preliminary experiments have shown a decrease in the dye removal % with an increase in the salt concentration. This will restrict the application of CNC-ALG hydrogel beads in real wastewater samples which contains higher salt concentration. Hence further design experiments should be carried out to modify the property of this adsorbent for use in such situation. Attempts have also been made to further increase the loading of CNCs in the nanocomposite. Preliminary studies have shown improved capability to adsorb MB with higher loadings. Comprehensive batch adsorption and mechanical testing studies using higher loadings of CNCs can provide valuable insight on the CNC loading threshold limit which is ideal for a nanocomposite with maximum adsorption capacity. Also, similar adsorbents based on CNCs and other biopolymers such as chitosan, gelatin, cellulose and starch etc. can be prepared. The design consideration for the development of these new adsorbents can be made based on the type of pollutant needed to be removed.

In chapter 4, adsorption behavior of MB by CNC-ALG hydrogel beads in a fixed bed column adsorption was investigated in detail. This study mainly explores the characteristic phenomenon occurred in the early stages of the breakthrough curve. However, more fixed bed column adsorption studies should be carried out to elucidate the long-term breakthrough behavior. Also, kinetic modelling of the fixed bed column adsorption experimental data using well-established models can help predict the breakthrough curves which are essential for the characterizing the performance of fixed bed columns.

In chapter 5, selective adsorption characteristics of the pristine and surface functionalized CNCs namely MF-CNCs and PD-CNCs were evaluated and the ability of PD-CNCs to tailor the characteristics of the nanocomposite was evaluated. Preliminary adsorption studies using MF-CNCs have demonstrated their very good adsorption capability for negatively charged

dyes. A filter cake based on cellulose pulp and MF-CNCs can be developed to further explore the capability of these MF-CNCs. Here the positively charged MF-CNCs could bind to the negatively charged cellulose pulp by electrostatic interaction and can act as nanofillers that aid in the selective adsorption of negatively charged water contaminants. The applicability of pristine and surface functionalized CNCs can be further exploited by developing new filtration platforms consisting of interchangeable CNC loaded cartridges. The choice of the CNCs loaded in these cartridges can be customized based on the water contaminant to be removed.

In chapter 6, a diffusion controlled simultaneous sensor-scavenger system based on atomically precise cluster – CNC composite was developed. This nanocomposite comprising of Au@BSA NCs loaded CNCs were selective for Hg^{2+} ion sensing. Similar nanocomposite with different nanocluster loaded CNCs can be developed for the selective sensing of other heavy metal ions in water. The time of sensing is sufficiently longer for the current nanocomposite as it is diffusion limited. This can be resolved by developing a forced diffusion cell setup that can enhance up the diffusion of ions into the nanocomposite. Also, at this stage of the development, the nanocomposite is not re-usable due to the poor recovery of fluorescence of Au@BSA NCs upon Hg^{2+} binding. This can be resolved by using new clusters with improved fluorescent recovery after binding with ions. The novel method proposed to visualize the diffusion phenomenon and calculate the mass transfer characteristics of Hg^{2+} ions into these hydrogel beads can be extended for other heavy metal ions and biomolecules by selecting an appropriate sensor moiety inside the hydrogel beads. The modelling of quenching dynamics used in this study also needs to be improved using better analysis and calculations encompassing several other parameters like binding rate, fluorescent decay coefficient etc.

The research work carried out as part of this doctoral thesis have explored in detail the adsorption characteristics of CNCs incorporated nanocomposites. These understandings can be further extended to the area of controlled release. Some studies have already shown that CNCs are very good candidates for the binding and controlled release of molecules. Surface functionalization of CNCs can be used to control the binding and release of molecules that would not normally bind to CNCs.[292] CNCs can also be incorporated in nanocomposites to

modulate their controlled release behavior.[25,69] Also, modelling the control release profiles of these nanocomposites can yield information on the influence of CNCs on the binding and controlled release of molecules. Studies can be performed to demonstrate that the controlled release and stimuli-responsive properties of these nanocomposites can be improved by functionalizing CNCs. Stimuli-responsive nature of the nanocomposites is advantageous for the controlled release of agrochemicals. The pH of the soil environment can be used to trigger the release of agrochemicals from the nanocomposite. CNCs can be functionalized by grafting with pH-responsive polymers like poly(acrylic acid) on its surface. The incorporation of these functionalized CNCs will make the nanocomposite pH responsive. The grafted poly(acrylic acid) chains will also introduce more negative charges on the surface CNCs which is beneficial for the enhanced binding and controlled release of positively charged agrochemicals.

References

(1) Ahuja, S. *Handbook of Water Purity and Quality*; Ahuja, S., Ed.; Academic press, 2009.

(2) Crini, G. Non-conventional low-cost adsorbents for dye removal: A review. *Bioresour. Technol.* **2006**, *97* (9), 1061–1085.

(3) Sharma, P.; Kaur, H.; Sharma, M.; Sahore, V. A review on applicability of naturally available adsorbents for the removal of hazardous dyes from aqueous waste. *Environ. Monit. Assess.* **2011**, *183* (1–4), 151–195.

(4) Unuabonah, E. I.; Adebowale, K. O.; Dawodu, F. a. Equilibrium, kinetic and sorber design studies on the adsorption of Aniline blue dye by sodium tetraborate-modified Kaolinite clay adsorbent. *J. Hazard. Mater.* **2008**, *157* (2–3), 397–409.

(5) Ho, Y. S.; McKay, G. Sorption of dyes and copper ions onto biosorbents. *Process Biochem.* **2003**, *38* (7), 1047–1061.

(6) Jain, A. K.; Gupta, V. K.; Bhatnagar, A.; Suhas. Utilization of industrial waste products as adsorbents for the removal of dyes. *J. Hazard. Mater.* **2003**, *101* (1), 31–42.

(7) Ali, I.; Gupta, V. K. Advances in water treatment by adsorption technology. *Nat. Protoc.* **2007**, *1* (6), 2661–2667.

(8) Bhatnagar, A.; Sillanpää, M. Utilization of agro-industrial and municipal waste materials as potential adsorbents for water treatment—A review. *Chem. Eng. J.* **2010**, *157* (2–3), 277–296.

(9) He, K. A calculation of the environmental footprint of a granular activated carbon regeneration facility. In *Climate and Energy section. Environmental Sciences Senior Thesis Symposium.*; UC Berkeley Environmental Sciences, 2012; Vol. 22.

(10) Peng, B. L.; Dhar, N.; Liu, H. L.; Tam, K. C. Chemistry and applications of nanocrystalline cellulose and its derivatives: A nanotechnology perspective. *Can. J. Chem. Eng.* **2011**, *89* (5), 1191–1206.

(11) Khin, M. M.; Nair, a. S.; Babu, V. J.; Murugan, R.; Ramakrishna, S. A review on nanomaterials for environmental remediation. *Energy Environ. Sci.* **2012**, *5* (8), 8075.

(12) Carpenter, A. W.; De Lannoy, C. F.; Wiesner, M. R. Cellulose nanomaterials in water

treatment technologies. *Environ. Sci. Technol.* **2015**, *49* (9), 5277–5287.

(13) Mahfoudhi, N.; Boufi, S. Nanocellulose as a Millennium Material with Enhancing Adsorption Capacities. In *Biodegradable and Biobased Polymers for Environmental and Biomedical Applications*; John Wiley & Sons, Inc.: Hoboken, NJ, USA, 2016; pp 349–383.

(14) Hokkanen, S.; Bhatnagar, A.; Sillanpää, M. A review on modification methods to cellulose-based adsorbents to improve adsorption capacity. *Water Res.* **2016**, *91*, 156–173.

(15) Mohammed, N.; Grishkewich, N.; Berry, R. M.; Tam, K. C. Cellulose nanocrystal–alginate hydrogel beads as novel adsorbents for organic dyes in aqueous solutions. *Cellulose* **2015**, *22* (6), 3725–3738.

(16) Mohammed, N.; Grishkewich, N.; Tam, K. C.; Berry, R. Pristine and surface functionalized cellulose nanocrystals (CNCs) incorporated hydrogel beads and uses thereof. US 14/976,564, 2016.

(17) Mohammed, N.; Grishkewich, N.; Waeijen, H. A.; Berry, R. M.; Tam, K. C. Continuous flow adsorption of methylene blue by cellulose nanocrystal-alginate hydrogel beads in fixed bed columns. *Carbohydr. Polym.* **2016**, *136*, 1194–1202.

(18) Mohammed, N.; Baidya, A.; Murugesan, V.; Kumar, A. A.; Ganayee, M. A.; Mohanty, J. S.; Tam, K. C.; Pradeep, T. Diffusion-Controlled Simultaneous Sensing and Scavenging of Heavy Metal Ions in Water Using Atomically Precise Cluster–Cellulose Nanocrystal Composites. *ACS Sustain. Chem. Eng.* **2016**, *4* (11), 6167–6176.

(19) Kabiri, K.; Omidian, H.; Zohuriaan-Mehr, M. J.; Doroudiani, S. Superabsorbent hydrogel composites and nanocomposites: A review. *Polym. Compos.* **2011**, *32* (2), 277–289.

(20) Peppas, N. A.; Hoffman, A. S. Hydrogels. In *Biomaterials Science: An Introduction to Materials in Medicine*; Elsevier, 2013; pp 166–179.

(21) Guvendiren, M.; Heiney, P. a.; Yang, S. Precipitated Calcium Carbonate Hybrid Hydrogels: Structural and Mechanical Properties. *Macromolecules* **2009**, *42* (17), 6606–

6613.

(22) Meenach, S. a; Otu, C. G.; Anderson, K. W.; Hilt, J. Z. Controlled synergistic delivery of paclitaxel and heat from poly(β-amino ester)/iron oxide-based hydrogel nanocomposites. *Int. J. Pharm.* **2012**, *427* (2), 177–184.

(23) Cao, X.; Habibi, Y.; Magalhães, W. Cellulose nanocrystals-based nanocomposites: fruits of a novel biomass research and teaching platform. *Curr. Sci.* **2011**, *100* (8), 1172–1176.

(24) Han, J.; Lei, T.; Wu, Q. Facile preparation of mouldable polyvinyl alcohol-borax hydrogels reinforced by well-dispersed cellulose nanoparticles: physical, viscoelastic and mechanical properties. *Cellulose* **2013**, *20* (6), 2947–2958.

(25) Zhang, X.; Huang, J.; Chang, P. R.; Li, J.; Chen, Y.; Wang, D.; Yu, J.; Chen, J. Structure and properties of polysaccharide nanocrystal-doped supramolecular hydrogels based on Cyclodextrin inclusion. *Polymer* **2010**, *51* (19), 4398–4407.

(26) Nechyporchuk, O.; Belgacem, M. N.; Pignon, F. Current Progress in Rheology of Cellulose Nanofibril Suspensions. *Biomacromolecules* **2016**, *17* (7), 2311–2320.

(27) Nechyporchuk, O.; Belgacem, M. N.; Bras, J. Production of cellulose nanofibrils: A review of recent advances. *Ind. Crops Prod.* **2016**, *93*, 2–25.

(28) Olivera, S.; Muralidhara, H. B.; Venkatesh, K.; Guna, V. K.; Gopalakrishna, K.; Kumar K., Y. Potential applications of cellulose and chitosan nanoparticles/composites in wastewater treatment: A review. *Carbohydr. Polym.* **2016**, *153*, 600–618.

(29) Moon, R. J.; Martini, A.; Nairn, J.; Simonsen, J.; Youngblood, J. Cellulose nanomaterials review: structure, properties and nanocomposites. *Chem. Soc. Rev.* **2011**, *40* (7), 3941–3994.

(30) Klemm, D.; Kramer, F.; Moritz, S.; Lindström, T.; Ankerfors, M.; Gray, D.; Dorris, A. Nanocelluloses: A New Family of Nature-Based Materials. *Angew. Chemie Int. Ed.* **2011**, *50* (24), 5438–5466.

(31) Eichhorn, S. J.; Baillie, C. A.; Zafeiropoulos, N.; Mwaikambo, L. Y.; Ansell, M. P.; Dufresne, A.; Entwistle, K. M.; Herrera-Franco, P. J.; Escamilla, G. C.; Groom, L.; et

al. Review: current international research into cellulosic fibres and composites. *J. Mater. Sci.* **2001**, *36* (9), 2107–2131.

(32) Favier, V.; Chanzy, H.; Cavaille, J. Polymer nanocomposites reinforced by cellulose whiskers. *Macromolecules* **1995**, 6365–6367.

(33) Dong, X. M.; Kimura, T.; Revol, J.-F.; Gray, D. G. Effects of Ionic Strength on the Isotropic−Chiral Nematic Phase Transition of Suspensions of Cellulose Crystallites. *Langmuir* **1996**, *12* (8), 2076–2082.

(34) Beck-Candanedo, S.; Viet, D.; Gray, D. G. Triphase Equilibria in Cellulose Nanocrystal Suspensions Containing Neutral and Charged Macromolecules. *Macromolecules* **2007**, *40* (9), 3429–3436.

(35) Lahiji, R. R.; Xu, X.; Reifenberger, R.; Raman, A.; Rudie, A.; Moon, R. J. Atomic force microscopy characterization of cellulose nanocrystals. *Langmuir* **2010**, *26* (6), 4480–4488.

(36) Lin, N.; Huang, J.; Dufresne, A. Preparation, properties and applications of polysaccharide nanocrystals in advanced functional nanomaterials: a review. *Nanoscale* **2012**, *4* (11), 3274.

(37) Braun, B.; Dorgan, J. R. Single-step method for the isolation and surface functionalization of cellulosic nanowhiskers. *Biomacromolecules* **2009**, *10* (2), 334–341.

(38) Hasani, M.; Cranston, E. D.; Westman, G.; Gray, D. G. Cationic surface functionalization of cellulose nanocrystals. *Soft Matter* **2008**, *4* (11), 2238.

(39) Habibi, Y.; Chanzy, H.; Vignon, M. R. TEMPO-mediated surface oxidation of cellulose whiskers. *Cellulose* **2006**, *13* (6), 679–687.

(40) Goussé, C.; Chanzy, H.; Excoffier, G. Stable suspensions of partially silylated cellulose whiskers dispersed in organic solvents. *Polymer* **2002**, *43*, 2645–2651.

(41) Morandi, G.; Heath, L.; Thielemans, W. Cellulose nanocrystals grafted with polystyrene chains through surface-initiated atom transfer radical polymerization (SI-ATRP). *Langmuir* **2009**, *25* (14), 8280–8286.

(42) Shi, Z.; Tang, J.; Chen, L.; Yan, C.; Tanvir, S.; Anderson, W. a.; Berry, R. M.; Tam, K. C. Enhanced colloidal stability and antibacterial performance of silver nanoparticles/cellulose nanocrystal hybrids. *J. Mater. Chem. B* **2015**, *3* (4), 603–611.

(43) Tang, J.; Shi, Z.; Berry, R. M.; Tam, K. C. Mussel-Inspired Green Metallization of Silver Nanoparticles on Cellulose Nanocrystals and Their Enhanced Catalytic Reduction of 4-Nitrophenol in the Presence of β-Cyclodextrin. *Ind. Eng. Chem. Res.* **2015**, *54* (13), 3299–3308.

(44) Wu, X.; Shi, Z.; Tjandra, R.; Cousins, A. J.; Sy, S.; Yu, A.; Berry, R. M.; Tam, K. C. Nitrogen-enriched porous carbon nanorods templated by cellulose nanocrystals as high performance supercapacitor electrodes. *J. Mater. Chem. A* **2015**, *3* (47), 23768–23777.

(45) Wu, X.; Shi, Z.; Fu, S.; Chen, J.; Berry, R. M.; Tam, K. C. Strategy for Synthesizing Porous Cellulose Nanocrystal Supported Metal Nanocatalysts. *ACS Sustain. Chem. Eng.* **2016**, *4* (11), 5929–5935.

(46) Liu, Y.; Ai, K.; Lu, L. Polydopamine and its derivative materials: synthesis and promising applications in energy, environmental, and biomedical fields. *Chem. Rev.* **2014**, *114* (9), 5057–5115.

(47) Lee, H.; Dellatore, S. M.; Miller, W. M.; Messersmith, P. B. Mussel-inspired surface chemistry for multifunctional coatings. *Science* **2007**, *318* (5849), 426–430.

(48) Dreyer, D. R.; Miller, D. J.; Freeman, B. D.; Paul, D. R.; Bielawski, C. W. Perspectives on poly(dopamine). *Chem. Sci.* **2013**, *4* (10), 3796.

(49) Lee, H.; Rho, J.; Messersmith, P. B. Facile Conjugation of Biomolecules onto Surfaces via Mussel Adhesive Protein Inspired Coatings. *Adv. Mater.* **2009**, *21* (4), 431–434.

(50) Sileika, T. S.; Kim, H.-D.; Maniak, P.; Messersmith, P. B. Antibacterial performance of polydopamine-modified polymer surfaces containing passive and active components. *ACS Appl. Mater. Interfaces* **2011**, *3* (12), 4602–4610.

(51) Bauer, D. R. Melamine/formaldehyde crosslinkers: characterization, network formation and crosslink degradation. *Prog. Org. Coatings* **1986**, *14* (3), 193–218.

(52) Haraguchi, K.; Li, H. J. Mechanical properties and structure of polymer-clay

nanocomposite gels with high clay content. *Macromolecules* **2006**, *39* (5), 1898–1905.

(53) Yang, X.; Bakaic, E.; Hoare, T.; Cranston, E. D. Injectable polysaccharide hydrogels reinforced with cellulose nanocrystals: morphology, rheology, degradation, and cytotoxicity. *Biomacromolecules* **2013**, *14* (12), 4447–4455.

(54) Kurecic, M.; Sfiligoj, M. Polymer Nanocomposite Hydrogels for Water Purification. In *Nanocomposites - New Trends and Developments*; InTech, 2012.

(55) Elisseeff, J. Hydrogels - Structure starts to gel. *Nat. Mater.* **2008**, *7* (April), 271–273.

(56) Patel, A.; Mequanint, K. Hydrogel Biomaterials. In *Biomedical Engineering - Frontiers and Challenges*; InTech, 2011; pp 275–296.

(57) Peppas, N. A.; Huang, Y.; Torres-Lugo, M.; Ward, J. H.; Zhang, J. Physicochemical Foundations and Structural Design of Hydrogels in Medicine and Biology. *Annu. Rev. Biomed. Eng.* **2000**, *2* (1), 9–29.

(58) Gulrez, S. K. .; Al-Assaf, S.; Phillips, G. O. Hydrogels: Methods of Preparation, Characterisation and Applications. **2011**.

(59) Hezaveh, H.; Muhamad, I. I. Effect of MgO nanofillers on burst release reduction from hydrogel nanocomposites. *J. Mater. Sci. Mater. Med.* **2013**, *24* (6), 1443–1453.

(60) Sivakumaran, D.; Maitland, D.; Hoare, T. Injectable microgel-hydrogel composites for prolonged small-molecule drug delivery. *Biomacromolecules* **2011**, *12* (11), 4112–4120.

(61) Schexnailder, P.; Schmidt, G. Nanocomposite polymer hydrogels. *Colloid Polym. Sci.* **2008**, *287* (1), 1–11.

(62) Aimé, C.; Coradin, T. Nanocomposites from biopolymer hydrogels: Blueprints for white biotechnology and green materials chemistry. *J. Polym. Sci. Part B Polym. Phys.* **2012**, *50* (10), 669–680.

(63) Yan, L. Y.; Chen, H.; Li, P.; Kim, D.-H.; Chan-Park, M. B. Finely dispersed single-walled carbon nanotubes for polysaccharide hydrogels. *ACS Appl. Mater. Interfaces* **2012**, *4* (9), 4610–4615.

(64) Wang, C.; Flynn, N. T.; Langer, R. Controlled Structure and Properties of Thermoresponsive Nanoparticle–Hydrogel Composites. *Adv. Mater.* **2004**, *16* (13),

1074–1079.

(65) Yang, J.; Han, C.-R.; Duan, J.-F.; Xu, F.; Sun, R.-C. *In situ* grafting silica nanoparticles reinforced nanocomposite hydrogels. *Nanoscale* **2013**, *5* (22), 10858–10863.

(66) Zhou, C.; Wu, Q.; Yue, Y.; Zhang, Q. Application of rod-shaped cellulose nanocrystals in polyacrylamide hydrogels. *J. Colloid Interface Sci.* **2011**, *353* (1), 116–123.

(67) Abitbol, T.; Johnstone, T.; Quinn, T. M.; Gray, D. G. Reinforcement with cellulose nanocrystals of poly(vinyl alcohol) hydrogels prepared by cyclic freezing and thawing. *Soft Matter* **2011**, *7* (6), 2373–2379.

(68) Yang, J.; Han, C.-R.; Duan, J.-F.; Xu, F.; Sun, R.-C. Mechanical and viscoelastic properties of cellulose nanocrystals reinforced poly(ethylene glycol) nanocomposite hydrogels. *ACS Appl. Mater. Interfaces* **2013**, *5* (8), 3199–3207.

(69) Lin, N.; Huang, J.; Chang, P. R.; Feng, L.; Yu, J. Effect of polysaccharide nanocrystals on structure, properties, and drug release kinetics of alginate-based microspheres. *Colloids Surf. B. Biointerfaces* **2011**, *85* (2), 270–279.

(70) Karaaslan, M. A.; Tshabalala, M. a.; Yelle, D. J.; Buschle-Diller, G. Nanoreinforced biocompatible hydrogels from wood hemicelluloses and cellulose whiskers. *Carbohydr. Polym.* **2011**, *86* (1), 192–201.

(71) Sanna, R.; Fortunati, E.; Alzari, V.; Nuvoli, D.; Terenzi, A.; Casula, M. F.; Kenny, J. M.; Mariani, A. Poly(N-vinylcaprolactam) nanocomposites containing nanocrystalline cellulose: a green approach to thermoresponsive hydrogels. *Cellulose* **2013**, *20* (5), 2393–2402.

(72) Goetz, L.; Mathew, A.; Oksman, K.; Gatenholm, P.; Ragauskas, A. J. A novel nanocomposite film prepared from crosslinked cellulosic whiskers. *Carbohydr. Polym.* **2009**, *75* (1), 85–89.

(73) Goetz, L.; Foston, M.; Mathew, A. P.; Oksman, K.; Ragauskas, A. J. Poly(methyl vinyl ether- co -maleic acid)−Polyethylene Glycol Nanocomposites Cross-Linked *In Situ* with Cellulose Nanowhiskers. *Biomacromolecules* **2010**, *11* (10), 2660–2666.

(74) Kelly, J. a; Shukaliak, A. M.; Cheung, C. C. Y.; Shopsowitz, K. E.; Hamad, W. Y.;

MacLachlan, M. J. Responsive photonic hydrogels based on nanocrystalline cellulose. *Angew. Chem. Int. Ed. Engl.* **2013**, *52* (34), 8912–8916.

(75) Spagnol, C.; Rodrigues, F. H. a.; Neto, A. G. V. C.; Pereira, A. G. B.; Fajardo, A. R.; Radovanovic, E.; Rubira, A. F.; Muniz, E. C. Nanocomposites based on poly(acrylamide-co-acrylate) and cellulose nanowhiskers. *Eur. Polym. J.* **2012**, *48* (3), 454–463.

(76) Spagnol, C.; Rodrigues, F. H. a.; Pereira, A. G. B.; Fajardo, A. R.; Rubira, A. F.; Muniz, E. C. Superabsorbent hydrogel nanocomposites based on starch-g-poly(sodium acrylate) matrix filled with cellulose nanowhiskers. *Cellulose* **2012**, *19* (4), 1225–1237.

(77) Eyholzer, C.; de Couraça, a B.; Duc, F.; Bourban, P. E.; Tingaut, P.; Zimmermann, T.; Månson, J. a E.; Oksman, K. Biocomposite hydrogels with carboxymethylated, nanofibrillated cellulose powder for replacement of the nucleus pulposus. *Biomacromolecules* **2011**, *12* (5), 1419–1427.

(78) Way, A. E.; Hsu, L.; Shanmuganathan, K.; Weder, C.; Rowan, S. J. pH-Responsive Cellulose Nanocrystal Gels and Nanocomposites. *ACS Macro Lett.* **2012**, *1* (8), 1001–1006.

(79) Dash, R.; Foston, M.; Ragauskas, A. J. Improving the mechanical and thermal properties of gelatin hydrogels cross-linked by cellulose nanowhiskers. *Carbohydr. Polym.* **2013**, *91* (2), 638–645.

(80) McKee, J. R.; Appel, E. a.; Seitsonen, J.; Kontturi, E.; Scherman, O. a.; Ikkala, O. Healable, Stable and Stiff Hydrogels: Combining Conflicting Properties Using Dynamic and Selective Three-Component Recognition with Reinforcing Cellulose Nanorods. *Adv. Funct. Mater.* **2014**, *24* (18), 2706–2713.

(81) Yang, J.; Han, C.-R.; Duan, J.-F.; Ma, M.-G.; Zhang, X.-M.; Xu, F.; Sun, R.-C.; Xie, X.-M. Studies on the properties and formation mechanism of flexible nanocomposite hydrogels from cellulose nanocrystals and poly(acrylic acid). *J. Mater. Chem.* **2012**, *22* (42), 22467.

(82) Yang, J.; Han, C.-R.; Duan, J.-F.; Ma, M.-G.; Zhang, X.-M.; Xu, F.; Sun, R.-C.

Synthesis and characterization of mechanically flexible and tough cellulose nanocrystals–polyacrylamide nanocomposite hydrogels. *Cellulose* **2013**, *20* (1), 227–237.

(83) Dai, Q.; Kadla, J. F. Effect of nanofillers on carboxymethyl cellulose/hydroxyethyl cellulose hydrogels. *J. Appl. Polym. Sci.* **2009**, *114* (3), 1664–1669.

(84) Cha, R.; He, Z.; Ni, Y. Preparation and characterization of thermal/pH-sensitive hydrogel from carboxylated nanocrystalline cellulose. *Carbohydr. Polym.* **2012**, *88* (2), 713–718.

(85) Nelson, K.; Retsina, T.; Iakovlev, M.; van Heiningen, A.; Deng, Y.; Shatkin, J. A.; Mulyadi, A. American Process: Production of Low Cost Nanocellulose for Renewable, Advanced Materials Applications. In *Springer Series in Materials Science*; Madsen, L. D., Svedberg, E. B., Eds.; Springer Series in Materials Science; Springer International Publishing: Cham, 2016; Vol. 224, pp 267–302.

(86) Hendicks, D. *Water Treatment Unit Processess: Physical and Chemical*; CRC Press, 2006.

(87) Noll, K. E. *Adsorption Technology for Air and Water Pollution Control*; CRC Press, 1991.

(88) Worch, E. *Adsorption Technology in Water Treatment: Fundamentals, Processes, and Modeling*; Walter de Gruyter, 2012.

(89) Inglezakis, V. J.; Poulopoulos, S. G. *Adsorption, Ion Exchange and Catalysis: Design of Operations and Environmental Applications*; Elsevier, 2006.

(90) Rafatullah, M.; Sulaiman, O.; Hashim, R.; Ahmad, A. Adsorption of methylene blue on low-cost adsorbents: A review. *J. Hazard. Mater.* **2010**, *177* (1–3), 70–80.

(91) He, X.; Male, K. B.; Nesterenko, P. N.; Brabazon, D.; Paull, B.; Luong, J. H. T. Adsorption and Desorption of Methylene Blue on Porous Carbon Monoliths and Nanocrystalline Cellulose. *ACS Appl. Mater. Interfaces* **2013**, *5* (17), 8796–8804.

(92) Batmaz, R.; Mohammed, N.; Zaman, M.; Minhas, G.; Berry, R. M.; Tam, K. C. Cellulose nanocrystals as promising adsorbents for the removal of cationic dyes.

Cellulose **2014**, *21* (3), 1655–1665.

(93) Yu, H.-Y.; Zhang, D.-Z.; Lu, F.-F.; Yao, J. New Approach for Single-Step Extraction of Carboxylated Cellulose Nanocrystals for Their Use As Adsorbents and Flocculants. *ACS Sustain. Chem. Eng.* **2016**, *4* (5), 2632–2643.

(94) Qiao, H.; Zhou, Y.; Yu, F.; Wang, E.; Min, Y.; Huang, Q.; Pang, L.; Ma, T. Effective removal of cationic dyes using carboxylate-functionalized cellulose nanocrystals. *Chemosphere* **2015**, *141*, 297–303.

(95) Eyley, S.; Thielemans, W. Imidazolium grafted cellulose nanocrystals for ion exchange applications. *Chem. Commun.* **2011**, *47*, 4177–4179.

(96) Jin, L.; Li, W.; Xu, Q.; Sun, Q. Amino-functionalized nanocrystalline cellulose as an adsorbent for anionic dyes. *Cellulose* **2015**, *22* (4), 2443–2456.

(97) Chan, C. H.; Chia, C. H.; Zakaria, S.; Sajab, M. S.; Chin, S. X. Cellulose nanofibrils: a rapid adsorbent for the removal of methylene blue. *RSC Adv.* **2015**, *5* (24), 18204–18212.

(98) Pei, A.; Butchosa, N.; Berglund, L. a.; Zhou, Q. Surface quaternized cellulose nanofibrils with high water absorbency and adsorption capacity for anionic dyes. *Soft Matter* **2013**, *9* (6), 2047–2055.

(99) Wang, Y.; Zhang, X.; He, X.; Zhang, W.; Zhang, X.; Lu, C. *In situ* synthesis of MnO2 coated cellulose nanofibers hybrid for effective removal of methylene blue. *Carbohydr. Polym.* **2014**, *110*, 302–308.

(100) Xie, K.; Zhao, W.; He, X. Adsorption properties of nano-cellulose hybrid containing polyhedral oligomeric silsesquioxane and removal of reactive dyes from aqueous solution. *Carbohydr. Polym.* **2011**, *83* (4), 1516–1520.

(101) Zhou, C.; Lee, S.; Dooley, K.; Wu, Q. A facile approach to fabricate porous nanocomposite gels based on partially hydrolyzed polyacrylamide and cellulose nanocrystals for adsorbing methylene blue at low concentrations. *J. Hazard. Mater.* **2013**, *263*, 334–341.

(102) Zhou, C.; Wu, Q.; Lei, T.; Negulescu, I. I. Adsorption kinetic and equilibrium studies

for methylene blue dye by partially hydrolyzed polyacrylamide/cellulose nanocrystal nanocomposite hydrogels. *Chem. Eng. J.* **2014**, *251*, 17–24.

(103) Jin, L.; Sun, Q.; Xu, Q.; Xu, Y. Adsorptive removal of anionic dyes from aqueous solutions using microgel based on nanocellulose and polyvinylamine. *Bioresour. Technol.* **2015**, *197*, 348–355.

(104) Nypelö, T.; Rodriguez-Abreu, C.; Kolen'ko, Y. V.; Rivas, J.; Rojas, O. J. Microbeads and Hollow Microcapsules Obtained by Self-Assembly of Pickering Magneto-Responsive Cellulose Nanocrystals. *ACS Appl. Mater. Interfaces* **2014**, *6* (19), 16851–16858.

(105) Chen, W.; Li, Q.; Wang, Y.; Yi, X.; Zeng, J.; Yu, H.; Liu, Y.; Li, J. Comparative Study of Aerogels Obtained from Differently Prepared Nanocellulose Fibers. *ChemSusChem* **2014**, *7* (1), 154–161.

(106) O'Connell, D. W.; Birkinshaw, C.; O'Dwyer, T. F. Heavy metal adsorbents prepared from the modification of cellulose: A review. *Bioresour. Technol.* **2008**, *99* (15), 6709–6724.

(107) Liu, P.; Sehaqui, H.; Tingaut, P.; Wichser, A.; Oksman, K.; Mathew, A. P. Cellulose and chitin nanomaterials for capturing silver ions (Ag+) from water via surface adsorption. *Cellulose* **2014**, *21* (1), 449–461.

(108) Liu, P.; Borrell, P. F.; Božič, M.; Kokol, V.; Oksman, K.; Mathew, A. P. Nanocelluloses and their phosphorylated derivatives for selective adsorption of Ag+, Cu2+ and Fe3+ from industrial effluents. *J. Hazard. Mater.* **2015**, *294*, 177–185.

(109) Yu, X.; Tong, S.; Ge, M.; Wu, L.; Zuo, J.; Cao, C.; Song, W. Adsorption of heavy metal ions from aqueous solution by carboxylated cellulose nanocrystals. *J. Environ. Sci.* **2013**, *25* (5), 933–943.

(110) Kardam, A.; Raj, K. R.; Srivastava, S.; Srivastava, M. M. Nanocellulose fibers for biosorption of cadmium, nickel, and lead ions from aqueous solution. *Clean Technol. Environ. Policy* **2014**, *16* (2), 385–393.

(111) Srivastava, S.; Kardam, A.; Raj, K. R. Nanotech Reinforcement onto Cellulosic Fibers:

Green Remediation of Toxic Metals. *Int. J. Green Nanotechnol.* **2012**, *4* (1), 46–53.

(112) Kardam, A.; Raj, K. R.; Srivastava, S. Novel nano cellulosic fibers for remediation of heavy metals from synthetic water. *Int. J. nanodimension* **2012**, *3* (2), 155–162.

(113) Singh, K.; Arora, J. K.; Sinha, T. J. M.; Srivastava, S. Functionalization of nanocrystalline cellulose for decontamination of Cr(III) and Cr(VI) from aqueous system: computational modeling approach. *Clean Technol. Environ. Policy* **2014**, *16* (6), 1179–1191.

(114) Sheikhi, A.; Safari, S.; Yang, H.; van de Ven, T. G. M. Copper Removal Using Electrosterically Stabilized Nanocrystalline Cellulose. *ACS Appl. Mater. Interfaces* **2015**, *7* (21), 11301–11308.

(115) Sirviö, J. A.; Hasa, T.; Leiviskä, T.; Liimatainen, H.; Hormi, O. Bisphosphonate nanocellulose in the removal of vanadium(V) from water. *Cellulose* **2016**, *23* (1), 689–697.

(116) Ma, H.; Hsiao, B. S.; Chu, B. Ultrafine Cellulose Nanofibers as Efficient Adsorbents for Removal of UO 2 2+ in Water. *ACS Macro Lett.* **2012**, *1* (1), 213–216.

(117) Sehaqui, H.; de Larraya, U. P.; Liu, P.; Pfenninger, N.; Mathew, A. P.; Zimmermann, T.; Tingaut, P. Enhancing adsorption of heavy metal ions onto biobased nanofibers from waste pulp residues for application in wastewater treatment. *Cellulose* **2014**, *21* (4), 2831–2844.

(118) Zhang, N.; Zang, G.-L.; Shi, C.; Yu, H.-Q.; Sheng, G.-P. A novel adsorbent TEMPO-mediated oxidized cellulose nanofibrils modified with PEI: Preparation, characterization, and application for Cu(II) removal. *J. Hazard. Mater.* **2016**, *316* (Ii), 11–18.

(119) Hokkanen, S.; Repo, E.; Suopajärvi, T.; Liimatainen, H.; Niinimaa, J.; Sillanpää, M. Adsorption of Ni(II), Cu(II) and Cd(II) from aqueous solutions by amino modified nanostructured microfibrillated cellulose. *Cellulose* **2014**, *21* (3), 1471–1487.

(120) Hokkanen, S.; Repo, E.; Sillanpää, M. Removal of heavy metals from aqueous solutions by succinic anhydride modified mercerized nanocellulose. *Chem. Eng. J.* **2013**, *223*, 40–

47.

(121) Hokkanen, S.; Repo, E.; Westholm, L. J.; Lou, S.; Sainio, T.; Sillanpää, M. Adsorption of Ni2+, Cd2+, PO43− and NO3− from aqueous solutions by nanostructured microfibrillated cellulose modified with carbonated hydroxyapatite. *Chem. Eng. J.* **2014**, *252*, 64–74.

(122) Hokkanen, S.; Repo, E.; Lou, S.; Sillanpää, M. Removal of arsenic(V) by magnetic nanoparticle activated microfibrillated cellulose. *Chem. Eng. J.* **2015**, *260*, 886–894.

(123) Dwivedi, A. D.; Dubey, S. P.; Hokkanen, S.; Sillanpää, M. Mechanistic investigation on the green recovery of ionic, nanocrystalline, and metallic gold by two anionic nanocelluloses. *Chem. Eng. J.* **2014**, *253*, 316–324.

(124) Suopajärvi, T.; Liimatainen, H.; Karjalainen, M.; Upola, H.; Niinimäki, J. Lead adsorption with sulfonated wheat pulp nanocelluloses. *J. Water Process Eng.* **2015**, *5*, 136–142.

(125) Zhou, Y.; Fu, S.; Zhang, L.; Zhan, H.; Levit, M. V. Use of carboxylated cellulose nanofibrils-filled magnetic chitosan hydrogel beads as adsorbents for Pb(II). *Carbohydr. Polym.* **2014**, *101* (1), 75–82.

(126) Zheng, Q.; Cai, Z.; Gong, S. Green synthesis of polyvinyl alcohol (PVA)–cellulose nanofibril (CNF) hybrid aerogels and their use as superabsorbents. *J. Mater. Chem. A* **2014**, *2* (9), 3110–3118.

(127) Anirudhan, T. S.; Shainy, F. Effective removal of mercury(II) ions from chlor-alkali industrial wastewater using 2-mercaptobenzamide modified itaconic acid-grafted-magnetite nanocellulose composite. *J. Colloid Interface Sci.* **2015**, *456*, 22–31.

(128) Anirudhan, T. S.; Deepa, J. R.; Christa, J. Nanocellulose/nanobentonite composite anchored with multi-carboxyl functional groups as an adsorbent for the effective removal of Cobalt(II) from nuclear industry wastewater samples. *J. Colloid Interface Sci.* **2016**, *467*, 307–320.

(129) Chen, L.; Berry, R. M.; Tam, K. C. Synthesis of β-Cyclodextrin-modified cellulose nanocrystals (CNCs)@Fe3O4@SiO2 superparamagnetic nanorods. *ACS Sustain. Chem.*

Eng. **2014**, *2* (4), 951–958.

(130) Hokkanen, S.; Repo, E.; Bhatnagar, A.; Tang, W. Z.; Sillanpää, M. Adsorption of hydrogen sulphide from aqueous solutions using modified nano/micro fibrillated cellulose. *Environ. Technol.* **2014**, *35* (18), 2334–2346.

(131) Huang, R.; Liu, Z.; Sun, B.; Fatehi, P. Preparation of dialdehyde cellulose nanocrystal as an adsorbent for creatinine. *Can. J. Chem. Eng.* **2016**, *94* (8), 1435–1441.

(132) Anirudhan, T. S.; Rejeena, S. R. Adsorption and hydrolytic activity of trypsin on a carboxylate-functionalized cation exchanger prepared from nanocellulose. *J. Colloid Interface Sci.* **2012**, *381* (1), 125–136.

(133) Anirudhan, T. S.; Rejeena, S. R. Selective adsorption of hemoglobin using polymer-grafted-magnetite nanocellulose composite. *Carbohydr. Polym.* **2013**, *93* (2), 518–527.

(134) Anirudhan, T. S.; Rejeena, S. R. Poly(methacrylic acid-co-vinyl sulfonic acid)-grafted-magnetite/nanocellulose superabsorbent composite for the selective recovery and separation of immunoglobulin from aqueous solutions. *Sep. Purif. Technol.* **2013**, *119*, 82–93.

(135) Korhonen, J. T.; Kettunen, M.; Ras, R. H. A.; Ikkala, O. Hydrophobic Nanocellulose Aerogels as Floating, Sustainable, Reusable, and Recyclable Oil Absorbents. *ACS Appl. Mater. Interfaces* **2011**, *3* (6), 1813–1816.

(136) Jiang, F.; Hsieh, Y.-L. Amphiphilic superabsorbent cellulose nanofibril aerogels. *J. Mater. Chem. A* **2014**, *2* (18), 6337–6342.

(137) Zhang, Z.; Sèbe, G.; Rentsch, D.; Zimmermann, T.; Tingaut, P. Ultralightweight and flexible silylated nanocellulose sponges for the selective removal of oil from water. *Chem. Mater.* **2014**, *26* (8), 2659–2668.

(138) Yang, X.; Cranston, E. D. Chemically cross-linked cellulose nanocrystal aerogels with shape recovery and superabsorbent properties. *Chem. Mater.* **2014**, *26* (20), 6016–6025.

(139) Lee, C. S.; Robinson, J.; Chong, M. F. A review on application of flocculants in wastewater treatment. *Process Saf. Environ. Prot.* **2014**, *92* (6), 489–508.

(140) Quinlan, P. J.; Tanvir, A.; Tam, K. C. Application of the central composite design to

study the flocculation of an anionic azo dye using quaternized cellulose nanofibrils. *Carbohydr. Polym.* **2015**, *133*, 80–89.

(141) Vandamme, D.; Eyley, S.; Van den Mooter, G.; Muylaert, K.; Thielemans, W. Highly charged cellulose-based nanocrystals as flocculants for harvesting Chlorella vulgaris. *Bioresour. Technol.* **2015**, *194*, 270–275.

(142) Zeng, X.; Xu, X.; Shenai, P. M.; Kovalev, E.; Baudot, C.; Mathews, N.; Zhao, Y. Characteristics of the electrical percolation in carbon nanotubes/polymer nanocomposites. *J. Phys. Chem. C* **2011**, *115* (44), 21685–21690.

(143) Suopajärvi, T.; Liimatainen, H.; Hormi, O.; Niinimäki, J. Coagulation–flocculation treatment of municipal wastewater based on anionized nanocelluloses. *Chem. Eng. J.* **2013**, *231*, 59–67.

(144) Suopajärvi, T.; Koivuranta, E.; Liimatainen, H.; Niinimäki, J. Flocculation of municipal wastewaters with anionic nanocelluloses: Influence of nanocellulose characteristics on floc morphology and strength. *J. Environ. Chem. Eng.* **2014**, *2* (4), 2005–2012.

(145) Arsad, N. J.; Ngadi, N. Chitosan-Grafted Nanocellulose Derived from Empty Fruit Bunch for Ethyl Orange Removal. *Appl. Mech. Mater.* **2014**, *625*, 784–787.

(146) Sun, X.; Danumah, C.; Liu, Y.; Boluk, Y. Flocculation of bacteria by depletion interactions due to rod-shaped cellulose nanocrystals. *Chem. Eng. J.* **2012**, *198–199*, 476–481.

(147) Jin, L.; Wei, Y.; Xu, Q.; Yao, W.; Cheng, Z. Cellulose nanofibers prepared from TEMPO-oxidation of kraft pulp and its flocculation effect on kaolin clay. *J. Appl. Polym. Sci.* **2014**, *131* (12), 40450 (1-8).

(148) Gaudreault, R.; Di Cesare, N.; Weitz, D.; van de Ven, T. G. M. Flocculation kinetics of precipitated calcium carbonate. *Colloids Surfaces A Physicochem. Eng. Asp.* **2009**, *340* (1–3), 56–65.

(149) Eyley, S.; Vandamme, D.; Lama, S.; Van den Mooter, G.; Muylaert, K.; Thielemans, W. CO 2 controlled flocculation of microalgae using pH responsive cellulose nanocrystals. *Nanoscale* **2015**, *7* (34), 14413–14421.

(150) Ge, S.; Champagne, P.; Wang, H.-D.; Jessop, P. G.; Cunningham, M. F. Microalgae Recovery from Water for Biofuel Production Using CO 2 -Switchable Crystalline Nanocellulose. *Environ. Sci. Technol.* **2016**, *50* (14), 7896–7903.

(151) Akhlaghi, S. P.; Zaman, M.; Mohammed, N.; Brinatti, C.; Batmaz, R.; Berry, R.; Loh, W.; Tam, K. C. Synthesis of amine functionalized cellulose nanocrystals: optimization and characterization. *Carbohydr. Res.* **2015**, *409*, 48–55.

(152) Lalia, B. S.; Guillen, E.; Arafat, H. A.; Hashaikeh, R. Nanocrystalline cellulose reinforced PVDF-HFP membranes for membrane distillation application. *Desalination* **2014**, *332* (1), 134–141.

(153) Metreveli, G.; Wågberg, L.; Emmoth, E.; Belák, S.; Strømme, M.; Mihranyan, A. A Size-Exclusion Nanocellulose Filter Paper for Virus Removal. *Adv. Healthc. Mater.* **2014**, *3* (10), 1546–1550.

(154) Quellmalz, A.; Mihranyan, A. Citric Acid Cross-Linked Nanocellulose-Based Paper for Size-Exclusion Nanofiltration. *ACS Biomater. Sci. Eng.* **2015**, *1* (4), 271–276.

(155) Asper, M.; Hanrieder, T.; Quellmalz, A.; Mihranyan, A. Removal of xenotropic murine leukemia virus by nanocellulose based filter paper. *Biologicals* **2015**, *43* (6), 452–456.

(156) Karim, Z.; Mathew, A. P.; Grahn, M.; Mouzon, J.; Oksman, K. Nanoporous membranes with cellulose nanocrystals as functional entity in chitosan: Removal of dyes from water. *Carbohydr. Polym.* **2014**, *112*, 668–676.

(157) Karim, Z.; Claudpierre, S.; Grahn, M.; Oksman, K.; Mathew, A. P. Nanocellulose based functional membranes for water cleaning: Tailoring of mechanical properties, porosity and metal ion capture. *J. Memb. Sci.* **2016**, *514*, 418–428.

(158) Karim, Z.; Mathew, A. P.; Kokol, V.; Wei, J.; Grahn, M. High-flux affinity membranes based on cellulose nanocomposites for removal of heavy metal ions from industrial effluents. *RSC Adv.* **2016**, *6* (25), 20644–20653.

(159) Mautner, A.; Lee, K.-Y.; Lahtinen, P.; Hakalahti, M.; Tammelin, T.; Li, K.; Bismarck, A. Nanopapers for organic solvent nanofiltration. *Chem. Commun.* **2014**, *50* (43), 5778–5781.

(160) Mautner, A.; Lee, K.-Y.; Tammelin, T.; Mathew, A. P.; Nedoma, A. J.; Li, K.; Bismarck, A. Cellulose nanopapers as tight aqueous ultra-filtration membranes. *React. Funct. Polym.* **2015**, *86*, 209–214.

(161) Mautner, A.; Maples, H. A.; Kobkeatthawin, T.; Kokol, V.; Karim, Z.; Li, K.; Bismarck, A. Phosphorylated nanocellulose papers for copper adsorption from aqueous solutions. *Int. J. Environ. Sci. Technol.* **2016**, *13* (8), 1861–1872.

(162) Qu, P.; Tang, H.; Gao, Y.; Zhang, L. P.; Wang, S. Polyethersulfone composite membrane blended With cellulose fibrils. *BioResources* **2010**, *5* (4), 2323–2336.

(163) Kong, L.; Zhang, D.; Shao, Z.; Han, B.; Lv, Y.; Gao, K.; Peng, X. Superior effect of TEMPO-oxidized cellulose nanofibrils (TOCNs) on the performance of cellulose triacetate (CTA) ultrafiltration membrane. *Desalination* **2014**, *332* (1), 117–125.

(164) Ma, H.; Burger, C.; Hsiao, B. S.; Chu, B. Ultra-fine cellulose nanofibers: new nano-scale materials for water purification. *J. Mater. Chem.* **2011**, *21* (21), 7507–7510.

(165) Ma, H.; Burger, C.; Hsiao, B. S.; Chu, B. Nanofibrous Microfiltration Membrane Based on Cellulose Nanowhiskers. *Biomacromolecules* **2012**, *13* (1), 180–186.

(166) Wang, R.; Guan, S.; Sato, A.; Wang, X.; Wang, Z.; Yang, R.; Hsiao, B. S.; Chu, B. Nanofibrous microfiltration membranes capable of removing bacteria, viruses and heavy metal ions. *J. Memb. Sci.* **2013**, *446*, 376–382.

(167) Ma, H.; Burger, C.; Hsiao, B. S.; Chu, B. Ultrafine Polysaccharide Nanofibrous Membranes for Water Purification. *Biomacromolecules* **2011**, *12* (4), 970–976.

(168) Ma, H.; Burger, C.; Hsiao, B. S.; Chu, B. Fabrication and characterization of cellulose nanofiber based thin-film nanofibrous composite membranes. *J. Memb. Sci.* **2014**, *454*, 272–282.

(169) Wang, Z.; Ma, H.; Hsiao, B. S.; Chu, B. Nanofibrous ultrafiltration membranes containing cross-linked poly(ethylene glycol) and cellulose nanofiber composite barrier layer. *Polymer* **2014**, *55* (1), 366–372.

(170) Wang, X.; Yeh, T.-M.; Wang, Z.; Yang, R.; Wang, R.; Ma, H.; Hsiao, B. S.; Chu, B. Nanofiltration membranes prepared by interfacial polymerization on thin-film

nanofibrous composite scaffold. *Polymer* **2014**, *55* (6), 1358–1366.

(171) Yang, R.; Aubrecht, K. B.; Ma, H.; Wang, R.; Grubbs, R. B.; Hsiao, B. S.; Chu, B. Thiol-modified cellulose nanofibrous composite membranes for chromium (VI) and lead (II) adsorption. *Polymer* **2014**, *55* (5), 1167–1176.

(172) Kaushik, M.; Moores, A. Review: nanocelluloses as versatile supports for metal nanoparticles and their applications in catalysis. *Green Chem.* **2016**, *18* (3), 622–637.

(173) Wei, H.; Rodriguez, K.; Renneckar, S.; Vikesland, P. J. Environmental science and engineering applications of nanocellulose-based nanocomposites. *Environ. Sci. Nano* **2014**, *1* (4), 302–316.

(174) Lam, E.; Male, K. B.; Chong, J. H.; Leung, A. C. W.; Luong, J. H. T. Applications of functionalized and nanoparticle-modified nanocrystalline cellulose. *Trends Biotechnol.* **2012**, *30* (5), 283–290.

(175) Wu, X.; Lu, C.; Zhang, W.; Yuan, G.; Xiong, R.; Zhang, X. A novel reagentless approach for synthesizing cellulose nanocrystal-supported palladium nanoparticles with enhanced catalytic performance. *J. Mater. Chem. A* **2013**, *1* (30), 8645–8652.

(176) Snyder, A.; Bo, Z.; Moon, R.; Rochet, J.-C.; Stanciu, L. Reusable photocatalytic titanium dioxide–cellulose nanofiber films. *J. Colloid Interface Sci.* **2013**, *399*, 92–98.

(177) Liu, S.; Tao, D.; Bai, H.; Liu, X. Cellulose-nanowhisker-templated synthesis of titanium dioxide/cellulose nanomaterials with promising photocatalytic abilities. *J. Appl. Polym. Sci.* **2012**, *126* (S1), E282–E290.

(178) Drogat, N.; Granet, R.; Sol, V.; Memmi, A.; Saad, N.; Klein Koerkamp, C.; Bressollier, P.; Krausz, P. Antimicrobial silver nanoparticles generated on cellulose nanocrystals. *J. Nanoparticle Res.* **2011**, *13* (4), 1557–1562.

(179) Díez, I.; Eronen, P.; Österberg, M.; Linder, M. B.; Ikkala, O.; Ras, R. H. A. Functionalization of Nanofibrillated Cellulose with Silver Nanoclusters: Fluorescence and Antibacterial Activity. *Macromol. Biosci.* **2011**, *11* (9), 1185–1191.

(180) Liu, H.; Song, J.; Shang, S.; Song, Z.; Wang, D. Cellulose Nanocrystal/Silver Nanoparticle Composites as Bifunctional Nanofillers within Waterborne Polyurethane.

ACS Appl. Mater. Interfaces **2012**, *4* (5), 2413–2419.

(181) Xiong, R.; Lu, C.; Zhang, W.; Zhou, Z.; Zhang, X. Facile synthesis of tunable silver nanostructures for antibacterial application using cellulose nanocrystals. *Carbohydr. Polym.* **2013**, *95* (1), 214–219.

(182) Wang, M. S.; Jiang, F.; Hsieh, Y.-L.; Nitin, N. Cellulose nanofibrils improve dispersibility and stability of silver nanoparticles and induce production of bacterial extracellular polysaccharides. *J. Mater. Chem. B* **2014**, *2* (37), 6226–6235.

(183) Dong, H.; Snyder, J. F.; Tran, D. T.; Leadore, J. L. Hydrogel, aerogel and film of cellulose nanofibrils functionalized with silver nanoparticles. *Carbohydr. Polym.* **2013**, *95* (2), 760–767.

(184) Azizi, S.; Ahmad, M.; Hussein, M.; Ibrahim, N. Synthesis, Antibacterial and Thermal Studies of Cellulose Nanocrystal Stabilized ZnO-Ag Heterostructure Nanoparticles. *Molecules* **2013**, *18* (6), 6269–6280.

(185) Jebali, A.; Hekmatimoghaddam, S.; Behzadi, A.; Rezapor, I.; Mohammadi, B. H.; Jasemizad, T.; Yasini, S. A.; Javadzadeh, M.; Amiri, A.; Soltani, M.; et al. Antimicrobial activity of nanocellulose conjugated with allicin and lysozyme. *Cellulose* **2013**, *20* (6), 2897–2907.

(186) Tang, J.; Song, Y.; Tanvir, S.; Anderson, W. A.; Berry, R. M.; Tam, K. C. Polyrhodanine Coated Cellulose Nanocrystals: A Sustainable Antimicrobial Agent. *ACS Sustain. Chem. Eng.* **2015**, *3* (8), 1801–1809.

(187) Chavan, R. Indian textile industry-environmental issues. *Indian J. Fibre Text. Res.* **2001**, *26*, 11–21.

(188) You, S.; Cheng, S.; Yan, H. The impact of textile industry on China's environment. *Int. J. Fash. Des. Technol. Educ.* **2009**, *2* (1), 33–43.

(189) Métivier-Pignon, H.; Faur-Brasquet, C.; Le Cloirec, P. Adsorption of dyes onto activated carbon cloths: approach of adsorption mechanisms and coupling of ACC with ultrafiltration to treat coloured wastewaters. *Sep. Purif. Technol.* **2003**, *31* (1), 3–11.

(190) Lee, K. Y.; Mooney, D. J. Alginate: properties and biomedical applications. *Prog.*

Polym. Sci. **2012**, *37* (1), 106–126.

(191) Fan, J.; Shi, Z.; Min, L.; Li, H.; Yin, J. Mechanically strong graphene oxide/sodium alginate/ polyacrylamide nanocomposite hydrogel with improved dye adsorption capacity. *J. Mater. Chem. A* **2013**, *1* (25), 7433–7443.

(192) Rocher, V.; Bee, A.; Siaugue, J.-M.; Cabuil, V. Dye removal from aqueous solution by magnetic alginate beads crosslinked with epichlorohydrin. *J. Hazard. Mater.* **2010**, *178* (1–3), 434–439.

(193) Zhao, F.; Yu, B.; Yue, Z.; Wang, T.; Wen, X.; Liu, Z.; Zhao, C. Preparation of porous chitosan gel beads for copper(II) ion adsorption. *J. Hazard. Mater.* **2007**, *147* (1–2), 67–73.

(194) Aravindhan, R.; Fathima, N. N.; Rao, J. R.; Nair, B. U. Equilibrium and thermodynamic studies on the removal of basic black dye using calcium alginate beads. *Colloids Surfaces A Physicochem. Eng. Asp.* **2007**, *299* (1–3), 232–238.

(195) Hameed, B. H.; Din, A. T. M.; Ahmad, A. L. Adsorption of methylene blue onto bamboo-based activated carbon: Kinetics and equilibrium studies. *J. Hazard. Mater.* **2007**, *141* (3), 819–825.

(196) Lagoa, R.; Rodrigues, J. R. Kinetic analysis of metal uptake by dry and gel alginate particles. *Biochem. Eng. J.* **2009**, *46* (3), 320–326.

(197) Lezehari, M.; Basly, J.-P.; Baudu, M.; Bouras, O. Alginate encapsulated pillared clays: removal of a neutral/anionic biocide (pentachlorophenol) and a cationic dye (safranine) from aqueous solutions. *Colloids Surfaces A Physicochem. Eng. Asp.* **2010**, *366* (1–3), 88–94.

(198) Liu, L.; Wan, Y.; Xie, Y.; Zhai, R.; Zhang, B.; Liu, J. The removal of dye from aqueous solution using alginate-halloysite nanotube beads. *Chem. Eng. J.* **2012**, *187*, 210–216.

(199) Parekh, P.; Parmar, A.; Chavda, S.; Bahadur, P. Modified Calcium Alginate Beads with Sodium Dodecyl Sulfate and Clay as Adsorbent for Removal of Methylene Blue. *J. Dispers. Sci. Technol.* **2011**, *32* (10), 1377–1387.

(200) Deng, H.; Yang, L.; Tao, G.; Dai, J. Preparation and characterization of activated carbon

from cotton stalk by microwave assisted chemical activation--application in methylene blue adsorption from aqueous solution. *J. Hazard. Mater.* **2009**, *166* (2–3), 1514–1521.

(201) Ozacar, M.; Sengil, I. A. Adsorption of metal complex dyes from aqueous solutions by pine sawdust. *Bioresour. Technol.* **2005**, *96* (7), 791–795.

(202) Saha, P.; Chowdhury, S.; Gupta, S.; Kumar, I.; Kumar, R. Assessment on the Removal of Malachite Green Using Tamarind Fruit Shell as Biosorbent. *CLEAN - Soil, Air, Water* **2010**, *38* (5–6), 437–445.

(203) Mall, I. D.; Srivastava, V. C.; Agarwal, N. K.; Mishra, I. M. Adsorptive removal of malachite green dye from aqueous solution by bagasse fly ash and activated carbon-kinetic study and equilibrium isotherm analyses. *Colloids Surfaces A Physicochem. Eng. Asp.* **2005**, *264* (1–3), 17–28.

(204) *CRC Handbook of Chemistry and Physics , 92nd Edition*, 92, Illust ed.; Haynes, W. M., Ed.; CRC Press, Taylor & Francis, 2011.

(205) Sun, L.; Fugetsu, B. Effect of encapsulated graphene oxide on alginate-based bead adsorption to remove acridine orange from aqueous solutions. *arXiv Prepr. arXiv1307.0223* **2013**.

(206) Maurya, N. S.; Mittal, A. K.; Cornel, P.; Rother, E. Biosorption of dyes using dead macro fungi: effect of dye structure, ionic strength and pH. *Bioresour. Technol.* **2006**, *97* (3), 512–521.

(207) Doğan, M.; Abak, H.; Alkan, M. Biosorption of Methylene Blue from Aqueous Solutions by Hazelnut Shells: Equilibrium, Parameters and Isotherms. *Water. Air. Soil Pollut.* **2008**, *192* (1–4), 141–153.

(208) Lim, S.-F.; Zheng, Y.-M.; Zou, S.-W.; Chen, J. P. Removal of copper by calcium alginate encapsulated magnetic sorbent. *Chem. Eng. J.* **2009**, *152* (2–3), 509–513.

(209) Jeon, Y. S.; Lei, J.; Kim, J.-H. Dye adsorption characteristics of alginate/polyaspartate hydrogels. *J. Ind. Eng. Chem.* **2008**, *14* (6), 726–731.

(210) Youssef, M. E.; Soliman, E. A.; Abu-Saied, M. A.; Mohdy Eldin, M. S.; Al-Deyab, S. S.; Kenawy, E.-R.; Elzatahray, A. A. Laboratory Studies and Numerical Modeling of

using Natural Micro beads for Environmental Applications. *Int. J. Electrochem. Sci.* **2010**, *5*, 1887–1897.

(211) Reddy, M. R.; Dunn, S. J. Distribution coefficients for nickel and zinc in soils. *Environ. Pollut. Ser. B, Chem. Phys.* **1986**, *1* (4), 303–313.

(212) Gomes, P. C.; Fontes, M. P. F.; Silva, A. G. da; Mendonca, E. de S.; Netto, A. R. Selectivity sequence and competitive adsorption of heavy metals by Brazilian soils. *Soil Sci. Soc. Am. J.* **2001**, *65* (4), 1115–1121.

(213) Gupta, V. K.; Mohan, D.; Sharma, S.; Sharma, M. Removal of Basic Dyes (Rhodamine B and Methylene Blue) from Aqueous Solutions Using Bagasse Fly Ash. *Sep. Sci. Technol.* **2000**, *35* (13), 2097–2113.

(214) Abramian, L.; El-Rassy, H. Adsorption kinetics and thermodynamics of azo-dye Orange II onto highly porous titania aerogel. *Chem. Eng. J.* **2009**, *150* (2–3), 403–410.

(215) Yu, Y.; Zhuang, Y.-Y.; Wang, Z.-H. Adsorption of Water-Soluble Dye onto Functionalized Resin. *J. Colloid Interface Sci.* **2001**, *242* (2), 288–293.

(216) Vimonses, V.; Lei, S.; Jin, B.; Chow, C. W. K.; Saint, C. Kinetic study and equilibrium isotherm analysis of Congo Red adsorption by clay materials. *Chem. Eng. J.* **2009**, *148* (2–3), 354–364.

(217) Chatterjee, S.; Chatterjee, S.; Chatterjee, B. P.; Guha, A. K. Adsorptive removal of congo red, a carcinogenic textile dye by chitosan hydrobeads: Binding mechanism, equilibrium and kinetics. *Colloids Surfaces A Physicochem. Eng. Asp.* **2007**, *299* (1–3), 146–152.

(218) Auta, M.; Hameed, B. H. Acid modified local clay beads as effective low-cost adsorbent for dynamic adsorption of methylene blue. *J. Ind. Eng. Chem.* **2013**, *19* (4), 1153–1161.

(219) Lagergren, S. Zur theorie der sogenannten adsorption gel`ster stoffe, Kungliga Svenska Vetenskapsakademiens. *Handlingar* **1898**, *24* (4), 1–39.

(220) Ho, Y. S.; McKay, G. Pseudo-second order model for sorption processes. *Process Biochem.* **1999**, *34* (5), 451–465.

(221) Weber, W. J.; Morris, J. C. Kinetics of adsorption on carbon from solution. *J. Sanit.*

Eng. Div. **1963**, *89* (2), 31–60.

(222) Wang, W.; Zong, L.; Wang, A. A nanoporous hydrogel based on vinyl-functionalized alginate for efficient absorption and removal of Pb2+ ions. *Int. J. Biol. Macromol.* **2013**, *62*, 225–231.

(223) Cheung, W. H.; Szeto, Y. S.; McKay, G. Intraparticle diffusion processes during acid dye adsorption onto chitosan. *Bioresour. Technol.* **2007**, *98* (15), 2897–2904.

(224) Krishni, R. R.; Foo, K. Y.; Hameed, B. H. Adsorptive removal of methylene blue using the natural adsorbent-banana leaves. *Desalin. Water Treat.* **2014**, *52* (31–33), 6104–6112.

(225) Allen, S. J.; McKay, G.; Khader, K. Y. Intraparticle diffusion of a basic dye during adsorption onto sphagnum peat. *Environ. Pollut.* **1989**, *56* (1), 39–50.

(226) Langmuir, I. The adsorption of gases on plane surfaces of glass, mica and platinum. *J. Am. Chem. Soc.* **1918**, *40* (9), 1361–1403.

(227) Yan, H.; Yang, L.; Yang, Z.; Yang, H.; Li, A.; Cheng, R. Preparation of chitosan/poly(acrylic acid) magnetic composite microspheres and applications in the removal of copper(II) ions from aqueous solutions. *J. Hazard. Mater.* **2012**, *229–230*, 371–380.

(228) Freundlich, H. Of the adsorption of gases. Section II. Kinetics and energetics of gas adsorption. *Trans. Faraday Soc.* **1932**, *28*, 195–201.

(229) Carmen, Z.; Daniel, S. Textile Organic Dyes – Characteristics, Polluting Effects and Separation/Elimination Procedures from Industrial Effluents – A Critical Overview. In *Organic Pollutants Ten Years After the Stockholm Convention - Environmental and Analytical Update*; Puzyn, D. T., Ed.; InTech, 2012; pp 55–86.

(230) Tan, I. A. W.; Ahmad, A. L.; Hameed, B. H. Adsorption of basic dye using activated carbon prepared from oil palm shell: batch and fixed bed studies. *Desalination* **2008**, *225* (1–3), 13–28.

(231) Higashijima, T.; Fuchigami, T. Determination of amino acids by capillary zone electrophoresis based on semiconductor laser fluorescence detection. *Anal. Chem.* **1992**,

64 (7), 711–714.

(232) Imasaka, T.; Tsukamoto, A.; Ishibashi, N. Visible semiconductor laser fluorometry. *Anal. Chem.* **1989**, *61* (20), 2285–2288.

(233) Cazetta, A. L.; Vargas, A. M. M.; Nogami, E. M.; Kunita, M. H.; Guilherme, M. R.; Martins, A. C.; Silva, T. L.; Moraes, J. C. G.; Almeida, V. C. NaOH-activated carbon of high surface area produced from coconut shell: Kinetics and equilibrium studies from the methylene blue adsorption. *Chem. Eng. J.* **2011**, *174* (1), 117–125.

(234) Liu, L.; Lin, Y.; Liu, Y.; Zhu, H.; He, Q. Removal of Methylene Blue from Aqueous Solutions by Sewage Sludge Based Granular Activated Carbon: Adsorption Equilibrium, Kinetics, and Thermodynamics. *J. Chem. Eng. Data* **2013**, *58* (8), 2248–2253.

(235) Beck, S.; Bouchard, J.; Berry, R. Dispersibility in water of dried nanocrystalline cellulose. *Biomacromolecules* **2012**, *13* (5), 1486–1494.

(236) Walker, C. Thinking small is leading to big changes. *Paper 360*. 2012, pp 8–13.

(237) Li, Q.; McGinnis, S.; Sydnor, C.; Wong, A.; Renneckar, S. Nanocellulose Life Cycle Assessment. *ACS Sustain. Chem. Eng.* **2013**, *1* (8), 919–928.

(238) Roman, M. Toxicity of Cellulose Nanocrystals: A Review. *Ind. Biotechnol.* **2015**, *11* (1), 25–33.

(239) Charumathi, D.; Das, N. Packed bed column studies for the removal of synthetic dyes from textile wastewater using immobilised dead C. tropicalis. *Desalination* **2012**, *285*, 22–30.

(240) Lazaridis, N. K.; Keenan, H. Chitosan beads as barriers to the transport of azo dye in soil column. *J. Hazard. Mater.* **2010**, *173* (1–3), 144–150.

(241) Xu, D.; Hein, S.; Loo, S. L.; Wang, K. The Fixed-Bed Study of Dye Removal on Chitosan Beads at High pH. *Ind. Eng. Chem. Res.* **2008**, *47* (22), 8796–8800.

(242) Lezehari, M.; Baudu, M.; Bouras, O.; Basly, J.-P. Fixed-bed column studies of pentachlorophenol removal by use of alginate-encapsulated pillared clay microbeads. *J. Colloid Interface Sci.* **2012**, *379* (1), 101–106.

(243) Fiol, N.; Escudero, C.; Poch, J.; Villaescusa, I. Preliminary studies on Cr(VI) removal from aqueous solution using grape stalk wastes encapsulated in calcium alginate beads in a packed bed up-flow column. *React. Funct. Polym.* **2006**, *66* (8), 795–807.

(244) Malkoc, E.; Nuhoglu, Y.; Dundar, M. Adsorption of chromium(VI) on pomace--an olive oil industry waste: batch and column studies. *J. Hazard. Mater.* **2006**, *138* (1), 142–151.

(245) Grant, G. T.; Morris, E. R.; Rees, D. a.; Smith, P. J. C.; Thom, D. Biological interactions between polysaccharides and divalent cations: The egg-box model. *FEBS Lett.* **1973**, *32* (1), 195–198.

(246) Morris, E. R.; Rees, D. a.; Thom, D.; Boyd, J. Chiroptical and stoichiometric evidence of a specific, primary dimerisation process in alginate gelation. *Carbohydr. Res.* **1978**, *66* (1), 145–154.

(247) Sikorski, P.; Mo, F.; Skjåk-Bræk, G.; Stokke, B. T. Evidence for egg-box-compatible interactions in calcium - Alginate gels from fiber x-ray diffraction. *Biomacromolecules* **2007**, *8* (7), 2098–2103.

(248) Richardson, J. F.; Harker, J. H.; Backhurst, J. R. . *Coulson and Richardson's Chemical Engineering Volume 2 - Particle Technology and Separation Processes*, 5th ed.; Elsevier, 2002.

(249) Aksu, Z.; Gönen, F. Biosorption of phenol by immobilized activated sludge in a continuous packed bed: prediction of breakthrough curves. *Process Biochem.* **2004**, *39* (5), 599–613.

(250) Al-Degs, Y. S.; Khraisheh, M. A. M.; Allen, S. J.; Ahmad, M. N. Adsorption characteristics of reactive dyes in columns of activated carbon. *J. Hazard. Mater.* **2009**, *165* (1–3), 944–949.

(251) Ghorai, S.; Pant, K. K. Equilibrium, kinetics and breakthrough studies for adsorption of fluoride on activated alumina. *Sep. Purif. Technol.* **2005**, *42* (3), 265–271.

(252) Hand, D. W.; Crittenden, J. C.; Thacker, W. E. Simplified Models for Design of Fixed Bed Adsorption Systems. *J. Environ. Eng.* **1984**, *110* (2), 440–456.

(253) Vortmeyer, D.; Michael, K. The effect of non-uniform flow distribution on

concentration profiles and breakthrough curves of fixed bed adsorbers. *Chem. Eng. Sci.* **1985**, *40* (11), 2135–2138.

(254) Cooney, D. O. The Importance of Axial Dispersion in Liquid-Phase Fixed-Bed Adsorption Operations. *Chem. Eng. Commun.* **1991**, *110* (1), 217–231.

(255) Tan, J. P. K.; Zeng, A. Q. F.; Chang, C. C.; Tam, K. C. Release kinetics of procaine hydrochloride (PrHy) from pH-responsive nanogels: theory and experiments. *Int. J. Pharm.* **2008**, *357* (1–2), 305–313.

(256) Lopez, V. C.; Hadgraft, J.; Snowden, M. J. The use of colloidal microgels as a (trans)dermal drug delivery system. *Int. J. Pharm.* **2005**, *292* (1–2), 137–147.

(257) Viessman, W.; Hammer, M.; Perez, E.; Chadik, P. *Water Supply and Pollution Control*; Pearson Prentice Hall: New Jersey, 2009.

(258) Dong, Z.; Wang, D.; Liu, X.; Pei, X.; Chen, L.; Jin, J. Bio-inspired surface-functionalization of graphene oxide for the adsorption of organic dyes and heavy metal ions with a superhigh capacity. *J. Mater. Chem. A* **2014**, *2* (14), 5034.

(259) Yang, Y.; Wei, Z.; Wang, C.; Tong, Z. Lignin-based Pickering HIPEs for macroporous foams and their enhanced adsorption of copper(II) ions. *Chem. Commun. (Camb).* **2013**, *49* (64), 7144–7146.

(260) Murali Mohan, Y.; Vimala, K.; Thomas, V.; Varaprasad, K.; Sreedhar, B.; Bajpai, S. K.; Mohana Raju, K. Controlling of silver nanoparticles structure by hydrogel networks. *J. Colloid Interface Sci.* **2010**, *342* (1), 73–82.

(261) Sharma, V. K.; Siskova, K. M.; Zboril, R.; Gardea-Torresdey, J. L. Organic-coated silver nanoparticles in biological and environmental conditions: fate, stability and toxicity. *Adv. Colloid Interface Sci.* **2014**, *204*, 15–34.

(262) Rai, M.; Yadav, A.; Gade, A. Silver nanoparticles as a new generation of antimicrobials. *Biotechnol. Adv.* **2009**, *27* (1), 76–83.

(263) Sankar, M. U.; Aigal, S.; Maliyekkal, S. M.; Chaudhary, A.; Anshup; Kumar, A. A.; Chaudhari, K.; Pradeep, T. Biopolymer-reinforced synthetic granular nanocomposites for affordable point-of-use water purification. *Proc. Natl. Acad. Sci. U. S. A.* **2013**, *110*

(21), 8459–8464.

(264) Loo, S.-L.; Fane, A. G.; Lim, T.-T.; Krantz, W. B.; Liang, Y.-N.; Liu, X.; Hu, X. Superabsorbent cryogels decorated with silver nanoparticles as a novel water technology for point-of-use disinfection. *Environ. Sci. Technol.* **2013**, *47* (16), 9363–9371.

(265) Fu, F.; Wang, Q. Removal of heavy metal ions from wastewaters: A review. *J. Environ. Manage.* **2011**, *92* (3), 407–418.

(266) Nata, I. F.; Sureshkumar, M.; Lee, C.-K. One-pot preparation of amine-rich magnetite/bacterial cellulose nanocomposite and its application for arsenate removal. *RSC Adv.* **2011**, *1* (4), 625–631.

(267) Trasande, L.; Landrigan, P. J.; Schechter, C. Public health and economic consequences of methyl mercury toxicity to the developing brain. *Environ. Health Perspect.* **2005**, *113* (5), 590–596.

(268) Nolan, E. M.; Lippard, S. J. Tools and Tactics for the Optical Detection of Mercuric Ion. *Chem. Rev.* **2008**, *108* (9), 3443–3480.

(269) Natarajan, G.; Mathew, A.; Negishi, Y.; Whetten, R. L.; Pradeep, T. A Unified Framework for Understanding the Structure and Modifications of Atomically Precise Monolayer Protected Gold Clusters. *J. Phys. Chem. C* **2015**, *119* (49), 27768–27785.

(270) Chen, L. Y.; Wang, C. W.; Yuan, Z.; Chang, H. T. Fluorescent gold nanoclusters: Recent advances in sensing and imaging. *Anal. Chem.* **2015**, *87* (1), 216–229.

(271) Zheng, J.; Nicovich, P. R.; Dickson, R. M. Highly fluorescent noble-metal quantum dots. *Annu. Rev. Phys. Chem.* **2007**, *58*, 409–431.

(272) Hu, D.; Sheng, Z.; Gong, P.; Cai, L. Highly selective fluorescent sensors for Hg(2+) based on bovine serum albumin-capped gold nanoclusters. *Analyst* **2010**, *135*, 1411–1416.

(273) Chevrier, D. M.; Chatt, A.; Zhang, P. Properties and applications of protein-stabilized fluorescent gold nanoclusters: short review. *J. Nanophotonics* **2012**, *6* (1), 064504 (1-16).

(274) Xavier, P. L.; Chaudhari, K.; Baksi, A.; Pradeep, T. Protein-protected luminescent noble

metal quantum clusters: an emerging trend in atomic cluster nanoscience. *Nano Rev.* **2012**, *3* (0), 1–16.

(275) Xie, J.; Zheng, Y.; Ying, J. Y. Highly selective and ultrasensitive detection of Hg(2+) based on fluorescence quenching of Au nanoclusters by Hg(2+)-Au(+) interactions. *Chem. Commun. (Camb).* **2010**, *46* (6), 961–963.

(276) Xie, J.; Zheng, Y.; Ying, J. Y. Protein-directed synthesis of highly fluorescent gold nanoclusters. *J. Am. Chem. Soc.* **2009**, *131* (3), 888–889.

(277) Ghosh, A.; Jeseentharani, V.; Ganayee, M. A.; Hemalatha, R. G.; Chaudhari, K.; Vijayan, C.; Pradeep, T.; Atanu Ghosh; Jeseentharani, V.; Ganayee, M. A.; et al. Approaching sensitivity of tens of ions using atomically precise cluster-nanofiber composites. *Anal. Chem.* **2014**, *86* (22), 10996–11001.

(278) Chau, M.; Sriskandha, S. E.; Pichugin, D.; Thérien-Aubin, H.; Nykypanchuk, D.; Chauve, G.; Méthot, M.; Bouchard, J.; Gang, O.; Kumacheva, E. Ion-Mediated Gelation of Aqueous Suspensions of Cellulose Nanocrystals. *Biomacromolecules* **2015**, *16* (8), 2455–2462.

(279) Shafiei-Sabet, S.; Hamad, W. Y.; Hatzikiriakos, S. G. Ionic strength effects on the microstructure and shear rheology of cellulose nanocrystal suspensions. *Cellulose* **2014**, *21* (5), 3347–3359.

(280) Mohanty, J. S.; Baksi, A.; Lee, H.; Pradeep, T. Noble metal clusters protected with mixed proteins exhibit intense photoluminescence. *RSC Adv.* **2015**, *5* (59), 48039–48045.

(281) Mohanty, J. S.; Xavier, P. L.; Chaudhari, K.; Bootharaju, M. S.; Goswami, N.; Pal, S. K.; Pradeep, T. Luminescent, bimetallic AuAg alloy quantum clusters in protein templates. *Nanoscale* **2012**, *4* (14), 4255–4262.

(282) Zhu, H.; Yu, T.; Xu, H.; Zhang, K.; Jiang, H.; Zhang, Z.; Wang, Z.; Wang, S. Fluorescent Nanohybrid of Gold Nanoclusters and Quantum Dots for Visual Determination of Lead Ions. *ACS Appl. Mater. Interfaces* **2014**, *6* (23), 21461–21467.

(283) Roy, S.; Palui, G.; Banerjee, A. The as-prepared gold cluster-based fluorescent sensor

for the selective detection of AsIII ions in aqueous solution. *Nanoscale* **2012**, *4* (8), 2734–2740.

(284) Yu, P.; Wen, X.; Toh, Y. R.; Huang, J.; Tang, J. Metallophilic bond-induced quenching of delayed fluorescence in Au 25@BSA Nanoclusters. *Part. Part. Syst. Charact.* **2013**, *30* (5), 467–472.

(285) Durgadas, C. V; Sharma, C. P.; Sreenivasan, K. Fluorescent gold clusters as nanosensors for copper ions in live cells. *Analyst* **2011**, *136* (5), 933–940.

(286) Golmohamadi, M.; Wilkinson, K. J. Diffusion of ions in a calcium alginate hydrogel-structure is the primary factor controlling diffusion. *Carbohydr. Polym.* **2013**, *94* (1), 82–87.

(287) Gehrke, S. H.; Fisher, J. P.; Palasis, M.; Lund, M. E. Factors Determining Hydrogel Permeability. *Ann. N. Y. Acad. Sci.* **2006**, *831* (1), 179–184.

(288) Legrand, J.; Dumont, E.; Comiti, J.; Fayolle, F. Diffusion coefficients of ferricyanide ions in polymeric solutions - comparison of different experimental methods. *Electrochim. Acta* **2000**, *45* (11), 1791–1803.

(289) Arthur, E. M.; O.Phillips, H. Diffusion Studies. Part II. Tracer Diffusion coefficient of Copper(II) in HCl and HClO4 at 25 C. *J. Chem. Soc. A Inorganic, Phys. Theor.* **1971**, 101–103.

(290) Quickenden, T. I.; Jiang, X. The diffusion coefficient of copper sulphate in aqueous solution. *Electrochim. Acta* **1984**, *29* (6), 693–700.

(291) Chen, D.; Lewandoswki, Z.; Roe, F.; Surapaneni, P. Diffusivity of Cu2+ in calcium alginate gel beads. *Biotechnol. Bioeng.* **1993**, *41*, 755–760.

(292) Jackson, J. K.; Letchford, K.; Wasserman, B. Z.; Ye, L.; Hamad, W. Y.; Burt, H. M. The use of nanocrystalline cellulose for the binding and controlled release of drugs. *Int. J. Nanomedicine* **2011**, *6*, 321–330.

Appendix

R-code to obtain the variation of red intensity along the bead diameter

```
library(jpeg)
readJPEG("/Users/Romy/Downloads/Quenching30.jpg")
r <- readJPEG("/Users/Romy/Downloads/Quenching30.jpg")
Red <- as.data.frame(r[,,1])
Green <- as.data.frame(r[,,2])
Blue <- as.data.frame(r[,,3])
center_red <- as.data.frame(Red[1024,])
center_green <- as.data.frame(Green[1024,])
center_blue <- as.data.frame(Blue[1024,])
center_red <- as.data.frame(t(center_red))
center_green <- as.data.frame(t(center_green))
center_blue <- as.data.frame(t(center_blue))
for (i in 1:nrow(center_red))
{
    center_red[i,2] <- i
    center_green[i,2] <- i
    center_blue[i,2] <- i
}
colnames(center_red) <- c("intensity","pixel.no")
colnames(center_green) <- c("intensity","pixel.no")
colnames(center_blue) <- c("intensity","pixel.no")
center_red[,3] <- "RED"
center_blue[,3] <- "BLUE"
center_green[,3] <- "GREEN"
center_pixels <- rbind(center_red,center_blue,center_green )
library(plotly)
plot_ly(center_pixels, y = intensity, color = V3, type =
"Scatter",mode = "markers")
```